Regulation of cyclic and pseudocyclic electron transport

Umama Hani

THÈSE DE DOCTORAT

NNT : 2024UPASB044

Regulation of cyclic and pseudocyclic electron transport

Régulation du transport cyclique et pseudocyclique des électrons

Thèse de doctorat de l'université Paris-Saclay

École doctorale n° 567, Sciences du végétal : du gène à l'écosystème (SEVE)
Spécialité de doctorat : Sciences végétales
Graduate School : BioSphERA. Référent : Faculté des sciences d´Orsay

Thèse préparée dans l´unité de recherche **Institute for Integrative Biology of the Cell (I2BC) (Université Paris-Saclay, CEA, CNRS)**, sous la direction de **Anja KRIEGER-LISZKAY**, DR CNRS.

Thèse soutenue à Paris-Saclay, le 15 octobre 2024, par

Umama HANI

Composition du Jury

Membres du jury avec voix délibérative

Sylvie DINANT Directrice de recherche, INRAE-Université Paris-Saclay	Présidente
Peter NIXON Professeur, Imperial College London	Rapporteur & Examinateur
Thomas ROACH Professeur associé (équiv. HDR), Universität Innsbruck	Rapporteur & Examinateur
Xenie JOHNSON Directeur de recherche, CEA Aix-Marseille Université	Examinatrice

université PARIS-SACLAY

ÉCOLE DOCTORALE
Sciences du végétal : du gène à l'écosystème (SEVE)

Titre : Régulation du transport cyclique et pseudocyclique des électrons

Mots clés : Manganèse, transport cyclique des électrons, transport pseudocyclique des électrons, photosystème I, plastocyanine, spectroscopie d'absorption in vivo, régulation redox, *Marchantia polymorpha*.

Résumé : La photosynthèse, principale voie de production d'énergie dans les environnements naturels, repose sur des flux d'électrons intervenant dans plusieurs complexes dans la membrane des thylakoïdes des organismes photosynthétiques. Le flux principal est le transport « linéaire » des électrons qui implique leur transfert de l'eau au $NADP^+$, le tout couplé à la synthèse d'ATP. L'oxydation de l'eau photosynthétique est catalysée par les clusters de manganèse (Mn_4CaO_5) au niveau du photosystème II (PSII). Pour assurer un équilibre optimal entre la quantité d'énergie produite et consommée, les organismes photosynthétiques détournent une partie de l'énergie lumineuse récoltée des voies de transport d'électrons "linéaires" vers des voies "alternatives". Parmi ces voies, on trouve les transports cyclique et pseudocyclique des électrons autour du photosystème I (PSI), qui fournit de l'ATP supplémentaire pour répondre aux besoins métaboliques. En outre, des systèmes redox spécialisés appelés " thiorédoxines " sont responsables du maintien de l'état redox et de l'acclimatation rapide des plantes à un environnement changeant. Dans le cas contraire, cela peut conduire à des niveaux toxiques d'espèces réactives de l'oxygène (ROS) dans les cellules.

Nous avons étudié les effets de l'excès et de la carence en manganèse (Mn) sur le transport des électrons au cours de la photosynthèse chez l'hépatique *Marchantia polymorpha*. Nous avons montré que l'homéostasie du Mn a un effet sur le-métabolisme mais aussi sur la photosynthèse. De plus, nous avons étudié les changements redox in vivo du P700 et du la plastocyanine (PC) en utilisant le spectrophotomètre KLAS-NIR. Il semble que la carence en Mn permet une augmentation du transport cyclique des électrons (TCE) ce qui indique la présence de supercomplexes contenant le PSI et le complexe du cytochrome b_6f. Dans un second temps, nous nous sommes concentrées sur la régulation redox de la réduction de l'oxygène (transport d'électrons pseudocyclique) du côté de l'accepteur du PSI. En utilisant la spectroscopie RPE par piégeage indirect de spin, nous avons montré que des plantes sauvages d'*Arabidopsis thaliana* génèrent plus de ROS en photopériode de jour court (JC) qu'en photopériode de jour long (JL). En outre, nous avons mis en évidence le rôle de plusieurs acteurs, y compris les thiorédoxines et plusieurs protéines du lumen et du stroma dans la régulation redox. De plus, j'ai découvert que le transfert du pouvoir réducteur du stroma au lumen est médié par une protéine appelée CCDA. Par ailleurs, l'attachement réversible de Trxm à la membrane des thylakoïdes agit comme une force motrice pour l'accumulation des ROS en JC. Dans l'ensemble, les résultats établissent un lien étroit entre le transport cyclique et pseudocyclique des électrons en termes de régulations redox médiées par les thiorédoxines. Une voie estégalement ouverte quant à une exploration plus approfondie du TCE dans différentes conditions de stress.

université PARIS-SACLAY

ÉCOLE DOCTORALE
Sciences du végétal : du gène à l'écosystème (SEVE)

Title : Regulation of cyclic and pseudocyclic electron transport

Keywords : Manganese, cyclic electron transport, pseudocyclic electron transport, photosystem I, plastocyanin, in vivo absorption spectroscopy, redox regulation, *Marchantia polymorpha*

Abstract: Photosynthesis acts as the main gateway for energy production in natural environments and relies on the electron flow via several complexes in the thylakoid membrane of photosynthetic organisms. The major flux is "linear" electron transport, which involves the transfer of electrons from water to $NADP^+$, coupled with the ATP synthesis. Photosynthetic water oxidation is catalyzed by manganese cluster (Mn_4CaO_5) at photosystem II (PSII). To ensure an optimal balance between the amount of energy produced and consumed, photosynthetic organisms divert part of the harvested light energy from "linear" to "alternative" electron transport pathways. Among those pathways are cyclic and pseudocyclic electron transport around Photosystem I (PSI), which supplies extra ATP to meet metabolic demands. Moreover, specialized redox systems, called " thioredoxins " are responsible for maintaining the redox status and fast acclimation of plants to constantly fluctuating environments, which could otherwise lead to toxic levels of reactive oxygen species (ROS) production.

We studied the effects of manganese (Mn) excess and deficiency on photosynthetic electron transport in the liverwort *Marchantia polymorpha*. We have shown that Mn homeostasis has an effect at both metabolic and photosynthetic levels. Moreover, we have studied the in vivo redox changes of P700 and PC using KLAS-NIR spectrophotometer and have shown that Mn deficiency seems to enhance cyclic electron transport (CET), that may indicate the presence of supercomplexes containing PSI and cytochrome b_6f complex. The second part of this PhD focused on the redox regulation of oxygen reduction (pseudocyclic electron transport) at the PSI acceptor side. By using indirect spin trapping EPR spectroscopy, we have shown that *Arabidopsis thaliana* wild type plants generate more ROS in short day (SD) photoperiod than in long day (LD) photoperiod. Further, the current study highlighted the role of several players in redox regulation; including thioredoxins and several other lumenal and stromal proteins. Moreover, I explored that the transfer of reducing powers from stroma to lumen is mediated by a protein called CCDA and that reversible attachment of Trxm to the thylakoid membrane acts as the driving force for higher ROS under the SD light regime. Overall, this research establishes a strong connection between cyclic and pseudocyclic electron transport in terms of thioredoxins mediated redox regulations and also paves the way to further explore CET under different stress conditions.

بِسْمِ ٱللَّهِ ٱلرَّحْمَٰنِ ٱلرَّحِيمِ

Dedicated to

my beloved Mother

میری پیاری امی کے لیے

&

To All the brave souls of Gaza, Palestine

Acknowledgements

Oh, what a roller coaster ride it has been !!!!

Completing these three years of PhD has been a truly transformative journey, and it would not have been possible without the support and guidance of many wonderful individuals.

First and foremost, I would like to specially thanks my thesis supervisor **Anja Krieger-Liszkay** for her insightful guidance and endless patience throughout these three years. I am so lucky that I have been supervised by such a good mentor like YOU. I highly appreciate our friendly scientific discussions that has deeply influenced my perspective on the natural world and scientific inquiry. Beyond all the scientific achievements, you are such a kind human being. I could never have imagined completing this PhD without your support. Despite the hardships that came my way when I started, you never turned your back on me. I was truly touched by your gestures and your unwavering commitment to my success.

I would also like to extend my heartfelt gratitude to **Sébastien Thomine** for hosting me in his lab throughout my PhD. I am deeply thankful for your generosity, kindness, support and the many other ways you contributed to my journey. Thanks once more for providing me with a nurturing and collaborative environment that was invaluable to my success.

I am also immensely grateful to the members of my thesis committee. Thanks **Emmanuelle Issakidis-Bourguet**, **Benjamin Bailleul** and **Benoît Alunni** for all the useful discussions and advices. Your expertise and critical insights have greatly enriched my work. Also, a special thanks to members of my thesis jury for accepting to review my manuscript. **Peter Nixon, Thomas Roach, Xenie Johnson** and **Sylvie Dinant**. Thanks for being part of my PhD Jury.

I also wants to say special thanks to **Ádám Solti** and **Éva Sárvári** for hosting me in their lab for one month. Thanks for all the valuable advices and suggestions.

I would like to say thanks to colleagues in CEA. Thanks **Marine** for introducing me with a cute plant “Marchantia”. I feel honored to have contributed to what you started. Thanks **Lucas** for all the friendly discussions.

Its incomplete without mentioning **MINIONS!!!** Oh, guys, you all are AMAZING. From the dizzying highs of successful experiments to the failed western blots, your lab became my second home. Your support, good humor and occasional rescue missions when I was “lost in the complexities of photosynthesis” were invaluable. Thank you for making this wild ride a memorable and enjoyable one!

A special thanks to **Jessica** for teaching me electron microscopy, you are amazing. Thanks, **Christelle** for helping me with everyday stuff in the lab and I will miss our cute little conversations in French. Thanks **Michele, Jean-Marie, and Sophie** for all the help, support and fantastic sense of humor that kept the atmosphere lively and fun, even during the most challenging times.

Anne-Sophie (my God Mother), I don't have words to express my gratitude. I am immensely grateful that our paths crossed. Thanks a lot for always listening to me, you have been a constant source of comfort throughout all these years. Thanks for teaching me molecular biology and helping me with all the tasks, no matter how big or small the task. I am incredibly grateful for your amazing presence in my life. Thank you for always being there for me.

Rubén, Rubén, Rubén!!!!!!! I could not have imagined this PhD without you. Thanks a lot for being my unpaid therapist and constant cheerleader. Your support and understanding is something that never let me feel down throughout this journey. You made hard days bearable and the good days even better simply by sharing a laugh over coffee. You are amazing, thanks for being such a great friend throughout this journey. You will be missed.

Guillaume, I am so happy that we met. Thanks for all the help and support. You are such a kindhearted and amazing person. I am extremely thankful for all the memories we share together. I will miss our chit-chat sessions ☺

Thanks **Pauline**, for being a good friend. Thanks for all the good memories and thanks for feeding us with tasty and fresh French brioche.

Nadine, I am so glad that I met you before ending my PhD. You are such an amazing and cute person. Thanks for all the help and all the cute conversations we had during this small time frame.

I would like to say special thanks to my close friends; **Julia Buggiani**, **Amir Maqbool**, **Busra Tas, Hamza Ramzan, Mohamed Mosalem, Reemana Fatima, Paul Adunola** and **Shaimaa Roshdy** for being a constant support throughout this journey.

A special thanks to my **mother**. I am nothing without you **"Ammi".** You have been an inspiration for me throughout my whole life. I dedicate all my success to you. Proud to be your daughter. And also special thanks to my only sister **Shahwana**, you are the best sister one could ask for and also, thanks to the rest of my family members.

Last but not least, a great and special thanks goes to **Danish (BOSS):** Thanks for believing in me. Your confidence in me has enhanced my ability to get to the end. Your love and support has been my greatest strengths.

Abbreviations

ΔpH :Transthylakoidal proton gradient

$^1O_2$:Singlet oxygen

2-Cys-Prx: 2- cysteine-peroxiredoxin

2Fe-2S: Rieske iron-sulphur protein

^{3}Chl*: Triplet state chlorophyll

A_1 :Phylloquinone

AA :Antimycin-A

ADP :Adenosine diphosphate

AET: Alternative electron transport

APX: Ascorbate peroxidase

ATP: Adenosine triphosphate

b_H :High potential heme

b_L :Low potential heme

BN-PAGE: Blue native polyacrylamide gel electrophoresis

CBB : Calvin-Benson-Bassham

CET : Cyclic electron transport

Chl : Chlorophyll

c_i :c type cytochrome

Cys : cysteine

Cyt b_6f: Cytochrome b_6f complex

Cyt c_6a: Cytochrome c_6a

DDM: n-dodecyl-beta-maltoside

ETC: Electron transport chain

Fd :Ferredoxin

FLV: Flavodiiron

FNR: Ferredoxin-$NADP^+$-reductase

FQR: Ferredoxin: plastoquinone oxidoreductase

FTR: Ferredoxin thioredoxin reductase

FTR-Trx : Ferredoxin-dependent thioredoxin system

H_2O: water

H_2O_2 :Hydrogen peroxide

KLAS: Kinetic LED array spectrophotometer

LD: Long day

LET: Linear electron transport

LHC: light-harvesting antenna complex

LHCII-a: LHCII assembly

LHCII-t: Trimeric LHCII

LTOI: Lumen Thiol Oxidoreductase1

Mn: Manganese

Mn_4CaO_5: manganese cluster /water splitting complex

NADPH: Nicotinamide adenine dinucleotide phosphate (reduced)

NIR: Near-infrared

NPQ : Non-photochemical quenching

NTRC: NADPH-dependent thioredoxin reductase system

$O_2^{\bullet-}$: Superoxide anion radical

OH• :Hydroxyl radical

PAM: Pulse amplitude modulation

PC: Plastocyanin

PCET: Pseudocyclic electron transport

PGR5: Proton gradient regulation 5

PGRL1: Pgr5 like -1

pmf: Proton motive force

PQ: Plastoquinone

PQH_2 :Plastohydroquinone

PSI: Photosystem I

PSII: Photosystem II

PSIIcc :Photosystem II core complex

PTOX : Plastid terminal oxidase

Q_A :Quinone A

Q_B :Quinone B

RC :Reaction center

ROS: Reactive oxygen species

SD: Short day

SOD :Superoxide dismutase

Trx: Thioredoxin

Table of Contents

Chapter 1: General Introduction

1.1. Chloroplast and Photosynthesis

Photosynthesis, which forms the basis of all life forms on earth takes place within specialized organelles of the green plant cell called the chloroplasts. Chloroplasts belong to plastids; which are organelles surrounded by the double membrane (outer and inner membrane) and contain their own genome. Oxygenic photosynthesis is believed to have evolved around 1.5 billion years ago from the cyanobacteria, in a process called endosymbiosis (Margulis, 1970; Maréchal, 2018). The primary reactions of photosynthesis takes place in the thylakoid membrane (detailed in section 1.1.1) which involve capturing sunlight energy and ultimately electron transfer through different protein complexes. This overall process leads to the generation of a proton (H^+) gradient which drives ATP synthesis and reduction of $NADP^+$. NADPH and ATP together, serve as substrates for the light-independent reactions, thus fixing carbon dioxide (CO_2) in the Calvin-Benson-Bassham (CBB) cycle.

1.1.1. Thylakoid membrane ultrastructure

The unique thylakoid membrane network hosts the photosynthetic machinery and is segregated into two domains: stacked (grana lamellae) and non-stacked (stroma lamellae) regions. The interface between stacked and non-stacked region is known as the grana margin and the space between two thylakoid membranes is named the thylakoid lumen. The space between the inner envelope membrane and thylakoid membrane is called the stroma, and it hosts all the light-independent carbon assimilation metabolic reactions (Kirchhoff, 2019). Besides hosting light-harvesting complex I (LHCI) and II (LHCII), it contains four main integral membrane complexes: photosystem II (PSII), cytochrome b_6f complex (Cyt b_6f), photosystem I (PSI) and ATP synthase complex (ATP synthase). These intrinsic supermolecular complexes together with other soluble extrinsic proteins are responsible for the primary reactions of photosynthesis, thus

catalyzing the synthesis of ATP and NADPH which are finally used for carbon assimilation reactions. Photosynthetic membrane complexes are unevenly distributed in the thylakoid membrane. The appressed grana region is mainly (80%) occupied by PSII-LHCII supercomplexes and the stromal exposed thylakoids are dominated by PSI-LHCI and ATP synthase. However, Cyt b_6f is equally distributed between the two domains (Anderson, 1982; Rantala et al., 2020).

1.2. Linear electron transport

The classical linear electron transport (LET) involves the flow of electrons from water (H_2O) to $NADP^+$ via the integral membrane protein complexes. The two photosystems are integrated via Cyt b_6f and two mobile electron carriers in the lipid bilayer and lumen i.e. plastoquinone (PQ) and plastocyanin (PC), respectively. Oxidation of water (H_2O) molecules by the water splitting complex of PSII reduces the PQ pool and leads to release of protons into the lumen. This generates a transthylakoidal proton gradient (ΔpH), which, together with the electrochemical gradient acts as a driving force for the ATP production. Further, a soluble copper containing protein PC is reduced by Cyt *f*, which is the electron donor to PSI. On the stromal side, PSI reduces ferredoxin (Fd) and the electrons generated here are used for the reduction of $NADP^+$ via ferredoxin-$NADP^+$-reductase (FNR) (Fig 1).

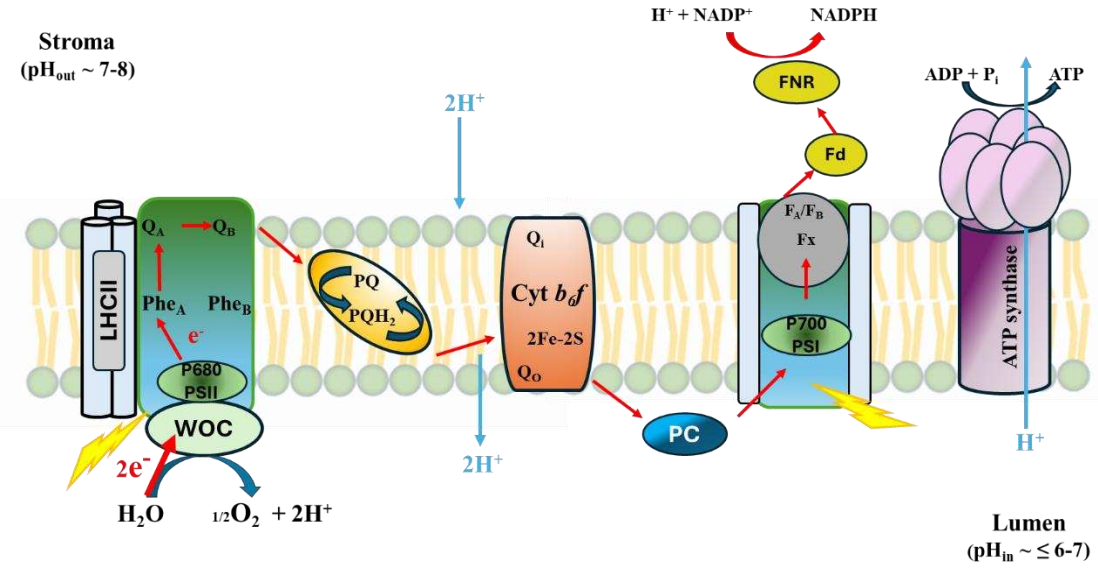

Figure 1: Linear electron transport in plants: A simplified scheme showing the interaction between different complexes (PSII, PSI, Cyt b_6f complex) and electron carriers; plastocyanin (PC), plastoquinone (PQ), plastoquinol (PQH_2) and ferredoxin (Fd). PSII upon extracting electron from H_2O reduces PQ. Cyt b_6f complex further transfers electrons to PSI via PC and finally to $NADP^+$ thus producing NADPH. Meanwhile, the acidification of lumen drives generation of ATP via ATP synthase. Red arrows indicates the path of electron transfer, and the transfer of protons is indicated by blue arrows. WOC (water oxidizing complex), LHCII (light harvesting complexes).

1.2.1. Light harvesting complex

One of the primary key events of photosynthetic process involves harvesting of sunlight energy. This process is carried out by pigment protein complexes called "light harvesting antenna complexes", that are subsequently responsible for the transfer of excitation energy to the reaction centers (RC) in the core complex of photosystem II and I, where charge separation occurs. The antenna systems have undergone a significant variation among different photosynthetic organisms in terms of evolution (Hohmann-Marriott and Blankenship, 2011). They belong to a large multigenic family of light-harvesting complex proteins (Lhc) (Jansson, 1999; Büchel, 2005). The land plant *Arabidopsis thaliana* has 15 LHC-II and 6 LHC-I encoding genes (Jansson, 1999), whereas 12 LHC-II (9 major and 3 minor) and 9 LHC-I encoding genes have been identified in the green alga *Chlamydomonas reinhardtii* (Minagawa and Takahashi, 2004). Lhcs are membrane proteins and have a similar structure that is composed of three transmembrane α-helices (Liu et al., 2004; Su et al., 2017) with an extraordinary number of chlorophylls (8 Chl a and 6 Chl b) and 3-4 xanthophyll molecules (Caffarri et al., 2014; Wei et al., 2016 ; van Bezouwen et al., 2017).

The most abundant light harvesting complex in green plants is LHC-II which exists as a trimer around the PSII core and coordinates about half of the total chlorophyll in the chloroplast (Peter and Thornber, 1991; Crepin and Caffarri, 2018). An X-ray structure of LHC-II has been resolved at 2.72 Å that provides deep insights into the positioning of the pigments and energy transfer amongst them (Liu et al., 2004; Standfuss et al., 2005). Moreover, imaging with

transmission electron microscopy and single-particle analysis has revealed PSII-LHCII supercomplexes with different antenna sizes (Caffarri et al., 2009). Besides the LHC-II heterotrimer which contains 3 gene products (Lhcb1-3), there also exist monomeric antenna complexes including Lhcb4, Lhcb5 and Lhcb6 which are also known as CP29, CP26 and CP24, respectively (Passarini et al., 2009; Pan et al., 2011). LHC-II also acts as a key player in photoprotection. To achieve this goal, plants have adapted two strategies. The first mechanism involves regulating the amount of light energy used by PSII, under circumstances when the amount of energy absorbed exceeds the photosynthetic capacity. To avoid oxidative stress, the excess energy is dissipated as heat in a process called energy-dependent non-photochemical quenching (qE-NPQ) (Müller et al., 2001; Horton and Ruban, 2005). Another approach for readjustment of redox poise of the electron transport chain upon fluctuation in light quantity and quality is achieved via the phosphorylation or re-distribution of mobile LHC-II antenna, which is commonly known as "state transitions" (Murata, 1969; Rochaix, 2014).

1.2.2. Photosystem II

PSII is a large multi-subunit pigment protein complex which stands out for its remarkable ability of catalyzing water oxidation, extracting electrons and thus providing oxygen that fuels life on the earth. In the past few decades, our knowledge of the PSII core complex has improved exponentially, with a series of high-resolution structures of PSII being published, ranging from 3.5 Å to 2.9 Å (Ferreira et al., 2004; Loll et al., 2005; Guskov et al., 2009; also reviewed in Cao et al., 2018). More recently, Umena and colleagues (2011) published a detailed atomic structure of PSII (1.9 Å) from *Thermosynechococcus vulcanus*, that is very detailed about the catalytic center of water splitting complex and truly enhanced our knowledge of understanding the complex reactions taking place at the PSII. The large multimeric PSII complex exists as a dimer in the thylakoid membrane (Gisriel et al., 2023).

The photosystem II core complex (PSIIcc) is composed of a reaction center, an inner antenna core and extrinsic thylakoid membrane proteins. It consists of more than 20 different subunits that vary depending on the organism (Qin et al., 2021). Moreover, PSII monomers also contain 11 β-carotenes, 35 Chls, a bicarbonate ion, around 20 lipid molecules and Mn, Ca and

chloride ions (Umena et al., 2011). The reaction center contains the membrane-intrinsic subunits including D1 (PsbA), D2 (PsbD), CP47 (PsbB) and CP43 (PsbC), that altogether makes the catalytic heart of the core (Fig 2). Cytochrome b_{559} , which is an important component of PSII and consists of two subunits (PsbE, PsbF), is essential for the proper functioning and assembly of PSII (Chiu et al., 2022). Together, the D1 and D2 subunits bind the co-factors of the internal electron transport chain, including the P680 reaction center chlorophylls, quinone acceptors, Q_A and Q_B, as well as the water splitting complex/manganese cluster (Mn_4CaO_5) on the donor (lumenal) side. Inner antenna proteins CP43 and CP47 bind the majority of chlorophylls (16 and 13 Chls respectively), thus funneling the absorbed energy into the reaction center and also stabilizing Mn_4CaO_5 cluster (Gisriel and Brudvig., 2022; Shevela et al., 2023). The last domain of PSII core includes extrinsic membrane proteins (PsbO, PsbP, PsbQ), that are bound on the lumenal side of the thylakoid membrane and are important for the stability of Mn_4CaO_5 cluster as well as allowing an enhanced binding of Ca^{+2} and Cl^- ions (Vinyard et al., 2022). Extrinsic membrane proteins vary greatly among plants, cyanobacteria and algae (Thornton et al., 2004; Ifuku and Noguchi., 2016). In addition, there also exists tiny low molecular mass membrane intrinsic subunits (PsbH, PsbX, PsbY, PsbZ and others) that are found in almost all organisms.

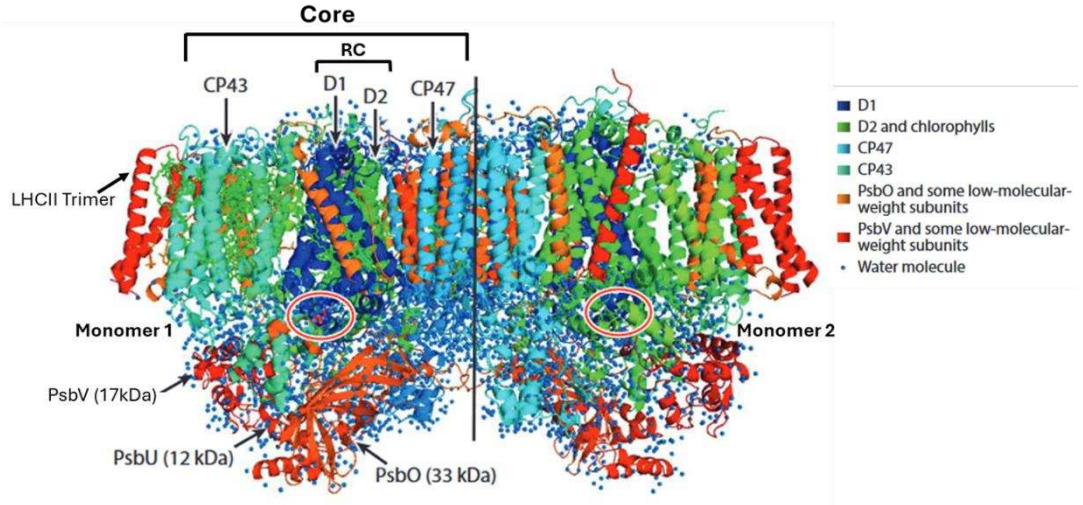

Figure 2. Structure of Photosystem II (PSII) dimer resolved at 1.9 Å from *Thermosynechococcus elongatus*: Two monomers are separated via non-crystallographic two-fold axis as shown by a vertical line. Peripheral antenna (LHCII) is indicated in red. Red circles are indicating water splitting center where Mn_4CaO_5 cluster binds. D1(PsbA) and D2(PsbD) are the largest subunits of PSII. CP43 (PsbC) and CP47 (PsbB) are the inner antenna (light harvesting) proteins. Membrane subunits (PsbO, PsbU and PsbV) on

the lumenal side are providing a protection cap for the Mn_4CaO_5 cluster. For better understanding a color code is available on the right side of the PSII structure. For clarity, other cofactors and intrinsic membrane subunits are not detailed here. Minor antennas are discussed in detail (Chapter 3). (This structure is chosen because of its better resolution as compared to plant PSII). S*tructure taken from Shen, 2015.*

Briefly, the overall reaction at PSII (Fig 3A, B) involves the absorption of photons by LHCs (in femtoseconds), that will funnel down the excitation energy to an ensemble of four pigment molecules (P_{D1}, P_{D2}, Chl_{D1}, Chl_{D2}) in the PSII RC. When this happens, P_{680} reaches its excited singlet state ($^1P_{680}$*) and transfers the electron to the primary electron acceptor pheophytin ($Pheo_{D1}$). This step occurs within ~ 3 ps and constitutes the primary charge separation thus producing a radical pair $P_{680}^{\bullet+}Pheo_{D1}^{\bullet-}$. It is important to mention here that $P_{680}^{\bullet+}$ has the highest known oxidizing potential in biology (~ +1.25 V). To ensure the stability of the radicals and to prevent charge recombination, a rapid electron transfer process occurs on both the donor and acceptor side of PSII. At the acceptor side, $Pheo_{D1}^{-}$ reduces the primary quinone acceptor (Q_A) within 250 ps, which ultimately reduces the secondary two electron acceptor quinone (Q_B), thus producing plastohydroquinone (PQH_2) within 1-20 ms. Whereas $P_{680}^{\bullet+}$ on the donor side is reduced (20 ns–35 µs) by tyrosine Z (Tyr Z), a redox active residue of D1, that extracts one electron from Mn_4CaO_5 cluster, a critical step for achieving water oxidation with high quantum yield (Shevela et al., 2023).

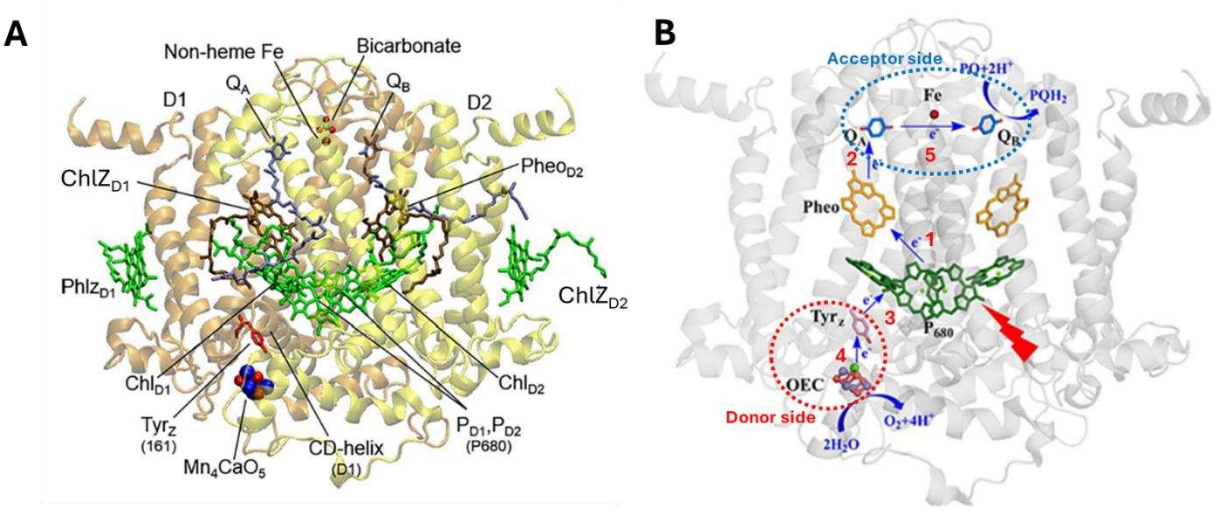

Figure 3. Localization of main cofactors involved in electron transfer in PSII: Figure based on structural data (PDB ID: 3WU2), showing the main redox cofactors embedded within the reaction center core (D1/D2 complex). Primary electron donor (P680) is the main cofactor, which is formed by the ensemble of different pigment molecules: a pair of Chls (P_{D1}/P_{D2}), two accessory chlorophylls (Chl_{D1}/Chl_{D2}), peripheral chlorophylls ($ChlZ_{D1}$ and $ChlZ_{D2}$ that make the connection to the antenna) and pheophytin as the primary electron acceptor. The acceptor side includes a non-heme Fe, binding a molecule of bicarbonate, located between the primary (Q_A) and secondary (Q_B) quinone acceptors. *Structure and inspired legend from Terentyev, 2022* **(A).** The successive steps in electron transfer within PSII reaction center are shown. P680, when photoexcited, transfers an electron to pheophytin (Pheo) and a primary radical pair $P680^{\bullet+}Pheo^{\bullet-}$ is produced. **(1)** $Pheo^{\bullet-}$ then reduces the primary quinone acceptor Q_A **(2).** Meanwhile, $P680^{\bullet+}$ on the donor side (red dotted circle) is filled by extracting an electron from the secondary electron donor (TyrZ) **(3),** which later drives the water oxidation at oxygen evolving center (OEC) at the PSII donor side **(4).** Finally secondary quinone acceptor Q_B at the acceptor side (blue dotted circle) is reduced by Q_A via non-heme Fe **(5).** *Modified scheme from Chen et al., 2022* **(B).**

The Mn_4CaO_5 cluster, which is considered the catalytic center of PSII, is responsible for water oxidation and is mainly coordinated by the amino acid residues from D1 on the lumenal side of thylakoid membrane. The water splitting complex cycles through series of five oxidation states ($S_0 \rightarrow S_4$). The oxidation of water (H_2O) leads to the formation of S_0 state with the release of oxygen (O_2) (Yano and Yachandra., 2014; Shen, 2015). Recently, study of mechanistic events involved in the transition from one intermediate state to the other have provided deep insights into photochemically induced reactions at the donor and acceptor sides (Ibrahim et al., 2020).

1.2.3. Cytochrome *b_6f* complex

Cytochrome *b_6f* (Cyt *b_6f*) is the third membrane complex in photosynthetic electron transport and acts as an oxidoreductase, thus mediating the electron transfer between PSII and PSI by oxidizing plastoquinol (PQH_2) and reducing soluble plastocyanin (PC) or cytochrome *c_6* in case of copper depletion in cyanobacteria and green algae (Cramer et al., 2004; Yamashita et al., 2007; Tikhonov, 2014). Like PSII, Cyt *b_6f* also exists as a functional dimer of ~220 kDa. As shown in Fig 4A, each monomer is composed of four large subunits containing two cytochromes

(cytochrome b_6 (PetA) and cytochrome *f* (PetB)), a Rieske iron-sulphur protein (2Fe-2S) and a protein IV (PetD), and four small subunits (PetG, L, M and N) with a structural role (Schwenkert, et al., 2007; Malone et al., 2021; Ruban et al., 2022). Redox cofactors exists within the large subunits. Cytochrome b_6 (cyt b_6) along with four transmembrane helices, possess three potential heme groups with different midpoint potentials: low potential heme (b_L), high potential heme (b_H) and a c type cytochrome (c_i). Each monomer of Cyt b_6f contains pigment molecules: a Chl molecule (Chl *a*) and a carotenoid (9-cis β-carotene). These pigments were found to be associated with subunit IV; however, their exact role is still unclear (Malone et al., 2021). Each monomer within the Cyt b_6f complex contains two binding pockets for quinone: luminal side (Q_o) and a stromal site (Q_i) which binds PQH_2 and PQ molecules, respectively (Tikhonov, 2014).

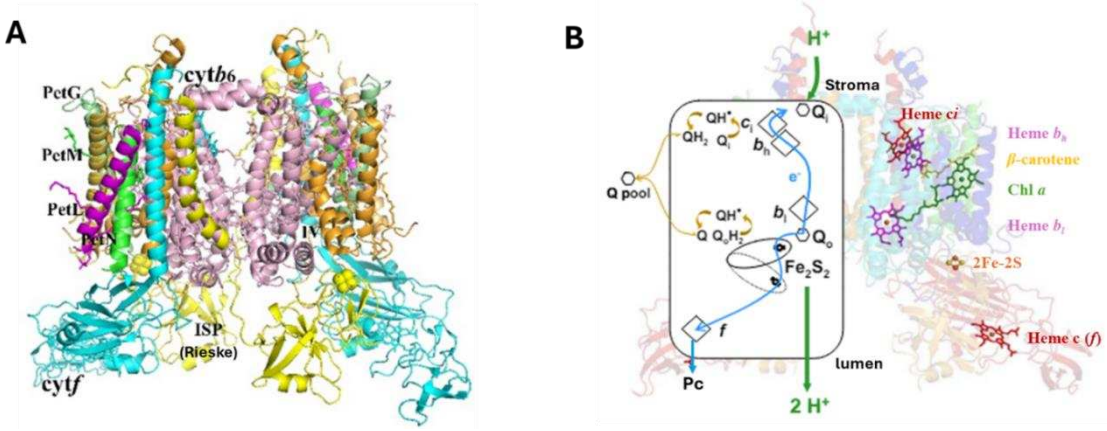

Figure 4. Structure of the cytochrome b_6f complex and Q cycle: Cryo-EM structure of Cyt b_6f dimer resolved at 3.58 Å from *Spinacia oleracea.* The following subunits are shown: cyt b_6 **(**light pink), cyt *f* (cyan), ISP-Rieske protein (yellow), subunit IV (orange), smaller subunits: PetG (pale green), PetM (wheat), PetL (magenta) and PetN (green). *Structure and legend from Qin et al., 2021* **(A).** Cyt b_6f complex operates through Q-cycle. Quinone binding pockets are shown as Qo (quinol (QH_2) oxidation site) and Qi (quinone (Q) reduction site). For each electron (blue arrows) transferred along high (2Fe-2S cluster and cyt *f*) and low potential chains (b_h, b_l, c_i hemes), two protons (green arrows) are translocated from stroma into the lumen. Cofactors are labelled in colors. Here the subunits are represented in different colors: cyt b_6 **(**cyan), cyt *f* (red), ISP-Rieske protein (yellow), subunit IV (blue). *Image from Stroebel et al., 2003; Malnoë, 2011* **(B).**

According to the Q cycle (Crofts, 2004), quinol oxidation is a bifurcated reaction and can be split into two half reactions. Oxidation of PQH_2 bound to the Q_o site (b_L), facilitates the transfer of one electron to PC via a high potential redox chain which contains 2Fe-2S cluster and cyt *f*. The other electron is directed from low (b_L) to high (b_H) redox potential hemes in cyt b_6 to reduce PQ on the stromal side (Q_i) (Tikhonov, 2014; Malone et al., 2021). Following the oxidation of a second PQH_2 at the Q_o site, semi-quinol at the Qi site is reduced and two protons are translocated from stroma into the lumen (Fig 4B), and generate a pH gradient, thus powering the Q cycle and increasing ATP synthesis. Moreover, evidence suggests that c_i may be involved in the direct reduction of PQ at the Qi binding site (Hasan et al., 2013) and might have role in cyclic electron transport (CET) around PSI. However, the exact nature of the electron donor to the PQ molecule still remains elusive (Johnson, 2011).

1.2.4. Photosystem I

PSI is a large multi-subunit protein complex and acts as a plastocyanin: ferredoxin oxidoreductase. It exists only in monomeric forms in higher plants whereas cyanobacterial PSI make trimers (Jordan et al., 2001). PSI crystal structures have remarkably helped in understanding the function and composition of the PSI core and its subunits (Klimmek et al., 2005; Nelson and Yocum., 2006). More recent refinement of the crystal structure of plant PSI resolved at 2.8-2.6 Å, has identified a total of 18 protein subunits, 15 β-carotenes, 175 Chls, 2 phylloquinones and 3 (4Fe-4S) clusters (Qin et al., 2015; Mazor et al., 2017). The PSI-LHCI supercomplex (see chapter 3) is organized into two functional moieties: core complex (reaction center) and a peripheral light-harvesting antenna complex (LHCI). The monomeric core hosts different subunits including PsaA and PsaB that binds most of the pigments, whereas LHCI is made up of six proteins (Lhca1-6). During state transitions, LHCII trimer gets attached to PSI (Jensen et al., 2007).

Two large transmembrane protein subunits; PsaA and PsaB together form heterodimer that initiates charge separation and the primary steps of the electron transport chain (ETC). This fundamental core houses P700 and certain other components of the ETC, including a 4Fe-4S cluster (F_x), A_0 (Chl a) and A_1 (phylloquinone) (Amunts and Nelson., 2009). The donor

(lumenal) side of PSI accommodates PsaF, which is a transmembrane protein and makes the docking site for soluble electron carriers PC or cyt c_6, which are directly involved in electron transfer (Xu et al., 1994; Busch and Hippler., 2011). Besides that, PsaF has an important role in binding and stabilizing LHCI trimers. PsaC, PsaD and PsaE together make a groove (docking site for Fd) on the acceptor (stromal) side of PSI (Fig 5A) (Yu et al., 1995; Fromme et al., 2001). The small intrinsic membrane subunits (PsaI, PsaJ, PsaK, PsaL) are attached peripherally to PsaA-PsaB and function to stabilize the antenna system, involved in state transitions (Lunde et al., 2000).

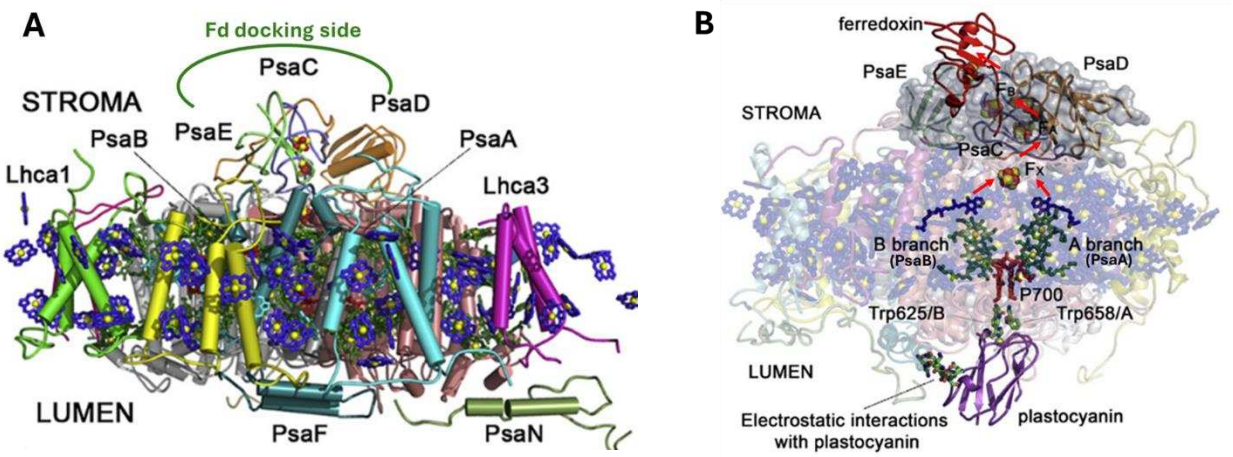

Figure 5. PSI structure and electron transfer: PSI is shown perpendicularly to the membrane normal. LHCI chlorophylls (Chls) are shown in blue and the rest of reaction center (RC) Chls are visible in green. PsaA and PsaB are large transmembrane protein subunits. Three extrinsic subunits (PsaC, PsaD and PsaE) on the stromal side forms the docking site for ferredoxin (Fd). PsaF binds plastocyanin (PC) and PsaN is interacting with Lhca3. Smaller subunits are omitted for clarity **(A)**. Proposed scheme for electron transport in PSI. A chain of organic cofactors, two Chls (green) and a phylloquinone (blue) are organized into two symmetrical branches; branch A (PsaA) and branch B (PsaB). PC is the electron donor, and it is recognized via its interaction and docking with PsaF and Trp658/PsaA, Trp625/PsaB, respectively. Once the electron reaches phylloquinone, it is transferred to Fe_4-S_4 clusters, Fx, F_A and F_B (shown in yellow-red spheres). Finally, the oxidized ferredoxin (red) in its docking site is reduced by electron donor F_B **(B)**. *Structure, modified scheme and legend from Amunts and Nelson; 2009*.

Electron transport in PSI (Fig 5B) occurs through two symmetrically active branches (however, only one branch is active in PSII) that are bound by either PsaA (A-branch) or PsaB (B-branch). The photoactive core contains a primary donor (P700) that exists as a Chl dimer (Chl a/a'), two Chls (accessory Chl and A_0) and a phylloquinone (A_1). Two branches intersect at the junction of 4Fe-4S cluster Fx, that is followed by PsaC bound terminal F_A/F_B clusters. Excited P700* is a very strong reductant (-1300 mV), which upon receiving energy from the antenna transfers an electron to the primary electron acceptor (A_{0A}/A_{0B}) forming $P700^+A_{0A}^-$ (A_{0B}^-) redox couple in ~3.7 ps, which afterwards transfers electron within 20-30 ps to phylloquinone (A_{1A}/A_{1B}), thus creating a more stable radical pair $P700^+A_{1A}^-$ (A_{1B}^-). This will successively reduce Fx (~200 ns), F_A or F_B (4Fe-4S clusters) and Fd, a soluble iron-sulfur protein (2Fe-2S) in the stroma which has a very negative redox potential (-430 mV). The final step involves reduction of $NADP^+$ via ferredoxin-NADP-reductase (FNR). At the same time $P700^+$ is re-reduced by accepting an electron from PC (Busch and Hippler., 2011; Petrova et al., 2017) (Ruban et al., 2022 [Chapter 2 from Book "Photosynthesis in Action"]).

1.2.5. ATP synthase

Adenosine triphosphate (ATP), which is also known as the "energy currency" of the cell, is generated when an anhydride bond is formed between adenosine diphosphate (ADP) and phosphate (Pi). ATP synthesis in the chloroplast is driven by a proton motive force (pmf) in a specialized complex called the CFo-CF_1 ATP synthase. The plastid ATP synthase is composed of many subunits and has a mass of around 500 kDa. It has a hydrophobic membrane bound part called Fo and a hydrophilic headpiece F_1. ATP synthase is thought to be regulated at the level of its γ subunit, where thioredoxin mediated thiol modulation is supposed to influence the pmf (Kohzuma et al., 2012). (For more details see Buchert, 2020)

1.3. The “dark reactions”

The reducing power stored in the form of ATP and NADPH is used to reduce CO_2 into organic compounds, which is important for plant growth and development. According to Bassham and colleagues (1954), besides fixing $6CO_2$; 18 ATP and 12 NADPH are consumed to generate one molecule of glucose, thus giving an ATP/NADPH ratio of 1.5. The CBB cycle involves three steps: carboxylation, reduction and regeneration (reviewed in Raines, 2003) that are not going to be detailed here. The most important enzyme in this cycle is ribulose-1,5-bisphosphate carboxylase/oxygenase (Rubisco), which is considered to be the most abundant protein in chloroplasts. Besides catalyzing the carboxylation reaction, it plays a very important role as an oxygenase in a process called photorespiration, which is considered as energy-dissipating mechanism (Zelitch, 1979).

1.4. Alternative electron transport

To efficiently use the captured light energy, all photosynthetic organisms needs a balance between the amount of energy produced and consumed. Any mismatch can severely damage the photosynthetic chain, by causing overreduction of the PQ pool, increased reactive oxygen species (ROS) production and PSI or PSII photoinhibition. To overcome these challenges, several alternative electron transfer (AET) pathways exists in plants. Most notable AET among them are cyclic electron transport (CET) and pseudocyclic electron transport (PCET) (Fig 6). Moreover, theoretically it is considered that the ATP/NADPH ratio of 1.28 produced during LET is not enough to meet the requirements for CO_2 fixation, which needs an ATP/NADPH ratio of 1.5. This is where AET pathways come into play to balance photosynthetic ETC by generating additional pmf, thus producing ATP without NADPH (Yamori et al., 2015). Besides that, a plethora of regulatory mechanisms also exists for protection of the ETC. I will discuss CET, PCET and the plastid terminal oxidase (PTOX), which is thought to protect PSII by acting as a “safety-valve”.

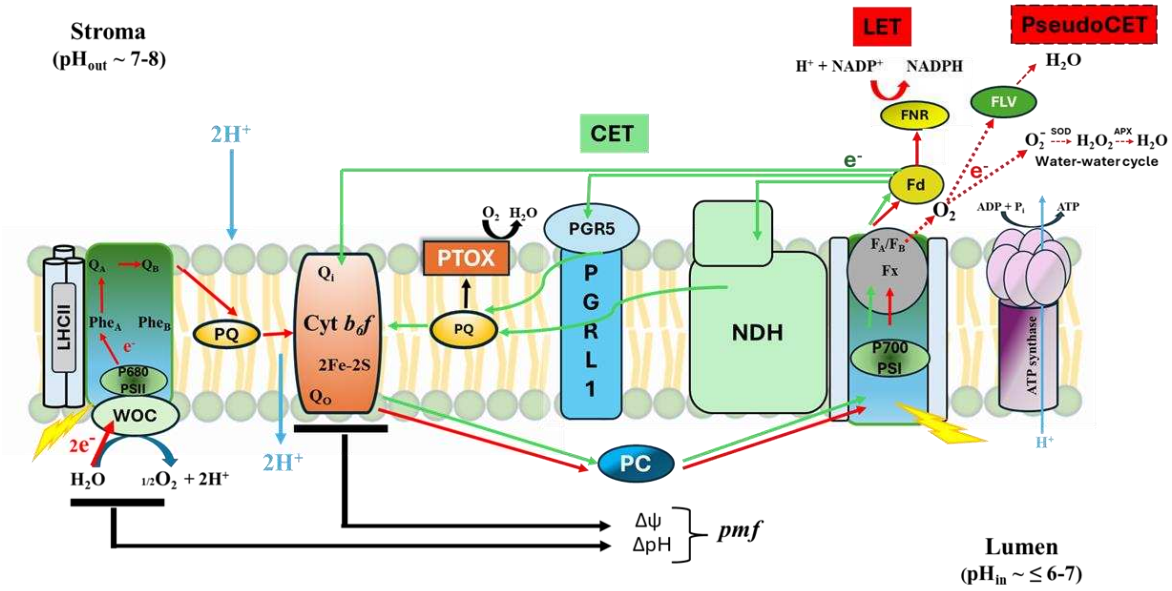

Figure 6: Alternative electron pathways in plants: A schematic representation of alternative electron transport (AET) in plants. Two main alternative electron pathways are shown here. Cyclic electron transport (CET) and pseudocyclic electron transport (PCET). CET (shown in green arrows) involves three different pathways: PGR5/PGRL1 antimycin A (AA) sensitive pathway; NDH-dehydrogenase like (NDH) complex AA insensitive and Ferredoxin (Fd) dependent pathway. PCET (red dotted arrows) involves Mehler reaction (water-water cycle) which involves reduction of oxygen (O_2) into superoxide anion radical ($O_2^{\bullet-}$), and ultimately into water (H_2O) via different enzymes; superoxide dismutase (SOD) and ascorbate peroxidase (APX), respectively. Note that flavodiiron (FLV) mediated Mehler reaction involves the direct reduction of O_2 into H_2O (in gymnosperms). Plastid terminal oxidase (PTOX), reduces O_2 into H_2O by accepting electrons from plastoquinone (PQ). To mention, Fd acts as an electron donor in CET, whereas PCET involves direct transfer from PSI to oxygen. The blue arrow indicates the proton gradient formed via Q-cycle in Cyt *b*$_6$*f* complex. Both linear and cyclic electron transport contribute towards pmf formation. Lumenal acidification contributes in photoprotection by limiting the electron transport through Cyt *b*$_6$*f* complex.

1.4.1. Cyclic electron transport

CET around PSI was first discovered around 50 years ago by Arnon and colleagues (Arnon, 1959). It is a bypass of normal LET, where it diverts energy for additional ATP production, without producing NADPH. CET explicitly shares the PQ pool, Cyt *b*$_6$*f*, PC, Fd and PSI with

LET. However, the molecular players involved in PQ reduction in CET are still not very clear and the mechanisms involved in CET remains a subject of controversy. Based on experimental evidence, two main pathways for CET have been proposed: NAD(P)H dehydrogenase-like (NDH) and PGR5/PGRL1 dependent pathways.

1.4.1.1. NAD(P)H dehydrogenase-like complex (NDH) dependent pathway

The first pathway involves the transfer of electrons from PSI acceptors to the PQ pool via the plastoquinone reductase (NDH), homologous to mitochondrial complex I, a NADH:ubiquinone(UQ)oxidoreductase (Joliot and Johnson, 2011). This pathway is usually referred to as NDH-CEF and is characteristically insensitive to antimycin-A (AA). NDH-1 from higher plants shares at least 11 subunits with the cyanobacterial and mitochondrial NADH:UQ oxidoreductase (complex I) (Peltier et al., 2016). However, from an evolutionary and functional viewpoint the chloroplast NDH complex holds more similarity with the cyanobacterial complex (Shikanai, 2007). Study of different subunits from NDH-1 complex and *in vitro* assays have revealed the absence of an NAD(P)H binding domain, which makes it dependent on using Fd as a substrate (Johnson, 2011; Yamamoto et al., 2011; Schuller et al., 2019). Moreover, like mitochondrial and bacterial complexes, chloroplast NDH-1 is capable of pumping additional protons per electron transferred (Strand et al., 2017). While both CET pathways contribute towards optimal photosynthetic performance, studies conducted on NDH-deficient mutants showed that, although conserved in plants, the NDH route only plays an important role during low light intensities (Yamori et al., 2015; Yamori and Shikanai, 2016). Moreover, reports from studies on rice (Yamori et al., 2011) and *Marchantia polymorpha* (Ueda et al., 2012) have shown that at low light intensities NDH deficient mutants show mutant phenotypes, which shows that chloroplast NDH acts as a safety valve and may contribute to redox homeostasis under low light intensities (Shikanai, 2014).

1.4.1.2. PGR5/PGRL1 dependent pathway

The second CET route i.e. the PGR5/PGRL1-dependent pathway remains more elusive. This pathway is antimycin-A (AA) sensitive and may be engaged by two molecular actors named as proton gradient regulation 5 (PGR5) and pgr5 like-1 (PGRL1) (Takahashi, 2022). PGR5 is a small thylakoid membrane protein with no redox cofactors and was discovered in *Arabidopsis thaliana,* while screening for mutants that exhibit distinctly low steady state qE (a major contributor to NPQ) (Munekage et al., 2002). Furthermore, under high light intensities, PGR5-deficient mutants exhibit a drop in the ratio of oxidized P700 to the total P700, thus limiting the electron flow at the PSI acceptor side (Munekage et al., 2002; Johnson et al., 2014; Zhou et al. 2022). Although a plethora of studies has already shown the involvement of PGR5 in regulating CET, still there is no clear evidence regarding the direct role of PGR5 in mediating CET. The PGR5 pathway through which electrons from Fd is thought to reduce PQ is still uncertain. Specifically, it's not fully elucidated whether Fd directly reduces PQ via PGR5/PGRL1, or it does so via interaction with Cyt b_6f. Moreover, PGR5 is tethered to its binding partner PGRL1 and forms a hetero dimer (DalCorso et al., 2008). Based on *in vitro* evidence, PGRLI was thought to facilitate the transfer of electrons from Fd to quinones thus supporting PGR5/PGRL1 as the prime complex for ferredoxin: plastoquinone oxidoreductase (FQR) (Hertle et al., 2013). However, later on, the idea suggesting a role of PGRL1 in driving CET was invalidated by Rühle and colleagues (2021). They proposed that PGRL1 plays a role in stabilizing PGR5 and shields it from degradation by PGRL1 homolog PGRL2. Moreover, Cyt b_6f complex potentially in collaboration with FNR has been suggested as an alternative FQR. However, to date no FNR-Cyt b_6f-PGR5 complex possessing the requisited FQR activity has been isolated (Joliot et al., 2004; Joliot and Johnson, 2011). PGR5 mutants from cyanobacteria did not show any evidence for PGR5 involvement in CET (Yeremenko et al., 2005; Margulis et al., 2020).

The absence of compelling evidence for sustained CET through two routes strongly implies the presence of an alternative pathway that involves the direct reduction of PQ by Cyt b_6f (Nawrocki et al., 2019). According to a proposed regulatory model in plants (Joliot and Johnson, 2011), docking of FNR to Cyt b_6f directly transfers electrons from Fd to cyt b_6f hemes (*ci* and b_H that are facing the stroma). The positioning of FNR is considered as an important factor and could control the balance between CET and LET. The proposed model somehow resembles the

classical Q-cycle (Mitchell, 1975), as the putative binding of Fd to stromal side of Cyt *b6f* suggests a very short edge to edge distance between its iron sulfur clusters and PQ or hemes at the Qi binding site, which ultimately allows an efficient electron transfer (Page et al., 1999). Moreover, Buchert and colleagues (2022) have put forward evidence, suggesting PGR5 as a mediator of Q-cycle at Cyt *b6f*. A recent cryo-EM structure of Cyt *b6f* suggests that a thylakoid soluble phosphoprotein (TSP9) could have a role in CET, which comes from the fact that it binds to a site, where the potential electron donor protein (Fd) is thought to interact with Cyt *b6f* (Sarewicz et al., 2023).

1.4.1.3. Photosynthetic control and redox regulation of CET

Different players involved in the regulation of CET have already been discussed briefly in the above sections. It has been proposed that CET is also involved in photoprotection. It is capable of decelerating PSII turnover through qE, thereby mitigating the absorption of excessive light energy. However, it also works the other way, where it is linked to photoprotection of PSI. This connection arises from the decrease in lumenal pH, which modulates the proton release during quinol oxidation at the Qo site of *b6f* complex. This step subsequently reduces the turnover rate of Cyt *b6f* complex and leads to PSI special pair oxidation. Under circumstances, when the PSI acceptor side is limited, CET contributes in preventing charge recombination within PSI, thus accumulating $P700^{+}$ which prevents the formation of triplet P700 ($^{3}P700$) and singlet oxygen. The slowing down of electron flow via the pH dependent modulation of *b6f* complex is called "photosynthetic control" (Fig 6), that creates a negative feedback loop ensuring the safety of photosynthetic machinery from potential damage (Tikhonov, 2013).

Thioredoxin (Trx) systems plays a very important role in the redox regulation of photosynthetic electron flow (Courteille et al., 2013; Nikkanen and Rintamäki, 2019). According to Wolf et al 2020, PGR5 is regulated in a redox dependent manner. Moreover, Okegawa and Motohashi (2020) recently proposed a model demonstrating the interaction of Trxm-4 (m type thioredoxins) with PGRL1 via its cysteine residues. Heterodimer formation of Trxm-4 with PGRL1 negatively regulates PGR5 under a steady state, which prevents the overstimulation of PGR5 pathway that could trigger the growth retardation (Okegawa et al., 2007). Moreover, Trx-

m4 dependent redox regulation is considered crucial for the redistribution of reductants towards both CO_2 assimilation and Trxs systems in terrestrial plants, which would otherwise hyperaccumulate in the downstream of PSI (Okegawa and Motohashi, 2020).

1.4.2. Pseudocyclic electron transport

Beyond the electron transport processes involved in $NADP^+$ reduction and driving of CET around PSI, the photosynthetic electron transport chain facilitates other redox reactions, notably involving molecular oxygen (O_2) which plays a pivotal role to photosynthetic function. Early studies showing the inhibitory effects of O_2 on CO_2 assimilation identified its role both as a product and electron acceptor and showed its significance in photosynthesis (Radmer and Kok, 1976). As an electron sink, O_2 can readily accept electrons from compounds with negative redox potential like PSI cofactors: phylloquinone, Fe-S clusters or most probably Fd and NADPH (Mehler, 1951) Under unfavorable environmental conditions that limit the rate of CBB cycle, excess electrons from PSII and PSI are photochemically quenched through a number of O_2 reducing pathways that are collectively referred to as pseudocyclic electron transport (PCET). PCET is also known as "water-water cycle", and unlike CET, here the electrons generated from H_2O at the oxygen evolving complex of PSII are used to reduce O_2 to H_2O via different enzymes and the only productive output of this reaction is the buildup of proton gradient and therefore ATP (Asada, 2000; Leister, 2020). Several O_2 reducing pathways associated with PCET (Fig 6) have been identified: "true" Mehler reaction (Asada, 2000), flavodiiron (FLV) mediated "Mehler reaction" (Shimakawa, 2023) and plastoquinone terminal oxidase (PTOX) mediated O_2 reduction (Nawrocki et al., 2019b).

1.4.2.1. Mehler reaction

The univalent photoreduction of O_2 to superoxide anion radical ($O_2^{\bullet-}$) in the photosynthetic machinery was early detected in 1950s by Mehler (Mehler, 1951) and termed as the "Mehler reaction". It is present in all photosynthetic organisms, spanning from cyanobacteria to angiosperms. To the best of our knowledge, PSI acceptor side, containing the low potential

electron carriers, (phylloquinone or the Fe-S cluster: F_AF_B and Fd) are suggested to be the most dominant source of electrons for $O_2^{\bullet-}$ production (Kozuleva et al., 2021; Krieger-Liszkay and Shimakawa, 2022). The superoxide ($O_2^{\bullet-}$) produced during the first step of Mehler reaction is itself not highly reactive. However, it dismutates to H_2O_2 in the presence of a transition metal ion like Fe(II) and generates the very reactive hydroxyl radical (OH•), which can cause potential photooxidative damage to photosystems that subsequently is a big harm to plant growth and development (Badger et al., 2000). However, antioxidant system of chloroplast helps in mitigating the negative impact of ROS production (Noctor and Foyer, 1998) by dismutating $O_2^{\bullet-}$ into hydrogen peroxide (H_2O_2) and into O_2 and H_2O in a reaction catalyzed by superoxide dismutase and ascorbate peroxidase (Tikhonov, 2023). Moreover, another site of $O_2^{\bullet-}$ reduction by the PQ pool is also known (Borisova-Mubarakshina et al., 2019). The precise quantification of Mehler´s reaction contribution in ROS production always remains ambiguous. Some studies suggests that it contributes ~10% of the maximal electron flow, however some debated that electron flow to O_2 accounts for almost 40% of total electron donation from PSII (Asada, 1999; Ivanov et al., 2014). Nevertheless, the Mehler reaction is a passive process: while not actively regulated, it still serves in maintaining the cellular balance against the oxidative stress. Its physiological significance is proven under certain stress conditions like drought and limited CO_2 availability (Ort and Baker, 2002). Moreover, growth photoperiod also influences the balance between LET and Mehler reaction in tobacco and *Arabidopsis* (Michelet and Krieger-Liszkay, 2012). Our paper (Hani et al., 2024) further shed light on the role of thioredoxins in regulating the Mehler reaction in response to growth photoperiod (See Article 3).

In comparison with the Mehler reaction, FLV-PCET represents an electron sink (shown in Fig 6) and safely reduces O_2 into H_2O using NADPH in chloroplast stroma, hence averting a possible emission of ROS. This electron sink has been lost in angiosperms during evolution (Shimakawa et al., 2017). Moreover, FLV mediated O_2 reduction is considered crucial in coping with fluctuating light intensities and CO_2 scarcity (Allahverdiyeva et al., 2011; Shimakawa et al., 2015).

1.4.2.2. PTOX

The Plastid terminal oxidase (PTOX), similar to the alternative oxidase (AOX) of mitochondria, catalyzes the PQH_2 oxidation coupled with reduction of O_2 to H_2O in the chloroplast (Laureau et al., 2013; Nawrocki et al., 2015). Two PTOX isoforms are known from studies in *Chlamydomonas* (Houille-Vernes et al., 2011), while angiosperms contains one PTOX isoform. Its PQH_2 oxidase activity has an important role in regulating the PQ pool redox state (Wang and Fu., 2016). PTOX has been shown to be important in carotenoid metabolism (Carol et al., 1999, Cazzonelli and Pogson., 2010). Carotenoids have an important role in photosynthesis, both in terms of their participation in energy dissipation (qE) and as an important constituent of PSII (where β-carotene serves as an important component of reaction centers). Plant carotenoid desaturase relies on PQ as an electron acceptor, and PTOX is needed to reoxidize PQH_2 (Carol and Kuntz, 2001; Houille-Vernes et al., 2011). Besides that, it has been suggested as a redox sensor in etioplasts (Kambakam et al., 2016). It also engages in chlororespiration and could be important for setting the redox poise for CET (Messant et al., 2021). PTOX serves as a safety valve, preventing photooxidative damage. Overexpression of PTOX1 in *Chlamydomonas* increased photoinhibition (Heyno et al., 2009; Ahmad et al., 2020) but behaved opposite in *Arabidopsis* (Rosso et al., 2006). This difference may stem from varying regulation between algal and plant-type PTOX isoforms. In our study (Messant et al., 2023), we have shed light on the new role of PTOX, both as an anti-oxidant and pro-oxidant. Most importantly, we argue against its protective function against PSII photoinhibition by showing that PTOX protects PSI under high light stress (See appendix for article 4).

1.5. Redox regulation of photosynthetic electron transport

Photosynthesis is a highly redox regulated metabolic process which is continuously exposed to fluctuating input factors, such as light intensity. One of the inevitable consequences of excited chlorophylls and electron transfer reactions throughout oxygenic photosynthesis is the production of reactive oxygen species (ROS). These include superoxide anion radical ($O_2^{\bullet-}$), hydrogen peroxide (H_2O_2), hydroxyl radical (OH•), and singlet oxygen ($^1O_2$). $O_2^{\bullet-}$ and H_2O_2 are

mainly produced at PSI (Mehler reaction already detailed above) (Asada et al., 1974), whereas site of $^1O_2$ production is mainly PSII (Telfer et al., 1994; Krieger-Liszkay, 2005). Under saturating light intensities or when the PQ pool is over reduced, triplet state chlorophyll (^{3}Chl*) reacts with ground state molecular oxygen ($^3O_2$) and generates $^1O_2$ (Dietz et al., 2016; Krieger-Liszkay, 2005). The ^{3}Chl* is produced either from singlet excited chlorophyll (^{1}Chl*) or by charge recombination of the primary radical pair ($P_{680}^{\bullet+}Pheo^{\bullet-}$) in PSII antenna complex by intersystem crossing or in the PSII reaction center, respectively. There is an increased probability of $^1O_2$ production when the forward electron transport is blocked, meaning the quinone acceptors of PSII are over reduced (Krieger-Liszkay and Shimakawa, 2022). In the antennae $^1O_2$ can be best quenched by nearby carotenoids and tocopherol (Nowicka et al., 2021).

In the case of limited number of electron acceptors, O_2 is reduced to $O_2^{\bullet-}$. The later then dismutates either spontaneously or in the presence of superoxide dismutase (SOD) to H_2O_2 and O_2 . Further, H_2O_2 in the presence of reduced transition metals like Fe^{+2} or Cu^{+2} can give rise to OH•; in a reaction best known as the Fenton reaction (See the equations below) (Michelet and Krieger-Liszkay, 2012). OH• radicals are very reactive and the damaging effects of OH• must be prevented through the action of antioxidant enzymes (catalase, ascorbate peroxidase (APX) and SOD) that detoxify its precursors $O_2^{\bullet-}$.and H_2O_2 .

$$O_2 + 1e^- \rightarrow O_2^{\bullet-}$$

$$2\ O_2^{\bullet-} + 2\ H^+ \rightarrow H_2O_2 + O_2 \quad \textbf{($O_2^{\bullet-}$ dismutation)}$$

$$Fe^{2+} + H_2O_2 \rightarrow Fe^{3+} + OH\bullet + OH^- \textbf{ (Fenton reaction)}$$

ROS is like a double edged sword: on one hand it can cause severe damage to the cellular components (Nawrocki et al., 2021), but on the other hand it participates in redox signaling and help plants to adapt to different metabolic and environmental triggers (Mittler et al., 2022). Plants have plenty of photoprotective (e.g. NPQ) and multilayered defense/regulatory mechanisms for maintaining ROS balance in the photosynthetic electron transport chain. These processes are contributing towards delicate equilibrium between photoprotection and photosynthetic efficiency. However, to achieve resilient and robust photosynthesis, one needs "fine-tuning" mechanisms, that will ultimately help in maintaining energy balance under

fluctuating environmental conditions like light quality and availability. One such approach is "thiol-disulphide" redox regulations that are mediated by a complex network of redox-regulated enzymes. I will detail here the mechanisms/pathways involved in maintaining the redox regulation at the stromal and lumenal side of the thylakoid membrane.

1.5.1. Thioredoxin-dependent redox regulation in plant chloroplasts

One of the widely known universal regulatory mechanism found in all type of living organism is dithiol-disulfide exchange, that largely relies on reductase activity of thioredoxins (Trxs) (Meyer et al., 2012). Trxs are ubiquitous proteins, widely found in bacteria, yeast, animals and plants. They exists as a small group of multifunctional acidic proteins, with a molecular weight of 12-14 kDa (Richter et al., 2018). Essentially, all the Trxs contains a highly conserved active site with the amino acid consensus sequence (WCGPC), that is involved in thiol-disulphide exchange reactions and hence participates in maintaining the redox homeostasis (Couturier et al., 2013; Geigenberger et al., 2017). Interestingly, only a few Trx encoding genes have been found in heterotrophic organisms, despite the large number of redox regulated proteins. However, photosynthetic organisms, most noticeably *Arabidopsis thaliana,* encode 20 Trx isoforms and based on sequence similarities they are classified into seven subgroups (f, h, m, o, x, y, z). Their distribution varies significantly across the subcellular compartment; Trx h is prevalent in the nucleus, endoplasmic reticulum, cytoplasm and mitochondria, Trx o is exclusive to mitochondria (Meyer et al., 2012), whereas the other five types of Trx (f, m, x, y, and z) prevail in the chloroplast (Ojeda et al., 2017; Kang et al., 2019) and exist as different isomers (Trx m1-4, Trx f1-2, Trx y1-2, Trx x and z) (Yoshida and Hisabori, 2017). Trx m is the most abundant Trx and makes upto 70% of total chloroplast Trxs. The chloroplast harbors two distinct thiol reduction systems; a Ferredoxin-dependent thioredoxin system (FTR-Trx system) and a NADPH-dependent thioredoxin reductase system (NTRC). These two systems make a significant contribution in stromal redox regulation and possess different electron donors (Fd and NADPH), but still hold some degree of redundancy regarding their target proteins (Nikkanen et al., 2017). I will briefly explain the two systems and how they interact with each other.

1.5.1.1. FTR/Trx system

The FTR-Trx system is primarily active in the light and driven by transferring electrons from PSI to Fd and then to ferredoxin thioredoxin reductase (FTR) (Schürmann and Buchanan, 2008). FTR is a heterodimeric iron sulfur protein with a variable and a conserved catalytic subunit. Mutant lines from *A.thaliana* showed that the FTR catalytic subunit harbors a redox active disulphide (Keryer et al., 2004), which finally reduces Trx thiol groups by transferring electrons from Fd to Trx (Fig 7A), thus acting as the primary reductant for free Trx (Yoshida and Hisabori, 2016). Later, reduced Trxs act on the stromal target proteins, modulating their function through strict light responsive regulation over both assimilatory and dissimilatory pathways (Thormählen et al., 2017).

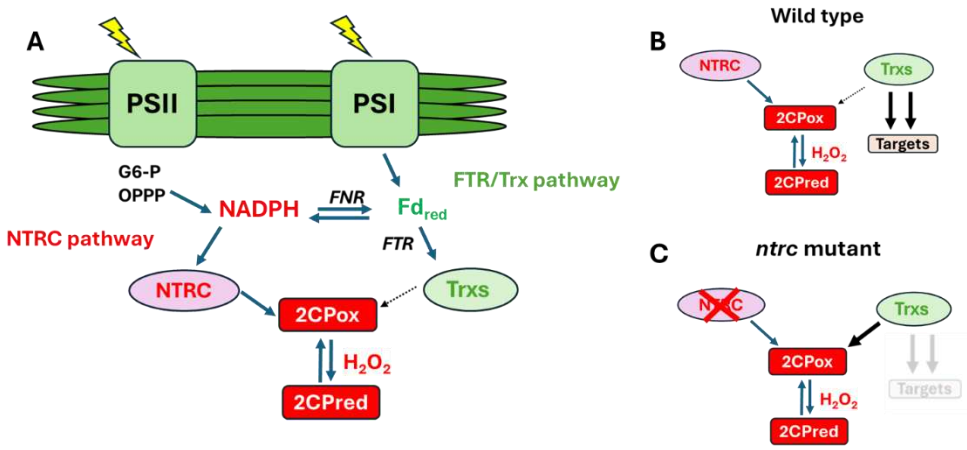

Figure 7: Scheme of redox regulation in stroma via the thioredoxin system: Two thioredoxin systems: FTR/Trx (in green) and NTRC (in red) are shown here. Light-driven reactions in photosynthetic electron transport chain reduces ferredoxin (Fd_{red}) and NADPH via the ferredoxin $NADP^+$ reductase (FNR). NADPH is also produced by sugars from the oxidative pentose phosphate pathway (OPPP). Fd_{red} feeds the reducing equivalents to plastid thioredoxins (Trxs) via ferredoxin thioredoxin reductase (FRT), whereas NTRC uses the reducing equivalents from NADPH for an efficient reduction of 2-Cys Prx (2CP) and supporting their hydrogen peroxide (H_2O_2) scavenging activity. 2CP can also be reduced by Trxs but less efficiently (dotted arrow). **(A).** Chloroplasts from the wild type plant allows efficient reduction of 2CP via NTRC, thus maintaining the redox state of these enzymes. Consequently, the redox state of Trxs is appropriate for the redox regulation of target proteins **(B)**. However, absence of NTRC leads to

overaccumulation of 2CP in its oxidized form, thereby draining the reducing equivalents from the pools of Trxs and impacting the redox regulation of targets downstream of Trxs **(C).** *Inspired scheme and modified legend from Cejudo et al., 2019; Pérez-Ruiz., 2017.*

The FTR-Trx system is responsible for the activation of enzymes of carbon assimilation reactions including sedoheptulose-1,7 bisphosphatase (SBPase), fructose-1,6-bisphosphatase (FBPase), glyceraldehyde-3-phosphate dehydrogenase (GAPDH) and phosphoribulokinase (PRK). Moreover, they also regulate the malate-oxaloacetate shuttle and some steps of starch and chlorophyll biosynthesis (Foyer, 2018). Based on *in vitro* studies, Trx m and f are involved in activating fructose-1,6-bisphosphatase (FBPase), NADP-malate dehydrogenase (MDH) and chloroplast ATP synthase (Sekiguchi et al., 2020). They are also involved in the regulation of other stromal enzymes associated with CBB cycle and starch synthesis (Yoshida et al., 2015). Moreover, *in vivo* studies showed that Trxm-4 has a role in CET, as it negatively regulates the PGR5-dependent electron flow (Courteille et al., 2013). Trx m1 and m2 mutants from *A.thaliana* revealed no growth phenotype (Laugier et al., 2013; Okegawa and Motohashi, 2015). However, when silenced together with Trxm-4, a pale green phenotype was observed which suggests the role of m-type Trxs in PSII biogenesis (Wang et al., 2013).

1.5.1.2. The NTRC system

In addition to FTR/Fd/Trx system, another chloroplast thiol regulatory system; NADPH-dependent thioredoxin reductase C (NTRC) was identified exclusively in oxygenic organisms mainly plants and algae. NTRC in *A.thaliana* is encoded by a single nuclear gene and functions as a bimodular enzyme containing both the NTR and Trx domain at its N and C-terminus, respectively, and that is why it is called NTRC (Serrato et al., 2004). The function of NTRC is considered complementary to the Fd/Trx system under day light conditions when the levels of reduced Fd are high. However, during the dark it becomes a prominent pathway for redox homeostasis, thus allowing the use of reducing powers of NADPH generated from oxidative pentose phosphate pathway (OPPP) (Cejudo et al., 2012). During dark or low light conditions, NTRC is a prominent pathway for chloroplast redox homeostasis by regulating starch

biosynthesis via OPPP pathway, independent of the FTR/Trx system (Eliyahu et al., 2015). Moreover, NTRC is also capable of reducing its own Trx domain (Wulff et al., 2011).

As shown in Fig 7A and based on biochemical and genetic studies, NTRC is considered as the major and most efficient reductant of 2-cysteine-peroxiredoxin (2-Cys Prx) in chloroplasts and interacts with it via its Trx domain (Bernal-Bayard et al., 2012). Typical 2-Cys-Prxs are homodimeric thiol-based peroxidases containing sulfhydryl groups, that are known for their H_2O_2 scavenging activity (Lee et al., 2018). In addition to the FTR system, NTRC was also found to be involved in regulating CBB cycle in response to varying light conditions (Thormählen et al., 2013). Moreover, a severe growth phenotype under short day conditions for NTRC mutant shows its importance under different growth photoperiods (Lepistö et al., 2009). Furthermore, an increased dissipation of light energy by NTRC deficient mutants under high light, shows their importance in controlling NPQ and thus photosynthetic electron transport (Naranjo et al., 2016). More recently, an increase in PSI oxidation was observed in *Arabidopsis* overexpressing NTRC (Nikkanen et al., 2019). These studies suggests an important role of NTRC in plant acclimation to fluctuating environment.

1.5.1.3. Cross talk between FTR/Trx and NTRC system

The identification of two redox pathways in chloroplasts raises the question of the functional relationship between these two pathways. Lately, extensive research employing reverse genetic approaches in *A. thaliana* has greatly expanded our understanding of this subject. It has been suggested that these two redox systems acts concertedly by sharing common targets (Cejudo et al., 2021). This issue was further addressed by the analysis of *Arabidopsis* mutants deficient in both pathways (Thormählen et al., 2015). Lack of NTRC and Trx f mutants (*ntrc-trxf1f2*) showed severe growth inhibition thus indicating these mutants were impaired in successful utilization of light energy (Ojeda et al., 2017). Similarly, the simultaneous deficiency of *ntrc-trxx*, unlike *trxx* (Paulido et al., 2010), had a dramatic effect on plant growth. Overall, these double mutants impacted the redox regulation of enzymes from CBB cycle (Ojeda et al., 2017). Moreover, Yoshida and Hisabori (2016) showed that the *ntrc-ftr* mutant is lethal, however overexpressing the mutated NTRC with inactivated Trx or NTR domain in *ntrc* background partially restored the

ntrc phenotype, suggesting communication between the two systems (Toivola et al., 2013). Bimolecular fluorescence complementation (BiFC) assays have shown that NTRC is capable of interacting *in vivo* with soluble Trxs and can also transfer the reducing equivalents to Trxf in vivo (Nikkanen et al., 2016).

The important issue in chloroplast biology is to establish the link between these two systems. Recent studies have shown the pleiotropic effects exerted by NTRC on variety of chloroplast regulated processes, indicating the role of 2-Cys Prx as a link between the two systems. *A.thaliana* plants devoid of NTRC recovered a growth phenotype like wild type with decreased levels of 2-Cys Prx. However, overexpressed 2-Cys Prx with no significant effect on wild type plant provoked a growth inhibition phenotype in *ntrc* mutant background, thus showing the dependence of *ntrc* phenotype on 2-Cys Prx levels (Pérez-Ruiz et al., 2017). These findings led to the proposal that NTRC plays an important role in upholding the redox equilibrium of 2-Cys Prx. Besides NTRC which is the main reducer of 2-Cys Prx in the dark, some chloroplast Trxs e.g ACTHI (Atypical Cysteine Histidine rich Trx1) are also capable of transferring reducing equivalents to 2-Cys Prx (Dangoor et al., 2012). Based on these findings, it is hypothesized that in wild type plants (Fig 7B), the redox status of 2-Cys Prx is under the control of NTRC which ultimately avoids the drainage of reducing equivalents from Trxs pool, thus keeping the downstream targets reduced. On the contrary, absence of NTRC (Fig 7C) causes impairment of the Trx dependent redox regulation, by keeping the levels of oxidized 2-Cys Prx high (Cejudo et al., 2021). Despite a lot of studies showing the interaction of NTRC with different chloroplast enzymes, there still remains an open question (that needs to be addressed) about the direct involvement of NTRC in regulating specific enzymes.

1.5.1.4. Connecting thiol regulation across thylakoid membrane

The importance of redox regulation in the thylakoid lumen cannot be overlooked by the fact that almost 40% of proteins in the thylakoid lumen are capable of disulfide formation, which in turn is regulated by redox signaling, making them indispensable for the protection and assembly of photosystem and the electron transport chain (ETC). Moreover, they also play an important role in protein translocation and folding (Kang and Wang, 2016). Recent studies have helped us

understand the role of thiol regulatory pathways in communicating the stromal and lumenal side of the chloroplast (Karamoko et al., 2013; Wu et al., 2021). Certain thiol modulated enzymes (Hall et al., 2010) are known to be involved in transporting the reducing equivalents across the thylakoid membrane (Brooks et al., 2013). However, unlike in the stroma, no Trx or Trx like soluble electron carriers have been yet identified in the thylakoid lumen (Motohashi and Hisabori, 2006; Buchanan, 2016). But it has been suggested that reduced Trx-m transfers reducing power into the thylakoid lumen via a "reducing equivalent transfer system". This system is comprised of CCDA (transmembrane transporter protein), HCF164 (membrane-anchored lumenal protein) and some other potential candidates (Karamoko et al., 2013).

1.5.2. HCF164 and CCDA transfers reducing equivalents from stroma to lumen

HCF164 was first identified by Meurer and colleagues, when they noticed a high chlorophyll fluorescence phenotype in a mutated plant (Meurer et al., 1996). The mutant was later found to be defective in Cyt b_6f assembly, thus suggesting a role of HCF164 in the maturation and assembly of Cyt b_6f (Lennartz et al., 2001). It is a membrane anchored lumenal protein that contains a Trx like domain with disulphide reductase activity. It has been suggested that Trxm-4, as an electron donor can reduce HCF164 and hence facilitates the transfer of the reducing power to its catalytic domain at the lumenal side. Moreover, Cytf, Rieske FeS center and PSI-N are the potential targets of HCF164 (Motohashi and Hisabori, 2006). Later, Motohashi and Hisabori (2010) proposed that chloroplasts must possess another system for transferring the reducing equivalents from stroma into the lumen, because the Cys residues of HCF164 resides close to the lumenal side and not towards stroma. They identified CCDA as a strong candidate for this purpose. CCDA is a prokaryotic homolog of thiol-disulphide transporters (Page et al., 2004) and it exists as a polytopic thylakoid membrane protein with six transmembrane regions in *A. thaliana.* Moreover, it contains two Cys residues embedded within the membrane, and it has been shown that its redox state is mediated by m-type Trxs. A similar phenotype like *hcf164* was also observed for some *ccda* mutants, indicating that CCDA is indispensable for Cyt b_6f assembly (Motohashi and Hisabori, 2010; reviewed in Hoh et al., 2023). Taken together, these findings suggest a redox control pathway across the thylakoid membrane where the reducing

equivalents are transferred from Trxm-4 (in the stroma) to the CCDA carrier, and then to HCF164 (in the lumen) which finally delivers them to lumenal target proteins (Fig 8).

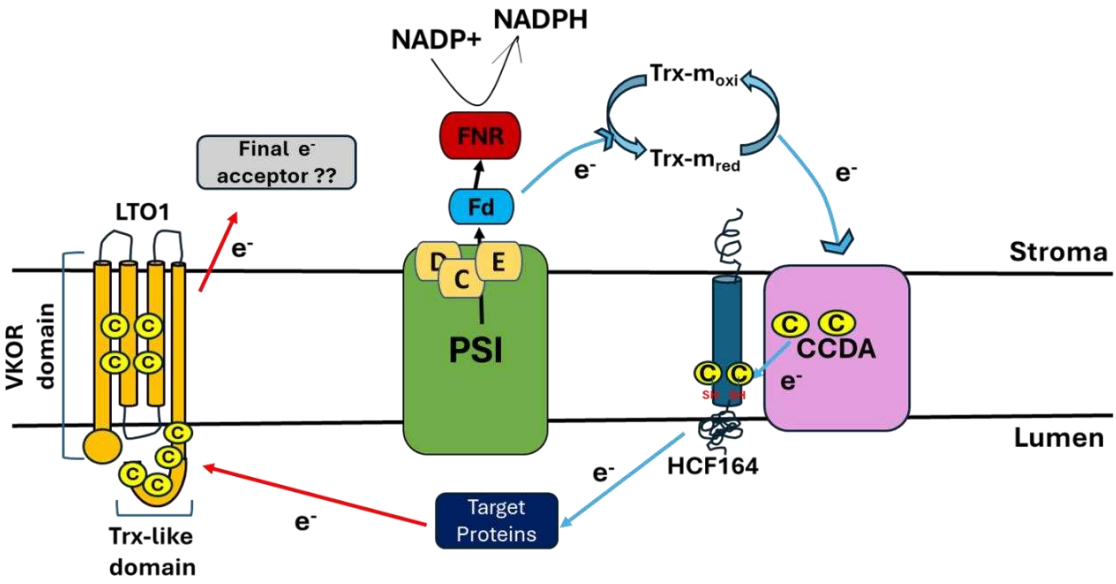

Figure 8: Hypothetical model for the redox regulation in the thylakoid lumen: Reducing equivalents are transferred from stroma to the lumen via Trxm, which acts as an electron donor for thylakoid lumen proteins. Trxm transfers electrons through CCDA and HCF164 which further conveys electrons to redox regulated target proteins in the lumen. LTO1 is an oxidoreductase, which finally oxidizes the redox regulated proteins. However, the final electron acceptor to LTO1 is unknown. Blue arrows for reduction and red for oxidation. Yellow circles indicate redox active cysteine residues. *Modified scheme and inspired legend from Hoh et al., 2023.*

1.5.3. Role of LTO1 and Cyt *c*$_6$*a* as potential candidates in redox regulatory pathway

In addition to the candidates explained above, LTO1 (Lumen thiol oxidoreductase 1) was proposed as lumen localized oxidoreductase that contain two domains: a VKOR domain and a Trx-like domain at its C-terminus, that is exposed to the thylakoid lumen. Lumenal proteins like

PsbO and STN7 are the potential targets of LTO1 (Lu et al., 2014; Wu et al., 2021). It has been proposed that maybe phylloquinone is the electron acceptor of LTO1 mediated disulphide formation pathway (Furt et al., 2010). However, to date, no final acceptor of LTO1 has been identified (Fig 8). Another potential oxidant that could function as electron acceptor in the lumen is Cyt c_6a. It holds some similarity with Cyt c_6 which can replace plastocyanin as electron donor to PSI in cyanobacteria and algae. The biological function of Cyt c_6a is unknown. Because of its relatively positive redox potential (+140 mV), it is unable to transfer electrons to PSI (Marcaida et al., 2006). But it has been suggested to act like a funnel for facilitating thiol oxidation in thylakoid lumen (Schlarb-Ridley et al., 2006).

However, many proposed pathways in lumenal redox regulation still remain hypothetical. In our study (Hani et al., 2024), we tried to answer some of these unresolved questions (see Article 3).

1.6. KLAS NIR: a tool for studying the in vivo redox changes in P700, PC and Fd in real time

Progress in our knowledge regarding photosynthetic mechanisms in living organisms relies largely on non-destructive techniques like pulse amplitude modulation (PAM) spectroscopic techniques. It emerged initially as a powerful tool for measuring the Chl fluorescence in PSII driven reactions, but shortly afterwards it expanded its utility for measuring transmittance changes in the near-infrared (NIR) spectral region for studying P700 redox changes in PSI (Harbinson and Woodward, 1987; Schreiber et al., 1988). Since then, it was widely used as non-intrusive tool for assessment of PSI quantum yield (YI) and the reactions at its donor and acceptor side. Many studies (Harbinson and Hedley, 1993; Klughammer and Schreiber, 1998; Oja et al., 2003) employed this technique for studying "P700" changes with commercially available devices, generating enormous amount of information on ETC, but still were unable to differentiate between P700, PC and Fd redox changes. The overlapping spectra of light-induced redox changes in P700, PC and Fd makes it relatively challenging to measure redox difference spectra of these electron carriers in an intact leaf.

However, Klughammer and Schreiber recently reported a new type of PAM-based measuring system. The new system "Dual-KLAS-NIR" (Kinetic LED array spectrophotometer) combines basic feature of KLAS-100 and Dual-PAM-100. In comparison to the Dual-PAM-100 that measures at two wavelengths, KLAS-NIR is capable of simultaneously measuring four dual wavelength difference signal (785–840, 795–970, 810–870 and 870–970 nm), which carry sufficient information for the routine deconvolution of P700, PC and Fd in real time (Schreiber and Klughammer, 2016). Moreover, it can also measure Chl fluorescence yield with both 635 and 440 nm excitation. To directly compare fluorescence changes with redox changes in PSI (P700, PC, Fd), it employs the same photodiode detector for both fluorescence and NIR transmittance measurements (Schreiber, 2017). According to Klughammer and Schreiber (2016), KLAS-NIR measuring system offers three major streams of novel information.

1- It is an excellent tool for studying the *redox state of P700 and PSI quantum yield,* as it allows the real time detection of $P700^+$, thus eliminating the assumptions about the extinction coefficients and redox equilibrium between P700 and PC. It also ensures precise analysis of $P700^+$ for thorough study of post-illumination re-reduction kinetics, which is vital for the estimation of CET around PSI. Moreover, reliable deconvolution exposes substantial variations in light responses of P700 and PC, which aligns well with the notably higher oxidation potential of P700.

2- It also offers an online deconvolution for the *redox state of PC.* Many *in vitro* studies have already shown the redox equilibrium between PC and P700, however very little is known about in vivo reactions. Schöttler and Toth (2014) recently emphasized that the photosynthetic apparatus adapts dynamically to a multitude of environmental factors, thus shaping the capacity of photosynthetic electron flow. They also demonstrated large changes in PC/P700 in comparison to photosynthetic capacity (Schöttler et al., 2004). With all these details, KLAS NIR can serve as an important tool in routine deconvolution of PC/P700, which may serve as a "proxy" for an estimate of relative differences in photosynthetic capacity.

3- Deconvoluted *redox changes in Fd* are important in terms of providing information about the secondary reactions at the PSI acceptor side. Moreover, binding of Fd to the stromal enzymes via different electron transfer reactions is a current topic of interest (Hanke and Mulo, 2013). With KLAS-NIR, Fd redox state can be studied in vivo by utilizing re-reduction kinetics approach as a function of different parameters that may modulate the activity of Fd-dependent pathways (Sétif et al., 2020).

1.7. *Marchantia polymorpha*: an emerging model plant

The emergence of land plants around 470 million years ago was one of the major evolutionary milestones in the history of green plants (Bowman et al., 2016b), and *Marchantia polymorpha* is considered as the first land colonizing plants (Bowman et al., 2017). In comparison with vascular plants, bryophytes are primitive small living organisms that includes non-vascular liverworts, mosses and hornworts (Mishler and Churchil, 1984). *Marchantia,* as a liverwort stands as a complex thalloid network with distinct dorsal-ventral structure; that is further characterized by the presence of air chambers and rhizoids (Bowman, 2022). The dorsal side of the vegetative thallus produces specialized cup shaped organs named “gemma cups”, which in turn leads to the production of “gemmae”. The ubiquity and its emergence as a “model plant” is primarily based on its short-life cycle, ease of propagation and its genomic attributes (Kato et al., 2020; Bowman, 2022).

Concerning the evolutionary aspect of photosynthesis in *Marchantia*, different studies highlighted the changes at the level of chloroplast (Zaitsev et al., 1998), chlorophyll biosynthetic pathways (Ueda et al., 2014) and supercomplexes (Harrer, 2003) in comparison with cyanobacteria and vascular plants. Moreover, Shimakawa and colleagues (2021) have shown the importance of flavodiiron proteins (absent in angiosperms) as an intermediate strategy in *Marchantia* that helps to keep the P700 oxidized and protects it thereby against photodamage. Besides that, this liverwort has bioaccumulator capacities (Samecka-Cymerman et al., 1997; Sharma, 2007) and has been widely used in research for understanding the impact of heavy metal stress like Cd, Cu, Pb and Zn on the physiological responses (lipid content, ROS, chlorophyll

content and growth). The morphology of thalli makes sure that ventral part and hyaline parenchyma of the plant is in direct contact with substrate, allowing the efficient uptake of metals thus bypassing a root system like in angiosperms (Ares et al., 2018).

1.8. Manganese as a tool for studying photosynthesis

Manganese (Mn) is one of the essential trace elements for plant growth and development. Photosynthetic organisms require Mn since it is the essential co-factor of the oxygen evolving complex (OEC) in PSII. The tetra-Mn cluster Mn_4O_5Ca drives the water splitting reaction at PSII by splitting two water molecules into electrons, protons and molecular oxygen (Ono et al., 1992; Bricker et al., 2012). Besides its importance in photosynthesis, Mn is crucial for ROS scavenging, pathogen defense, respiration and hormone signaling. Certain enzymes like Mn superoxide dismutase (MnSOD) and oxalate oxidase exclusively require Mn for ROS detoxification in mitochondria, peroxisomes and apoplast respectively (Lane, 2002; Corpas et al., 2017).

Moreover, in some enzymes, Mn is interchangeable with certain divalent cations like calcium (Ca), cobalt (Co), copper (Cu), zinc (Zn) and magnesium (Mg). For example, it has been shown that Mn is interchangeable with Mg at the active site of Ribulose-1,5-bisphosphate carboxylase/oxygenase (Rubisco), thus balancing the carboxylase and oxygenase activity of Rubisco by promoting photorespiration when Mn is bound instead of Mg (Bloom and Lancaster, 2018; Bloom, 2019).

To sustain the optimal plant growth, plants need an adequate supply of Mn, which, if not available, could lead to Mn deficiency. The amount of available Mn^{2+} in soil depends on several factors like soil pH, redox potential and soil porosity. As a result, plants grown on alkaline soils are more susceptible to Mn deficiency, thus favoring the oxidation of Mn^{2+} to unavailable MnOx (Mn oxides) (Husted et al., 2009). The exact distribution and prevalence of Mn deficiency is difficult to obtain since Mn deficiency appears as a latent disorder. However, prolonged Mn starvation leads to leaf necrosis indicating the overaccumulation of ROS in chloroplast.

Moreover, Mn deficiency destabilizes the PSII complexes and directly impacts the thylakoid structure (Schmidt et al., 2016).

Keeping in mind the importance of water splitting reaction, it is important to understand the Mn import into the chloroplast and into the thylakoid lumen. Recently, two members of PAM71 family named CMT1 (Chloroplast Manganese Transporter 1), and PAM71 (Photosynthesis Affected Mutant 71) have been shown to have an important role in Mn import into the chloroplast. CMT1 was found to be localized in the inner envelope membrane of the chloroplast. A pale yellow phenotype and difference in the grana stacking were observed in *cmt1*, thus indicting an important role of CMT1 transporter in photosynthesis (Eisenhut et al., 2018; Zhang et al., 2018). Furthermore, PAM71 was shown to be important for Mn import into the thylakoid lumen (Schneider et al., 2016). Further research is required to elucidate the selectivity and transport mechanisms of CMT1 and PAM71. It would also be interesting to investigate the presence of such transporters or their orthologues in *Marchantia polymorpha.*

Despite the importance of Mn in plant growth and development, little is known about its effects on photosynthesis. Using *M. polymorpha,* we have studied the effects of Mn excess and deficiency on PSII (See Article 1). In the current thesis, I further elaborated the effects of Mn deficiency on redox changes in P700 and PC and its possible role in CET (See Article 2).

Aims

The main questions that I asked during my PhD was under which physiological conditions alternative electron transport pathways are important and how their activity is regulated. It is very well known that besides the major electron flux, i.e. "linear electron flow", there are alternative electron fluxes like "cyclic" and "pseudocyclic" electron transport around PSI that come into play under certain physiological conditions. However, the exact mechanisms behind their regulation and interplay among these two systems remain unknown. Redox regulatory cascades have an important role in maintaining the metabolic state of plants. Thioredoxins are one of them and are known to negatively regulate cyclic electron transport, however very little is known about redox regulation of pseudocyclic electron transport. I have tried to establish the link between these two important electron transport pathways by studying in detail photosynthetic electron transport and the possibility of supercomplex formation under manganese deficiency in *Marchantia polymorpha* and by understanding the redox regulation of oxygen reduction at photosystem I acceptor side under different light regimes in *Arabidopsis thaliana.*

I am briefly highlighting two topics as the main aim of my PhD thesis.

1. **Studying the effects of manganese (Mn) deficiency on photosynthetic electron transport in the liverwort *Marchantia polymorpha*.**

- I contributed to a study entitled "Manganese concentration affects chloroplast structure and the photosynthetic apparatus in *Marchantia polymorpha*", where, besides showing in vivo changes in the photosynthetic electron transport, I performed electron microscopy (with the help of the I2BC imaging platform) and compared the images with images obtained by super-resolution microscopy to show changes in the structural organization of thylakoids under Mn deficiency.
- *Marchantia* was grown under Mn deficiency to study in vivo redox changes in P700 and PC using the KLAS NIR spectrophotometer. To better characterize the role of cyclic electron transport (CET) under Mn deficiency, I studied the re-reduction kinetics by specifically using far-red light. Further, I studied the probability of supercomplex

formation under Mn deficiency by performing the blue native (BN) PAGE assay. Moreover, using X-ray fluorescence microscopy, I looked into the Mn distribution in *Marchantia* thalli under Mn deficiency.

2. Redox Regulation of Superoxide Production at Photosystem I in *Arabidopsis thaliana*

- It is known that CET is negatively regulated by thioredoxin m. Since CET and pseudocyclic electron transport are in competition, it was of interest to investigate whether pseudocyclic electron flow also undergoes a redox regulation. A specific redox-mediating protein system embedded in the thylakoid membrane was studied here in plants grown under different photoperiods. The main aim was to show the interaction between Trxm-4 and the thylakoid membrane. Moreover, to investigate if the change in photoperiod alters the properties of electron transport and the amount of ROS generated in the light, indirect-spin-trapping EPR spectroscopy was performed on different redoxin mutants including *ccda* and *cyt* c_6*a* that are proposed as mediator proteins in this study. These mutants were further characterized in vivo using chlorophyll fluorescence.

Chapter 2: Deciphering Manganese homeostasis: Its impact on photosynthesis and metabolism in liverwort *Marchantia polymorpha*.

2.1. Introduction

Manganese (Mn) is considered as an essential trace element for plant growth and development and has a prominent role as an important constituent of the Manganese cluster (also called the oxygen-evolving complex) on the donor side of photosystem II (PSII). Any disturbances in Mn homeostasis can severely disrupt photosynthetic electron transport, specifically affecting PSII, which is the main site of water oxidation. Mn homeostasis and its considerable effects are well studied in *Arabidopsis thaliana*, however very little is known about its impact on the land plant *Marchantia polymorpha*. *Marchantia* is a liverwort and naturally considered as a well-known bio-indicator of heavy metals that can hyperaccumulate certain heavy metals, like lead (Pb), thus making it an ideal model for studying metal stress. The study basically covers the aspects of Mn excess and deficiency on *Marchantia* and its possible effects on photosynthesis and metabolism. This article defines the culture conditions for growing *Marchantia* in both Mn excess and deficiency and a detailed overview is given in context of effects of Mn homeostasis at the plant and organelle (chloroplast) level. Metabolomic analysis showed that excess of Mn seems to target plant metabolism; however, deficiency mainly affects photosynthesis. Moreover, transmission electron microscopy and super-resolution microscopy was employed to study changes in the organization of the thylakoid membrane. Chlorophyll fluorescence measurements and P700 absorption changes were studied using DUAL-PAM. Another important finding of this study is that Mn deficiency may favor cyclic electron transport in *Marchantia polymorpha.*

2.2. Article 1: Manganese concentration affects chloroplast structure and the photosynthetic apparatus in *Marchantia polymorpha* (published)

My contributions in this article includes growing of *Marchantia*, transmission electron microscopy with the help of Claire BOULOGNE (I2BC imaging platform), additional experiments for the paper (Chlorophyll fluorescence measurements (Fig S5), photoinhibition experiments (Fig S4, S6) in the presence and absence of lincomycin). Moreover, I also participated in critical reading of the manuscript.

https://doi.org/10.1093/plphys/kiad052 PLANT PHYSIOLOGY 2023: 192: 356–369

Plant Physiology®

Research Article

Manganese concentration affects chloroplast structure and the photosynthetic apparatus in *Marchantia polymorpha*

Marine Messant,[1] Umama Hani,[1] Thaïs Hennebelle,[1] Florence Guérard,[2] Bertrand Gakière,[2] Andrew Gall,[1] Sébastien Thomine[1] and Anja Krieger-Liszkay[1,*]

1 Institute for Integrative Biology of the Cell (I2BC), CEA, CNRS, Université Paris-Saclay, 91198 Gif-sur-Yvette cedex, France
2 Institute of Plant Sciences Paris-Saclay, CNRS, Université Paris-Sud, Institut National de la Recherche Agronomique, Université d'Evry, Université Paris-Diderot, Université Paris-Saclay, 91405 Orsay Cedex, France

*Author for correspondence: anja.liszkay@i2bc.paris-saclay.fr (A.K.-L.)
The author responsible for distribution of materials integral to the findings presented in this article in accordance with the policy described in the Instructions for Authors (https://academic.oup.com/plphys/pages/General-Instructions) is A.K.-L. (anja.liszkay@i2bc.paris-saclay.fr).

Abstract

Manganese (Mn) is an essential metal for plant growth. The most important Mn-containing enzyme is the Mn_4CaO_5 cluster that catalyzes water oxidation in photosystem II (PSII). Mn deficiency primarily affects photosynthesis, whereas Mn excess is generally toxic. Here, we studied Mn excess and deficiency in the liverwort *Marchantia polymorpha*, an emerging model ideally suited for analysis of metal stress since it accumulates rapidly toxic substances due to the absence of well-developed vascular and radicular systems and a reduced cuticle. We established growth conditions for Mn excess and deficiency and analyzed the metal content in thalli and isolated chloroplasts. In vivo super-resolution fluorescence microscopy and transmission electron microscopy revealed changes in the organization of the thylakoid membrane under Mn excess and deficiency. Both Mn excess and Mn deficiency increased the stacking of the thylakoid membrane. We investigated photosynthetic performance by measuring chlorophyll fluorescence at room temperature and 77 K, measuring P700 absorbance, and studying the susceptibility of thalli to photoinhibition. Nonoptimal Mn concentrations changed the ratio of PSI to PSII. Upon Mn deficiency, higher non-photochemical quenching was observed, electron donation to PSI was favored, and PSII was less susceptible to photoinhibition. Mn deficiency seemed to favor cyclic electron flow around PSI, thereby protecting PSII in high light. The results presented here suggest an important role of Mn in the organization of the thylakoid membrane and photosynthetic electron transport.

Introduction

Manganese (Mn) is an essential element for plant growth. Mn homeostasis is disturbed under suboptimal or excessive Mn availability (Schmidt et al. 2016; Alejandro et al. 2020). The most important Mn-containing enzyme is the Mn_4CaO_5 cluster at photosystem II (PSII) that catalyzes water oxidation. Although Mn is involved as a cofactor in a range of biochemical pathways, the primary effect of Mn deficiency in photosynthetic organisms is a decrease in photosynthetic activity (Marschner 1995). Furthermore, Mn is involved in reactive oxygen species (ROS) metabolism and in the antioxidant response. Manganese is the cofactor of the manganese superoxide dismutase (MnSOD) found in mitochondria and peroxisomes (Bowler et al. 1994; Corpas et al. 2017). Oxalate oxidase (OxOx) present in the apoplast also requires Mn. This enzyme catalyzes the oxidation of oxalate to carbon dioxide coupled with the reduction of oxygen to hydrogen peroxide (Requena and Bornemann 1999), the latter having an essential role in the defense against pathogens (Lane 2002). When accumulated in excess, Mn can be toxic causing oxidative stress (Marschner 1995; Pittman 2005; Delhaize et al. 2007; Peiter et al. 2007; Eroglu et al. 2016).

Received September 9, 2022. Accepted December 6, 2022. Advance access publication February 1, 2023

In the presence of excess Mn in the soil, there is a competition between the uptake of Mn and other metals that are also essential for the plant (Alam et al. 2005; St. Clair and Lynch, 2005; Blamey et al. 2015; Lešková et al. 2017). Indeed, at the level of the roots, plants do not have transporters that are completely selective for a single metal. Thus, a high abundance of Mn can lead to a decrease in the absorption of other essential metals such as calcium, magnesium, iron, or even phosphorus, thereby negatively affecting photosynthesis (Nable et al. 1988; Amao and Ohashi 2008) and inhibiting chlorophyll synthesis (Clairmont et al. 1986; Subrahmanyam and Rathore 2001). Manganese excess causes chlorosis followed by necrosis leading to plant death, but these symptoms are very variable and species dependent (Millaleo et al. 2010). To overcome Mn toxicity, plants have developed different ways of Mn storage in vacuoles (Ducic and Polle 2007), cell walls (Führs et al. 2010), and even Golgi vesicles (Marschner 1995; Pittman 2005). In the literature, plant species have been divided into tolerant and non-tolerant to Mn excess. Some species can hyperaccumulate Mn at levels above 10,000 $mg.kg^{-1}$ dry weight (DW) (Van der Ent et al. 2013).

The effect of Mn deficiency on photosynthetic electron transport and chloroplast structure has been studied for decades in a number of different organisms ranging from cyanobacteria to angiosperms (e.g. Homann 1967; Salomon and Keren 2011). In general, a decline in PSII activity is observed although symptoms of Mn deficiency are species dependent (Homann 1967). Depending on the severity of Mn deficiency, the ultrastructure of chloroplasts may be perturbed. In slightly Mn-deficient spinach (*Spinacia oleracea*) plants, the stroma lamellae are affected, while the grana stacks are normal. Under more severe Mn deficiency, grana stacks are also disorganized (Mercer et al. 1962). More recently, similar observations were reported in the Arabidopsis (*Arabidopsis thaliana*) knockout mutant chloroplast Mn transporter1 (CMT1), a transporter localized in the inner envelope membrane, where chloroplast development was abnormal and thylakoids appeared disorganized, with either hypo- or hyper-stacked grana lamellae (Eisenhut et al. 2018; Zhang et al. 2018). In this mutant, a large heterogeneity between the chloroplasts was observed with chloroplasts containing a well-structured, normal organization of the thylakoid membranes next to chloroplasts with completely disorganized architectures (Eisenhut et al. 2018). The consequences of the loss of PSII activity and the disorganization of the thylakoid membrane on the ratio of linear and cyclic photosynthetic electron transport have not been investigated in previous studies.

In this present study, we investigated the consequences of both excess and deficiency of Mn on photosynthesis in the liverwort *Marchantia polymorpha*, an emerging model system. Marchantia has been described in the 1990s as being able to hyperaccumulate certain metals such as, for example, lead (Samecka-Cymerman et al. 1997). Due to the morphology of the thalli, the ventral part and hyaline parenchyma of the plant are in direct contact with the substrate allowing the uptake of the metals from the medium without having to pass through the root system as occurs in vascular plants. Compared to vascular plants, the leaf anatomy of Marchantia is simpler and the tissues are thinner. Chloroplasts are less structured than in vascular plants (Tanaka et al. 2017) with smaller grana stacks, making these chloroplasts an ideal system for super-resolution fluorescence microscopy.

We have established conditions for cultivating Marchantia on plates under Mn deficiency and excess. The metal content, metabolome, and antioxidant activities as well as photosynthetic activity and chloroplast structure were determined to investigate the response of Marchantia to non-optimal Mn supply. Manganese excess and deficiency affect these processes in different ways. Manganese excess led to a strong response of the metabolome but subtle defects in photosynthesis, whereas, in contrast, Mn deficiency affected the activity of PSII and promoted cyclic electron transport around PSI. Under Mn deficiency, an increase in non-photochemical fluorescence quenching was observed, protecting PSII against photoinhibition.

Results

Part I: Mn excess induces a stress response and affects the photosynthetic apparatus

In order to determine the effect of Mn excess on *M. polymorpha*, plants were cultivated on media containing different $MnCl_2$ concentrations, ranging from 33 µM (Agar Control) to 6.5 mM (200×) manganese. Gemmae were cultured on a standard Gamborg's B5 medium (33 µM $MnCl_2$) for 2 weeks before being transferred for 1 week to the different Mn concentrations before analysis. Figure 1A shows that thalli were able to grow normally up to 1 mM Mn. However, thalli showed reduced growth from 2 up to 6.6 mM Mn, with signs of stress visible as brown spots. The chlorophyll content of the thalli was significantly decreased in excess Mn conditions (SI Table 1). The determination of Mn concentration in thalli (Figure 1B) showed that there is a positive correlation between Mn accumulation and Mn concentration in the medium. In addition to Mn, we determined Fe and Mg content since high Mn may negatively impact Fe import into the chloroplasts and thereby the assembly of FeS clusters in PSI (Millaleo et al. 2013), and Mg is important for stacking of the thylakoid membranes. Neither Fe nor Mg content was affected by the high Mn concentrations.

In the following, we focus on the conditions of Mn excess 30 × and 200 ×. The first being the highest concentration at which Marchantia showed no obvious signs of stress and the second being the most stressful condition. We conducted a metabolomic analysis by gas chromatography–mass spectrometry (GC-MS) on thalli. In total, 94 metabolites have been identified and quantified (Supplemental Figure S1, Tables S2 and S3). Regarding the

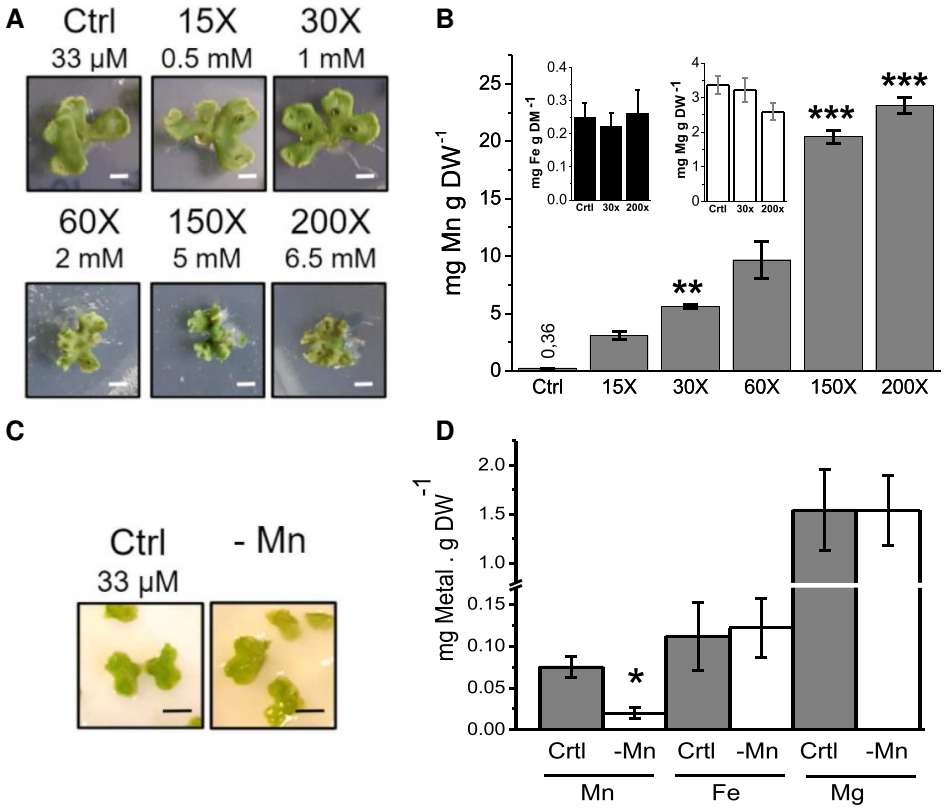

Figure 1. Effect of nonoptimal Mn supply on growth and metal content of *Marchantia polymorpha*. Mn excess: **A)** 2-wk-old thalli were transferred for 1 week to agar plates containing 33 µM (control, Crtl), 0.5 mM (15×), 1 mM (30×), 2 mM (60×), 5 mM (150×), and 6.5 mM (200×) $MnCl_2$, respectively. White scale bars represent 1 cm. **B)** Manganese, iron, and magnesium concentrations were determined after 1-week growth with the given Mn concentrations. Mn deficiency: **C)** 2-week-old thalli were transferred and grown for 1 week on starch plates with or without the addition of 33 µM $MnCl_2$. Black scale bars represent 1 cm. **D)** Manganese, iron, and magnesium concentrations in thalli were measured after 1 week of growth on starch plates with (Ctrl, hatched bars) or without $MnCl_2$ (-Mn, white bars) in the medium. Error bars in **B** and **D** represent standard errors. Stars in **B** and **D** indicate significant differences, compared to the control condition, based on a Mann–Whitney test (*$P < 0.05$, **$P < 0.01$, ***$P < 0.001$; $N \geq 3$ biological replicates).

200× condition, certain metabolites involved in the response to heavy metal or oxidative stresses were strongly increased, while all other metabolites decreased compared to the control. A very high concentration of Mn was associated with a strong induction of polyamine synthesis with an accumulation of ornithine, citrulline, and putrescine (Table 1). Among sugars and their derivatives, strong increases in trehalose, rhamnose, and galacturonic acid were also observed. All these compounds are known to accumulate in plants and other organisms upon exposure to heavy metals (Sharma and Dietz 2006; Singh et al. 2016; Liu et al. 2017; Hasanuzzaman et al. 2019; Alejandro et al. 2020). Most striking, *N*-methylalanine content was 30 and 50 times higher in 30× and 200× conditions, respectively. To further investigate the response to oxidative stress, the activity of a few antioxidant enzymes was measured (Table 2). A 2-fold increase in superoxide dismutase (SOD) activity was observed at the highest Mn concentration. The activity of class III peroxidases was also slightly increased at 200×, while catalase activity gradually decreased.

Table 1. Increase in metabolites involved in oxidative stress response upon growth on high Mn concentration

Metabolite	Experimental condition		
	Ctrl	30×	200×
Citrulline	0.001 ± 0	0.001 ± 0	0.003 ± 0.001
Galacturonic acid	0.004 ± 0	0.004 ± 0.001	0.008 ± 0.001
L-ornithine	0.003 ± 0.001	0.003 ± 0	0.007 ± 0.001
N-Methylalanine	0.021 ± 0.002	0.67 ± 0.237	1.101 ± 0.038
Putrescine	0.003 ± 0.001	0.002 ± 0	0.008 ± 0.001
Rhamnose	0.004 ± 0	0.004 ± 0.001	0.008 ± 0.001
Trehalose	0.053 ± 0.003	0.049 ± 0.008	0.083 ± 0.012

List of selected metabolites showing an increase in plants grown in 200× condition. The mean value and SD are given ($N = 4$). $P < 0.05$ for all values, according to the 2-way ANOVA test. See Supplemental Table S2 for the full list.

Next, we studied the impact of Mn excess on chloroplast ultrastructure and photosynthetic activity. The concentration of Mn, Fe, and Mg was measured in isolated intact chloroplasts (Figure 2A). The results show a gradual and significant increase of Mn comparable with the observation made in the

Table 2. Antioxidant enzymes activities in thalli from control and manganese excess and deficiency conditions

Parameter	Experimental condition				
	Ctrl	30×	200×	Starch + Mn	Starch − Mn
SOD activity	3.01 ± 0.63	4.19** ± 0.86	6.00*** ± 1.48	5.63 ± 1.43	5.08 ± 0.63
CAT activity	1.18 ± 0.16	0.87** ± 0.26	0.54*** ± 0.12	0.72 ± 0.16	0.70 ± 0.13
PRX activity	1.27 ± 0.38	1.17 ± 0.25	1.59* ± 0.42	1.52 ± 0.20	1.04** ± 0.40
ROS	—	—	—	44.4 ± 4.2	100 ± 1.4

Superoxide dismutase, Catalase, and peroxidase activities (μmol substrate mg proteins^{-1} min^{-1}) were measured in crude extracts. $^{\bullet}OH$ derived from $H_2O_2/O_2^{\bullet-}$ was measured using electron paramagnetic resonance (EPR) as a hydroxyethyl-*N*-tert-butyl-α-(4-pyridyl)nitrone *N*′-oxide.
(4-POBN) adduct. Mean value and SD are given. Stars indicate a significant difference compared to the control condition, based on a Mann–Whitney test (*$P < 0.01$, **$P < 0.01$, ***$P < 0.001$, $N = 3$ biological replicates).

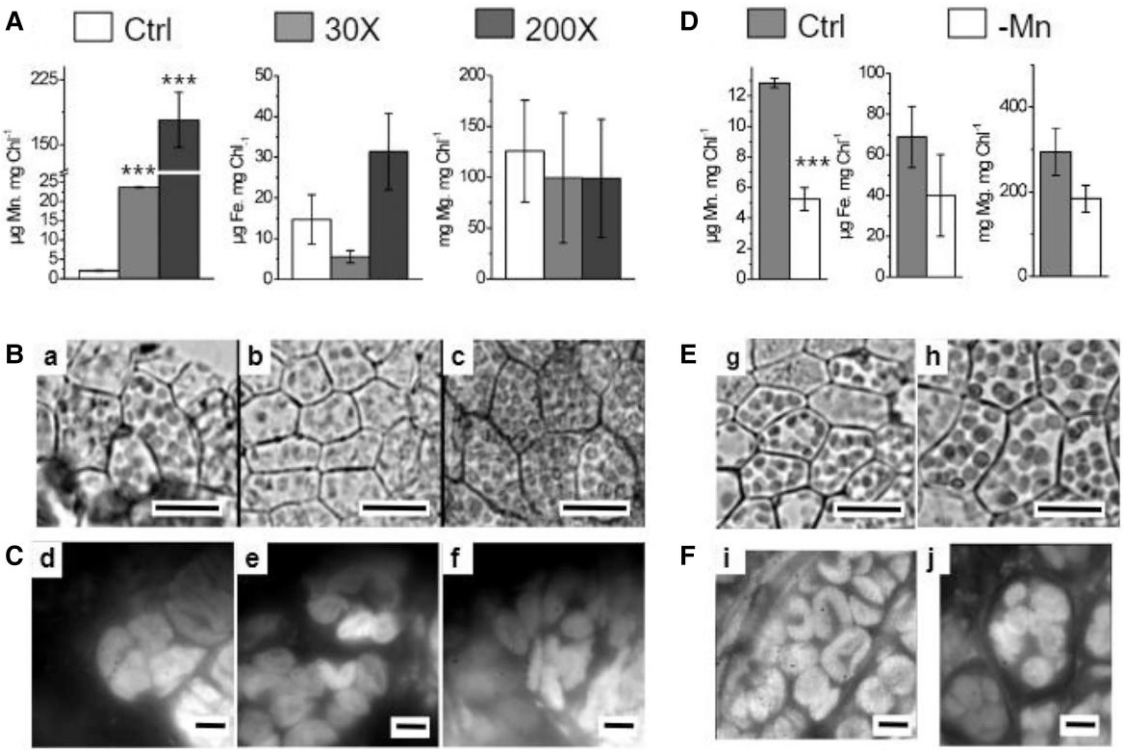

Figure 2. Chloroplast metal content and structure in *Marchantia polymorpha* grown on nonoptimal Mn supply. Mn excess: **A)** Metal content of intact chloroplasts isolated from thalli cultured on agar (control, 33 μM; 30×, 1 mM; 200×, 6.5 mM $MnCl_2$). **B)** Microscopy images of thalli cultured on agar (a, Control; b, 30×; c, 200×). **C)** Epifluorescence microscopy images of chloroplast surfaces of thalli (d, Control; e, 30×; f, 200×). Mn deficiency: **D)** Metal content of intact chloroplasts isolated from thalli cultured on starch (Starch + Mn, 33 μM Mn; Starch − Mn, without Mn). **E)** Microscopy images of chloroplasts in thalli (g, Starch + Mn; h, Starch − Mn). **F)** Epifluorescence microscopy images of chloroplast surfaces of thalli (i, Starch + Mn; j, Starch − Mn). Scale bars in B and E represent 200 μm; scale bars in C and F represent 10 μm. Error bars in A and D represent standard errors. Stars in A and D indicate significant differences, compared to the control condition, based on a Mann–Whitney test (***$P < 0.001$; $N \geq 3$ biological replicates).

whole thalli. We observed an increase from 2 to 175 μg Mn mg Chl^{-1} in the 200× condition compared to the Control. We determined the total chlorophyll content of the thalli to determine the proportion of Mn allocated to chloroplasts (Figures 1B and 2A; Supplemental Table S1). About 7% to 13% of the total Mn content of the thalli was detected inside the isolated chloroplasts with 13% in Control and 30× and 7% in 200×. There were no significant changes in the chloroplast Fe and Mg concentrations under Mn excess.

We used first bright-field and epifluorescence microscopy to see whether Mn excess changes the morphology of the cells as well as the number of chloroplasts (Figure 2B). In Control Agar, most chloroplasts show typical plant-type spherical morphology, while in 30×, there was a divergence from this typical architecture. Some chloroplasts had a deformed shape. In 200×, this progression of deformation of the morphology was further enhanced and the chloroplasts were smaller on average (Figure 2C, Supplemental Figure S2). Next, we used

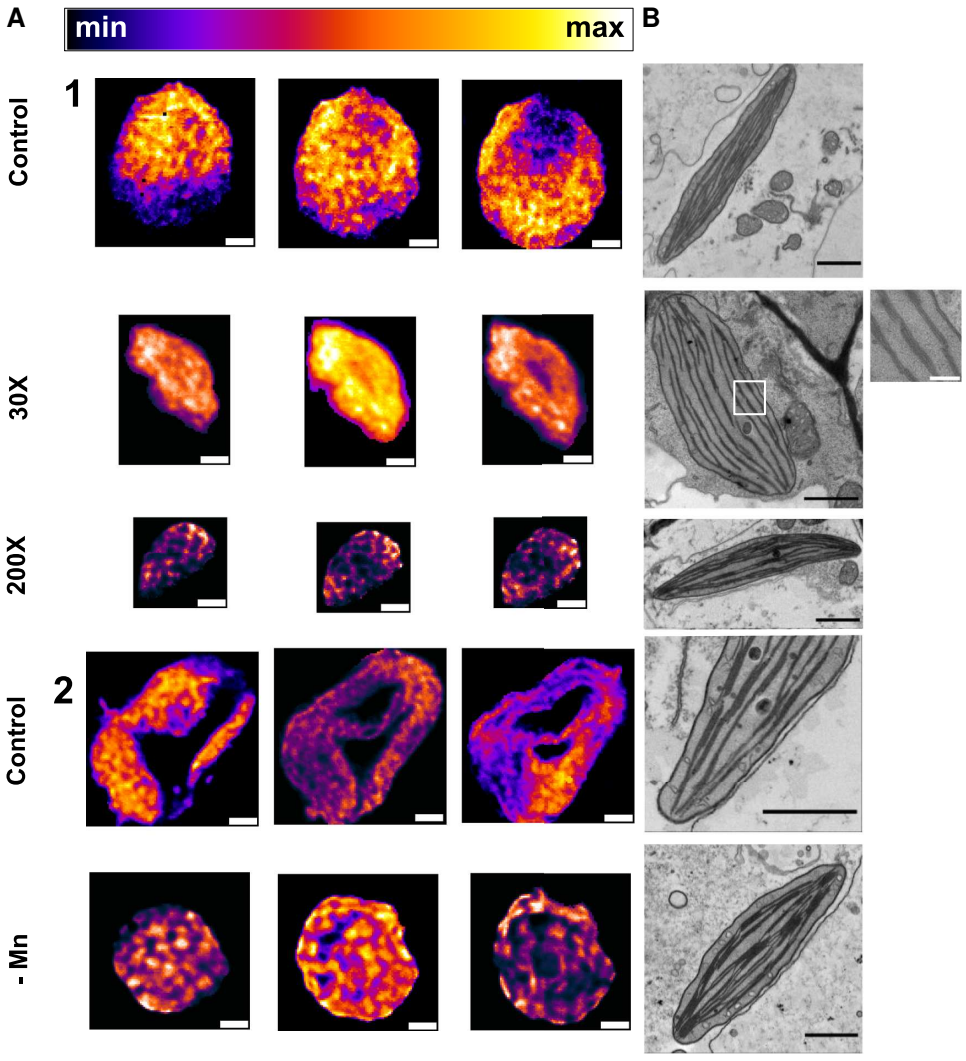

Figure 3. Organization of chloroplast membranes as evidenced by room temperature in vivo super-resolution chlorophyll fluorescence emission nanoscopy and by TEM. **A)** Super-resolution fluorescence microscopy. 1) Agar Control, 30× and 200× conditions and 2) Starch Control and Starch − Mn. For each culture condition, reading from left to right, the 3 reconstructed fluorescence maps are separated by 300 nm in the axial (z) direction. The false-color scale is represented by horizontal color bar (minimum, black; maximum, white). Scale bar: 1 µm. One chloroplast is represented by a total of 10 chloroplasts analyzed for each condition. **B)** TEM images. 10–20 chloroplasts were analyzed, exhibiting the same features for each culture condition. Scale bar: 1 µm (except for the digitally enhanced insert, 200 nm).

super-resolution fluorescence nanoscopy and transmission electron microscopy (TEM) to determine better the change in the organization of the thylakoid membranes triggered by excess Mn (Figure 3). At physiological temperatures, chlorophyll fluorescence is mainly due to PSII emission, which is essentially concentrated in the grana lamellae (for reviews, see Dekker and Boekema 2005; Kirchhoff 2019). Hence, the fluorescence images partly represent the spatial organization and relative abundance of grana stacks in in vivo chloroplasts. The organization of the chloroplast in the Control (Figure 3A top panel) is similar to that of *Arabidopsis thaliana* (Iwai et al. 2018; Streckaite 2021) with a "round" shape and the presence of numerous grana stacks visualized as highly fluorescent yellow/orange patches in the false-color images, albeit with a less clear separation between stroma and grana lamellae. Under the 30× condition, the chloroplast is smaller, indicating a more compact spatial organization of the interconnected granae. Furthermore, the presence of a non-fluorescent region was observed in the center corresponding to a void in bright-field images. In 200×, the smaller chloroplasts still exhibited strong chlorophyll fluorescence emissions with a well-developed distribution of patches indicative of thylakoid grana stacks. Electron microscopy images confirm clear grana stacking under control and 200× conditions, while the organization at 30× was different with 3 thylakoid membranes always attached to each other concomitant with a lack of major grana stack formation (Figure 3B, TEM insert). This uniform distribution of attached membranes under

Table 3. Chl *a*/*b* ratio and electron transport capacities of thylakoids from thalli cultured on manganese excess and deficiency

Parameter	Experimental condition				
	Ctrl	30×	200×	Starch + Mn	Starch − Mn
Chl *a*/*b*	1.23 ± 0.09	1.30 ± 0.10	0.97 ± 0.06	0.95 ± 0.22	0.91 ± 0.20
F_v/F_m	0.775 ± 0.005	0.773 ± 0.003	0.765 ± 0.004	0.772 ± 0.012	0.751* ± 0.004
PSI/PSII	1.47 ± 0.02	1.42 ± 0.01	1.19* ± 0.02	1.11 ± 0.02	1.51* ± 0.01
PSII activity	48 ± 13	43 ± 17	15.0*** ± 5.1	30 ± 9	22 ± 8
PSI activity	116 ± 20	114 ± 27	100 ± 40	59 ± 8	75* ± 16

Chlorophyll content was determined after extraction in acetone. PSI to PSII ratio was determined by integrating the area of the fluorescence at 77 K ($\lambda_{max725}/\lambda_{max685}$). PSII and PSI activities (μmol O_2 μg chl^{-1} h^{-1}) were measured using an O_2 electrode. PSII activity was measured as oxygen evolution in the presence of 1 mM 2,6-dichloro-1,4-benzoquinone (DCBQ), 10 mM NH_4Cl. PSI activity was measured as oxygen uptake in the presence of 10 μM DCMU, 5 mM ascorbate, 30 μM DCPIP, 500 μM methylviologen, and 10 mM NH_4Cl. Mean value and SE are given. Stars indicate significant difference compared to the control condition, based on a Mann–Whitney test (*$P < 0.01$, ***$P < 0.001$, $N = 6$).

30× Mn is in agreement with the quasi-uniform false-color chlorophyll emission maps observed using in vivo fluorescence nanoscopy, attributed to mainly PSII emission.

Since the size of the chloroplasts and the distribution of the chlorophyll fluorescence within the chloroplasts were affected by the growth conditions, photosynthesis was studied in more detail. Table 3 presents that the Chl *a*/*b* ratio remained unchanged at 30× but decreased at 200× Mn, indicating that the antenna size relative to the reaction center increased since Chl *b* is a major constituent of the light-harvesting complex II (LHCII). The 77 K fluorescence emission spectra (Figure 4A) showed 3 characteristic peaks at 685, 695, and 725 nm; the former 2 peaks are attributed to LHCII and PSII, and the latter to PSI with its antenna (Satoh and Butler 1978). For chloroplasts isolated from thalli grown at 200×, the emission attributed to PSI decreased relative to that of PSII, while there was no change when grown at 30× (Figure 4A). In line with the lower PSI fluorescence relative to PSII fluorescence in 200×, the capacity of PSI electron transport was slightly lower although the effect was not statistically significant (Table 3). However, the capacity of PSII electron transfer was significantly decreased. A damaging effect of high Mn concentration on PSII activity was confirmed by fluorescence induction curves (Figure 4B). The appearance of the K-phase under 200× condition can be attributed to the damage to the Mn_4CaO_5 cluster at the PSII donor side according to Strasser (1997). In 200×, maximum quantum yield of PSII (F_v/F_m) and chlorophyll quenching fluorescence were altered during illumination with actinic light, but there was no increase in the susceptibility of PSII to photoinhibition (Table 3, Supplemental Figures S3 and S4).

Part II: Mn deficiency affects the photosynthetic apparatus and may favor cyclic electron flow

In the following, we investigated the effect of Mn starvation on *M. polymorpha*. Agar plates were not suitable to induce Mn deficiency since agar contains too much Mn as an impurity (12.8 ± 0.4 μM). Therefore, we substituted agar with starch as a gelling agent. Gemmae were cultured for 2 wk on Gamborg's B5 Agar medium (33 μM $MnCl_2$) before young thalli were transferred to Mn-free Gamborg's B5 Starch medium with or without the addition of Mn (33 μM Mn). It was not possible to culture gemmae directly on starch because they were not able to develop. Figure 1C shows that plants exhibited no visible growth defect after 1 week culturing on Starch Control or without Mn. However, chlorophyll fluorescence showed a clear decrease in the quantum yield of PSII (F_v/F_m) was lower when no $MgCl_2$ had been added to the medium (Supplemental Figure S5). The amount of metals in thalli was measured (Figure 1D). The use of starch allowed a reduction of Mn content from 75 μg Mn g DW^{-1} (Starch Control) to 20 μg Mn g DW^{-1} (Starch − Mn). Fe and Mg contents were not affected.

As for Mn excess, a metabolic analysis was carried out. No significant difference in the metabolomics profiles was observed between the 2 starch conditions (Supplemental Table S1), while there were clear differences between Agar Control and Starch Control (Supplemental Table S2). The activity measurements of the antioxidant enzymes showed a significant decrease in the activity of type III peroxidases (Table 2). Using a spin-trapping assay, the generation of $^{\bullet}OH$ derived from $H_2O_2/O_2^{\bullet-}$ was detected in starch-grown plants. ROS levels were 2 times higher in the Starch − Mn condition.

Next, the impact of Mn deficiency on chloroplasts was investigated. The measurements (Figure 2D) revealed a decrease in the Mn content by about 50% in the Starch − Mn condition compared with the Starch Control. There was a tendency that the Starch − Mn growth condition lowers slightly the Fe and Mg content; however, the differences were not statistically significant. Overall, the metal content (Mn, Fe, and Mg) of the chloroplasts under starch conditions was almost double compared to chloroplasts from thalli grown under Agar Control conditions. This may be due to effects on the metal uptake and transport system or also be connected to a higher intactness of the isolated chloroplasts. The epifluorescence microscopy images (Figure 2F) showed more "horseshoe-shaped" chloroplasts under the Starch Control condition. In Starch − Mn, chloroplasts appeared rounder. These observations were confirmed by super-resolution nanoscopy (Figure 3B); however, the area of the chloroplasts was unaltered (Supplemental Figure S2). In the Starch Control, the thylakoid membranes were organized in grana/lamellae-like structures. In the Starch − Mn condition, the chloroplasts had fewer voids in the 3D volume.

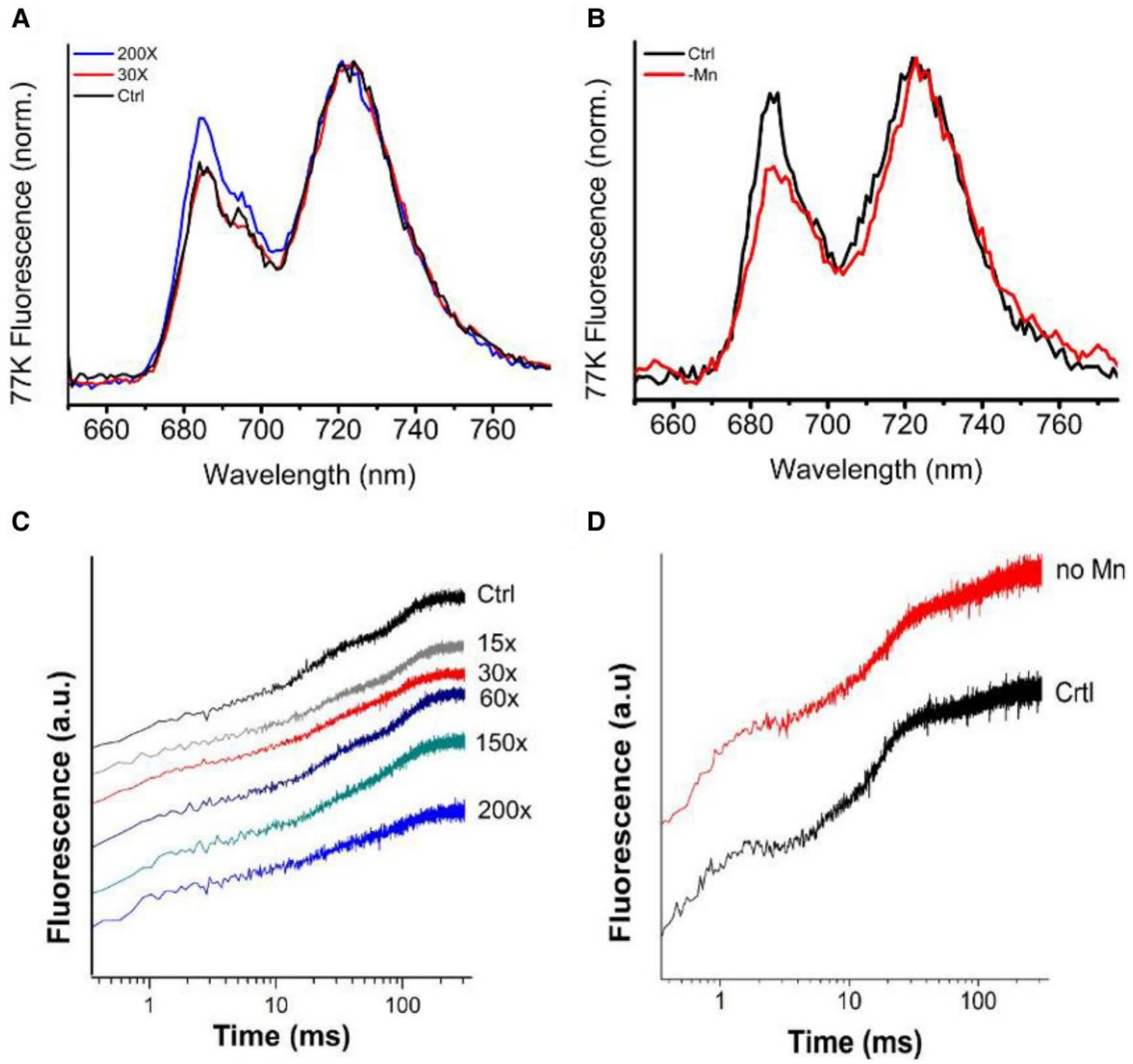

Figure 4. Chlorophyll fluorescence at 77 K and room temperature. **A)** 77 K fluorescence emission of chloroplasts extracted from thalli grown on agar: Ctrl (black), 30× (red), and 200× (blue, upper trace at 685 nm) ($N = 3$, biological replicates). **B)** Same as (a) carried out on starch-cultivated thalli with (Ctrl, black) or without $MnCl_2$ (−Mn, red, upper trace at 685 nm). Spectra in A and B were normalized to the maximum emission at 725 nm. **C)** Room-temperature fluorescence induction curves (OJIP) were measured on 5-min dark-adapted thalli by the application of a saturating flash with 300 ms duration. Culture conditions as in A. **D)** Fluorescence induction curves on thalli grown as in B. One representative curve is shown for each condition.

Compared with a standard chloroplast as represented in the Agar Control (Figure 3A, top panel), or Arabidopsis (Iwai et al. 2018; Streckaite 2021), the strongly fluorescent regions were localized more distinctly, indicating a change in the mesoscopic organization of the thylakoid membrane. This indicates smaller grana stacks with a more pronounced segregation between them and the stroma lamellae as confirmed by TEM. The TEM image shows a much higher degree of stacking of the thylakoid membranes (Figure 3B).

The 77 K fluorescence (Figure 4B) showed a decrease in the emission at 680 nm in chloroplasts isolated from Starch – Mn thalli, indicating a loss of PSII content compared with PSI. PSII activity was lower (Table 3). The quantum yield of PSII, F_v/F_m, was significantly lower upon Mn deficiency. PSI activity increased significantly, confirming the change in the PSI/PSII ratio under Mn deficiency seen in 77 K fluorescence spectra. In the Starch – Mn condition, the fluorescence induction curves showed a dip phase at about 2 ms, indicative of damage to the Mn_4CaO_5 cluster at the PSII donor side (Figure 4D).

Figure 5 shows changes in room temperature chlorophyll fluorescence upon illumination with actinic light. Upon Mn deficiency, energy dissipation as the heat was enhanced (qN; Figure 5C). However, photochemical quenching (qP; Figure 5D) was not affected. Furthermore, the slightly higher minimum fluorescence level during the recovery phase (post-illumination fluorescence transient, PIFT) upon Mn deficiency indicates an increase in chlororespiratory and/or cyclic electron flow. To show whether the stability of PSII or the repair of damaged PSII was affected under Mn deficiency, photoinhibition experiments were carried out with or without the protein synthesis inhibitor lincomycin

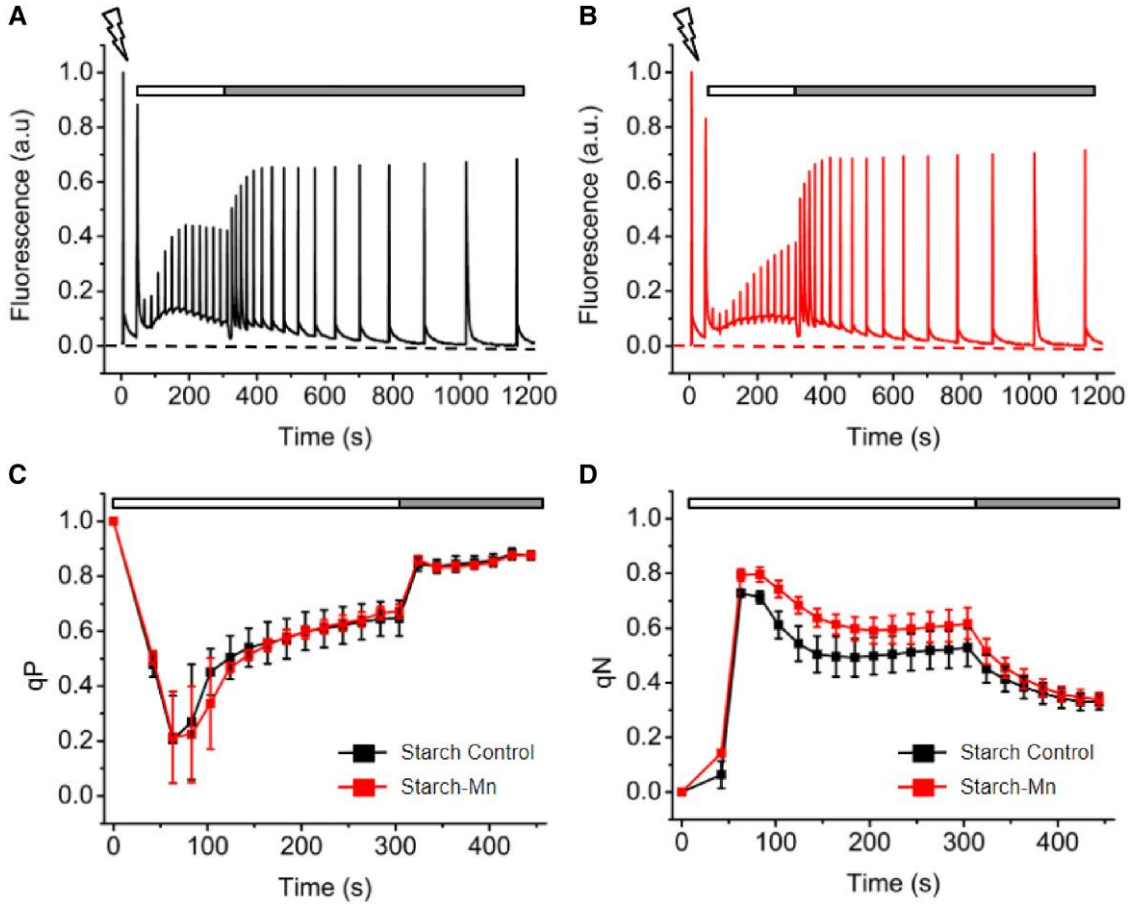

Figure 5. Analysis of variable chlorophyll fluorescence in Mn deficiency. **A)** and **B)** Induction and recovery fluorescence curves were measured on thalli transferred for 1 week to starch medium with (black) or without added $MnCl_2$ (red). After 5 min dark adaptation, thalli were exposed to a measuring light to determine the minimum fluorescence level (dashed lines) and to a saturating flash to obtain the maximum fluorescence level. Actinic light (50 µmol photons m^{-2} s^{-1}) was applied for 5 min (white bar). Recovery in the dark was followed (gray bar). **C)** qN and **D)** qP parameters were calculated, thanks to saturating flashes applied during the light and dark period. Mean values and standard deviation are given in **C** and **D** ($N = 12$, 3 biological replicates). C: lower trace, without added $MnCl_2$; D: upper trace, without added $MnCl_2$.

(Figure 6). Plants cultivated on Starch – Mn were more susceptible to high light in the absence of lincomycin. In the presence of lincomycin, the opposite was observed with PSII in plants cultivated on Starch – Mn being more resistant to the photoinhibitory treatment. This may be explained by the higher nonphotochemical quenching (NPQ) protecting the photosynthetic apparatus. A higher NPQ was observed also in the presence of lincomycin (Supplemental Figure S6).

The higher PSI fluorescence at 77 K, the higher NPQ, and the protection of PSII against photoinhibition in plants cultivated on Starch – Mn may indicate that cyclic electron transport is favored under these conditions. Absorption changes of P700 show that P700 is more slowly oxidized, both in red actinic and in far-red light, in plants cultivated on Starch – Mn indicating that more electrons are available in the electron transport chain (Figure 7A). To show that indeed more electrons are available for $P700^+$ reduction at the luminal side, we determined the yield of donor-side limitation, Y(ND) as a function of the intensity of the actinic light. Figure 7B shows the less donor-side limitation of PSI over a wide range of light intensities in plants cultivated on Starch – Mn compared to those cultivated on Starch Control. These data further indicate a higher activity of cyclic electron flow under Mn deficiency. Under both conditions, acceptor side limitation at the stromal side of PSI was not observed because Marchantia possesses flavodiiron proteins that use ferredoxin as an electron donor to reduce oxygen to water (Shimakawa et al. 2021).

Discussion

In this study, we established growth conditions for manganese excess and deficiency in *M. polymorpha*. Marchantia can absorb up to 25 mg Mn g DW^{-1} (Figure 1B) which is higher than the hyperaccumulator *Polygonum lapathifolium* that contains approximately 18 mg Mn g DW^{-1} in its aerial parts (Liu et al. 2016). However, Marchantia shows symptoms of toxicity under the 200× conditions, and thalli

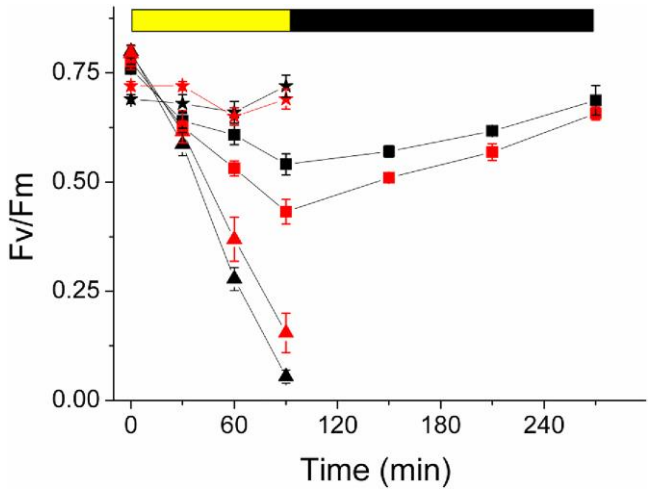

Figure 6. Photoinhibition in Mn deficiency in the absence and presence of lincomycin. Photoinhibition was measured on starch-cultivated thalli with (black symbols) or without $MnCl_2$ (red symbols). F_v/F_m was followed during exposure to high light (800 µmol photons $m^{-2}s^{-1}$) for 90 min (yellow bar) and during the recovery at room light (black bar). Squares: without lincomycin; lower trace without $MnCl_2$, triangles: with lincomycin; upper trace without $MnCl_2$ As a control, lincomycin samples incubated in the dark are shown (stars). Mean values and standard errors are given ($N = 6$, 2 biological replicates).

only survive for a few weeks. Therefore, Marchantia does not qualify as a hyperaccumulator despite its high Mn uptake capacity. Mn excess conditions induced an increase in SOD and peroxidase (PRX) activity, while catalase activity decreased (Table 2). An increase in SOD activity could reflect a higher amount of MnSOD present under Mn excess conditions. The metabolomics analysis showed that known stress-induced metabolites accumulate upon excess Mn (Table 1; Supplemental Figure S2 and Tables S2 and S3); however, the metabolomics response of Marchantia is distinct from that of angiosperms and requires in-depth functional analysis of metabolites and metabolic pathways. An excess of Mn affected the ratio between it and other metals (e.g. Fe and Mg) in both thalli and chloroplasts. Indeed, cation transporters are known not to be completely selective under stressed conditions (Vert et al. 2002; Ducic et al. 2005; Lei et al. 2007; Millaleo et al. 2010; Barberon et al. 2011); well-documented examples of excess of Mn in the soil are known to perturb the absorption and translocation of other elements, including iron, magnesium, and phosphorus (Ducic et al. 2005; Lei et al. 2007; Millaleo et al. 2010), causing Fe deficiency in plants. However, Marchantia grown at 200 × does not show alterations in the Fe and Mg content inside the thalli (Figures 1B and 2A). Nevertheless, an alteration in the Mn/Fe ratio may induce Fe deficiency through competitive binding. Fe deficiency is known to affect primarily PSI that is rich in 4Fe4S clusters. As shown in Figure 4B, PSI content is lowered in comparison to PSII in 200×. A similar reduction of PSI upon exposure to Mn excess has been reported for Arabidopsis (Millaleo et al. 2013). Aside PSI, the water-splitting activity of PSII seems also to be affected in the 200 × condition as seen by the appearance of the K-phase in fluorescence induction curves (Figure 4C) and the decrease in PSII activity (Table 2). A toxic effect of Mn excess on PSII activity is in accordance with data on angiosperms (Liang et al. 2019); 200 × Mn not only negatively affected the photosynthetic apparatus but also led to a reduction in chloroplast size and an alteration of the well-separated grana stack and stroma lamellae distribution (Figures 2 and 3).

Transfer of thalli from agar to starch plates allowed to establish Mn deficiency conditions. Growth in starch allowed lowering the Mn content drastically in the thalli to 21 µg Mn g DW^{-1}. According to Mengel and Kirkby (1987), the minimum Mn content required for the growth of angiosperms is about 20 to 40 mg Mn kg DW^{-1}, and most angiosperms usually contain 30 to 500 mg Mn kg DW^{-1}. Manganese deficiency led to a decrease in F_v/F_m, a change in the ratio of the activity PSI/PSII (Table 3), and less PSII content relative to PSI according to 77 K fluorescence (Figure 4B). In angiosperms, Mn deficiency lowers PSII activity while PSI activity remains unaffected (Homann 1967; for review see Schmidt et al. 2016). Furthermore, the structural organization of the thylakoids was affected (Figure 3). It is known that Mn deficiency leads to disorganization of the thylakoid membrane in angiosperms (Mercer et al. 1962; Homann 1967). In *M. polymorpha*, the smaller compartmentation of the grana stacks could be partly responsible for the changes in electron transport. In addition to a change in the stoichiometry between active PSI and active PSII, a different distribution of photosynthetic complexes may favor cyclic electron flow around PSI by allowing the formation of supercomplexes likely to be required for cyclic electron flow (Iwai et al. 2010). As shown in Figure 7, thalli grown on Starch – Mn show less limitation of electron donation to $P700^+$ than those of the Starch Control indicating a stimulation of cyclic electron flow under Mn deprivation. Cyclic electron flow is known to be induced under specific physiological conditions like anaerobiosis in *Chlamydomonas reinhardtii* (Joliot et al. 2022). Changes in the organization of PSI complexes were also observed under Mn limitation in cyanobacteria (Salomon and Keren 2011). Increased cyclic electron flow generates a higher proton gradient across the thylakoid membrane and thereby an increase in NPQ (Figure 5C). A higher NPQ protects PSII against photoinhibition as seen when thalli grown on Starch – Mn were exposed to high light in the presence of lincomycin (Figure 6), while they were more susceptible to photoinhibition in the absence of lincomycin (Figure 6) likely due to a slowdown of PSII repair. A slowdown of PSII repair under Mn deficiency has been observed previously in the Mn transporter mutant *nramp3nramp4* in Arabidopsis (Lanquar et al. 2010). The repair of PSII may be slowed down in the light because of the higher ROS levels in Starch – Mn (Table 2) that affects the synthesis of the D1 protein (Nishiyama et al. 2011).

In conclusion, we show here that unfavorable Mn concentrations during the growth of Marchantia affect not only the

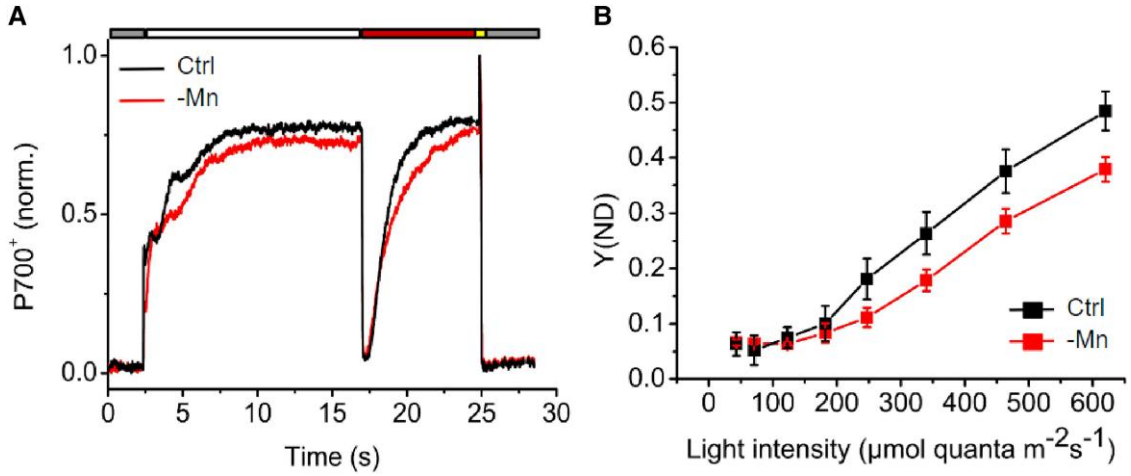

Figure 7. Activity of PSI in Mn deficiency. **A)** Normalized $P700^+$ signal was obtained on thalli cultivated on Starch (+Mn, black, upper trace; −Mn, red, lower trace). The redox state of the PSI primary donor P700 was monitored through the changes in absorbance at 830 versus 875 nm. Leaves were kept in the dark for 5 min prior to the measurements. Thalli were exposed to actinic light for 15 s (white bar) and to far-red light until reaching a plateau (red bar). Then, a saturating flash was applied (yellow bar) and the decay was observed in the dark (gray bar). **B)** PSI donor-side limitation Y(ND) based on saturating pulse analyses. Following the initial determination of maximal oxidation of P700, actinic light of the indicated intensities was given for 180 s. Mean values and standard deviation are given ($N = 6$, 2 biological replicates).

photosynthetic apparatus but also the organization of the thylakoid membrane. Future work is needed to explore the link between changes in the organization and stacking of the thylakoid membrane and stimulation of cyclic electron flow under Mn deficiency.

Materials and methods

Plant growth conditions

Gemmae from *M. polymorpha*, Takaragaike (Tak-1) accession (male) were asexually cultured on ½ Gamborg's GB5 1% (w/v) Agar medium (Gamborg et al. 1968) for 2 weeks under a light–dark cycle of 16-h light, 22°C, 120 µmol quanta $m^{-2}s^{-1}$, white fluorescent lamp/8 h dark, 20°C. For Mn excess condition, young thalli were transferred to ½ Gamborg's GB5 1% Agar medium containing 33 µM (control), 0.5 mM (15×), 1 mM (30×), 2 mM (60×), 5 mM (150×), or 6.5 mM (200×) $MnCl_2$ for 1 week before measurements. According to the metal quantification, the control medium contained 2.52 ± 0.27 µg Mn g^{-1} fresh weight of the solid medium. For Mn deficiency, young thalli were transferred on ½ Gamborg's GB5 6% starch (w/v) medium with or without the addition of 33 µM $MnCl_2$ for 1 week before performing measurements. According to the metal quantification, the starch medium with $MnCl_2$ contained 2.03 ± 0.13 µg Mn g^{-1}, and the medium without the addition of $MnCl_2$ contained 0.26 ± 0.08 µg Mn g^{-1} fresh weight of the solid medium.

Chloroplast and thylakoid isolation

About 10 g of thalli was collected, the media carefully mechanically removed, and grounded in 100 ml of GR buffer (50 mM Hepes-KOH pH 7.5, 0.33 M sorbitol, 1 mM $MgCl_2$, 2 mM EDTA, 5 mM Na-ascorbate) with a spatula of BSA. The slurry was filtered through 2 layers of Miracloth and centrifuged at 1,200 × *g* (4°C) for 7 min. Pellets were resuspended in 2 m of GR buffer and then layered on the top of a Percoll gradient [15 ml of 30% Percoll/GR buffer (v/v) and 10 ml of 70% Percoll/GR buffer v/v], centrifuged at 7,000 × *g* (4°C) for 17 min (no brake). Intact chloroplasts were collected and washed in 25 ml of GR buffer; centrifugation 1,500 × *g* (4°C) for 5 min. The intactness was checked by light microscopy. For thylakoids, the same procedure was used without the percoll gradient.

Metal quantification

Thalli were collected and dried at 70°C for 2 days before being weighed. About 1 ml of nitric acid (65%) was added to 1 mg of plant material. For intact chloroplasts, the chlorophyll concentration was adjusted to 100 µg chl ml^{-1} before the addition of 2.5 volume of nitric acid. After 10-fold dilution in trace-metal-free water, the metal content of the samples was determined by atomic emission spectroscopy using an MP AES 1200 spectrometer (Agilent, USA).

Super-resolution microscopy

For each sample, a small quantity of thallus was placed in a sandwich of 2 glass coverslips (22 mm diameter, Paul Marienfeld GmbH & Co. KG), sealed, and placed inside an in-house built sample holder. The sample holder was fixed to a nano-positioning system (P-733.2CD, P-725.4CD, E-725.3CD, Physikinstrumente) coupled to an inverted microscope (Ti-U, Nikon) equipped with a CFI Apochromat Lambda 100× oil immersion objective. Room-temperature fluorescence emission was recorded by an iXon ULTRA 897 camera in conventional mode, gain 3 (Andor Technology Ltd.,

Belfast), coupled to the microscope with a custom-made Optomask (Cairn Research Ltd, Faversham). The total chlorophyll fluorescence emission was isolated using a dichroic mirror/emission filter doublet (59022BS/ET655LP, Chroma Technology Corporation). Epifluorescence images were recorded using an excitation provided by a plasma light source (HPLS245 Thorlabs Inc.) and an excitation filter (MF469-35 Thorlabs Inc.). The excitation source for the laser-scanning measurements was a 445-nm emitting laser (OBIS LX, Coherent Inc.) at 100 nW intensity at the sample. Laser scanning and final image reconstruction [resolution (d) $d_{xy} = 126$ nm, $d_z = 320$ nm] were as previously described (Streckaite 2021) with a dwell time of 10 to 30 ms, 60-nm X/Y-scan steps, and 300-nm Z-scan steps.

Transmission electron microscopy

About 1-mm strips of thalli were cut under glutaraldehyde/paraformaldehyde fixative and impregnated by the 1% osmium (w/v) and 1.5% potassium hexacyanoferrate (w/v) en bloc staining protocol as described (Hawes et al. 1981; Juniper et al. 1982); 70-nm-thick sections were cut with an EM UC6 ultramicrotome (Leica Microsystems) and deposited on to copper grids. Ultrathin sections were stained with 2% uranyl acetate (w/v) (Merck) and Reynolds lead citrate according to standard procedures. Grids were examined under a JEOL 1400 TEM operating at 80 kV (JEOL, http://www.jeol.com). Images were acquired using a 9-megapixel high-speed camera (RIO9; Gatan, http://www.gatan.com) and processed using Digital Micrograph (Gatan).

Pigment analysis

Thalli were weighed and incubated in 100% acetone for 16 h in the dark. For complete pigment extraction, acetone incubation was repeated 3 times. The pigment extract was diluted to 80% acetone (v/v) before measurement. Chlorophyll *a* and chlorophyll *b* contents were calculated according to Porra and Scheer (2019).

77K Chlorophyll fluorescence measurements

Fluorescence spectra of intact chloroplasts diluted in GR buffer were measured with a Carry Eclipse fluorimeter (Agilent, USA); excitation wavelength: 430 nm. The spectra were normalized to the intensity of the PSI emission.

Chlorophyll fluorescence analysis at room temperature

Chlorophyll fluorescence analysis was performed on 5 min dark-adapted thalli using a Dual-PAM-100 fluorimeter (Walz, Effeltrich, Germany). F_m and F_m' were determined using saturating flashes (10,000 µmol quanta $m^{-2}s^{-1}$, duration 300 ms). F_o, minimum and F_m, maximum fluorescence in a dark-adapted sample; F_m', maximum fluorescence and F', fluorescence emission from a light-adapted sample. Induction and recovery curves were measured using actinic light of 50 µmol quanta $m^{-2}s^{-1}$: $F_v/F_m = (F_m - F_0)/F_m$, $qN = (F_m - F_m')/(F_m - F_0')$, and $qP = (F_m' - F)/(F_m' - F_0')$. For induction curves (OJIP), one saturating flash was given.

Photoinhibition

Thalli were placed on wet filter paper and illuminated with white light (800 µmol quanta $m^{-2}s^{-1}$) LED panel SL3500 (Photon Systems Instrument, Drasov, Czech Republic). For recovery, samples were placed in low light (10 µmol quanta $m^{-2}s^{-1}$). When indicated, thalli were incubated in lincomycin (1 g L^{-1}) for 4 h prior to the photoinhibition treatment. F_v/F_m was measured using an Imaging-PAM (Walz, Effeltrich, Germany).

P700 measurements

P700 absorbance was measured using a Dual-PAM-100 fluorometer (Walz, Effeltrich, Germany). Near-infrared measuring lights (830 and 870 nm) were applied to measure the transmittance of oxidized P700. Prior to the measurements, the plants were kept in the light in the growth chamber so that the Calvin–Benson cycle enzymes were active. Five minutes dark-adapted thalli were exposed to actinic light followed by far-red light. Then, a saturating flash was given at the end of the far-red light period. To determine quantum yields of PSI donor, Y(ND), and acceptor side limitations, Y(NA), saturating pulse analysis was used (Klughammer and Schreiber 1994). Each actinic light intensity was applied for 180 s before determining Y(ND) and Y(NA).

Antioxidant enzymes activity

Thalli were harvested and ground in 50-mM HEPES buffer pH 6.5. The slurry was filtered through one layer of Miracloth, centrifuged for 5 min at 10.000 × g (4°C). Protein concentration in the crude extract was determined by amido black since the supernatant contained pigments (Schaffner and Weissmann 1973). About 10 µg ml^{-1} protein was used for the enzymatic tests. Guaiacol peroxidase activity was determined spectrophotometrically by measuring the oxidation of guaiacol to tetraguaiacol at 470 nm (ϵ: 26.6 $mM^{-1}cm^{-1}$) (Chance and Maehly 1955). The reaction mixture contained 50 mM NaH_2PO_4/Na_2HPO_4 pH 7.5, 3 mM H_2O_2, and 0.01% (v/v) guaiacol. Catalase activity was measured polarographically at 20°C with a Clark-type electrode in 50 mM Tris buffer pH 8.5 and 1 mM H_2O_2 as substrate. SOD activity was measured using a solution of 500 µM Xanthine, 20 mM HEPES buffer pH 7, 0.2 U ml^{-1} xanthine oxidase, and 100 µM XTT (Na,3′-(1-(phenylaminocarbonyl)-3,4-tetrazolium)-bis-(4-methoxy-6-nitro) benzene sulfonic acid hydrate) as substrate. The kinetics of superoxide production were measured as increase in absorbance at 470 nm, and the SOD activity was determined by following the inhibition of the superoxide production after the addition of the crude extract (Molins et al. 2013). For $^{\bullet}OH$ detection, 15 mg thalli were incubated for 1 h in 3 ml 10 mM phosphate buffer, pH 6.0, 50 mM *N*-tert-butyl-α-(4-pyridyl)nitrone *N*′-oxide (4-POBN), and 4% ethanol (v/v) (Heyno et al. 2008).

Metabolite analysis

GC-MS profiling of metabolites was performed on thalli cultured on Agar Control, 30× and 200× conditions and thalli grown on Starch Control and Starch − Mn. Dried and grounded samples (5 mg of dry weight) were incubated in 1 ml of H_2O/ACN/isopropanol (2/3/3) with 4 mg l^{-1} of ribitol for 10 min at 4°C with shaking at 250 *g* in an Eppendorf Thermomixer. Insoluble material was removed by centrifugation at 20,400 × *g* for 10 min; 700 µl of supernatant was recovered, and 70 µl of a mix of H_2O/MeOH/isopropanol (2/5/2) with 0.3 g L^{-1} of myristic acid d27 was added as an internal standard for retention time locking. Aliquots of each extract (100 µl) extracts were dried for 4 h at 30°C in a Speed-Vac and stored at −80°C. After thawing, samples were dried again in a Speed-Vac for 1 h at 30°C before adding 10 µl of 20 mg ml^{-1} methoxyamine in pyridine to the samples. The reaction was performed for 90 min at 30°C under continuous shaking in an Eppendorf thermomixer. A volume of 90 µl of *N*-methyl-*N*-trimethylsilyl-trifluoroacetamide was then added and the reaction continued for 30 min at 37°C. After cooling, 80 µl were transferred to an Agilent vial for injection. Four hours after derivatization, 1 µl sample was injected in splitless mode on an Agilent 7890B gas chromatograph coupled to an Agilent 5977A mass spectrometer (column: RESTEK RXI 5SIL MS 30MX0.25MMX0.25UM). An injection in split mode with a ratio of 1:30 was systematically performed for the quantification of saturated compounds. Raw Agilent data files were analyzed with AMDIS https://chemdata.nist.gov/dokuwiki/doku.php?id=chemdata:amdis. The Agilent Fiehn GC-MS Metabolomics RTL Library was employed for metabolite identifications. Peak areas were determined with the Masshunter Quantitative Analysis (Agilent) in splitless and split 30 modes. Peak areas were normalized to ribitol and dry weight. Metabolite contents are expressed in arbitrary units (semi-quantitative determination).

Acknowledgments

We thank Claire Boulogne (I2BC) for performing electron microscopy.

Author contributions

M.M. and A.K.-L. designed the project. M.M., U.H., T.H., F.G., B.G., A.G., S.T., and A.K.-L. performed the experiments and analyzed the data. M.M. and A.K.-L. wrote the initial version of the manuscript that was read and revised by all authors.

Supplemental data

The following materials are available in the online version of this article.

Supplemental Table S1. Chlorophyll and Mn content in thalli grown in Mn excess.

Supplemental Table S2. List of 96 metabolites identified by GC-MS in *M. polymorpha*.

Supplemental Table S3. Metabolites significantly decreased in starch condition compared with agar control in *M. polymorpha*.

Supplemental Figure S1. Metabolite analysis in *M. polymorpha* grown in Mn excess condition.

Supplemental Figure S2. Estimation of the chloroplast size under the different growth conditions.

Supplemental Figure S3. Chlorophyll fluorescence at room temperature in *M. polymorpha* grown in control and Mn excess conditions.

Supplemental Figure S4. Photoinhibition of photosystem II in *M. polymorpha* grown in control and Mn excess condition in the presence and absence of lincomycin.

Supplemental Figure S5. Chlorophyll fluorescence (F_v/F_m) in *M. polymorpha* grown on starch plates in low Mn concentrations.

Supplemental Figure S6. qN determination in the presence of lincomycin in *M. polymorpha* grown on starch in control and Mn-deficient conditions.

Funding

This work was supported by the Labex Saclay Plant Sciences-SPS (ANR-17-EUR-0007), the platform of Biophysics of the I2BC supported by the French Infrastructure for Integrated Structural Biology (FRISBI; grant number ANR-10-INSB-05), and IBiSA and France-BioImaging infrastructure supported by the Agence Nationale de la Recherche (ANR-10-INBS-04, call "'investissements d'Avenir"). M.M. is supported by a CEA PhD fellowship.

Conflict of interest statement. None declared.

Data availability

Data will be made available on demand.

References

Alam S, Akiha F, Kamei S, Huq SMI, Kawai S. Mechanism of potassium alleviation of manganese phytotoxicity in barley. J Plant Nutr. 2005:**28**(5):889–901. https://doi.org/10.1081/PLN-200055572

Alejandro S, Höller S, Meier B, Peiter E. Manganese in plants: from acquisition to subcellular allocation. Front Plant Sci. 2020:**11**: article 300. https://doi.org/10.3389/fpls.2020.00300

Amao Y, Ohashi A. Effect of Mn ion on the visible light induced water oxidation activity of photosynthetic organ grana from spinach. Catal Commun. 2008:**10**(2):217–220. https://doi.org/10.1016/j.catcom.2008.08.022

Barberon M, Zelazny E, Robert S, Conéjéro G, Curie C, Friml J, Vert G. Monoubiquitin-dependent endocytosis of the iron-regulated transporter 1 (IRT1) transporter controls iron uptake in plants. Proc Natl Acad Sci U S A. 2011:**108**(32):E450–E458. https://doi.org/10.1073/pnas.1100659108

Blamey FPC, Hernandez-Soriano M, Cheng M, Tang C, Paterson D, Lombi E, Hong Wang W, Scheckel KG, Kopittke PM. Synchrotron-based techniques shed light on mechanisms of plant sensitivity and tolerance to high manganese in the root environment. Plant Physiol. 2015:**169**(3): 2006–2020. https://doi.org/10.1104/pp.15.00726

Bowler C, Van Camp W, Van Montagu M, Inzé D, Asada K. Superoxide dismutase in plants. CRC Crit Rev Plant Sci. 1994:**13**(3): 199–218. https://doi.org/10.1080/07352689409701914

Chance B, Maehly AC. Assay of catalases and peroxidases. Methods Enzymol. 1955:**2**:764–775. https://doi.org/10.1016/S0076-6879(55)02300-8

Clairmont KB, Hagar WG, Davis EA. Manganese toxicity to chlorophyll synthesis in tobacco callus. Plant Physiol. 1986:**80**(1):291–293. https://doi.org/10.1104/pp.80.1.291

Corpas FJ, Barroso JB, Palma JM, Rodriguez-Ruiz M. Plant peroxisomes: a nitro-oxidative cocktail. Redox Biol. 2017:**11**:535–542. https://doi.org/10.1016/j.redox.2016.12.033

Dekker JP, Boekema EJ. Supramolecular organization of thylakoid membrane proteins in green plants. Biochim Biophys Acta. 2005:**1706**(1–2):12–39. https://doi.org/10.1016/j.bbabio.2004.09.009

Delhaize E, Gruber BD, Pittman JK, White RG, Leung H, Miao Y, Jiang L, Ryan PR, Richardson AE. A role for the AtMTP11 gene of Arabidopsis in manganese transport and tolerance. Plant J. 2007:**51**(2):198–210. https://doi.org/10.1111/j.1365-313X.2007.03138.x

Ducic T, Polle A. Manganese toxicity in two varieties of douglas fir (*Pseudotsuga menziesii* var. *viridis* and *glauca*) seedlings as affected by phosphorus supply. Funct Plant Biol. 2007:**34**(1):31–40. https://doi.org/10.1071/FP06157

Eisenhut M, Hoecker N, Schmidt SB, Basgaran RM, Flachbart S, Jahns P, Eser T, Geimer S, Husted S, Weber APM, et al. The plastid envelope CHLOROPLAST MANGANESE TRANSPORTER1 is essential for manganese homeostasis in Arabidopsis. Mol Plant. 2018:**11**(7): 955–969. https://doi.org/10.1016/j.molp.2018.04.008

Eroglu S, Meier B, von Wiren N, Peiter E. The vacuolar manganese transporter MTP8 determines tolerance to iron deficiency-induced chlorosis in Arabidopsis. Plant Physiol. 2016:**170**(2):1030–1045. https://doi.org/10.1104/pp.15.01194

Führs H, Behrens C, Gallien S, Heintz D, Van Dorsselaer A, Braun HP, Horst WJ. Physiological and proteomic characterization of manganese sensitivity and tolerance in rice (*Oryza sativa*) in comparison with barley (*Hordeum vulgare*). Ann Bot. 2010:**105**(7):1129–1140. https://doi.org/10.1093/aob/mcq046

Gamborg OL, Miller RA, Ojima K. Nutrient requirements of suspension cultures of soybean root cells. Exp Cell Res. 1968:**50**(1): 151–158. https://doi.org/10.1016/0014-4827(68)90403-5

Hasanuzzaman M, Alhaithloul HA, Parvin K, Borhannuddin Bhuyan MHM, Tanveer M, Moshin SM, Nahar K, Soliman MH, Al Mahmud J, Fujita M. Polyamine action under metal/metalloid stress: regulation of biosynthesis, metabolism, and molecular interactions. Int J Mol Sci. 2019:**20**(13):315. https://doi.org/10.3390/ijms20133215

Hawes CR, Juniper BE, Horne JC. Low and high-voltage electron microscopy of mitosis and cytokinesis in maize roots. Planta. 1981:**152**(5):397–407. https://doi.org/10.1007/BF00385355

Heyno E, Klose C, Krieger-Liszkay A. Origin of cadmiuminduced reactive oxygen species production: mitochondrial electron transfer versus plasma membrane NADPH oxidase. New Phytol. 2008:**179**(3): 687–699. https://doi.org/10.1111/j.1469-8137.2008.02512.x

Homann P. Studies on the manganese of the chloroplast. Plant Physiol. 1967:**42**(7):997–1007. https://doi.org/10.1104/pp.42.7.997

Iwai M, Roth MS, Niyogi KK. Subdiffraction-resolution live-cell imaging for visualizing thylakoid membranes. Plant J. 2018:**96**(1): 233–243. https://doi.org/10.1111/tpj.14021

Iwai M, Takizawa K, Tokutsu R, Okamuro A, Takahashi Y, Minagawa J. Isolation of the elusive supercomplex that drives cyclic electron flow in photosynthesis. Nature. 2010:**464**(7292):1210–1213. https://doi.org/10.1038/nature08885

Joliot P, Sellés J, Wollman FA, Verméglio A. High efficient cyclic electron flow and functional supercomplexes in *Chlamydomonas* cells. Biochim Biophys Acta Bioenerg. 2022:**1863**(8):148909. https://doi.org/10.1016/j.bbabio.2022.148909

Juniper BE, Hawes CR, Horne JC. The relationships between the dictyosomes and the forms of endoplasmic-reticulum in plant-cells with different export programs. Bot Gaz. 1982:**143**(2):135–145. https://doi.org/10.1086/337282

Kirchhoff H. Chloroplast ultrastructure in plants. New Phytol. 2019:**223**(2):565–574. https://doi.org/10.1111/nph.15730

Klughammer K, Schreiber U. An improved method, using saturating light pulses for the determination of photosystem I quantum yield via $P700^+$-absorbance changes at 830 nm. Planta. 1994:**192**(2): 261–268. https://doi.org/10.1007/BF01089043

Lane BG. Oxalate, germins, and higher-plant pathogens. IUBMB Life. 2002:**53**(2):67–75. https://doi.org/10.1080/15216540211474

Lanquar V, Ramos MS, Lelièvre F, Barbier-Brygoo H, Krieger-Liszkay A, Krämer U, Thomine S. Export of vacuolar manganese by AtNRAMP3 and AtNRAMP4 is required for optimal photosynthesis and growth under manganese deficiency. Plant Physiol. 2010:**152**(4): 1986–1999. https://doi.org/10.1104/pp.109.150946

Lei Y, Korpelainen H, Li C. Physiological and biochemical responses to high Mn concentrations in two contrasting *Populus cathayana* populations. Chemosphere. 2007:**68**(4):686–694. https://doi.org/10.1016/j.chemosphere.2007.01.066

Lešková A, Giehl RFH, Hartmann A, Fargašová A, von Wirén N. Heavy metals induce iron deficiency responses at different hierarchic and regulatory levels. Plant Physiol. 2017:**174**(3):1648–1668. https://doi.org/10.1104/pp.16.01916

Liang HZ, Zhu F, Wang RJ, Huang XH, Chu JJ. Photosystem II of *Ligustrum lucidum* in response to different levels of manganese exposure. Sci Rep. 2019:**9**(1):12568. https://doi.org/10.1038/s41598-019-48735-8

Liu K, Yu F, Chen M, Zhou Z, Chen C, Li MS, Zhu J. A newly found manganese hyperaccumulator – *Polygonum lapathifolium* Linn. Int J Phytoremediation. 2016:**18**(4):348–353. https://doi.org/10.1080/15226514.2015.1109589

Liu T, Zhu L, Zhang Z, Huang H, Zhang Z, Jiang L. Protective role of trehalose and heavy metal stress in *Aureobasidium subglaciale* F134. Sci Rep. 2017:**7**(1):1–9. https://doi.org/10.1038/s41598-017-15489-0

Marschner H. Mineral nutrition of higher plants. Ann Bot. 1995:**78**(4): 527–528. https://doi.org/10.1006/anbo.1996.0155

Mengel K, Kirkby EA. Principles of plant nutrition. Ann Bot. 1987:**93**(4): 479–480. https://doi.org/10.1093/aob/mch063

Mercer FV, Nittim M, Possigham JV. The effect of manganese deficiency on the structure of spinach chloroplasts. J Cell Biol. 1962:**15**(2):379–381. https://doi.org/10.1083/jcb.15.2.379

Millaleo R, Reyes-Díaz M, Alberdi M, Ivanov AG, Krol M, Hüner NP. Excess manganese differentially inhibits photosystem I versus II in *Arabidopsis thaliana*. J Exp Bot. 2013:**64**(1):343–354. https://doi.org/10.1093/jxb/ers339

Millaleo R, Reyes-Diaz M, Ivanov AG, Mora ML, Alberdi M. Manganese as essential and toxic element for plants: transport, accumulation and resistance mechanisms. J Plant Nutr Soil Sci. 2010:**10**(4):470–481. https://doi.org/10.4067/S0718-95162010000200008

Molins H, Michelet L, Lanquar V, Agorio A, Giraudat J, Roach T, Krieger-Liszkay A, Thomine S. Mutants impaired in vacuolar metal mobilization identify chloroplasts as a target for cadmium hypersensitivity in *Arabidopsis thaliana*. Plant Cell Environ. 2013:**36**(4): 804–817. https://doi.org/10.1111/pce.12016

Nable RO, Houtz RL, Cheniae GM. Early inhibition of photosynthesis during development of Mn toxicity in tobacco. Plant Physiol. 1988:**86**(4):1136–1142. https://doi.org/10.1104/pp.86.4.1136

Nishiyama Y, Allakhverdiev SI, Murata N. Protein synthesis is the primary target of reactive oxygen species in the photoinhibition of photosystem II. Physiol Plant. 2011:**142**(1):35–46. https://doi.org/10.1111/j.1399-3054.2011.01457.x

Peiter E, Montanini B, Gobert A, Pedas P, Husted S, Maathuis FJ, Blaudez D, Chalot M, Sanders D. A secretory pathway-localized cation diffusion facilitator confers plant manganese tolerance. Proc Natl Acad Sci U S A. 2007:**104**(20):8532–8537. https://doi.org/10.1073/pnas.0609507104

Pittman JK. Managing the manganese: molecular mechanisms of manganese transport and homeostasis. New Phytol. 2005:**167**(3): 733–742. https://doi.org/10.1111/j.1469-8137.2005.01453.x

Porra RJ, Scheer H. Towards a more accurate future for chlorophyll a and b determinations: the inaccuracies of Daniel Arnon's assay. Photosynth Res. 2019:**140**(2):215–219. https://doi.org/10.1007/s11120-018-0579-8

Requena L, Bornemann S. Barley (*Hordeum vulgare*) oxalate oxidase is a manganese-containing enzyme. Biochem J. 1999:**343**(1):185–190. https://doi.org/10.1042/bj3430185

Salomon E, Keren N. Manganese limitation induces changes in the activity and in the organization of photosynthetic complexes in the cyanobacterium *Synechocystis* sp. strain PCC 6803. Plant Physiol. 2011:**155**(1):571–579. https://doi.org/10.1104/pp.110.164269

Samecka-Cymerman A, Marczonek A, Kempers AJ. Bioindication of heavy metals in soil by liverworts. Arch Environ Contam Toxicol. 1997:**33**(2):162–171. https://doi.org/10.1007/s002449900238

Satoh K, Butler WL. Low temperature spectral properties of subchloroplast fractions purified from spinach. Plant Physiol. 1978:**61**(3): 373–379. https://doi.org/10.1104/pp.61.3.373

Schaffner W, Weissmann C. A rapid, sensitive, and specific method for the determination of protein in dilute solution. Anal Biochem. 1973:**56**(2):502–514. https://doi.org/10.1016/0003-2697(73)90217-0

Schmidt SB, Jensen PE, Husted S. Manganese deficiency in plants: the impact on photosystem II. Trends Plant Sci. 2016:**21**(7):622–632. https://doi.org/10.1016/j.tplants.2016.03.001

Sharma SS, Dietz K-J. The significance of amino acids and amino acid-derived molecules in plant responses and adaptation to heavy metal stress. J Exp Bot. 2006:**57**(4):711–726. https://doi.org/10.1093/jxb/erj073

Shimakawa G, Hanawa H, Wada S, Hanke GT, Matsuda Y, Miyake C. Physiological roles of flavodiiron proteins and photorespiration in the liverwort *Marchantia polymorpha*. Front Plant Sci. 2021:**19**(12): 668805. https://doi.org/10.3389/fpls.2021.668805

Singh S, Parihar P, Singh R, Singh VP, Prasad SM. Heavy metal tolerance in plants: role of transcriptomics, proteomics, metabolomics, and ionomics. Front Plant Sci. 2016:**8**:1143. https://doi.org/10.3389/fpls.2015.01143

St. Clair SB, Lynch JP. Differences in the success of sugar maple and red maple seedlings on acid soils are influenced by nutrient dynamics and light environment. Plant. Cell Environ. 2005:**28**(7):874–885. https://doi.org/10.1111/j.1365-3040.2005.01337.x

Strasser BJ. Donor side capacity of photosystem II probed by chlorophyll a fluorescence transients. Photosynth Res. 1997:**52**(2): 147–155. https://doi.org/10.1023/A:1005896029778

Streckaite S. Thylakoids: from molecular to membrane organisation. A spectroscopic and nanoscopic study of the photosynthetic apparatus [PhD thesis]. [Amsterdam]: Vrije Universiteit Amsterdam; 2021.

Subrahmanyam D, Rathore VS. Influence of manganese toxicity on photosynthesis in ricebean (*Vigna umbellata*) seedlings. Photosynthetica. 2001:**38**(3):449–453. https://doi.org/10.1023/A:1010998226323

Tanaka H, Sato M, Ogasawara Y, Hamashima N, Buchner O, Holzinger A, Toyooka K, Kodama Y. Chloroplast aggregation during the cold-positioning response in the liverwort *Marchantia polymorpha*. J Plant Res. 2017:**130**(6):1061–1070. https://doi.org/10.1007/s10265-017-0958-9

Van der Ent A, Baker AJM, Reeves RD, Pollard AJ, Schat H. Hyperaccumulators of metal and metalloid trace elements: facts and fiction. Plant Soil. 2013:**362**(1–2):319–334. https://doi.org/10.1007/s11104-012-1287-3

Vert G, Grotz N, Dédaldechamp F, Gaymard F, Guerinot ML, Briat JF, Curie C. IRT1, an Arabidopsis transporter essential for iron uptake from the soil and for plant growth. Plant Cell. 2002:**14**(6):1223–1233. https://doi.org/10.1105/tpc.001388

Zhang B, Zhang C, Liu C, Jing Y, Wang Y, Jin L, Yang L, Fu A, Shi J, Zhao F, et al. Inner envelope CHLOROPLAST MANGANESE TRANSPORTER 1 supports manganese homeostasis and phototrophic growth in Arabidopsis. Mol Plant. 2018:**11**(7):943–954. https://doi.org/10.1016/j.molp.2018.04.007

Supplemental

Messant *et al.*

Manganese excess and deficiency affect chloroplast structure and the photosynthetic apparatus in *Marchantia polymorpha*

Table S1. Chlorophyll and Mn content in thalli grown in Mn excess

sample	mg Chl/g DW	mg Mn/g DW	µg Mn/mg Chl	µg Mn in Chloroplast/ g DW
Crtl (agar)	14.6 ± 1.2	0.23	2.1	30.3 ± 0.10
30x	10.6 ± 1.7*	2.71	23.6	250.8 ± 0.09***
200x	8.8 ± 1.3*	23.12	178.7	1566.2 ± 0.06***

Chlorophyll content and dry weight was determined by three consecutive acetone extractions (N=6). Values of Mn content are the same as in Figs 1. 2 of the main manuscript. Mean value and SE is given. Stars indicate significant differences based on a Mann and Whitney test (* $p<0.05$. *** $p<0.001$). Chlorophyll content was determined according to Porra and Scheer (2019).

Table S2. List of 96 metabolites identified by GC-MS in *Marchantia polymorpha*

	Control		30X		200X		Starch+Mn		Starch-Mn	
Metabolites	Mean	SD	Mean	SD	Mean	SD	Mean	SD	Mean	SD
1.3-propanediol	0.011	0.000	0.012	0.000	0.011	0.000	0.011	0.001	0.011	0.001
1.6-anhydro-glucose	0.005	0.001	0.004	0.000	0.002	0.000	0.002	0.001	0.002	0.001
2.3-butanediol	0.005	0.001	0.005	0.000	0.004	0.000	0.005	0.000	0.004	0.000
2-hydroxypyridine	0.021	0.003	0.017	0.002	0.014	0.001	0.015	0.001	0.012	0.002
3.4-dihydroxymandelic acid	0.003	0.001	0.002	0.000	0.008	0.002	0.002	0.000	0.001	0.000
3-hydroxy-3-methylglutaric acid	0.005	0.000	0.004	0.000	0.003	0.000	0.003	0.001	0.002	0.001
4-hydroxypyridine	0.003	0.000	0.002	0.000	0.002	0.000	0.002	0.000	0.002	0.000
acetohydroxamic acid	0.030	0.004	0.028	0.003	0.034	0.006	0.030	0.005	0.034	0.006
allantoin	0.007	0.004	0.012	0.008	0.008	0.003	0.001	0.001	0.000	0.000
alpha ketoglutaric acid	0.029	0.004	0.006	0.006	0.000	0.000	0.011	0.010	0.010	0.009
arabinose	0.003	0.000	0.003	0.000	0.003	0.000	0.001	0.000	0.001	0.000
arbutin	0.002	0.000	0.002	0.000	0.002	0.000	0.001	0.000	0.000	0.000
aspartic acid	0.750	0.207	0.585	0.114	0.385	0.053	0.086	0.027	0.155	0.130
benzoic acid	0.003	0.000	0.003	0.000	0.003	0.000	0.003	0.000	0.003	0.000
Beta- alanine	0.004	0.001	0.003	0.001	0.004	0.001	0.001	0.000	0.001	0.001
beta-cyano-L-alanine	0.002	0.000	0.004	0.002	0.020	0.007	0.001	0.000	0.001	0.000
beta-sitosterol	0.004	0.001	0.004	0.001	0.004	0.001	0.002	0.001	0.002	0.001
citramalic acid	0.005	0.000	0.004	0.000	0.002	0.000	0.004	0.001	0.004	0.003
citric acid	0.285	0.010	0.295	0.017	0.037	0.005	0.289	0.063	0.247	0.091
citrulline	0.001	0.000	0.001	0.000	0.003	0.001	0.000	0.000	0.000	0.000
D-(+) trehalose	0.053	0.003	0.049	0.008	0.083	0.012	0.036	0.011	0.021	0.008
dehydroascorbic acid	0.007	0.001	0.004	0.000	0.005	0.001	0.001	0.000	0.001	0.000
D-glucose	0.239	0.035	0.252	0.068	0.218	0.058	0.411	0.233	0.234	0.081
D-glucose-6-phosphate	0.015	0.002	0.010	0.003	0.005	0.001	0.010	0.005	0.006	0.003
DL-isoleucine	0.060	0.015	0.061	0.010	0.046	0.014	0.028	0.006	0.023	0.009
D-malic acid	0.453	0.067	0.288	0.051	0.048	0.009	0.654	0.299	0.618	0.257
D-mannitol	0.013	0.010	0.009	0.007	0.009	0.006	0.023	0.022	0.024	0.019
D-mannose	0.005	0.000	0.004	0.000	0.004	0.000	0.045	0.042	0.002	0.000
dopamine (hydroxytyramine)	1.589	0.178	1.144	0.201	1.810	0.252	0.612	0.074	0.260	0.019
D-sorbitol	0.008	0.001	0.007	0.000	0.006	0.000	0.007	0.001	0.006	0.000
D-threitol	0.010	0.003	0.008	0.002	0.008	0.003	0.017	0.013	0.023	0.013
fructose	0.182	0.027	0.203	0.060	0.173	0.045	0.261	0.134	0.166	0.065
fructose 6-phosphate	0.008	0.001	0.006	0.001	0.003	0.001	0.005	0.002	0.003	0.001
fumaric acid	0.180	0.031	0.126	0.030	0.022	0.002	0.070	0.008	0.067	0.028

galactonic acid	0.001	0.000	0.001	0.000	0.000	0.000	0.092	0.088	0.009	0.005
galacturonic acid	0.004	0.000	0.004	0.001	0.008	0.001	0.013	0.008	0.005	0.003
gluconic acid	0.003	0.000	0.003	0.000	0.002	0.000	0.002	0.001	0.002	0.000
glyceric acid	0.016	0.001	0.014	0.001	0.006	0.001	0.016	0.005	0.013	0.006
glycerol	0.014	0.001	0.013	0.001	0.011	0.001	0.011	0.002	0.010	0.002
glycerol 1-phosphate	0.021	0.002	0.016	0.002	0.011	0.002	0.010	0.003	0.007	0.001
glycine	0.007	0.001	0.006	0.001	0.006	0.001	0.002	0.000	0.003	0.001
glycolic acid	0.013	0.001	0.015	0.001	0.014	0.001	0.009	0.000	0.009	0.002
L-(+) lactic acid	0.012	0.001	0.016	0.004	0.012	0.001	0.014	0.003	0.012	0.002
L-alanine	0.010	0.002	0.010	0.002	0.004	0.001	0.003	0.001	0.003	0.002
L-asparagine	0.372	0.021	0.461	0.074	0.478	0.085	0.059	0.036	0.108	0.095
leucrose	0.003	0.000	0.004	0.001	0.005	0.001	0.001	0.000	0.001	0.000
L-glutamic acid	2.642	0.178	2.568	0.065	2.024	0.148	1.143	0.298	1.078	0.449
L-glutamine	0.107	0.013	0.080	0.022	0.202	0.078	0.023	0.019	0.023	0.022
L-homoserine	0.002	0.000	0.002	0.000	0.002	0.000	0.001	0.000	0.000	0.000
L-leucine	0.004	0.001	0.007	0.001	0.007	0.001	0.007	0.002	0.006	0.001
L-lysine	0.003	0.001	0.002	0.001	0.004	0.002	0.001	0.000	0.000	0.000
L-methionine sulfoxide	0.001	0.000	0.001	0.000	0.001	0.000	0.000	0.000	0.000	0.000
L-norleucine	0.059	0.013	0.066	0.015	0.043	0.015	0.025	0.007	0.018	0.005
L-ornithine	0.003	0.001	0.003	0.000	0.007	0.001	0.001	0.000	0.001	0.001
L-proline	0.010	0.002	0.011	0.001	0.009	0.001	0.004	0.000	0.005	0.002
L-serine	0.625	0.028	0.617	0.037	0.616	0.113	0.157	0.040	0.138	0.069
L-threonine	0.080	0.008	0.070	0.010	0.042	0.006	0.028	0.007	0.024	0.010
L-threonine	0.025	0.005	0.036	0.018	0.070	0.019	0.005	0.001	0.004	0.000
L-tryptophan	0.043	0.019	0.036	0.017	0.134	0.035	0.005	0.002	0.003	0.002
L-valine	0.046	0.007	0.054	0.014	0.060	0.013	0.026	0.005	0.022	0.006
maltose	0.002	0.001	0.003	0.000	0.002	0.001	0.084	0.067	0.022	0.011
myo-inositol	0.042	0.003	0.041	0.001	0.031	0.003	0.022	0.005	0.018	0.004
myristic acid	0.005	0.000	0.004	0.001	0.004	0.000	0.005	0.001	0.004	0.000
N-ethylglycine	0.849	0.030	0.888	0.093	1.101	0.039	0.755	0.089	0.743	0.053
N-methylalanine	0.021	0.002	0.670	0.237	1.101	0.038	0.607	0.210	0.743	0.053
norepinephrine (noradrenalin)	0.008	0.002	0.006	0.002	0.020	0.003	0.007	0.003	0.003	0.001
norvaline	0.086	0.015	0.092	0.015	0.069	0.020	0.047	0.008	0.044	0.019
oleic acid	0.005	0.000	0.004	0.001	0.004	0.000	0.004	0.001	0.005	0.001
O-phosphocolamine	0.005	0.001	0.003	0.001	0.002	0.000	0.002	0.001	0.001	0.001
oxalic acid	0.024	0.004	0.023	0.002	0.018	0.003	0.013	0.002	0.013	0.005
palmitic acid	0.146	0.019	0.134	0.025	0.140	0.025	0.164	0.034	0.146	0.021
phenanthrene	0.007	0.001	0.006	0.001	0.007	0.001	0.006	0.000	0.007	0.001
Phenylalanine	0.018	0.002	0.019	0.002	0.009	0.002	0.006	0.003	0.005	0.001
phosphoric acid	0.615	0.138	0.318	0.124	0.093	0.019	0.589	0.176	0.510	0.280
phytol	0.050	0.002	0.046	0.006	0.089	0.024	0.016	0.007	0.011	0.005
porphine	0.032	0.003	0.030	0.002	0.039	0.002	0.029	0.001	0.024	0.001
putrescine	0.003	0.001	0.002	0.000	0.008	0.001	0.000	0.000	0.001	0.000
pyruvic acid	0.006	0.001	0.005	0.000	0.003	0.000	0.001	0.001	0.002	0.001
rhamnose	0.004	0.000	0.004	0.001	0.008	0.001	0.002	0.000	0.001	0.000
shikimic acid	0.209	0.043	0.168	0.031	0.068	0.010	0.265	0.106	0.127	0.074
stearic acid	0.076	0.017	0.073	0.021	0.087	0.019	0.098	0.022	0.098	0.023

stigmasterol	0.022	0.003	0.023	0.003	0.021	0.002	0.009	0.002	0.007	0.002
succinic acid	0.074	0.006	0.080	0.008	0.040	0.007	0.093	0.019	0.096	0.041
Sucrose	2.261	0.326	2.004	0.232	1.473	0.293	1.571	0.421	1.042	0.277
tagatose	0.005	0.000	0.004	0.000	0.074	0.071	0.079	0.046	0.085	0.084
talose	0.005	0.000	0.004	0.000	0.004	0.000	0.004	0.001	0.002	0.000
threonic acid	0.102	0.010	0.120	0.016	0.098	0.008	0.082	0.008	0.062	0.010
Threonic acid-1.4-lactone	0.007	0.001	0.008	0.001	0.016	0.003	0.004	0.000	0.003	0.001
trans-aconitic acid	0.475	0.054	0.362	0.049	0.031	0.006	0.407	0.151	0.324	0.151
tyramine	0.073	0.006	0.074	0.015	0.106	0.020	0.076	0.036	0.021	0.012
tyrosine	0.044	0.007	0.043	0.007	0.052	0.013	0.018	0.009	0.011	0.008
uracil	0.003	0.001	0.003	0.000	0.002	0.000	0.002	0.000	0.002	0.000
urea	0.011	0.002	0.010	0.002	0.003	0.001	0.005	0.002	0.002	0.001
xylitol	0.005	0.000	0.003	0.001	0.001	0.000	0.001	0.000	0.001	0.000
xylose	0.004	0.000	0.004	0.000	0.002	0.000	0.002	0.000	0.001	0.000
xylulose	0.007	0.000	0.005	0.000	0.003	0.000	0.004	0.001	0.003	0.001

List of 96 metabolites identified and quantified in plants grown in Agar Control. 30X. 200X. Starch Control and Starch-Mn condition. N=4 biological replicates. $P<0.05$ for all values according to two-way ANOVA test.

Table S3. Metabolites significantly decreased in Starch condition compared to Agar Control in *Marchantia polymorpha*

	Agar Control		Starch (+/-)	
Metabolites	Mean	SD	Mean	SD
1.6-anhydro-glucose	0.005	0.001	0.002	0.001
2-hydroxypyridine	0.021	0.003	0.013	0.003
3.4-dihydroxymandelic acid	0.003	0.001	0.001	0.001
arabinose	0.003	0.000	0.001	0.001
arbutin	0.002	0.000	0.001	0.000
aspartic acid 2	0.750	0.207	0.120	0.177
beta-cyano-L-alanine	0.002	0.000	0.001	0.000
citrulline 2	0.001	0.000	0.000	0.000
D-(+) trehalose	0.053	0.003	0.029	0.020
dopamine (hydroxytyramine)	1.589	0.178	0.436	0.213
fumaric acid	0.180	0.031	0.068	0.038
glycerol 1-phosphate	0.021	0.002	0.008	0.005
L-alanine 1	0.010	0.002	0.003	0.003
L-asparagine 2	0.372	0.021	0.083	0.136
leucrose	0.003	0.000	0.001	0.001
L-glutamic acid 3 (dehydrated)	2.642	0.178	1.110	0.707
L-glutamine 1	0.107	0.013	0.023	0.038
L-homoserine 2	0.002	0.000	0.000	0.000
L-lysine 2	0.003	0.001	0.000	0.001
L-methionine sulfoxide 3	0.001	0.000	0.000	0.000
L-norleucine 1	0.059	0.013	0.022	0.012
L-serine 1	0.625	0.028	0.148	0.105
L-threonine 1	0.080	0.008	0.026	0.016
L-valine 2	0.046	0.007	0.024	0.010
myo-inositol	0.042	0.003	0.020	0.009
N-methylalanine	0.021	0.002	0.675	0.293
O-phosphocolamine	0.005	0.001	0.002	0.001
Phenylalanine 1	0.018	0.002	0.005	0.004
phytol 1	0.050	0.002	0.013	0.012
putrescine	0.003	0.001	0.000	0.001
pyruvic acid	0.006	0.001	0.001	0.002
rhamnose 1	0.004	0.000	0.002	0.001

stigmasterol	0.022	0.003	0.008	0.005
talose 1	0.005	0.000	0.003	0.002
threonic acid	0.102	0.010	0.072	0.019
Threonic acid-1.4-lactone	0.007	0.001	0.003	0.002
tyrosine 2	0.044	0.007	0.015	0.016
urea	0.011	0.002	0.004	0.003
xylitol	0.005	0.000	0.001	0.001
xylose 2	0.004	0.000	0.002	0.001
xylulose	0.007	0.000	0.003	0.001

List of 41 metabolites significantly different between Agar Control and both Starch Control and Starch-Mn conditions combined ($p<0.05$). The column Starch (+/-) represents the mean of all starch samples (Starch Control and Starch-Mn). A statistical test ANOVA 2 was conducted. Absolute values represent the mean of 4 biological replicates for each condition.

Figure S1. Metabolite analysis in *M. polymorpha* grown in Mn excess condition.

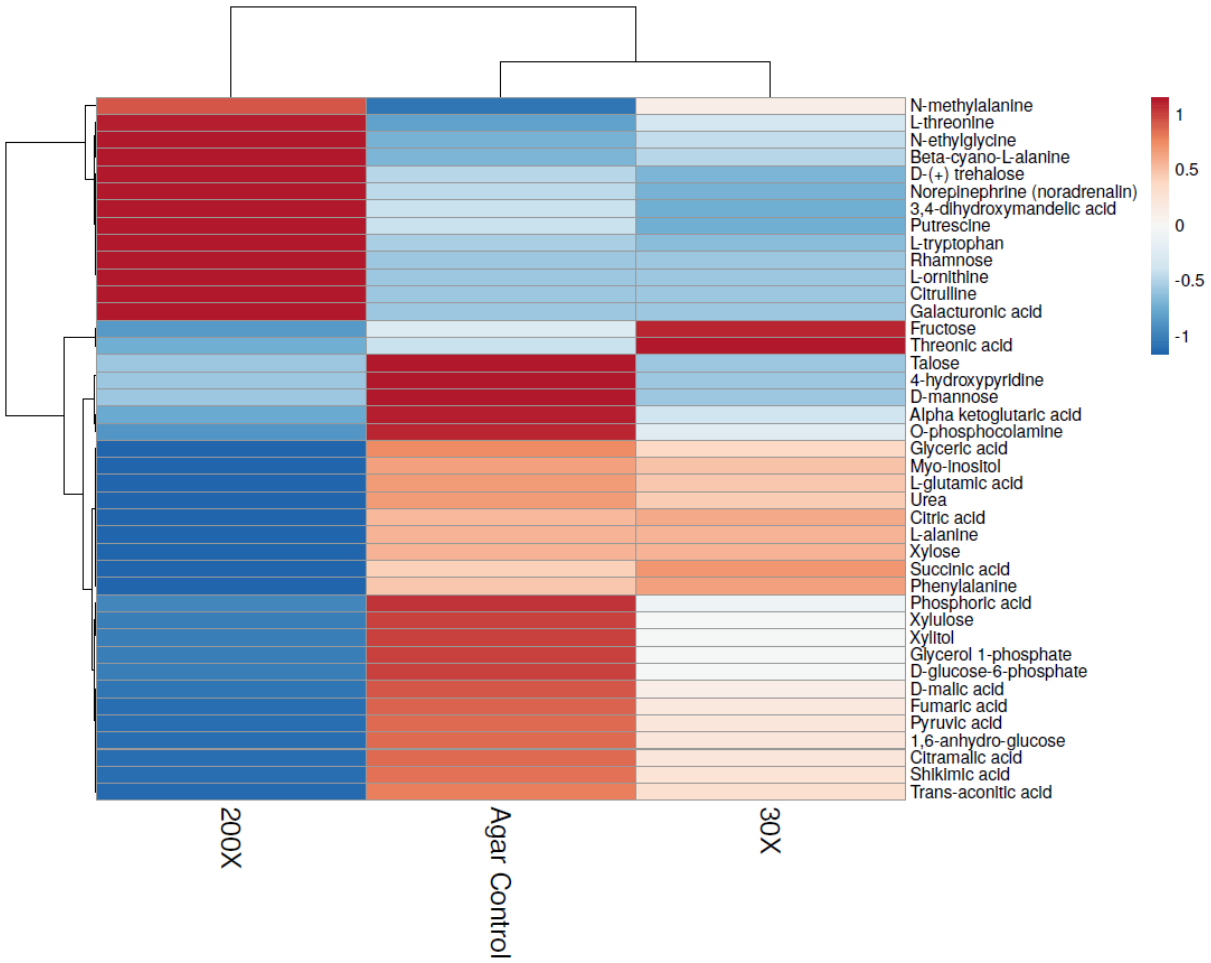

Heatmap showing significantly different metabolites in whole thalli grown under Control. 30X and 200X conditions. This figure is a result of an ANOVA 2 statistical test. The color scale represents the changes between the three conditions taking into account the maximum and the minimum value for a given metabolite in each condition.

Figure S2. Estimation of the chloroplast size under the different growth conditions

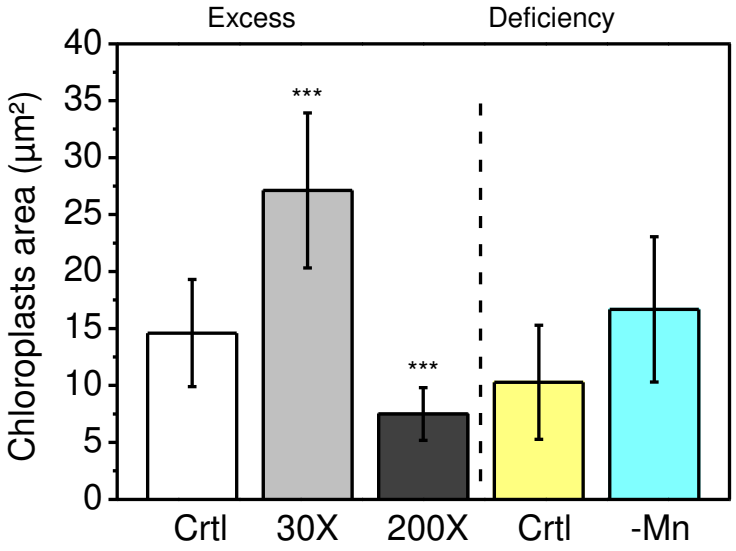

Area of the chloroplasts was determined from super-resolution fluorescence microscopy images using ImageJ. Number of images analyzed: Crtl agar: N=12, 30X: N=12; 200X: N=23; Crtl starch: N=25, starch –Mn : N=7. Mean value and SD are given. Stars indicate significant differences, compared to the control, based on a Mann and Whitney test (*** $p<0.001$).

Figure S3. Chlorophyll fluorescence at room temperature in *M. polymorpha* grown in control and Mn excess conditions

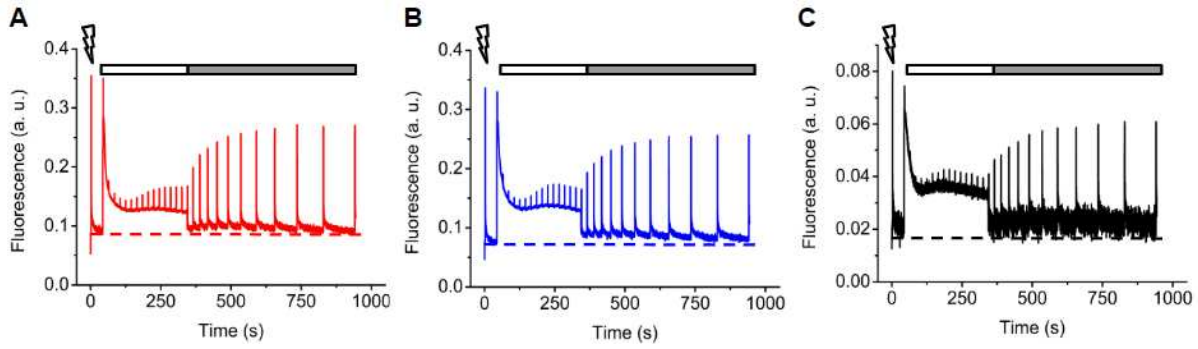

Induction and recovery of chlorophyll measured on thalli grown in Control (red), 30X (blue) and 200X (black) conditions. After 5 min dark adaptation, thalli were exposed to a measuring light to determine the minimum fluorescence level (dashed lines) and to a saturating flash to obtain the maximum fluorescence level. Actinic light (50 µmol photons m^{-2} s^{-1}) was applied for 5 min (white bar). Recovery in the dark was followed (grey bar). Representative curves are shown (N=3).

Figure S4. Photoinhibition of photosystem II in *M. polymorpha* grown in control and Mn excess condition in the presence and absence of lincomycin

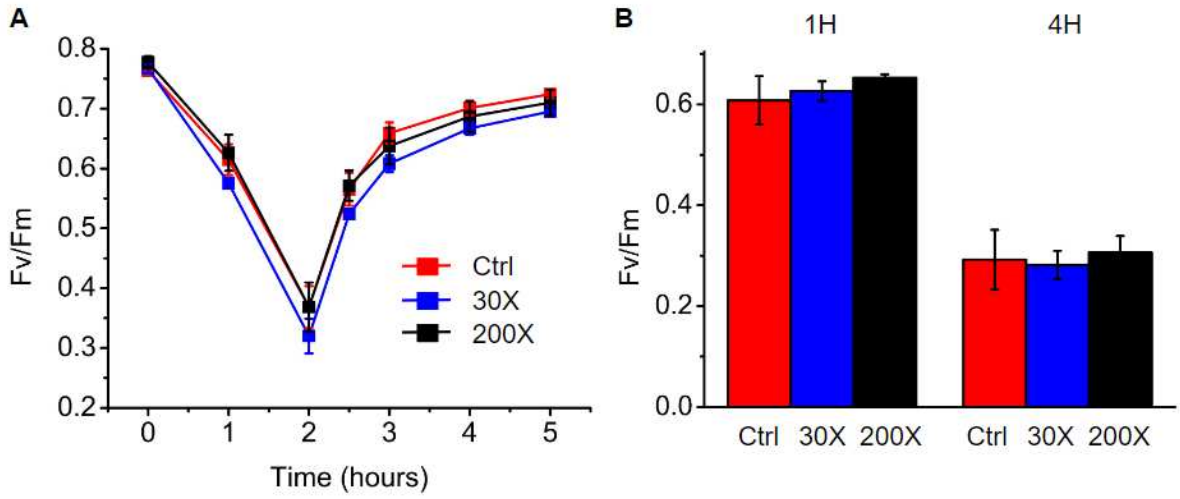

(A) Photoinhibition without lincomycin was measured in thalli cultivated in Control (red), 30X (blue) and 200X (black) conditions. Fv/Fm was followed on plants exposed to a strong light (800 µmol photons $m^{-2}s^{-1}$) for 2h and during the recovery at room light. **(B)** Fv/Fm was recorded during photoinhibition of thalli preincubated with lincomycin for 4h. Mean and SD are shown (N=3, biological replicates).

Figure S5. Chlorophyll fluorescence (Fv/Fm) in *M. polymorpha* grown on starch plates in low Mn concentrations

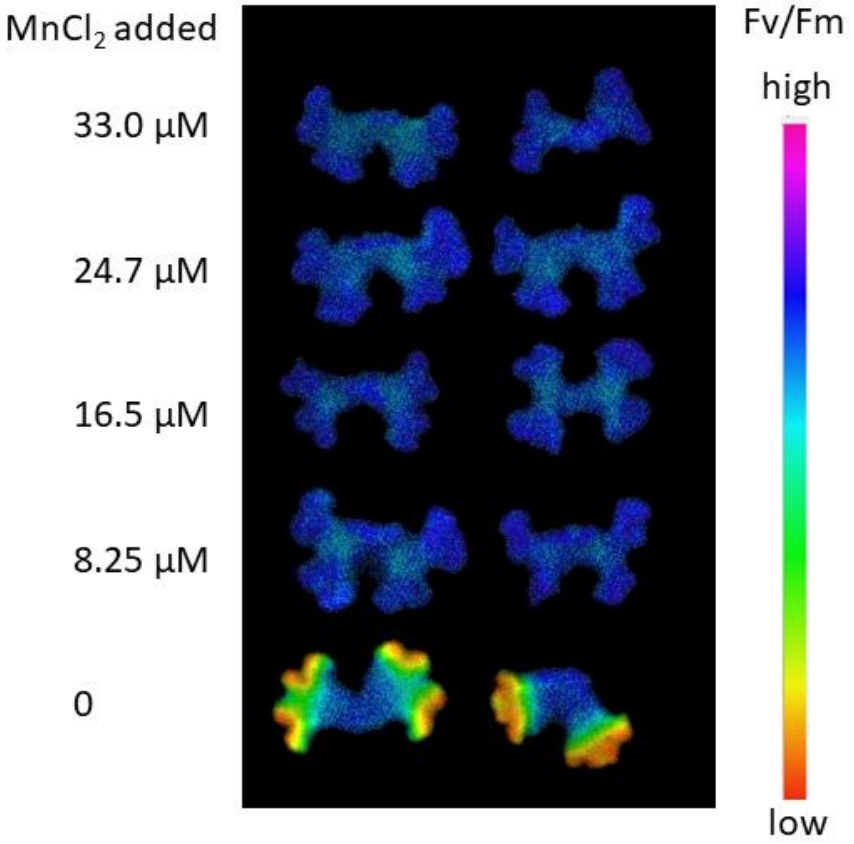

Thalli were grown for 2 weeks on standard medium before transferred for 1 week to starch media with the addition of the indicated Mn concentration. After 1 week growth on starch medium, thalli were dark-adapted for 5 min before Fv/Fm values were determined using an Imaging-PAM (Walz, Effeltrich, Germany). Right: Colour scale corresponds to Fv/Fm value between 1 (pink/high) and 0 (red/low).

Figure S6. qN determination in the presence of lincomycin in *Marchantia polymorpha* grown on starch in control and Mn-deficient conditions

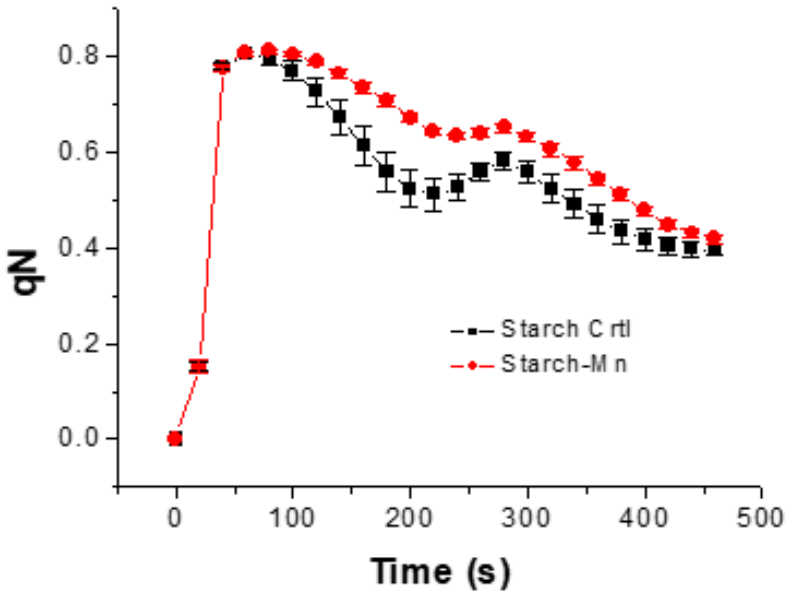

Thalli were incubated for 4 h in lincomycin solution (1g L^{-1}) prior to the measurements. After 5 min dark adaptation. thalli were exposed to measuring light and to saturating flashes. Actinic light (55 µmol quanta $m^{-2}s^{-1}$) was applied during 5 min. Mean and SD are shown (N=4).

Chapter 3: Study of cyclic electron transport under Mn deficiency in *Marchantia polymorpha*

3.1. Introduction

Plants are continuously exposed to changing environmental conditions and to cope with them they have developed certain regulatory mechanisms and some alternative electron pathways. Cyclic electron transport (CET) is one of them and already detailed in Chapter 1 (General Introduction). Based on our previous findings (Article 1) it is known that CET is favored under manganese (Mn) deficiency. In this study, I mainly investigated the in vivo redox changes of P700 and plastocyanin (Pc) under Mn deficiency in *Marchantia* using KLAS-NIR spectrophotometer. Further, I showed that $P700^+$ and PC^+ re-reduction in the dark are faster under Mn deficiency and this was interpreted as a sign of enhanced CET. With the use of BN-PAGE, I further looked into the possible supercomplex formation under Mn deficiency and the preliminary results suggests that maybe there is some sort of supercomplex formation around PSI.

3.2. Article 2: Manganese deficiency alters photosynthetic electron transport in *Marchantia polymorpha* (published)

I performed all experiments (KLAS-NIR measurements, western blotting, BN-PAGE, X-ray fluorescence imaging), including data analysis, writing and critical reading of manuscript.

Plant Physiology and Biochemistry 215 (2024) 109042

Contents lists available at ScienceDirect

Plant Physiology and Biochemistry

journal homepage: www.elsevier.com/locate/plaphy

Manganese deficiency alters photosynthetic electron transport in *Marchantia polymorpha*

Umama Hani, Anja Krieger-Liszkay *

Université Paris-Saclay, Institute for Integrative Biology of the Cell (I2BC), CEA, CNRS, 91198, Gif-sur-Yvette cedex, France

ARTICLE INFO

Handling Editor: Dr. Mario De Tullio

Keywords:
Cyclic electron transport
In vivo absorption spectroscopy
Marchantia polymorpha
Photosystem I
Plastocyanin

ABSTRACT

Manganese (Mn) is considered as an essential element for plant growth. Mn starvation has been shown to affect photosystem II, the site of the Mn_4CaO_5 cluster responsible for water oxidation. Less is known on the effect of Mn starvation on photosystem I. Here we studied the effects of Mn deficiency *in vivo* on redox changes of P700 and plastocyanin (Pc) in the liverwort *Marchantia polymorpha* using the KLAS-NIR spectrophotometer. Far-red illumination is used to excite preferentially photosystem I, thus facilitating cyclic electron transport. Under Mn starvation, we observed slower oxidation of P700 and a decrease in the Pc signal relative to P700. The lower Pc content under Mn deficiency was confirmed by western blots. Re-reduction kinetics of $P700^+$ and Pc^+ were faster in Mn deficient thalli than in the control. The above findings show that the kinetics studied under Mn deficiency not only depend on the number of available reductants but also on how quickly electrons are transferred from stromal donors via the intersystem chain to Pc^+ and $P700^+$. We suggest that under Mn deficiency a structural reorganization of the thylakoid membrane takes place favoring the formation of supercomplexes between ferredoxin, cytochrome b_6f complex, Pc and photosystem I, and thus an enhanced cyclic electron transport.

1. Introduction

Manganese (Mn) is one of the essential trace elements for plant growth and development. Mn is known as an indispensable constitutive element of the Mn_4O_5Ca cluster in photosystem II (PSII), where it oxidizes water molecules and thus provides the necessary electrons for oxygenic photosynthesis (Shen, 2015; Alejandro et al., 2020). Plants require an optimal supply of Mn to maintain homeostatic balance (Alejandro et al., 2020). Besides its role in PSII, Mn has an important role as co-factor of various enzymes including catalase (MnCAT), superoxide dismutase (MnSOD), decarboxylases of tricarboxylic acid (TCA) cycle (Marschner, 2011; Corpas et al., 2017) and in other metabolic processes (Schmidt et al., 2016; Bhat et al., 2020). Mn deficiency strongly impacts photosynthesis, mainly PSII, accompanied by subtle perturbation in chloroplast ultrastructure (Papadakis et al., 2007; Messant et al., 2023). Initial signs of Mn deficiency typically appear first in younger leaves, which includes paleness accompanied by interveinal chlorosis (Schmidt et al., 2016). However, symptoms of Mn deficiency vary depending on the species (Homann, 1967).

Contrary to the research done on effects of Mn deficiency on PSII, very limited information concerning its consequences on PSI is available. We have previously studied the effects of Mn excess and deficiency in liverwort *Marchantia polymorpha*, for which we established the conditions for Mn concentration for optimal growth and a condition to induce Mn deficiency (Messant et al., 2023). With well-explored taxonomy and morphology, *M. polymorpha* stands as a complex thalloid liverwort (Bowman, 2016), residing mainly at the marginal area between aquatic and land environments. Today's use of *M. polymorpha* as a model plant is primarily based on its genomic simplicity (Bowman et al., 2016; Bowman, 2022) and ease of propagation (Naramoto et al., 2022). In our recent study, we investigated the effect of Mn deficiency on photosynthesis in *M. polymorpha*. Under Mn starvation, a change in the ratio of PSI/PSII capacities was observed. Moreover, we also showed changes in structural organization of thylakoid membrane. Most importantly for the present study, less limitation of electron donation to $P700^+$ in actinic light was observed under Mn deficiency. We interpreted the difference in stoichiometry of PSI/PSII and the lower donor-side limitation of PSI as an increase in cyclic electron transport (CET) under Mn starvation (Messant et al., 2023). CET is one of the alternative electron pathways that comes into play under certain physiological conditions, especially upon stress (Sunil et al., 2019) with the main aim of balancing the ATP/NADPH ratio. CET involves cycling of

* Corresponding author.
E-mail address: anja.liszkay@i2bc.paris-saclay.fr (A. Krieger-Liszkay).

https://doi.org/10.1016/j.plaphy.2024.109042
Received 29 March 2024; Received in revised form 7 August 2024; Accepted 11 August 2024
Available online 16 August 2024

electrons around PSI, generating a proton gradient and thereby ATP without generating NADPH (for recent reviews see e.g., Nawrocki et al., 2019; Takahashi, 2022).

The current study aims to further explore the effects of Mn deficiency on PSI in *M. polymorpha*, with the main objective of investigating changes in oxido-reduction of P700 and plastocyanin (Pc) using KLAS-NIR spectrophotometer. KLAS-NIR is a pulse-amplitude modulation spectrophotometer that has been developed by Klughammer and Schreiber (2016) to study deconvoluted signals in the near infra-red of P700 and Pc *in vivo*, i.e. in thalli in our case. We particularly have chosen the approach of inducing CET by irradiating thalli with far-red (FR) light, thus facilitating the measurement of CET. FR light is preferentially absorbed by PSI and maximally oxidizes P700 to the extent of 80–90% (Chow et al., 2012; Pettai et al., 2005).

2. Materials and methods

2.1. Plant material

Gemmae from Takaragaike (Tak-1) male accession of *M. polymorpha* were cultured for two weeks under a light-dark cycle (16 h light, 22 °C, 100 μmol photons $m^{-2}s^{-1}$, white fluorescent lamp; 8 h-dark, 20 °C) on one-half-strength Gamborg's B5 media (GB5) with 1% Agar (Gamborg et al., 1968). To create Mn deficiency, thalli were transferred to ½ GB5 media containing 6% starch with or without addition of 33 μM $MnCl_2$ for a week prior to performing desired experiments (Messant et al., 2023).

2.2. Thylakoids isolation and immunoblots

Thalli from three-weeks old *M. polymorpha* were harvested and after careful washing with water to remove starch, were grounded in a buffer containing 0.33 M sorbitol, 1 mM EDTA, 1 mM $MgCl_2$, 50 mM KCl, 25 mM MES-KOH (pH 6.1). The resulting slurry was filtered through two layers of cheese cloth and one layer of miracloth. After centrifugation, the pellet was re-suspended in 25 mM HEPES-KOH (pH 6.7), 0.33 M sorbitol, 1 mM EDTA, 1 mM $MgCl_2$, 50 mM KCl and washed twice. Finally, the isolated thylakoids were re-suspended and stored in 25 mM HEPES-KOH (pH 7.6), 0.33 M sorbitol, 1 mM $MgCl_2$, 50 mM KCl. All centrifugation steps were performed at 3,000×*g* for 3 min at 4 °C. Chlorophyll content was measured according to Arnon (1949).

For immunodetection, proteins from the thylakoids extract were separated using 12% (w/v) sodium dodecyl polyacrylamide gel electrophoresis (SDS-PAGE). After electrophoresis, proteins were transferred to nitrocellulose membrane (Amersham™ Protran, 0.45 μm pore size) and incubated with primary antibodies (Pc, PsaC, PetB and cytb_{559}) at room temperature in TBS-T (0.1 % Tween-20 (v/v), containing 5% non-fat milk powder). After washing with TBS-T, the membranes were decorated with anti-rabbit peroxidase-linked secondary antibodies. Bands were visualized with enhanced chemiluminescence (ChemiDoc™ Touch Imaging System, Bio-Rad) after 1–2 min incubation with ECL solution (Amersham ECL Prime Western Blotting Detection Reagent). Antibodies directed against Pc (AS06 141), PsaC (AS10 939), PetB (AS18 4169) were purchased from Agrisera (Vännäs, Sweden), antibodies directed against cytb_{559} were kindly provided by P. Beyer, Freiburg University, Germany. Densitometric analysis of blots was performed with image J (https://imagej.nih.gov/ij/).

2.3. RT-PCR

Plant Mini RNeasy kit (Qiagen, Venlo, Netherlands) was used for total RNA extraction, and samples were homogenized with RLT lysis buffer. RT reactions were done with the SuperScript IV Reverse Transcriptase kit (Invitrogen, Carlsbad, USA). cDNA was diluted 4 times with LightCycler 480 SYBR Green I Master (Roche, Penzberg, Germany) reaction medium (1X final concentration) containing 2.5 μM of each primer (Table S1). The mRNA levels of plastocyanin (Mp4g02720.1_Sequence extracted from "MarpolBase"; genome database for *Marchantia*) were normalized to reference housekeeping gene ACTIN 1 (*MpACT1*: Mp6g10990).

2.4. Chlorophyll fluorescence and P700 measurements

Chlorophyll fluorescence and P700 absorbance were measured using a Dual-PAM-100 fluorometer (Walz, Effeltrich, Germany). Effective quantum yield of PSII: Y(II) = (Fm'-F)/Fm' and non-photochemical quenching: qN=(Fm–Fm')/Fm, were measured as a function of light intensity. Each actinic light intensity was applied for 180 s. For P700 measurements, dark adapted thalli were exposed to three different actinic light intensities (64, 175 and 803 μmol quanta $m^{-2}s^{-1}$) and far-red light followed by a saturating flash at the end of far-red light period.

2.5. KLAS-NIR measurements

All the measurements were made with kinetic-LED-array-spectrophotometer (KLAS) (Walz, Effeltrich, Germany) that utilizes pulse amplitude modulation within the NIR-Infrared (NIR) spectral range and operates in the dual-wavelength difference mode (785–840, 810–870, 870–970 and 795–970 nm) (Schreiber and Klughammer, 2016; Schreiber, 2017). Technical details of the KLAS-NIR spectrophotometer and the principle behind the deconvolution of P700, Pc and Fd are explained in detail by Klughammer and Schreiber (2016). All measurements were done under "Slow kinetics window". Transmittance changes were recorded with high-resolution trigger run file called "NIR max" along with data acquisition every ms (Fig. 2). Kinetics recording and illumination steps were fully automated. NIR max protocol includes three main components. After dark adaptation, the sample was illuminated with Actinic Light (AL10, 572 μmol quanta $m^{-2}s^{-1}$) for 3 s and 30 ms pulse of light at saturating light intensity (6500 μmol quanta $m^{-2}s^{-1}$) was applied during illumination with AL. The second component involves switching on the FR light (FR18) for 10 s that lead to almost maximal oxidation of P700 and Pc. At the end, a 300 ms saturating flash was given to fully induce oxidation of P700 and Pc (P700 and Pc MAX values). Kinetics of P700 oxidation (Fig. 4) and $P700^+$ and Pc^+ re-reduction (Figs. 5 and 6) were studied with FR-on (FR10) and FR-off respectively.

2.6. Transmission electron microscopy

About 1 mm strips of thalli were cut and fixed with glutaraldehyde/paraformaldehyde fixative and later infused with 1% osmium (w/v) and 1.5% potassium hexacyanoferrate (w/v) en bloc staining protocol as described (Hawes et al., 1981; Juniper et al., 1982); EM UC6 ultramicrotome (Leica microsystems) was used for cutting 70 mm thick sections to be deposited on to copper grids. Ultrathin sections were stained with 2% uranyl acetate (w/v) (Merck) and Reynolds lead citrate according to standard procedures. Grids were examined under a JEOL 1400 TEM operating at 80 kV (JEOL, http://www.jeol.com). Images were acquired using a 9-megapixel high-speed camera (RIO9; Gatan, http://www.gatan.com) and processed using Digital Micrograph (Gatan).

3. Results

In the current study, we aimed to investigate the effect of Mn deficiency on photosynthetic electron transport in *M. polymorpha* in more detail compared with the study by Messant et al. (2023). Fig. 1 shows that Y(II) was lower and qN was higher in Mn-deficient thalli than in thalli grown in control conditions. In addition to PSII, P700 oxidation is also affected under Mn deficiency. At light intensities higher than growth light, P700 oxidation was slower and a lower steady state oxidation level was reached at an actinic red light intensity of 175 μmol quanta $m^{-2}s^{-1}$. We have reported previously that limitation of electron donation to PSI was lower in Mn-deficient thalli than in thalli grown in

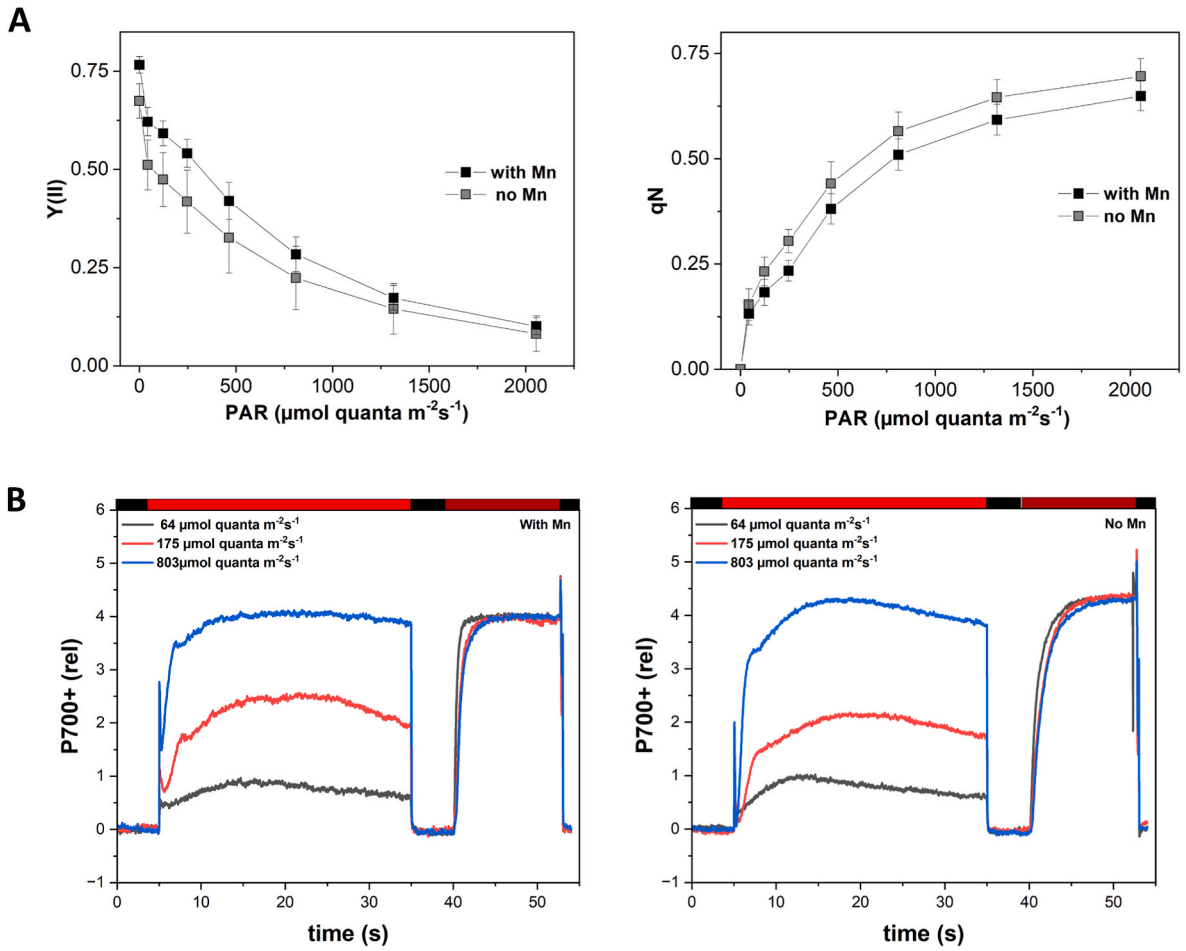

Fig. 1. Chlorophyll fluorescence and P700 measurements in response to different light intensities in *Marchantia* thalli grown in control and Mn-deficient conditions. Effective quantum yield of PSII (YII) and non-photochemical quenching (qN) measured as function of light intensity. Data are represented as the mean ± SD of 5 biological replicates (A). For P700 oxidation measurements, red actinic light (803, 175 and 64 µmol quanta $m^{-2}s^{-1}$) and far-red light were given as indicated in the coloured bars. To get the maximum oxidation amplitude of P700, a saturation flash was given at the end of the far-red illumination. Measurements with three independent biological replicates were performed and representative traces are shown (B).

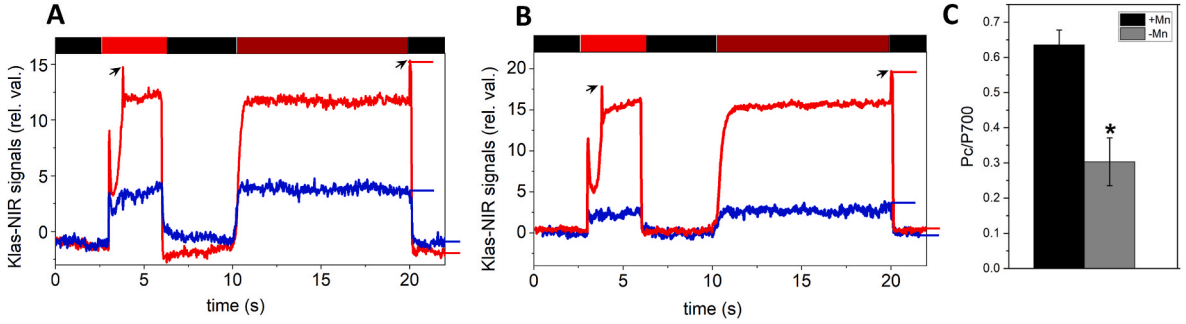

Fig. 2. Redox changes in P700 and Plastocyanin in *Marchantia* thalli grown in control and Mn-deficient conditions. Changes in the redox states of P700 (red) and plastocyanin (Pc; blue) in thalli grown in control conditions (+Mn; **A**) and in Mn-deficiency (-Mn**; B**) upon illumination with red actinic light (570 µmol quanta $m^{-2}s^{-1}$) and far-red light. Saturation flashes were applied at 4 s and 20 s as indicated by black arrows. Horizontal marks indicate the maximum intensity levels (under far-red light) and the zero levels (in the dark) for P700 and Pc. Top of the figure indicates the illumination protocol (red = Actinic light, dark red = Far-red light). Figures A, B show representative traces. The mean absorption values of the calculated ratio (Pc/P700) for + Mn and –Mn are given in **C**, 3 independently grown biological replicates, n = 9. Statistically significance (*$P < 0.05$) was assessed by Student's *t*-test.

control conditions while the capacity of PSII electron transport was lowered (Messant et al., 2023). To study oxidation of P700 and Pc in parallel, we used the KLAS NIR spectrophotometer. The kinetics shown in Fig. 2 were obtained using the "NIR-Max" protocol of KLAS NIR spectrophotometer. Changes in the redox states of P700 and Pc in response to red-actinic and far-red light are shown for 3-weeks old thalli of *Marchantia polymorpha*. The maximum oxidation levels for P700 and Pc were determined through a saturation flash following the far-red light. Calculated "relative" values indicate the amount of photo-oxidized (and reduced) P700 and Pc. Compared with $P700^{+}$

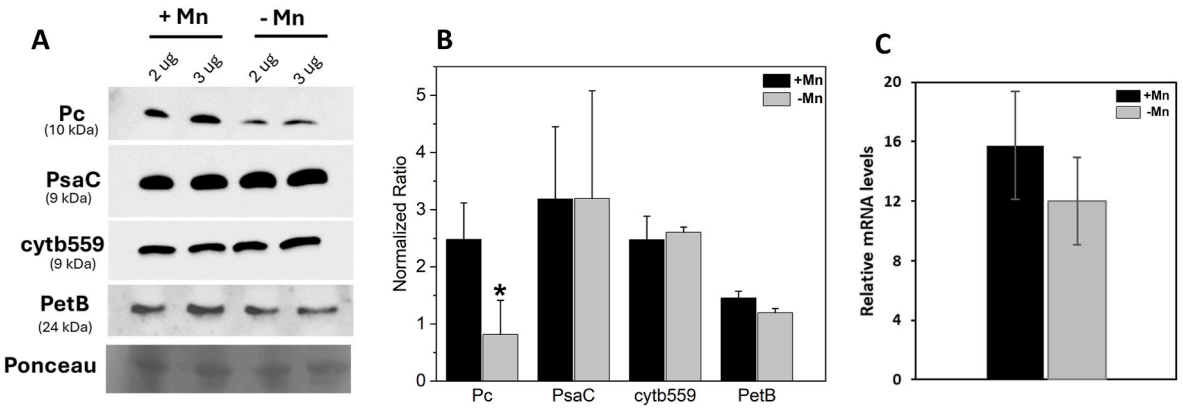

Fig. 3. Western blots and RT-PCR analysis of plastocyanin in *Marchantia* grown in control and Mn-deficient conditions. Representative immunoblots showing the content of Pc (Plastocyanin), PsaC (PSI subunit),cytb_{559} (PSII subunit) and PetB (cyt b_6f subunit) in thylakoids extracted from *Marchantia polymorpha*, grown in the presence of Mn (+Mn) and under Mn deficiency (-Mn). Gels were loaded based on chlorophyll content and ponceau red staining is shown as loading control (**A**). Densitometric analysis (**B**), mean value ± SE of three to six biological replicates are shown. Statistically significance (*P < 0.05) was assessed by Student's *t*-test. RT-PCR data for Pc (mean value ± SE) of two biological replicates are shown (C).

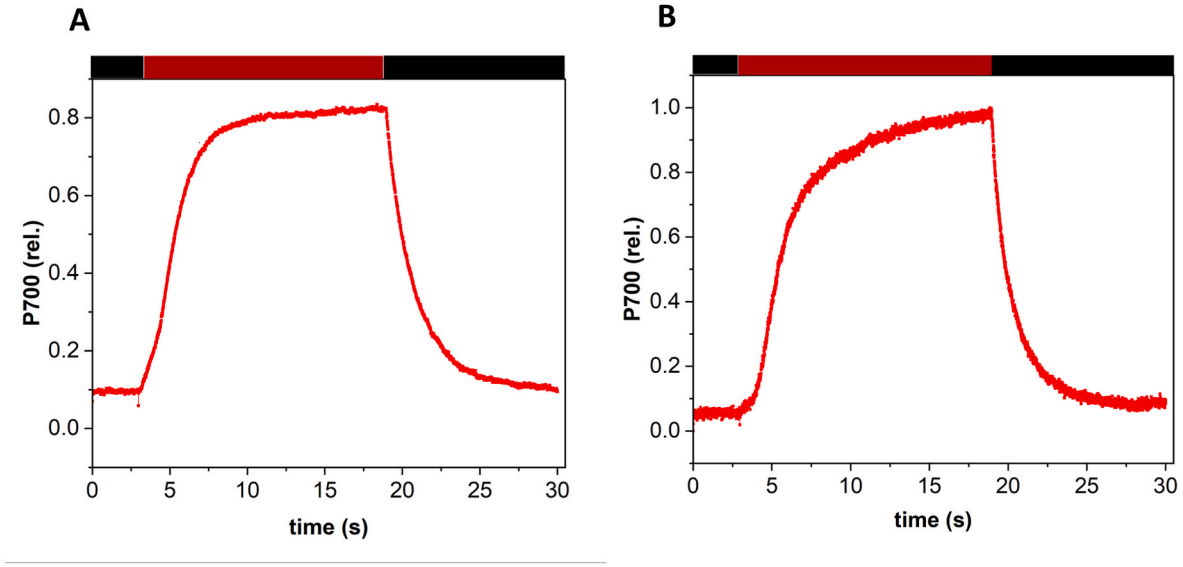

Fig. 4. Far-red light (FR) illumination shows differences in the kinetics of P700 oxidation in Mn-deficient samples. Thalli grown in control (A) and Mn-deficient (B) conditions were illuminated with FR light for 15 s. Top of the figure indicates the illumination protocol. The representative curves shown are an average of 10 traces. In total, 3 biological replicates were measured, each with 2 technical replicates.

amplitude, in far-red light, the amplitude of Pc oxidation was significantly smaller (≤50 %) under Mn deficiency (Fig. 2B) than in the presence of Mn (Fig. 2A). Fig. 2C shows significant changes for the calculated Pc to P700 ratio. The decrease in Pc content was confirmed by immunoblotting using specific antibodies. A clear decrease in the Pc content was visible under Mn deficiency (Fig. 3A), while PsaC (PSI subunit), cytb_{559} (PSII subunit) and PetB (cyt b_6f subunit) remained stable under both conditions. RT-PCR analysis of Pc (Fig. 3C) showed no significant differences between the two growth condition, indicating that it is not the expression levels but rather the protein stability that is responsible for the low Pc content under Mn deficiency.

The question arises how a low content of Pc affects electron donation to $P700^+$. We reported earlier lower donor-side limitation in Mn-deficient *Marchantia* when illuminated with red actinic light. Fig. 4 shows P700 oxidation kinetics induced by far-red light of dark-adapted *Marchantia* thalli. A considerable difference in P700 oxidation was noticed between control (+Mn) and Mn-deficient (-Mn) samples. In the presence of Mn (Fig. 4A), far red light triggered P700 oxidation within 8s, whereas under Mn deficiency (Fig. 4B) P700 is oxidized more slowly, indicating that more electrons are available to be donated to $P700^+$, thereby delaying the time until maximum $P700^+$ accumulation is observed. This slow rise of P700 oxidation may indicate a higher cyclic electron transport.

To further see the effect of Mn deficiency on PSI, reduction of $P700^+$ was studied after turning off the far-red light. Fig. 5 shows a significantly slower re-reduction of $P700^+$ under control conditions than under Mn deficiency. Half times ($t_{1/2}$) of $P700^+$ were determined as 3.7 s ± 0.01 and 1.9 s ± 0.007 for + Mn and -Mn, respectively. The faster re-reduction of $P700^+$ indicates again that more electrons are available to be donated to $P700^+$, suggesting a higher CET or less strong photosynthetic control under Mn deficiency. Moreover, we also reported faster re-reduction of Pc^+ in Mn-deficient thalli than in control thalli (Fig. 6). Pc^+ reduction was about 2.5-fold slower in comparison with $P700^+$. In the presence of the uncoupler nigericin the opposite effect was observed (Fig. S1). Both, the $t_{1/2}$ for $P700^+$ reduction and for Pc^+ reduction were slower under Mn deficiency than in control conditions. This shows that in the presence of nigericin under Mn deficiency less electron donors are available to reduce $P700^+$ and Pc^+.

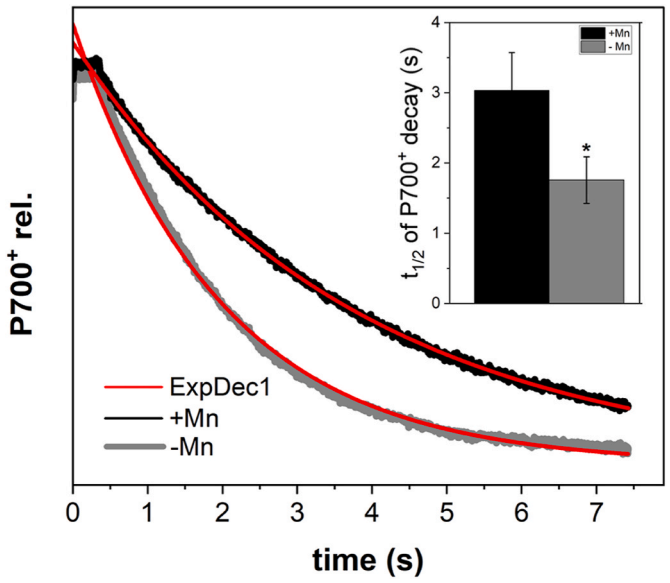

Fig. 5. Re-reduction kinetics of P700$^+$ after FR illumination. The kinetics of P700$^+$ re-reduction in Marchantia thalli indicated in black and grey for + Mn and –Mn, respectively, were monitored in the dark, after 5s exposure to FR light. Decay signals for P700$^+$ were fitted with single exponential function (red traces). The curves represent an average of 6 measurements for each sample. The inset show the half times ($t_{1/2}$) calculated for P700$^+$ decay (samples from three independent cultures, n = 6). Statistical significance (*P < 0.05) was assessed by Student's *t*-test.

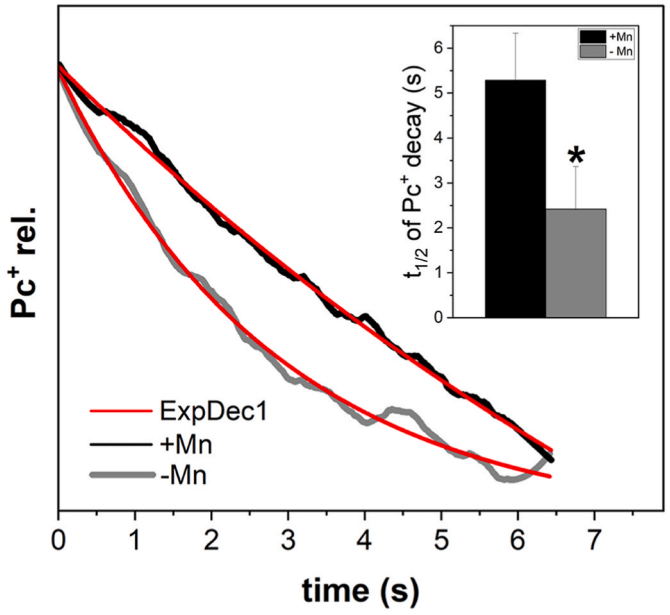

Fig. 6. Re-reduction kinetics of Pc$^+$ after FR illumination. The kinetics of Pc$^+$ re-reduction in *Marchantia* thalli indicated as black and grey for + Mn and –Mn respectively, were monitored in the dark, after 5s exposure to FR light. Decay signals for P700$^+$ were fitted with single exponential function (red traces). The curves represent an average of 6 measurements for each sample. The inset show the half times ($t_{1/2}$) calculated for Pc$^+$ decay (samples from three independent cultures, n = 6). Statistical significance (*P < 0.05) was assessed by Student's *t*-test.

4. Discussion

Here, we studied transient absorption changes in P700 and Pc using the KLAS-NIR spectrophotometer in the liverwort *M. polymorpha* grown in control and Mn-deficient conditions. According to the maximum signals for Pc$^+$ (Fig. 2) and immunoblot analysis (Fig. 3), the Pc signal relative to the P700 signal is drastically decreased upon Mn deficiency (Fig. 2). In *Arabidopsis*, it has been shown that the Pc content can be significantly decreased without pronounced changes in the overall photosynthetic activity, suggesting that Pc is present in large excess under control growth conditions (Pesaresi et al., 2009). However, in tobacco Schöttler et al. (2004) observed a reduction of electron transport and assimilation capacity when the amount of Pc was decreased. A decrease in Pc content has previously also been reported in early stages of senescence in tobacco and barley (Schöttler et al., 2004; Shimakawa et al., 2020). In Marchantia, lower Pc content induced by Mn deprivation, affects electron donation to PSI. The slower rate of P700 oxidation upon illumination of dark-adapted sample with red and FR light under Mn deficiency (Fig. 2B and 4B, see also Fig. 7 in Messant et al., 2023) and the faster re-reduction of P700$^+$ (Fig. 5) and Pc$^+$ (Fig. 6), show that either more electron donors are available for the reduction of these compounds, or that the electron transport becomes faster. Extra electron donation could originate from enhanced chlororespiration; lower photosynthetic control or from enhanced cyclic electron transport under Mn deficiency. Since lower donor-side limitation is also observed upon illuminations with actinic red light, a condition that outcompetes the chlororespiration pathway, we suggest that either less strong photosynthetic control or more cyclic electron transport is taking place under Mn deficiency than under control conditions. In Figs. 4–6, we have studied the effect of FR illumination. FR light excites preferentially PSI and cyclic electron transport is favored compared with red light illumination (Heber et al., 1978). In KLAS-NIR, using FR light at 720 nm, in a leaf the quantum yield of PSII of absorbed light is about 15% compared with illumination at 620 nm (Pettai et al., 2005). This low PSII activity is sufficient to supply electrons at a low rate via linear electron flow to sustain cyclic flow. After illumination with FR light, the re-reduction kinetics of P700$^+$ takes place with a $t_{1/2}$ of 3.7 s ± 0.01 in control and 1.9 s ± 0.007 in Mn-deficient samples (Fig. 5). These kinetics are rather slow compared to the kinetics observed after illumination with red actinic light in higher plants (see for example Shimakawa et al., 2020). However, comparable half-time of 1.7 s for PSI CET has been previously reported for *Arabidopsis thaliana* (Jensen et al., 2000). The faster reduction of P700$^+$ and Pc$^+$ could also be explained by a lower photosynthetic control under Mn deficiency. Donor-side limitation to PSI is lower under Mn deficiency as we have reported earlier (Messant et al., 2023). This could be either caused by increased cyclic flow or lower photosynthetic control. qN was higher under Mn deficiency (Fig. 1), speaking for a larger proton gradient and, presumably, a higher photosynthetic control. When the thalli had been infiltrated with nigericin the reduction of P700$^+$ and Pc$^+$ was slower under Mn deficiency (Fig. S1), opposite to what has been observed in the absence of an uncoupler (Figs. 5 and 6). This observation could be explained by lower photosynthetic electron transport and lower NADPH production since the PSII activity is decreased under Mn deficiency (Fig. 1A, see also data in Messant et al., 2023).

A comparison between P700$^+$ and Pc$^+$ reduction kinetics shows that Pc$^+$ reduction is 2.5-fold slower than that of P700$^+$, both in control and under Mn deficiency. This can be explained by an amount of Pc larger than that of PSI reaction centers. Upon Mn deficiency, the ratio Pc/P700 decreased by about 50% while the reduction of P700$^+$ and Pc$^+$ was accelerated. The faster reduction of P700$^+$ and of Pc$^+$ under Mn deficiency shows clearly that the kinetics not only depend on the number of available reductants in stroma and Pc electron carriers in the lumen but also on how quickly electrons can transfer from the stromal donors via the intersystem chain to Pc$^+$ and from there to P700$^+$. It has been reported previously that a decrease in the amount of Pc limits electron transport on the donor side of PSI probably caused by the limitation of lateral diffusion of Pc between the cyt b_6f complex and PSI (Drepper et al., 1996; Haehnel, 1982; Cruz et al., 2001). In the present case, however, the electron transport is accelerated when the Pc pool is small.

Using the data shown in Fig. 2 and the extinction coefficient of P700 and Pc determined *in vitro* (Sétif et al., 2019), the molar ratio of Pc to P700 is about 1.6 in control and 0.8 under Mn starvation. Even if this determination is an underestimation of the Pc content, under Mn deficiency too few Pc would be available for maintaining efficient electron transport between cyt b_6f complex, Pc and PSI. This speaks for a structural reorganization of the complexes and the formation of supercomplexes formed between ferredoxin, cytb_6f complex, Pc and PSI. According to the study conducted by Joliot and Joliot (2002), PSI, cytb_6f complex, Fd and Ferredoxin $NADP^+$-reductase (FNR) are physically associated and serve as a platform for Fd-dependent CET, leading to slow leakage of electrons and ultimately limited photo-oxidation of P700. In the green alga *Chlamydomonas reinhardtii* supercomplexes composed of PSI, Pc, cytb_6f complex, Fd have been biochemically isolated (Iwai et al., 2010), and functional supercomplexes have been biophysically characterized (Joliot et al., 2022). Moreover, a low-resolution structure of a PSI-LHCI-cytb_6f complex has been also revealed in *C. reinhardtii* (Steinbeck et al., 2018). Alterations of the organization of the thylakoid membrane may favor the formation of such supercomplexes. According to transmission electron microscopy images (Fig. S2), the organization of the thylakoid membrane is affected by Mn deprivation. In *in vivo* super-resolution chlorophyll fluorescence emission microscopy strongly fluorescent regions were localized more distinctly in chloroplasts of Mn-deficient thalli, indicating a change in the mesoscopic organization of the thylakoid membrane (Messant et al., 2023). This indicates smaller grana stacks with a more pronounced segregation between them and the stroma lamellae.

Enhancement of cyclic electron transport upon abiotic stress conditions allows to generate a higher pmf and a higher ATP/NADPH ratio. CET is known to increase under certain stress conditions like drought, low CO_2, low N, low temperature, and heavy metal stress (for review, see Sunil et al., 2019). CET is crucial for protecting PSI by alleviating the over-reduction of the acceptor side of PSI. *Marchantia* possess flavodiiron proteins and over-reduction of the acceptor side of PSI is less critical than in angiosperms (Shimakawa et al., 2017), however, upon Mn deficiency the capacity of linear electron flow is diminished and maintaining a high ATP level may be physiologically important to survive photoautrophically. Future work is needed to show if CET is increased under deprivation of other micronutrients than Mn. In addition, the biochemical composition of the putative supercomplex involved in CET under Mn deficiency in *Marchantia* should be analyzed.

Author contribution

U. H., and A.K-L. designed the project. U.H. performed the experiments; U.H. and A.K-L. analyzed the data. U. H., and A.K-L. wrote the manuscript.

Funding

This work was supported by the Labex Saclay Plant Sciences-SPS (ANR-17-EUR-0007), the platform of Biophysics of the I2BC supported by the French Infrastructure for Integrated Structural Biology (FRISBI; grant number ANR-10-INSB-05), IBiSA and France-BioImaging infrastructure (ANR-10-INBS-04, call “investissements d’Avenir”). U.H. is supported by a CNRS PhD contract.

Declaration of competing interest

The authors declare the following financial interests/personal relationships which may be considered as potential competing interests: Anja Krieger-Liszkay reports financial support was provided by French National Research Agency. If there are other authors, they declare that they have no known competing financial interests or personal relationships that could have appeared to influence the work reported in this paper.

Data availability

Data will be made available on request.

Acknowledgements

We would like to thank Sébastien Thomine (I2BC) for hosting U.H. in his laboratory, Claire Boulogne (I2BC) for her help with electron microscopy and Ginga Shimakawa (Kobe university, Japan) for scientific discussions.

Appendix A. Supplementary data

Supplementary data to this article can be found online at https://doi.org/10.1016/j.plaphy.2024.109042.

References

Alejandro, S., Höller, S., Meier, B., Peiter, E., 2020. Manganese in plants: from acquisition to subcellular allocation. Front. Plant Sci. 11, 517877.
Arnon, D.I., 1949. Copper enzymes in isolated chloroplasts. Polyphenoloxidase in Beta vulgaris. Plant Physiol. 24 (1), 1.
Bhat, B.A., Islam, S.T., Ali, A., Sheikh, B.A., Tariq, L., Islam, S.U., Hassan Dar, T.U., 2020. Role of micronutrients in secondary metabolism of plants. Plant Micronutrients: Def. Toxic. Manag. 311–329.
Bowman, J.L., 2016. A brief history of Marchantia from Greece to genomics. Plant Cell Physiol. 57 (2), 210–229.
Bowman, J.L., 2022. The liverwort Marchantia polymorpha, a model for all ages. In: Current Topics in Developmental Biology, vol. 147. Academic Press, pp. 1–32.
Bowman, J.L., Araki, T., Arteaga-Vazquez, M.A., Berger, F., Dolan, L., Haseloff, J., et al., 2016. The naming of names: guidelines for gene nomenclature in Marchantia. Plant Cell Physiol. 57 (2), 257–261.
Chow, W.S., Fan, D.Y., Oguchi, R., Jia, H., Losciale, P., Park, Y.I., et al., 2012. Quantifying and monitoring functional photosystem II and the stoichiometry of the two photosystems in leaf segments: approaches and approximations. Photosynth. Res. 113, 63–74.
Corpas, F.J., Barroso, J.B., Palma, J.M., Rodriguez-Ruiz, M., 2017. Plant peroxisomes: a nitro-oxidative cocktail. Redox Biol. 11, 535–542.
Cruz, J.A., Salbilla, B.A., Kanazawa, A., Kramer, D.M., 2001. Inhibition of plastocyanin to P_{700}^+ electron transfer in Chlamydomonas reinhardtii by hyperosmotic stress. Plant Physiol. 127, 1167–1179.
Drepper, F., Hippler, M., Nitschke, W., Haehnel, W., 1996. Binding dynamics and electron transfer between plastocyanin and photosystem I. Biochemistry 35 (4), 1282–1295.
Gamborg, O.L., Miller, R., Ojima, K., 1968. Nutrient requirements of suspension cultures of soybean root cells. Exp. Cell Res. 50 (1), 151–158.
Haehnel, W., 1982. On the functional characterization of electron transport from plastoquinone to photosystem I. Biochim. Biophys. Acta 682, 245–257.
Hawes, C.1., Juniper, B.E., Horne, J.C., 1981. Low and high voltage electron microscopy of mitosis and cytokinesis in maize roots. Planta 152, 397–407.
Heber, U., Egneus, H., Hanck, U., Jensen, M., Köster, S., 1978. Regulation of photosynthetic electron transport and photophosphorylation in intact chloroplasts and leaves of Spinacia oleracea L. Planta 143 (1), 41–49.
Homann, P., 1967. Studies on the manganese of the chloroplast. Plant Physiol. 42 (7), 997–1007.
Iwai, M., Takizawa, K., Tokutsu, R., Okamuro, A., Takahashi, Y., Minagawa, J., 2010. Isolation of the elusive supercomplex that drives cyclic electron flow in photosynthesis. Nature 464 (7292), 1210–1213.
Jensen, P.E., Gilpin, M., Knoetzel, J., Scheller, H.V., 2000. The PSI-K subunit of photosystem I is involved in the interaction between light-harvesting complex I and the photosystem I reaction center core. J. Biol. Chem. 275 (32), 24701–24708.
Joliot, P., Sellés, J., Wollman, F.A., Verméglio, A., 2022. High efficient cyclic electron flow and functional supercomplexes in Chlamydomonas cells. Biochim. Biophys. Acta Bioenerg. 1863 (8), 148909.
Joliot, P., Joliot, A., 2002. Cyclic electron transfer in plant leaf. Proc. Natl. Acad. Sci. USA 99 (15), 10209–10214.
Juniper, B.E., Hawes, C.R., Horne, J.C., 1982. The relationships between the dictyosomes and the forms of endoplasmic reticulum in plant cells with different export programs. Bot. Gaz. 143 (2), 135–145.
Klughammer, C., Schreiber, U., 2016. Deconvolution of ferredoxin, plastocyanin, and P700 transmittance changes in intact leaves with a new type of kinetic LED array spectrophotometer. Photosynth. Res. 128, 195–214.
Marschner, H. (Ed.), 2011. Marschner’s Mineral Nutrition of Higher Plants. Academic press.
Messant, M., Hani, U., Hennebelle, T., Guérard, F., Gakière, B., Gall, A., et al., 2023. Manganese concentration affects chloroplast structure and the photosynthetic apparatus in Marchantia polymorpha. Plant Physiol. 192 (1), 356–369.
Naramoto, S., Hata, Y., Fujita, T., Kyozuka, J., 2022. The bryophytes Physcomitrium patens and Marchantia polymorpha as model systems for studying evolutionary cell and developmental biology in plants. Plant Cell 34 (1), 228–246.

Nawrocki, W.J., Bailleul, B., Picot, D., Cardol, P., Rappaport, F., Wollman, F.A., Joliot, P., 2019. The mechanism of cyclic electron flow. Biochim. Biophys. Acta Bioenerg. 1860 (5), 433–438.
Papadakis, I.E., Giannakoula, A., Therios, I.N., Bosabalidis, A.M., Moustakas, M., Nastou, A., 2007. Mn-induced changes in leaf structure and chloroplast ultrastructure of Citrus volkameriana (L.) plants. J. Plant Physiol. 164 (1), 100–103.
Pesaresi, P., Scharfenberg, M., Weigel, M., Granlund, I., Schröder, W.P., Finazzi, G., Rappaport, F., Masiero, S., Furini, A., Jahns, P., Leister, D., 2009. Mutants, overexpressors, and interactors of Arabidopsis plastocyanin isoforms: revised roles of plastocyanin in photosynthetic electron flow and thylakoid redox state. Mol. Plant 2 (2), 236–248.
Pettai, H., Oja, V., Freiberg, A., Laisk, A., 2005. Photosynthetic activity of far-red light in green plants. Biochim. Biophys. Acta 1708 (3), 311–321.
Schmidt, S.B., Jensen, P.E., Husted, S., 2016. Manganese deficiency in plants: the impact on photosystem II. Trends Plant Sci. 21 (7), 622–632.
Schöttler, M.A., Kirchhoff, H., Weis, E., 2004. The role of plastocyanin in the adjustment of the photosynthetic electron transport to the carbon metabolism in tobacco. Plant Physiol. 136 (4), 4265–4274.
Schreiber, U., 2017. Redox changes of ferredoxin, P700, and plastocyanin measured simultaneously in intact leaves. Photosynth. Res. 134, 343–360.
Schreiber, U., Klughammer, C., 2016. Analysis of photosystem I donor and acceptor sides with a new type of online-deconvoluting kinetic LED-array spectrophotometer. Plant Cell Physiol. 57 (7), 1454–1467.
Sétif, P., Boussac, A., Krieger-Liszkay, A., 2019. Near-infrared *in vitro* measurements of photosystem I cofactors and electron-transfer partners with a recently developed spectrophotometer. Photosynth. Res. 142 (3), 307–319.
Shen, J.R., 2015. The structure of photosystem II and the mechanism of water oxidation in photosynthesis. Annu. Rev. Plant Biol. 66, 23–48.
Shimakawa, G., Ishizaki, K., Tsukamoto, S., Tanaka, M., Sejima, T., Miyake, C., 2017. The liverwort, Marchantia, drives alternative electron flow using a flavodiiron protein to protect PSI. Plant Physiol. 173 (3), 1636–1647.
Shimakawa, G., Sétif, P., Krieger-Liszkay, A., 2020. Near-infrared *in vivo* measurements of photosystem I and its lumenal electron donors with a recently developed spectrophotometer. Photosynth. Res. 144 (1), 63–72.
Steinbeck, J., Ross, I.L., Rothnagel, R., Gäbelein, P., Schulze, S., Giles, N., et al., 2018. Structure of a PSI–LHCI–cyt b6f supercomplex in Chlamydomonas reinhardtii promoting cyclic electron flow under anaerobic conditions. Proc. Natl. Acad. Sci. USA 115 (41), 10517–10522.
Sunil, B., Saini, D., Bapatla, R.B., Aswani, V., Raghavendra, A.S., 2019. Photorespiration is complemented by cyclic electron flow and the alternative oxidase pathway to optimize photosynthesis and protect against abiotic stress. Photosynth. Res. 139 (1–3), 67–79.
Takahashi, H., 2022. Cyclic electron flow A to Z. J. Plant Res. 135 (4), 539–541.

Fig S1. Re-reduction kinetics of $P700^+$ and Pc^+ in the presence of uncoupler Nigericin

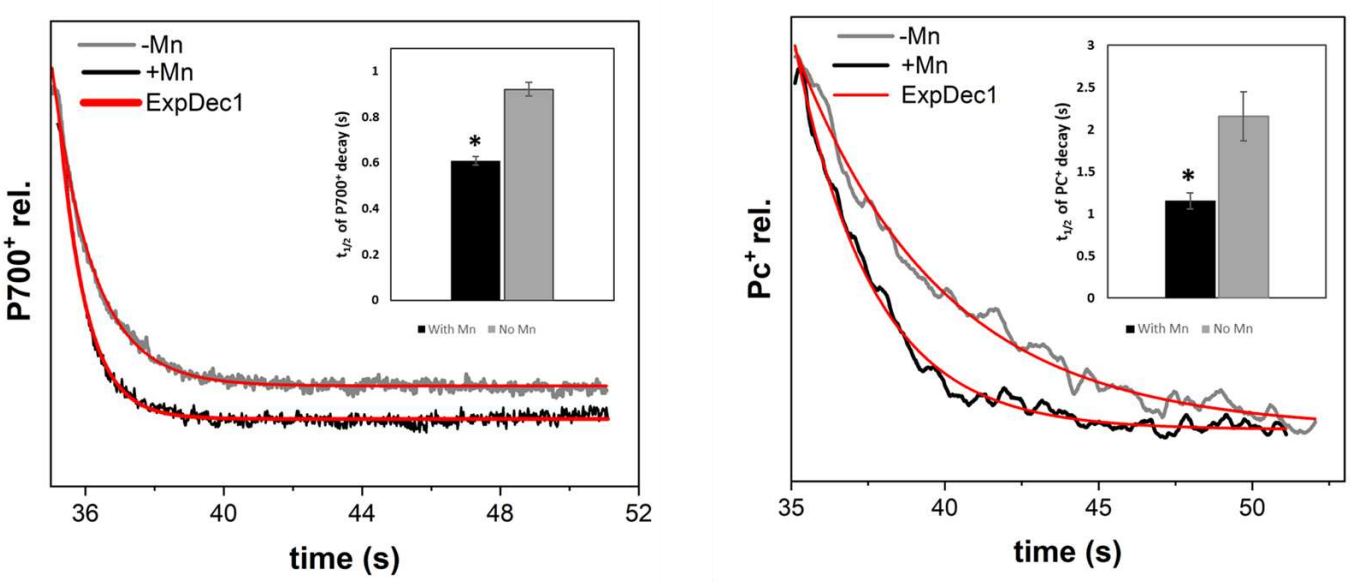

Thalli was incubated for 30 min in 100 nM nigericin. Thalli were illuminated for 5s with far-red light. $P700^+$, Pc^+ reduction kinetics were recorded after turning off far-red light (t=35s). Decay signals were fitted with single exponential function (red traces). Typical curves are shown (average of 4 measurements for each sample). The inset show the half times ($t_{1/2}$) calculated for $P700^+$ and Pc^+ decay (two biological replictaes (n=4). Statistical significance (*$P < 0.05$) was assessed by Student´s t-test.

Fig S2. Chloroplast membrane organization as shown by transmission electron microscopy (TEM) .

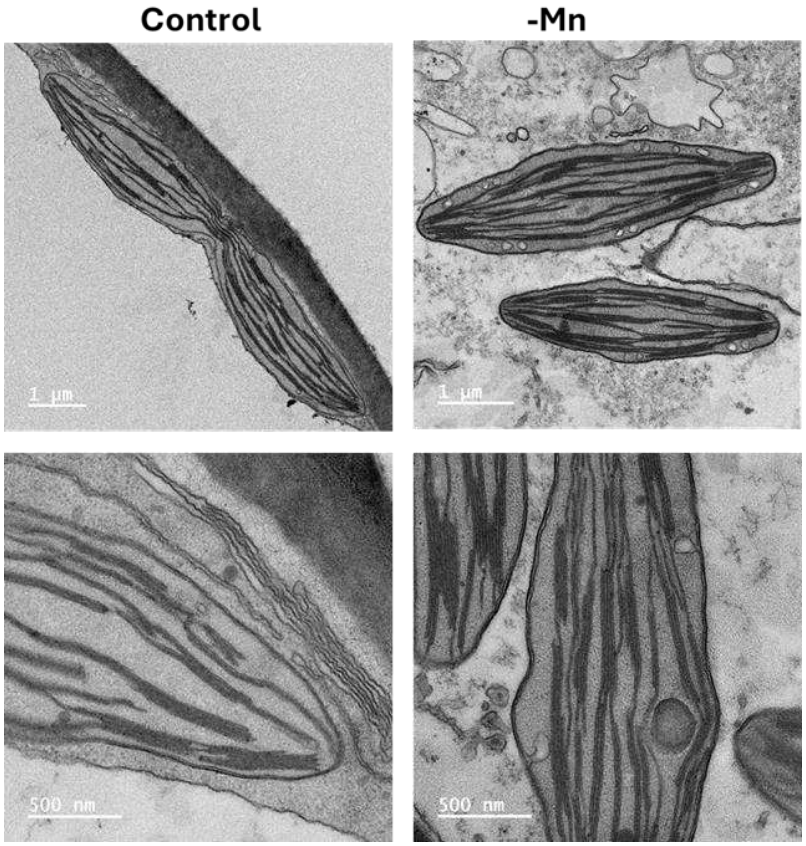

10-20 chloroplasts were analyzed for each condition. Scale bar: 1µm (and 500 nm for zoomed micrographs)

Table S1. List of Primers used in RT-PCR analysis

Gene/Transcript Name	F Primer	R primer
MP_Pc	CTCCCATCGAGAGCAACTGG	CTGGGGCACGAAGATGAGTT
MP_Act1	AGCGCGGTTACTCTTTCACC	TGGTGATGACTTGACCGTCG

3.3. Studying the supercomplex formation in *Marchantia polymorpha* under Mn deficiency

3.3.1. Introduction

Based on the previous results (See Article 2), it is assumed that there is some sort of supercomplex formation around cyclic electron transport (CET) under manganese (Mn) deficiency in *Marchantia polymorpha.* PSI can also bind LHC-II thus forming a PSI-LHC-II complex that plays a very important role in distribution of excitation energy during the light acclimation process (Galka et al., 2012) and state transitions (Rochaix et al., 2012). In the green alga *Chlamydomonas reinhardtii,* supercomplexes composed of PSI, PC, *cyt* b_6f complex and Fd have been biochemically isolated (Iwai et al., 2010). Moreover, a low resolution structure of PSI-LHCI-Cyt b_6f complex has also been revealed in *C. reinhardtii* (Steinbeck et al., 2018) A physical interaction between PSI-LHCI and Cyt b_6f or type 1-NDH dehydrogenase complex (NDH-1 complex) was also reported for *Arabidopsis*, that may have role either in cyclic electron flow or chlororespiration (Yadav et al., 2017).

Since we suppose that Mn depletion leads to an increase in cyclic flow, I tried to isolate the supercomplexes from *M. polymorpha* (both in the presence and deficiency of Mn) using BN PAGE. Moreover, Mn distribution in control conditions and Mn-deficiency in *Marchantia* thalli was studied using x-ray fluorescence imaging. For the analyses and the understanding of the BN PAGE, more detailed information on LHC composition is needed than provided in chapter 1. Here I will focus on light harvesting complex (LHC) proteins involved in supercomplex formation for both PSII and PSI.

The major light harvesting complex LHCII is the most abundant antenna complex in vascular plants and contains 6 different Lhcb proteins (that bind pigments), that are associated with PSII dimeric core (Liu et al., 2004). Lhcb1, Lhcb2 and Lhcb3 are major apoproteins that forms heterotrimers in vivo with different stoichiometric ratios (Jackowski et al., 2001). A ratio of 7:3:1 has been estimated for Lhcb (1:2:3) in *A. thaliana* (Galka et al., 2012; Crepin and Caffarri,

2018), that may vary depending on light conditions. Moreover, homotrimers of Lhcb1 or Lhcb2 were also reported in some *in vitro* studies (Caffarri et al., 2004; Standfuss and Kühlbrandt, 2004). The major trimeric Lhcb proteins are attached to PSII core via three minor Lhcb proteins; named as Lhcb4 (CP29), Lhcb5 (CP26) and Lhcb6 (CP24) (Rantala et al., 2020). The Lhcb isoforms exists in different sub-isoforms and evolved differently (Crepin and Caffarri, 2018). PSII-LHCII supercomplexes involves the PSII dimeric core and peripheral light harvesting antenna proteins (LHCII). Based on their affinities with PSII core (C), the trimeric LHC-II are classified as loosely (L), strongly (S) and moderately (M) bound (Boekema et al., 1999). Fluctuations in the light intensity triggers the formation of PSII-supercomplexes (PSII-s) with varying antenna sizes, including $C_2S_2M_2$, C_2S_2M, C_2S_2 and C_2S (Caffarri et al., 2009). The most abundant among them is $C_2S_2M_2$ and its cryo-EM structure has been resolved at 2.7-3.2 Å in pea (Su et al., 2017). In $C_2S_2M_2$ complex, the dimeric PSII core is bound with S-LHCII (via Lhcb5) and M-LHCII-trimers (via Lhcb4/Lhcb6) (Dekker and Boekema, 2005). Besides that, L-LHCII trimers exist likely at the periphery of PSII and play a very important role in the adjustment of the antenna size of the two photosystems (Grieco et al., 2015) via an important regulatory process called state transitions (Goldschmidt-Clermont and Bassi, 2015). However, their composition is not very well known but they may probably contain Lhcb1 and Lhcb2 (Koskela et al., 2020).

The monomeric PSI complex forms a stable supercomplex with LHCI-antenna, that contains Lhca pigment proteins Lhca1-4; organized in dimers (Lhca1/Lhca4 and Lhca2/Lhca3) (Pan et al., 2020). Further, these LHC-1 subunits are attached to the PsaF subunit of the PSI core complex by forming a semispherical belt (also called as LHCI belt) (Boekema et al., 2001; Wientjes and Croce, 2011). Studies have shown great evolutionary diversity in PSI-LHCI, where *Chlamydomonas reinhardtii* has been reported to contain nine LHCI proteins (Kargul et al., 2003). Interestingly, the genome from *Physcomitrella patens* revealed greater diversity among the LHC genes than found in *A.thaliana and C. reinhardtii* (Alboresi et al., 2008).

3.3.2 Materials and Methods

3.3.2.1. Plant material

Gemmae from Tak-1 male accession of *Marchantia polymorpha* were grown initially for two weeks on ½ Gamborg´s B5 (GB5) media with 1% agar (Gamborg et al., 1968) under a light-dark cycle (16h light, 22°C, 100 µmol photons m^{-2} s^{-1}, white fluorescent lamp/8h-dark, 20°C). Later young thalli were transferred onto ½ GB5 media with (33 µM $MnCl_2$) and without Mn, with starch (6%) as a gelling agent. Thalli were grown on starch for one week before performing the desired experiments (Messant et al., 2023).

3.3.2.2. Thylakoids isolation

Thylakoids from *M. polymorpha* were isolated as described in (Sárvári et al., 2022) and (Sárvári and Nyitrai, 1994). Thalli were harvested and starch was removed carefully from the thalli by washing 3-4 times with distilled water. Harvested material was homogenized in grinding (GR) buffer [50 mM HEPES-KOH (pH 7.0), 330 mM sorbitol, 2 mM EDTA, 2 mM $MgCl_2$, 0.1% (w/v) BSA, 0.1% (w/v) Na-ascorbate] at 4°C for 3x5 s using a blender. The resulting slurry was filtered through two layers of Miracloth and centrifuged at 1200x*g* for 7 min at 4°C. The pellet contains intact chloroplasts and thylakoids. The pellet was resuspended in washing buffer (50 mM HEPES-KOH (pH 7.0), 330 mM sorbitol, 2 mM EDTA, 2 mM $MgCl_2$) and centrifuged at 1500x*g* for 7 min. In order to remove envelope membrane and soluble enzymes from the intact chloroplast, samples were kept under osmotic shock (10 mM $Na_4P_2O_7$-pH 7.4) for 5 minutes (on ice) and later centrifuged at 5000x*g* for 7 min. For the removal of CF1, samples were treated with (5 mM Tricine-$(CH_3)_4NOH$ (pH 7.5), 0.1 M sorbitol) and centrifuged at 10,000x*g* for 10 minutes. Osmotic shock and CF1 removal steps were done according to (Fuad et al., 1983). Finally, the thylakoids were stored in storage buffer (2 mM Tris-maleate (pH 7.0), 40% (w/v) glycerol) and kept in liquid nitrogen. All steps were carried out at 4°C.

3.3.2.3. Chlorophyll content determination

For chlorophyll determination, pigments from fresh thalli and thylakoids were extracted with 5 mM N-(tri(hydroxymethyl)methyl) glycine (Tricine)-KOH pH 7.8), 80% (v/v) acetone and the extracts were centrifuged at 10,000x*g* (4 °C) for 5 min. Chl content was determined according to Porra (Porra et al., 1989).

3.3.2.4. BN PAGE

Thylakoid complexes were separated under native conditions using BN-PAGE based on the method of Schagger and von Jagow (1991). The whole procedure was performed using Mini-Protean apparatus (BioRad) with 1.5 mm acrylamide gradient separating gels [4.5-12% (w/v), and 4% stacking (w/v)], containing 8.5% (w/v) glycerol. For the sample preparation, thylakoids containing 500 µg Chl ml^{-1}, were washed with washing buffer (330 mM sorbitol, 50 mM Bis-Tris-HCl, pH 7.0, and 250 µg/ml Pefabloc, a protein inhibitor cocktail) and centrifuged for 10 min at 10,000x*g*. Further, the samples were solubilized in solubilizing buffer (SB) (750 mM aminocaproic acid, 50 mM Bis-Tris-HCl, pH 7.0, 0.5 mM EDTA, 250 µg/mL Pefabloc) along with 1% (w/v) n-dodecyl-ß-D-maltoside (DDM) and 1% (w/v) digitonin. To achieve the final concentration of solubilization buffer and Chls, a two-fold concentrated stock (2xSB) was combined with an equal volume of deionized water relative to the volume of thylakoids samples. The thylakoid pellet was resuspended well with a pipette and incubated on ice for 30 minutes with two short vortexing in between. Samples were then centrifuged at 18,000x*g* for 15 min at 4 °C and later supplemented with Serva Blue G (SBG) solution (750 mM aminocaproic acid, 5% (w/v) SBG). After a brief vortex, 10-20 µl of solubilized samples were applied per lane. Note that prior to loading, the residual ammonium persulphate from the wells were rinsed with cathode buffer containing 5x diluted SBG. BN PAGE was performed with a cathode buffer containing 0.02% SBG. Electrophoresis was carried out [5 mA/ cm^2 gel surface)] with a constant voltage of 50 V (30 min), 100 V (30 min) and 150 V (30 min). Once the dye reaches 2/3 of the separating gel, the upper buffer was changed with a cathode buffer containing 1000x diluted SBG and the electrophoresis was continued with 200 V until the dye front reaches the end (about 2-2.5 hrs).

SDS-PAGE (5% stacking, 10-18% linear gradient and 8.5% w/v glycerol) was performed according to Laemmli (1970). To determine the polypeptide patterns of thylakoid complexes, 3 mm wide gel strips were cut out from the BN-PAGE lanes and aligned well on the surface of denaturing gels, where the strips were solubilized with solubilizing buffer (1% (w/v) β-DM, 5% (w/v) SBG, and 0.5% (w/v) agarose). A constant current of 20 mA/gel was applied for about 2 hrs to separate proteins. Blue-Silver method (Candiano et al., 2004) was employed for gel staining. Gels were scanned using an Epson Perfection V750 PRO.

3.3.2.5. X-ray fluorescence (XRF)

Manganese (Mn) distribution in *Marchantia* thalli was analyzed by X-ray fluorescence (XRF) imaging. Thalli were harvested and after careful removal of starch, were subjected to drying under press at 60°C for 24 h, thus ensuring the smooth and flat surface of the thalli. A 5 mm diameter window was designed to hold the thallus in place. XRF imaging was conducted by XGT-7200V (Horiba, Japan) that was equipped with a silicone drift detector (for photons detection) and an Rh x-ray tube. Sample was set in vacuum and the areas/regions of interest were measured by applying an x-ray guide tube (100 mm) with an acceleration voltage and current of 50 kV and 1 mA, respectively. Mn distribution was assessed by detecting the characteristic $K\alpha_1$ photons emitted at 5.90 keV peak. Data analysis was performed in Python 3 (3.11).

3.3.3. Results

3.3.3.1. Identification of thylakoid complexes in *M. polymorpha*

Composition of protein complexes found in the isolated thylakoids from *Marchantia* was analyzed by BN/SDS PAGE. With a combination of DDM (n-Dodecyl-Beta-Maltoside) and digitonin, PSII and PSI complexes in various combination with LHC were resolved (Fig 9). PSII-PSI megacomplexes were not resolved well on the gels and altogether they can be referred to as “aggregates or mc (megacomplexes)”. Moreover, no PSI-NDH supercomplex was observed in *Marchantia,* which is in line with the earlier studies showing that NDH does not exist in a

complex form with PSI in *Marchantia* (Ueda et al., 2012). This could be explained by the evolutionary loss of *Lhca5* (Kato et al., 2018). Bands exhibiting low mobility are typically identified as PSII-supercomplexes (sc) that dissociate into four PSII-LHCII sc ($C_2S_2M_2$, C_2S_2M, C_2S_2 or C_2SM, C_2S or C_2M) and into a dimer (C2) (Caffarri et al., 2009). Within PSI, PSI core monomers were found alongside Lhca1-4, while PSI-LHCII complexes binding to the trimeric LHCII (LHCII-t) were also identified. Large amounts of LHCII are found to be associated with PSI (Prakash et al., 2001) and Bell with his colleagues found that spinach PSI-LHCII can host as many as five LHC-II trimers (Bell et al., 2015). PSII- dimer (C2) showed a comparable mobility to PSI in BN-PAGE (upper end of the band). Moreover, another PSII monomer; probably CS that contains some tightly bound LHCII-t antenna was detected at the lower end of the band with PSI. This kind of complex was also seen in poplar but migrated a bit further than PSII-dimer (Caffarri et al., 2009; Sárvári et al., 2020). Free Lhc bands emerged as LHCII assembly complexes (LHCII-a) comprising LHCII-t along with CP24 and CP29, LHCII-t and Lhc-m. Complexes binding Chl are labelled as "x" in the gel pictures. Cytochrome b_6f dimer (cyt b_6f/d) appeared below the PSII-monomer (C) band. An unknown band (?-blue arrow) can be seen running below LHCII-t band. Sometimes, when the solubilization was too strong, monomeric cyt b_6f band can also be seen below LHCII-t. Lhc-m band is not clearly visible because of overlap with the coomassie dye front. Moreover, Lhca are rarely found in the Lhc-m band, as Lhca are bound very tightly with PSI-core. In order to solubilize thylakoids with low amount of detergents, most of the coupling factor (CF1) was washed out from thylakoids surface and that's why it cannot be seen on the gels. Moreover, a band labelled (PSI-?) can be seen running below C_2S and above PSI-LHCII. This large supercomplex could be "PSIcore-6Lhca-LHCII", which has already been shown to bind extra Lhca1,4 dimer and abundantly found in state 2 (Crepin et al., 2020; Sárvári et al., 2022). A big PSI complex "PSI-LHCI-Lhcb9-LHCII" can be seen running above C_2S, which was also featured in bryophytes, specifically in *Physcomitrella*, which helps them to cope naturally with high and low light irradiance. The presence of such big complexes in mosses is possibly due to the presence of flavodiiron proteins (Gerotto et al., 2022; Zhang et al., 2023). All the complexes explained above were seen under both conditions (control and Mn deficient) in *Marchantia.* Interestingly, an unknown band (? Red arrow) was found running below cyt b_6f/d in Mn deficient sample (Fig 9-B) and was absent in control sample (Fig 9-A). The spot can be

further seen down near cyt b_6f subunit Pet B. Till now, nothing like this has been seen before and currently mass spectrometric identification is going on in this part of the project. More BN PAGE analysis including the densitometry analysis and mass spectrometry analysis is needed to solve this mystery and to see if there is a new kind of complex present under Mn deficiency that could have a role in CET in *Marchantia.* Note that these are only preliminary results and biochemical composition of putative supercomplexes should be identified.

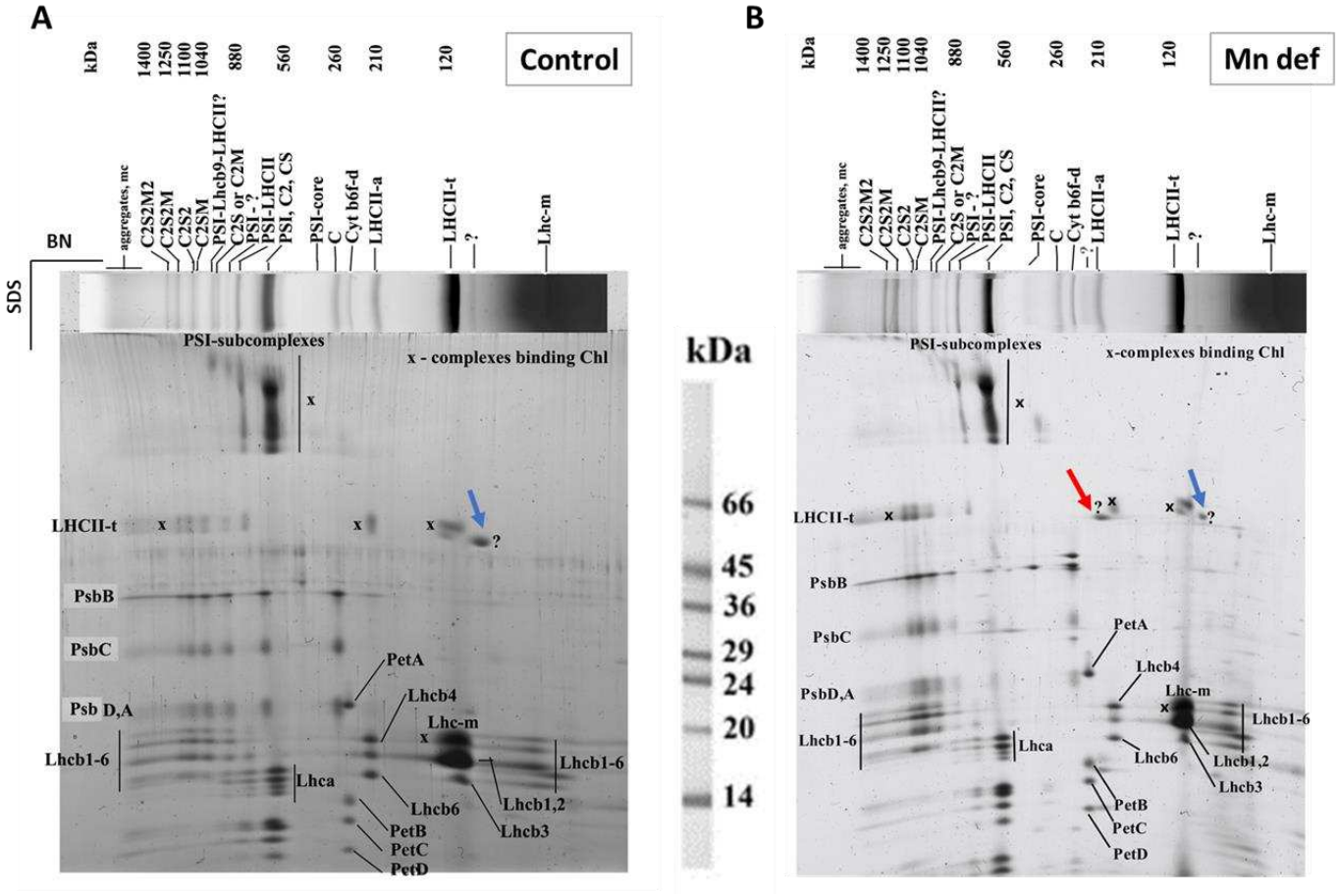

Figure 9: BN/SDS PAGE pattern of thylakoid complexes from *Marchantia polymorpha* with Mn (A) and Mn deficiency(B) Thylakoids were solubilized with 1% (w/v) DDM and 1% (w/v) digitonin and were separated by 4.5-12 % BN gradient gel followed by SDS PAGE.

3.3.3.2. Manganese distribution in *Marchantia* thalli

Element intensity maps were collected using XRF, with a 5 mm diameter window to hold the thalli in place. Intensity profiles were created using rectangular "region of interests" (ROIs), where data points were averaged along the axis perpendicular to the direction of ROI. Further, based on smoothed intensity profiles (using a Savitzky-Golay filter), linear regression was performed. Mn is clearly detectable in the total energy spectrum of control sample; however Mn was barely detectable according to the total energy spectrum of Mn deficient thalli (Fig 10).

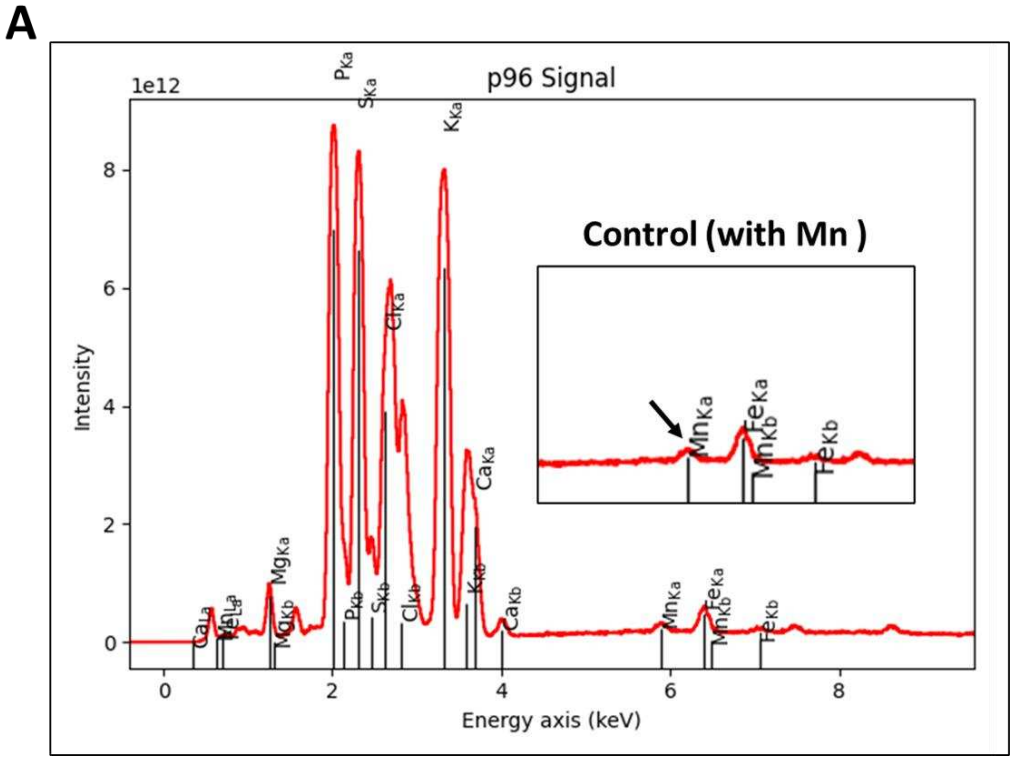

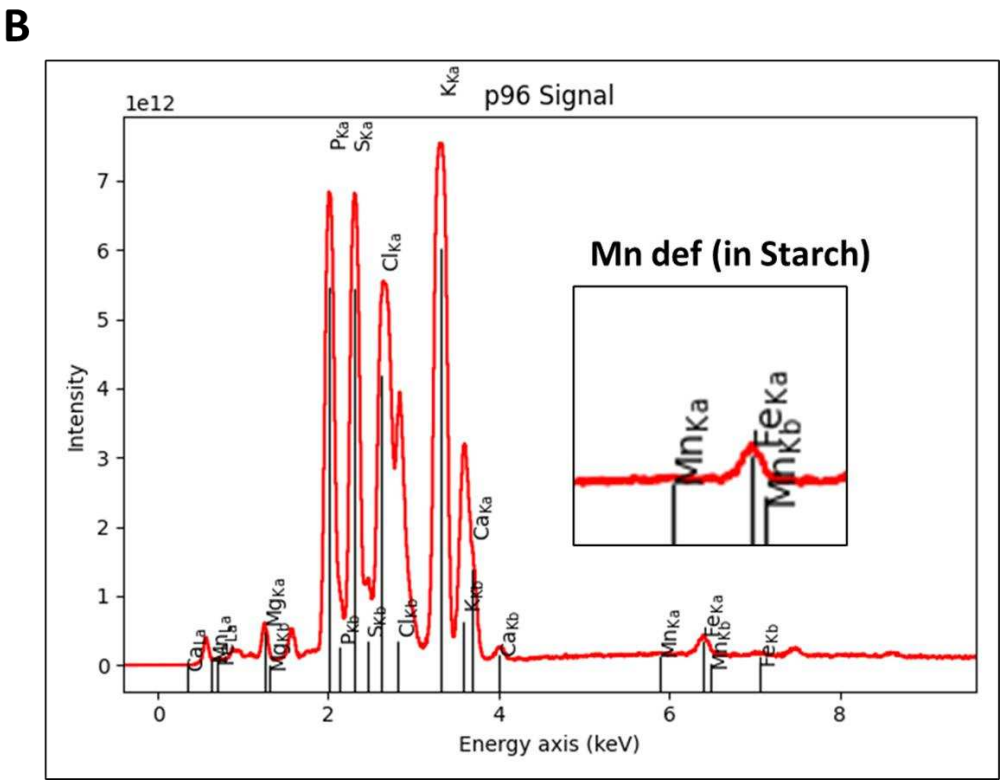

Fig 10: Total energy spectrum of *Marchantia* thalli in the presence (A) and deficiency (B) of manganese.

In figure 11, the direction of ROI is shown by blue arrow and the graphs indicate Mn distribution (left to right) in the direction of blue arrow. Under control conditions (Fig 11-A), it was seen that there is a clear linear decrease in Mn signal towards the edge of thallus for ROIs 1 and 2. However, in ROI-3, where the edge of thallus seems to be thicker, Mn signals are increasing towards the edge of thallus first. Perpendicular to the thallus (ROI-4), Mn signal shows a notable increase towards the right side of the thallus, which may explain the different profile of Mn in ROI-3. Under Mn deficiency (Fig 11-B), a decrease in signal intensity can be see towards the thallus, however this decrease is lower in the centre of thallus for ROI 1 and 2. Let's not forget that Mn signal intensities are quite low for this sample. When considering the perpendicular profile of ROI-3, a general decrease of signal intensity can be seen further away

from the tip of the thallus. In ROI-4, the area prior to the peak intensity of ROI-2 is considered, and Mn signal seems to increase more prior to the edge.

The most important information that can be deduced from these results is, that there is always a signal peak at the tip of Mn-deficient thalli that is lacking in control sample. This situation very much resembles to what has been seen in higher plants under transition metal deficiencies. They always allocate metals to the developing tissues. Under severe Iron (Fe) deficiency, even if all the leaves are severely chlorotic, the young still developing leaves contain higher amounts of Fe because of Fe remobilization (Zhang et al., 1995). Based on these signal intensities, it seems that *Marchantia* does the same with Mn, while the old thallus part starts senescence, the developing thallus part (developing photosynthetic machineries) gets sufficient amount of Mn. In future, it would be interesting to further investigate Mn distribution at the cellular level in *Marchantia* using an equipment that allows to get images with higher resolution.

A

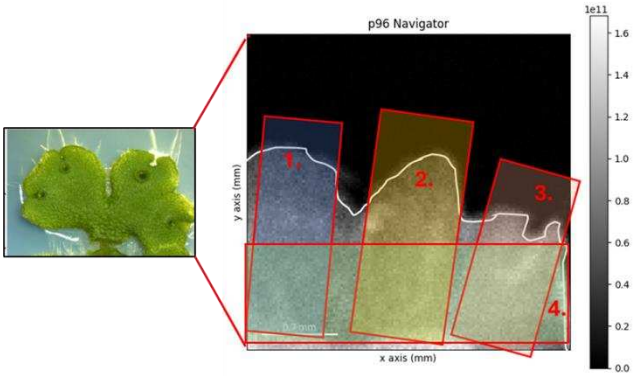
p96 Navigator
1e11
1.6
1.4
1.2
1.0
0.8
0.6
0.4
0.2
0.0
y axis (mm)
1.
2.
3.
4.
0.2 mm
x axis (mm)

B

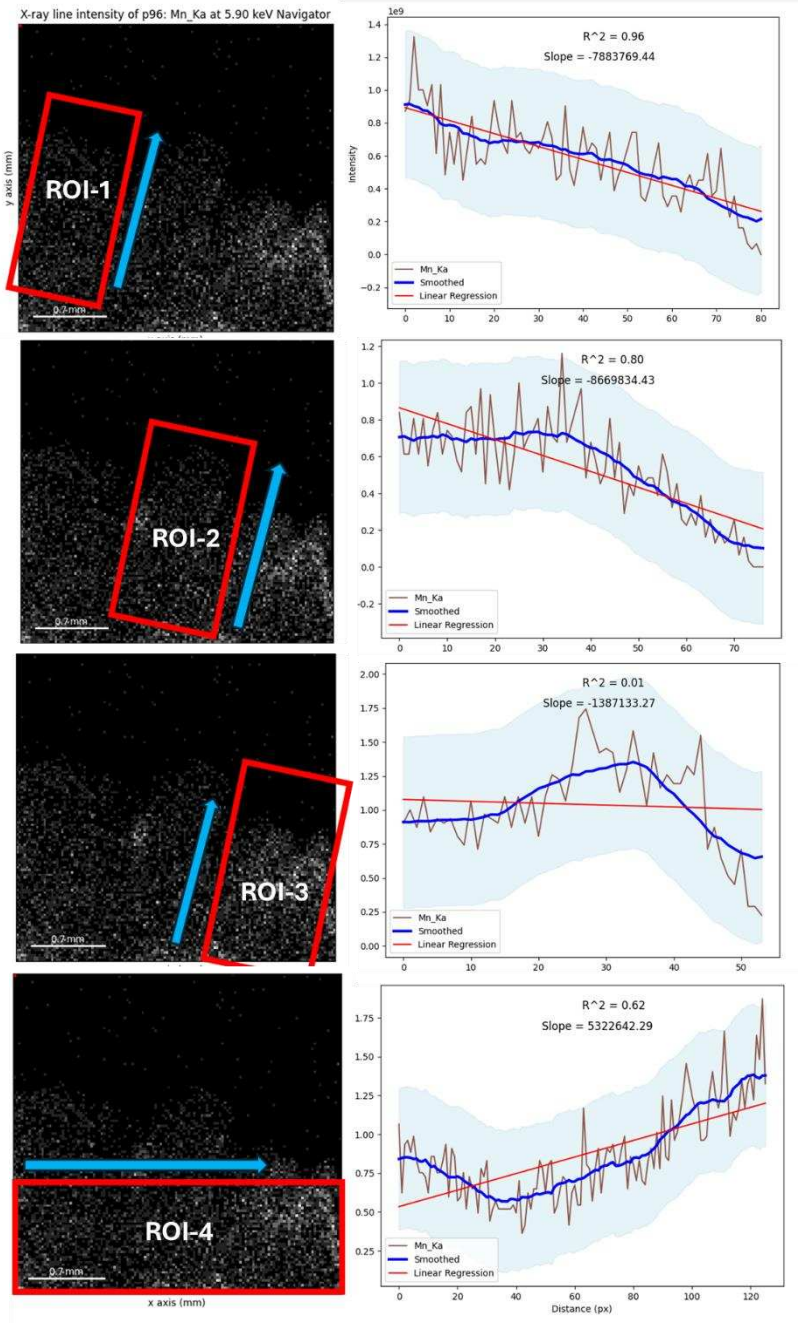
X-ray line intensity of p96: Mn_Ka at 5.90 keV Navigator
y axis (mm)
ROI-1
0.2 mm
1e9
Intensity
R^2 = 0.96
Slope = -7883769.44
Mn_Ka
Smoothed
Linear Regression
ROI-2
R^2 = 0.80
Slope = -8669834.43
ROI-3
R^2 = 0.01
Slope = -1387133.27
ROI-4
R^2 = 0.62
Slope = 5322642.29
x axis (mm)
Distance (px)

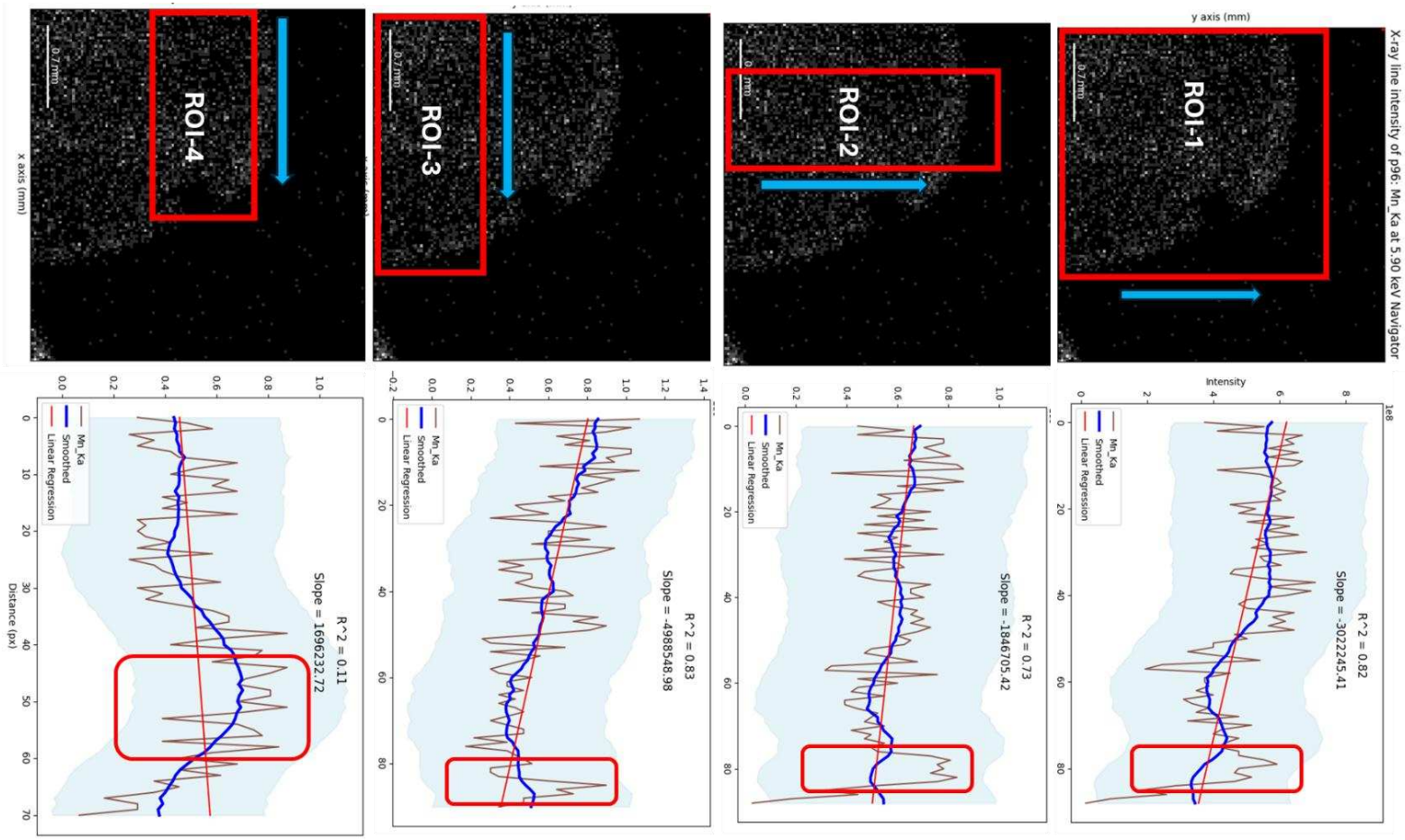

Fig 11: X-ray fluorescence intensity profiles showing the distribution of Mn Kα1 throughout the thalli under control (B) and Mn deficiency (C). Intensity signal peaks are shown in graphs and distribution of Mn in the selected region of interests (ROIs) is shown by vertical and horizontal profiles. The blue arrow indicates the direction of ROI. A navigator window is showing the way thalli is analyzed; by selecting different ROIs depending on the shape and size of thalli (A).

Chapter 4: Study of the redox regulation of oxygen reduction at photosystem I

4.1. Introduction

Plants need a striking balance between the amount of energy produced and consumed, any unfavorable condition can lead to a metabolic collapse. To maintain the redox balance, plants have a specialized system called “thioredoxin system”, that undergo redox regulatory modifications of target proteins, that have important roles in metabolic pathways. These thiol-dependent redox regulations also have an important role in regulating alternative electron flows. (For more details see Chapter 1). In this study we have shown the effect of photoperiod on the redox regulation of oxygen reduction at the photosystem I (PSI) acceptor side. Mostly, we employed indirect spin trapping electron paramagnetic resonance (EPR) spectroscopy to measure the changes in the reactive oxygen species (ROS) under two different light regimes in mutants defective in the stromal and lumenal thiol-regulatory network. The most interesting finding of this paper is the thioredoxin mediated redox regulation of PSI. Moreover, we have proposed a model for the redox regulation of oxygen reduction depending on the photoperiod and redox networking among stromal, thiol and lumenal proteins.

4.2. Article 3: A complex and dynamic redox network regulates oxygen reduction at photosystem I in *Arabidopsis* (published)

I have done genotyping for *ccda* and *cytc$_6$a* and further characterized the role of *ccda* and *cytc$_6$a* in the regulation of the Mehler reaction. I also contributed in EPR spectroscopy and analyzing data. Moreover, I actively participated in critical reading and discussions of manuscript.

Plant Physiology®

Plant Physiology, 2024, 00, 1–10
https://doi.org/10.1093/plphys/kiae501
Advance access publication 26 September 2024
Research Article

A complex and dynamic redox network regulates oxygen reduction at photosystem I in Arabidopsis

Umama Hani,[1] Belen Naranjo,[2] Ginga Shimakawa,[1] Christophe Espinasse,[3] Hélène Vanacker,[3] Pierre Sétif,[1] Eevi Rintamäki,[4] Emmanuelle Issakidis-Bourguet,[3,*] Anja Krieger-Liszkay[1,*]

[1]CEA, CNRS, Institute for Integrative Biology of the Cell (I2BC), Université Paris-Saclay, 91198 Gif-sur-Yvette, France
[2]Departamento de Bioquímica Vegetal y Biología Molecular, Instituto de Bioquímica Vegetal y Fotosíntesis, Universidad de Sevilla, 41092 Sevilla, Spain
[3]CNRS, INRAE, Université Paris-Saclay, Université Evry, Institute of Plant Sciences Paris-Saclay (IPS2), 91190 Gif-sur-Yvette, France
[4]Molecular Plant Biology, Department of Life Technologies, University of Turku, 20014 Turku, Finland
*Author for correspondence: anja.liszkay@i2bc.paris-saclay.fr (A.K.-L.), emmanuelle.issakidis-bourguet@universite-paris-saclay.fr (E.I.-B.)
The author responsible for the distribution of materials integral to the findings presented in this article in accordance with the policy described in the Instructions for Authors (https://academic.oup.com/plphys/pages/General-Instructions) is Anja Krieger-Liszkay.

Abstract

Thiol-dependent redox regulation of enzyme activities plays a central role in regulating photosynthesis. Besides the regulation of metabolic pathways, alternative electron transport is subjected to thiol-dependent regulation. We investigated the regulation of O_2 reduction at photosystem I. The level of O_2 reduction in leaves and isolated thylakoid membranes depends on the photoperiod in which plants are grown. We used a set of Arabidopsis (*Arabidopsis thaliana*) mutant plants affected in the stromal, membrane, and lumenal thiol network to study the redox protein partners involved in regulating O_2 reduction. Light-dependent O_2 reduction was determined in leaves and thylakoids of plants grown in short-day and long-day conditions using a spin-trapping electron paramagnetic resonance assay. In wild-type samples from short-day conditions, reactive oxygen species generation was double that of samples from long-day conditions, while this difference was abolished in several redoxin mutants. An in vitro reconstitution assay showed that thioredoxin m, NADPH-thioredoxin reductase C, and NADPH are required for high O_2-reduction levels in thylakoids from plants grown in long-day conditions. Using isolated photosystem I, we also showed that reduction of a photosystem I protein is responsible for the increase in O_2 reduction. Furthermore, differences in the membrane localization of m-type thioredoxins and 2-Cys peroxiredoxin were detected between thylakoids of short-day and long-day plants. Overall, we propose a model of redox regulation of O_2 reduction according to the reduction power of the stroma and the ability of different thiol-containing proteins to form a network of redox interactions.

Introduction

Thiol-dependent redox regulation of enzyme activities plays a central role in regulating photosynthesis. It has been well established that key enzymes of the Calvin–Benson–Basham cycle are redox-regulated via the thioredoxin (Trx) system (Buchanan 2016). In the chloroplast, Trxs are reduced in the light by ferredoxin in a reaction catalyzed by the Ferredoxin Thioredoxin Reductase (FTR). NADPH-thioredoxin reductase C (NTRC), a protein with both a NADPH-thioredoxin reductase and a Trx domain, has also been found in chloroplasts (Serrato et al. 2004). NTRC has been shown to be involved in controlling the level of H_2O_2 via its interaction with 2-cys peroxiredoxin (2-Cys-PRX), it participates in redox regulation of a key enzyme in starch biosynthesis (Michalska et al. 2009; Lepistö et al. 2013), of enzymes of the chlorophyll biosynthesis pathway (Richter et al. 2013; Perez-Ruiz et al. 2014) and in regulating the activity of the chloroplast ATP synthase (Carrillo et al. 2016; Naranjo et al. 2016; Nikkanen et al. 2016; for a recent review see Cejudo et al. 2019). A severe growth inhibition phenotype has been reported for a mutant lacking NTRC and Trx f1 (Thormählen et al. 2015) and in the triple mutant *ntrc-trxf1f2* and the double mutant *ntrc-trxx* (Ojeda et al. 2017). Both, *ntrc-trxf1f2* and *ntrc-trxx* mutants showed high mortality at the seedling stage (Ojeda et al. 2017) indicating that NTRC is important for chloroplast redox regulation, for controlling the redox state of several thioredoxins and showing that both redox regulation systems, FTR and the NTRC, are linked via 2-Cys-Prxs (Perez-Ruiz et al. 2017). Interaction between NTRC and Trx m1, Trx m3, and Trx y1 have been shown by bifluorescence complementation assays in vivo (Nikkanen et al. 2016). Trx m4 has been suggested to regulate negatively cyclic electron flow around photosystem I (PSI) (Courteille et al. 2013). Recently, evidence has been provided that m-type thioredoxins form a complex with PROTON GRADIENT REGULATION 5-LIKE 1 (PGRL1), a protein that is supposed to participate together with PGR5 in cyclic electron flow (Okegawa and Motohashi 2020; Wolf et al. 2020). Trx m1, Trx m2, and Trx m4 have also been reported to be implicated in the biogenesis of PSII (Wang et al. 2013), showing a broad implication of m-type thioredoxins in the photosynthetic light reactions. Compared to the other isoforms, Trx m3 seems not to be relevant for controlling these processes. A mutant of Trx m3, the less abundant protein of the m-type thioredoxins in chloroplast stroma (Okegawa and Motohashi 2015), shows unaltered chloroplast performance (Benitez-Alfonso et al. 2009). *Nicotiana tabacum* plants overexpressing Trx m were shown to be impaired in photosynthesis but being more tolerant to oxidative stress conditions (Rey et al. 2013). Furthermore, Trx m1, Trx m2, and NTRC have been shown to be indispensable for acclimation of photosynthesis

Received May 10, 2024. Accepted July 1, 2024.

under fluctuating light conditions (Thormählen et al. 2017). Taken together, these reports provide experimental evidence for an important role played by NTRC and Trx m isoforms for the rapid acclimation of plants to changes in the light regime, for controlling alternative photosynthetic electron flow and for coping with oxidative stress. Another important protein in the thiol-based chloroplast redox regulatory network is 2-Cys PRX, the most abundant peroxiredoxin in the chloroplast (Muthuramalingam et al. 2009). 2-Cys PRXs are reduced by NTRC and by Trxs and detoxify H_2O_2. Most importantly, they also act as a system to reoxidize reduced thioredoxins (Telman et al. 2020).

In the thylakoid lumen, candidates for controlling the redox state of protein disulfide bridges are the LUMEN THIOL OXIDOREDUCTASE 1 (LTO1) and the atypical cytochrome c_{6A} (Marcaida et al. 2006). The LTO1 protein is a transmembrane protein carrying a C-terminal thioredoxin-like domain typical of oxidoreductases belonging to the protein disulfide isomerase family. The *lto1* mutant has been shown previously to be affected in the assembly of active PSII while PSI electron transport was unaltered upon excitation with far-red light (Karamoko et al. 2011). Since the cysteine residues of LTO1 are at the lumen side of the thylakoid membrane, the redox state of the stroma has to be transmitted to these cysteines. Possible candidates are the transmembrane proteins CCDA and HCF164 (Motohashi and Hisabori 2010; Karamoko et al. 2013; Kang and Wang 2016).

There is a strong link between the level of reactive oxygen species (ROS) and the thiol system. Superoxide anion radicals ($O_2^{\bullet-}$) are mainly generated by the photosynthetic electron transport at PSI by the classical "Mehler reaction" or pseudocyclic electron flow. It has been reported that leaves of Arabidopsis (*Arabidopsis thaliana*) plants grown under short-day conditions (SD, 8 h light, 16 h dark) generate the double amount of superoxide compared with plants grown under long-day conditions (LD, 16 h light, 8 h dark) (Michelet and Krieger-Liszkay 2012). This extra electron transport in SD plants is used to generate a higher proton gradient and more ATP than found in thylakoids from LD plants. In the presence of an uncoupler, the difference in ROS generation was abolished between the 2 different thylakoid preparations. Addition of NADPH but not of NADH increased the level of ROS generation in LD thylakoids to the same amount as observed in SD thylakoids. Addition of NADPH to SD thylakoids had no important effect. In thylakoids from plants lacking NTRC the ROS production was like in SD wild type (wt) thylakoids and the difference between SD and LD thylakoids was abolished (Lepistö et al. 2013). These results point to a redox regulation of ROS generation at the level of PSI.

It remains an open question whether NTRC interacts with a protein of PSI at the thylakoid membrane, whether a Trx is involved in the redox regulation of ROS generation at PSI and how the redox state of the stroma is transmitted to the thylakoid lumen. In this study, we aimed to establish the interaction between different players of the chloroplast thioredoxin network and their ability to alter the capacity of O_2 reduction at the PSI acceptor side. We measured light-dependent ROS generation on leaves and isolated thylakoids of *A. thaliana* grown under SD or LD conditions in wt, in single mutants: *ntrc*, *trxm4*, *ccda, lto1*, *cyt* c_{6A}, in double mutants: *trxm1trxm2* and *2cpab*, and in plants overexpressing NTRC (oeNTRC). The sub-chloroplast localization of NTRC and Trx m was studied using immunoblots. In vitro reconstitution experiments were performed using thylakoids and purified recombinant Trx m and/or NTRC protein in order to directly test their effect on light-induced ROS generation.

Results

Leaves and thylakoid membranes isolated from *A. thaliana* wt plants grown in SD conditions generate in the light about twice the amount of ROS compared to those from plants grown in LD conditions (Fig. 1) as has been previously reported (Michelet and Krieger-Liszkay 2012). ROS production was measured using an indirect spin-trapping assay. In this assay hydroxyl radicals are detected which derive from superoxide anion radicals and hydrogen peroxide in a Haber–Weiss reaction catalyzed by Fe(II) (Ramos et al. 1992). In the light, the Mehler reaction generates superoxide that dismutates to hydrogen peroxide. Using the spin trap 5-diethoxyphosphoryl-5-methyl-1-pyrroline-N-oxide (DEMPO) that forms specific and distinguishable adducts with superoxide and with hydroxyl radicals, we have shown previously that it is indeed the level of superoxide that is twice higher in thylakoids isolated from SD plants compared with those from LD plants (Michelet and Krieger-Liszkay 2012). A comparison between ROS production in leaf disks and isolated thylakoids shows that the same differences in ROS production were found in both types of samples (Fig. 1B and C). This demonstrates that in the light the majority of superoxide/hydrogen peroxide is generated by the photosynthetic electron transport chain. Mutants affected in Trx m isoforms or in NTRC lost the difference between SD and LD. The single mutant *trxm4* and the double mutant *trxm1m2* generated similar amounts of ROS like LD plants, while *ntrc* generated high amounts of ROS like SD plants, independently of the photoperiod during their growth. Overexpression of NTRC increased the difference between SD and LD compared to wt. In a similar manner, the mutant devoid of 2-Cys PRX A and B showed an overall increase in the ROS production, however, the difference between SD and LD was maintained in *2cpab* (Fig. 1). There was no significant difference in protein levels of Trxm isoforms, NTRC and 2-Cys PRX in leaf extracts from wt grown in SD or LD conditions (Supplementary Fig. S1)

Furthermore, we found that 2-Cys PRX was slightly more abundant in leaf protein samples from plants grown in LD than in SD when prepared in presence of SDS but not in absence of detergent (Fig. 2A and B), suggesting that 2-Cys PRX is mainly stromal and the difference between SD and LD samples would be attributable to a differential association to thylakoid membranes. Indeed, thylakoids from LD grown plants showed a marked higher amount of 2-Cys PRX (recovered from thylakoid membranes in the presence of SDS) compared to SD, confirming that the difference of global (stromal plus thylakoid-associated) abundance in leaf extracts between photoperiods was attributable to the fraction of membrane-bound protein. In LD, the protein was present mainly in its dimeric form, most probably corresponding to the oxidized form as evidenced by the shift of the signal from an apparent mass of about 40 kDa to about 20 kDa produced by reduction with DTT giving the monomeric form. In PSI preparations, we could not immune-detect 2-Cys PRX (Fig. 2C) suggesting that the protein was not directly associated with PSI complexes, or lost upon sample preparation due to a loosening of the association to the photosystem. This latter possibility is strongly suggested by the detection of a faint signal in the supernatant of LD thylakoids resuspended in buffer devoid of detergent.

To see whether the localization of Trx m and/or NTRC is altered in plants grown in the 2 different light regimes, immunoblots were performed using leaf extracts and isolated thylakoids. As shown in Fig. 3, no difference in the total amount of Trx m4 and NTRC was found in leaf extracts. However, the attachment of Trx m differed in SD and LD thylakoids. Trx m4 was found in the thylakoid fraction in SD thylakoids but not in LD thylakoids. A similar

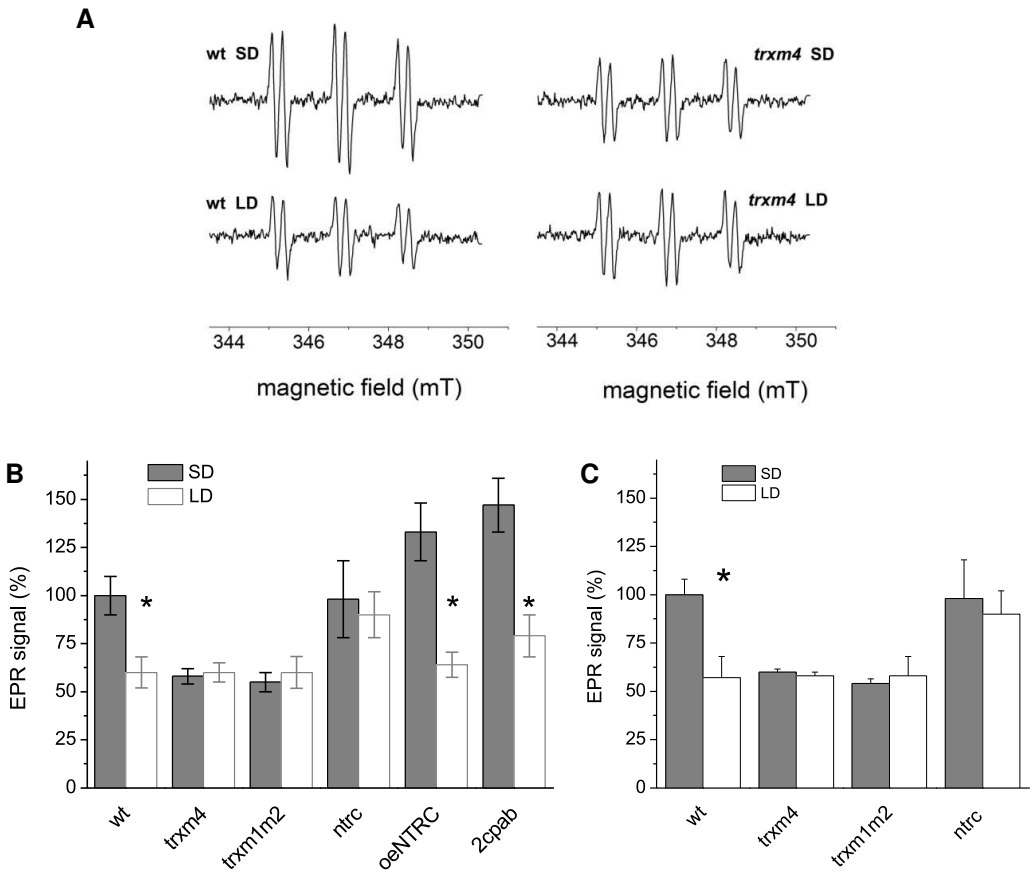

Figure 1. Light-induced hydroxyl radical formation in SD and LD leaf disks and washed thylakoid membranes in wt and redoxin mutants. Generation of hydroxyl radicals originating from $O_2^{\bullet-}/H_2O_2$ was detected by spin trapping with 4-POBN. **A)** Typical EPR spectra of the 4-POBN/α-hydroxyethyl adduct are shown. After infiltration with assay medium containing 4-POBN/ethanol/Fe-EDTA, leaf disks were incubated in the same medium for 30 min in light (200 μmol quanta m^{-2} s^{-1}) before detection of the radicals in the medium. Relative EPR intensities in leaves **(B)** and thylakoid membranes **(C)**. Thylakoid membranes (20 μg chlorophyll [Chl] μg ml^{-1}) were illuminated for 2 min (500 μmol quanta $m^{-2}s^{-1}$) in the presence of the spin-trapping assay before detection of the radical. Gray bars: SD, white bars: LD. All EPR signals were normalized to the signal of SD thylakoids without addition (100%). Mean values with SE are shown ($n \geq 6$, biological replicates; *$P < 0.05$ (comparison between SD and LD growth conditions for each genotype) according to Tukey test.

membrane localization like for Trx m4 was observed for Trx m2 (Supplementary Fig. S2).

Attachment of Trx m seems to be required for allowing enhanced electron transport to oxygen at PSI. To test whether the lack of membrane-associated Trx was indeed responsible for the lower ROS generation in LD thylakoids, we reconstituted LD thylakoids with purified Trx m4 and/or NTRC proteins in the presence of NADPH (Fig. 4). Addition of NADPH alone stimulated slightly the ROS production in LD thylakoids. A further increase in signal size was observed when Trxm4 or NTRC were added together with NADPH. However, these differences were statistically not significant. When Trxm4 was added together with NADPH and NTRC, LD thylakoids generated 3-fold more ROS than without any protein addition. In the absence of NADPH, addition of TRxm4 and NTRC had no effect. The different additives had only a small effect on SD thylakoids. This result points to a redox regulation of O_2 reduction at the level of PSI. To investigate whether there is a direct effect of thiol reduction on the O_2-reduction capacity of PSI, we incubated isolated PSI with the reducing agent tris(2-carboxyethyl)phosphine (TCEP) and followed light-dependent O_2 consumption using an O_2 electrode. As shown in Fig. 5, O_2 consumption was 2 times higher in the presence of TCEP. These data show that it is redox regulation of PSI itself that is crucial for the level of O_2 reduction at the acceptor side of PSI.

The question arises which subunit of PSI may be redox-regulated. Several subunits of PSI contain cysteines, however most of them are ligands of the iron-sulphur clusters F_x, F_A, and F_B, and can therefore be excluded as candidates undergoing reversible regulatory redox modifications. In addition, there are 2 proteins, PsaN and PsaF that may be candidates for disulfide bridge formation. It has been shown previously that the PSI subunit PsaN contains four cysteine residues that can form 2 disulfide bridges (Motohashi and Hisabori 2006). PsaF contains at its luminal site 2 cysteine residues that are close enough to form a disulfide bridge. PsaF is a transmembrane protein that forms the docking site for plastocyanin at the donor side of PSI and at the acceptor side its C terminus is in direct neighborhood with PsaE. PsaE forms together with PsaC and PsaD the docking site for ferredoxin. O_2 reduction is supposed to take place at this site. Since PsaF is the most likely candidate for redox regulation, and we did not observe any significant quantitative difference of this protein when comparing SD and LD thylakoid and PSI protein preparations (Fig. 2), we performed redox immunoblot assays to explore the influence of light regime on its redox state. Thylakoid membranes were treated with 4′-acetamido-4′-maleimidylstilbene-2,2′-disulfonic acid (AMS) that reacts with thiol groups (alkylation reaction), we separated the proteins by SDS-PAGE and analyzed the apparent mass of PsaF by immunodetection. Supplementary Fig. S3 shows that 2 bands were detected when the thylakoids had been

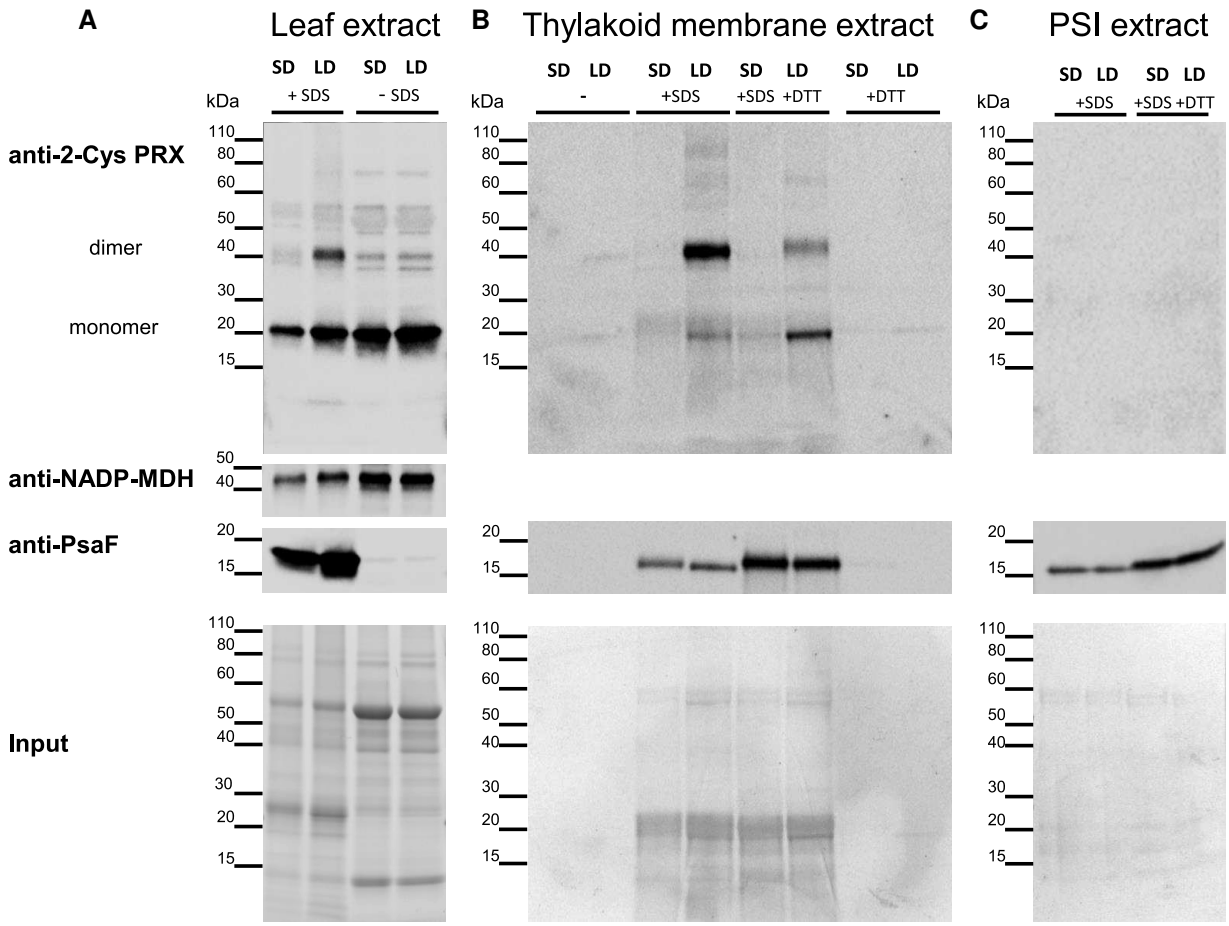

Figure 2. Association of 2-Cys PRX with thylakoid membranes depends on the photoperiod. Immunodetection of 2-Cys PRX in **A)** soluble leaf extracts (50 μg protein per well), **B)** thylakoid membranes (5 μg Chl per well), and **C)** PSI complexes (0.5 μg Chl per well) prepared from plants grown in SD and LD conditions. Immunodetection of chloroplastic NADP-malate dehydrogenase and PsaF were taken as controls as stromal and membrane-associated protein, respectively. Coomassie staining of the blot (input) was taken for gel loading control. For thylakoid and PSI membrane samples, SDS (2% [w/v]) and DTT (10 mM) treatments were performed for 10 min at room temperature (RT). After centrifugation, the supernatant was collected and analyzed. All samples were supplemented with nonreducing loading blue prior heat treatment and gel loading.

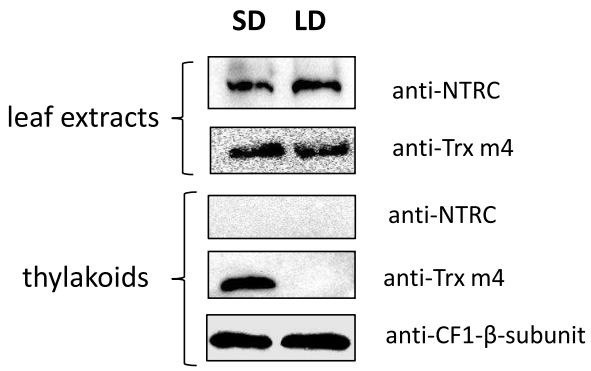

Figure 3. Membrane association of Trx m and 2-Cys PRX. Immunodetection of NTRC and Trx m4 in leaf extracts and thylakoid membranes prepared from plants grown in SD and LD conditions. Samples corresponding to 5 μg chlorophyll were loaded in each well. The results shown are representative of 3 biologically independent experiments.

chemically reduced with TCEP prior to the AMS treatment. This indicates that PsaF exists in an oxidized form with cysteines potentially forming a disulfide bridge and, upon addition of a reductant, in a reduced form with AMS-accessible thiols. However, without exogenous reductant, in isolated thylakoids from both SD and LD plants, only the oxidized form was found, probably due to spontaneous oxidation during membrane sample preparation. Redox immunoblots were performed on the mutants used for detection of the ROS levels in Fig. 1. In leaf extracts prepared in presence of SDS and m-PEG-mal (Fig. 6 and Supplementary Figs. S3 and S4) PsaF was immuno-detected as 2 well distinguishable redox variants that could be quantified by densitometry. We found that relative abundance of PsaF oxidized and reduced forms strongly varied between light and dark samples. In LD, PsaF was reduced equally in all genotypes with a reduction percentage ranging from 24.6% to 32.4% in the dark, and from 1.5% to 2.9% in the light. However, we did not observe significant differences in the redox state of PsaF in the 2 light regimes or between the different mutant lines, with the exception of *ntrc* where PsaF was significantly more reduced in SD (39.7% in the dark and 8.4% in the light) than in LD (24.6% in the dark and 2.4% in the light), and in comparison to wt (28.4% in the dark and 2.2% in the light) and the other mutants analyzed. However, there was no correspondence with the ROS levels found in *ntrc*. We concluded that the reduction of PsaF may be not stable enough to catch it during the alkylation treatment procedure.

The redox state of the stroma has to be transmitted to the thylakoid lumen to be able to act on thiol/disulfide groups of

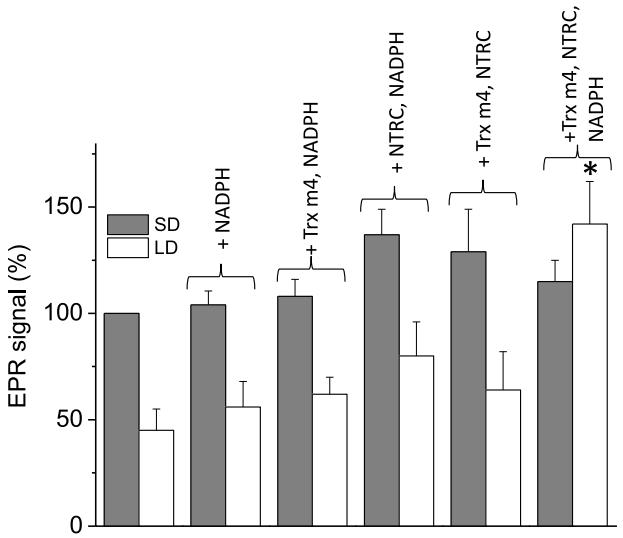

Figure 4. Reconstitution of ROS generation in LD thylakoids by Trx m, NTRC, and NADPH. Light-induced hydroxyl radical formation in SD and LD thylakoids is shown by spin trapping with 4-POBN. Thylakoid membranes (20 μg Chl ml^{-1}) were illuminated for 2 min (500 μmol quanta m^{-2}s^{-1}) before detection of the radical. When indicated, 200 μM NADPH, 0.3 μM Trx m4, and 0.3 μM NTRC were added to the assay before starting the illumination. All EPR signals were normalized to the signal of SD thylakoids without addition (100%). Gray bars: SD, white bars: LD. Mean values with SE are shown ($n = 3$; *$P < 0.05$ comparison with LD no protein added) according to the Tukey's test.

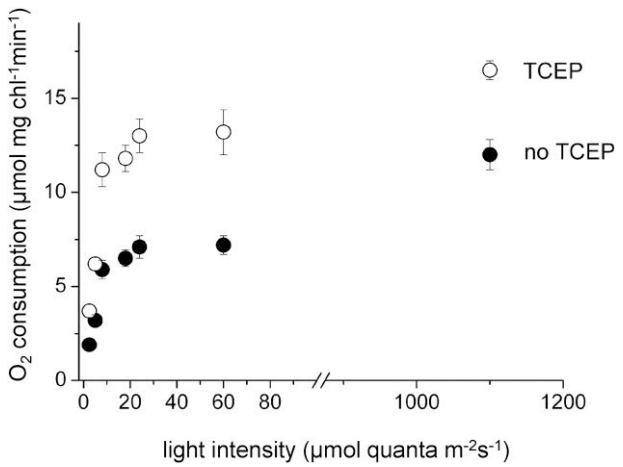

Figure 5. Dependence of O_2 consumption by isolated PSI on the redox state. O_2 consumption was measured with an O_2 electrode using DCPIP/ascorbate as electron donor. Samples were illuminated with green actinic light. When indicated, isolated PSI had been incubated with 1 mM TCEP for 15 min prior to the measurement. Mean values with SE are shown ($n = 4$).

PsaF. The transmembrane proteins CCDA and HCF164 are likely candidates for the transmission of the redox state from the stromal site to the lumenal site of the thylakoid membrane (Motohashi and Hisabori 2010). LTO1 (Karamoko et al. 2011) and the atypical cytochrome c_{6A} (Marcaida et al. 2006) may act as candidates for redox modifications inside the lumen. Figure 7 shows that the mutants of CCDA (*ccda3* and *ccda4*) and of LTO1 have indeed lost the difference in superoxide production between SD and LD, while lack of cyt c_{6A} has no effect.

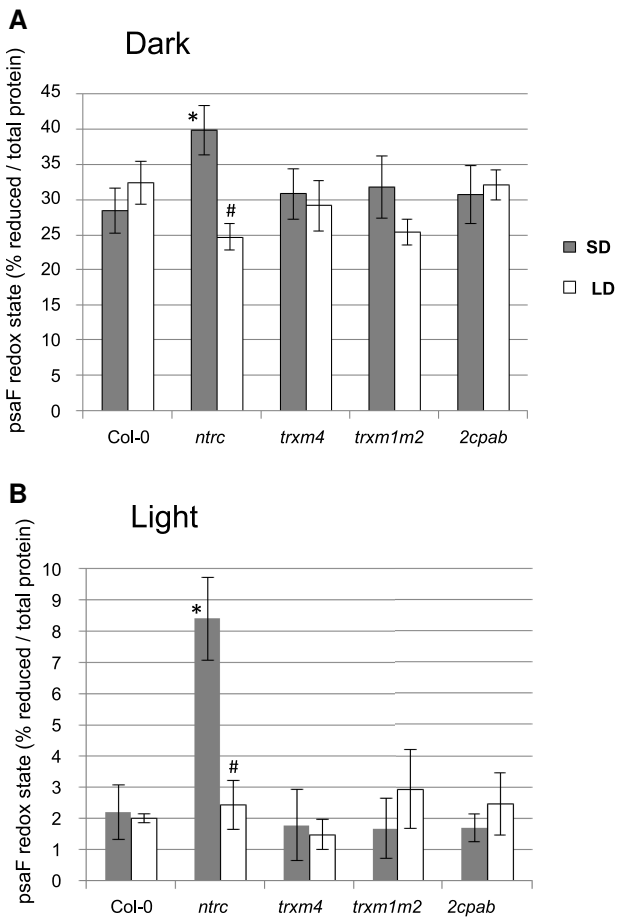

Figure 6. Redox state of PsaF in dark- and light-adapted plants. Total leaf protein extracts from WT (Col-0) and redoxins (*ntrc*, *trxm4*, *trxm1m2*, and *2cpab*) mutant plants grown in SD or LD conditions were prepared in the presence of the thiol alkylating agent mPEG-maleimide as described in methods. After SDS-PAGE, proteins (50 μg per well) were electro-transferred onto a PVDF membrane for PsaF immunodetection (chemiluminescence). See Supplementary Figs. S3 and S4 for details about the quantification method used and an example of redox immunoblot signals. **A)** and **B)** PsaF redox state in leaves in the dark and in the light, respectively. Values correspond to the mean of 5 to 6 experiments. Error bars correspond to SD. * and # designate significant differences between mutant and wt genotypes, and between SD and LD (for each genotype), respectively; according to Student's *t*-test, $P < 0.05$.

Discussion

Redox regulation of linear photosynthetic electron transport and alternative pathways has been reported previously (Johnson 2003). Courteille et al. (2013) showed that cyclic electron transport involving the NDH complex was altered in Trx m4 mutants, Nikkanen et al. (2018) reported the involvement of NTRC in the control of NDH complex-dependent and Naranjo et al. (2021) in PGR5-dependent cyclic flow. Both alternative electron transport pathways, cyclic and pseudocyclic flow, are in competition and downregulation of cyclic flow is therefore supposed to stimulate pseudocyclic flow. We have shown previously (Michelet and Krieger-Liszkay 2012) that O_2 reduction at PSI is higher in SD thylakoids than in LD thylakoids and that this difference is abolished in the presence of uncouplers. This observation points to a pH- or redox-regulated process taking place at the luminal side of the thylakoid membrane and controlling O_2 reduction at PSI. Indeed, O_2 reduction of isolated PSI is stimulated by the thiol-reducing agent TCEP (Fig. 5). At low light intensities, such

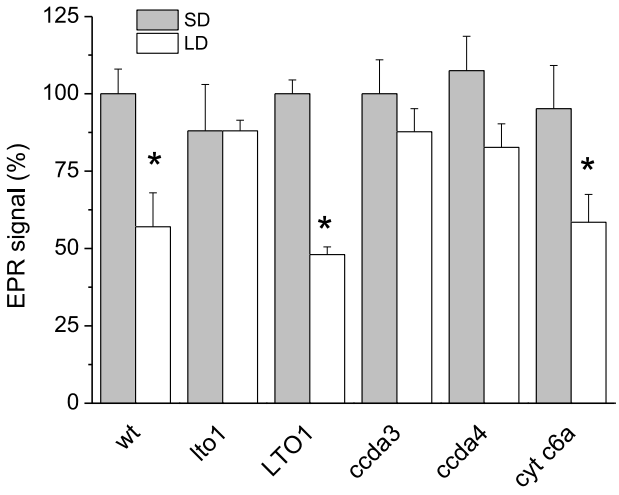

Figure 7. Light-induced hydroxyl radical formation in SD and LD leaf disks of mutants affected in LTO1, CCDA (*ccda3* and *ccda4*), and Cyt c_{6A}. Generation of hydroxyl radicals originating from $O_2^{\bullet-}/H_2O_2$ was detected in leaves by spin trapping with 4-POBN. Gray bars: SD, white bars: LD. All EPR signals were normalized to the signal of SD thylakoids without addition (100%). Mean values with SE are shown ($n = 8$, 2 to 3 biological replicates; *$P < 0.05$ comparison between growth conditions for each genotype) according to Tukey test.

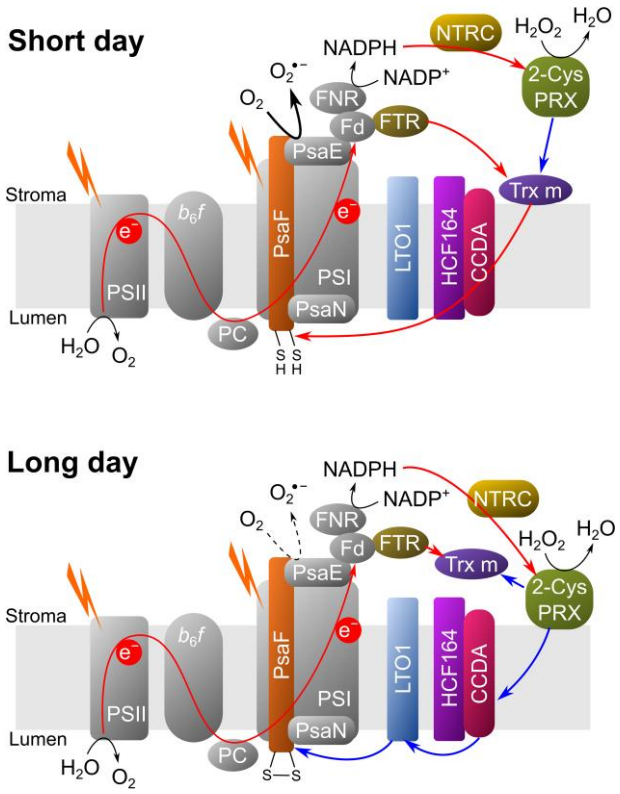

Figure 8. Model of redox regulation of O_2 reduction at PSI. Red arrows indicate also photosynthetic electron transport. Black arrow shows strong reduction of O_2, while the dashed black arrows shows weak reduction of O_2. Reduced cysteine residues in PsaF favor higher O_2 reduction activity. The redox state of PsaF is modified by 2 thiol modulating redox systems. The first one is required for reduction of the disulfide bond (red arrows), the second one for their oxidation (blue arrows). Trx m is a central player for controlling the reduction state of PsaF. Trx m is reduced by FTR. Under SD conditions, Trx m associates to the thylakoid membrane and reduces CCDA which reduces via HCF164 finally PsaF. In LD conditions, reduced PsaF is oxidized by LTO1, which itself is oxidized by CCDA (blue arrows. 2-Cys-PRX attaches to the membrane, allowing the oxidation of CCDA. In addition, it can oxidize Trx m (blue arrows).

as those used for the measurements shown in Fig. 5, O_2 is reduced by the terminal electron acceptors, the 4Fe4S clusters F_A and F_B, while at higher light intensities it is reduced by the acceptor A_1, a phylloquinone (Kozuleva et al. 2021). PsaN and PsaF are the only constitutive protein subunits of PSI containing cysteine residues that can form a disulfide bridge. In the structure published by Pan et al. (2018) for maize (*Zea mays*) PSI, PsaN forms close contacts with the N-terminal extension of PsaF. In a spin-trapping experiment on leaves of the *psan* mutant, the same difference between SD and LD was observed as in wt, ruling out PsaN as a candidate for the redox regulation of O_2 reduction (Supplementary Fig. S5). The most likely candidate for the redox modification affecting O_2 reduction is PsaF for the following reasons: (i) PsaF was found in PSI X-ray structures from pea either in the reduced state (Mazor et al. 2015) or with a disulfide bond (Qin et al. 2015), and (ii). PsaF has been identified by a proteomics approach as a redox-affected protein (Ströher and Dietz 2008). PsaF is a transmembrane protein, and we hypothesize here that, upon a modification of the redox state of its cysteines, a long-range structural change affects the neighboring subunit PsaE and thereby the ferredoxin docking site at the PSI acceptor side. Accordingly, O_2 reduction is favored when the disulfide bridge in PsaF is reduced while Fd reduction becomes less efficient. The subunit PsaE seems to be crucial for O_2 reduction at PSI in Arabidopsis (Krieger-Liszkay et al. 2020). Unfortunately, we were not able to detect significant differences in the reduction level of PsaF in the two light regimes and in the mutant lines analyzed for which distinct O_2 reduction levels were clearly found (Fig. 1).

We also addressed the question how the redox state of PsaF is controlled in the lumen. The *Lto1* mutant has lost the difference between SD and LD (Fig. 7), implying a role of this protein in redox regulation of PSI. The difference between SD and LD is also lost in the mutants *ccda3* and *ccda4* (Fig. 7), demonstrating the importance of CCDA in transmitting the stromal redox state to the lumen in vivo. The CCDA and LTO1 mutants show high ROS levels independent of the growth photoperiod. We hypothesize that LTO1 keeps PsaF oxidized under LD conditions, while CCDA keeps LTO1 oxidized, leading to low O_2 reduction in LD. In SD conditions, where the redox state of CCDA and LTO1 is highly reduced, the situation changes. Under these circumstances, reduction of PsaF seems feasible (Fig. 8).

Trx m has been shown to be the electron donor to CCDA in vitro (Motohashi and Hisabori 2010). We propose here that Trx m association to the thylakoid membrane is required for an efficient electron donation to CCDA and onwards to redox-regulated proteins in the thylakoid lumen, reduction of PsaF and increase in O_2 reduction (Fig. 7). Trx m association to the membrane in SD conditions (Fig. 3 and Supplementary Fig. S2) may be facilitated by the higher proton motive force generated in thylakoids from SD plants (Michelet and Krieger-Liszkay 2012). Such a mechanism has been shown to play a role for the attachment of the plastid terminal oxidase to the thylakoid membrane (Bolte et al. 2020). Future experiments using leaves harvested toward the end of the dark period compared with leaves harvested from plants exposed to high light or using leaves infiltrated with uncouplers could answer whether Trx m association is controlled by the proton motive force.

The question arises how to integrate 2-Cys-PRX and NTRC into this model. According to a previous report (Bohrer et al. 2012) and

our measurements of 5,5-dithio-bis-(2-nitrobenzoic acid) reduction (Supplementary Fig. S6), NTRC is not able to reduce m-type Trxs in a direct manner when tested at physiologically relevant concentrations. Furthermore, 2-Cys-PRXs are mainly reduced by NTRC and act as an oxidizing system toward reduced Trxs (Nikkanen et al. 2016; Perez-Ruiz et al. 2017; Vaseghi et al. 2018; Telman et al. 2020) as well as they are responsible for H_2O_2 detoxification in the stroma (König et al. 2002). We suggest that membrane association of 2-Cys-PRX in LD is important to keep CCDA oxidized. As shown in Fig. 2, 2-Cys PRX is associated to the membrane only in LD conditions, and it is found mostly in its dimeric form. H_2O_2 detoxification may be more efficient if 2-Cys PRX is attached to the membrane close to the site of superoxide production and conversion into H_2O_2 by membrane-associated superoxide dismutase (SOD). In the absence of NTRC or 2-Cys PRX, however, the redox state of the chloroplast is strongly disturbed, which complicates the interpretation of the experiments with these mutants (Fig. 1).

In conclusion, our hypothesis for the redox regulation of pseudocyclic electron flow is based on three mechanisms: (i) The availability of electron acceptors other than O_2 for photosynthetic electron transport, (ii) Redox regulation of the different players according to the redox state of the stroma and the capabilities of the different players to form a network of redox-driven interactions, and (iii) The reversible membrane attachment of Trx m and 2-Cys-PRX that may depend on changes in pH and ion concentration controlled by the proton motive force. Attachment of Trx m seems to be necessary to achieve a high reduction state of CCDA and PsaF in SD resulting in high O_2-reduction levels at PSI, while detachment of Trx m and attachment of 2-Cys-PRX in LD seems to favor oxidation of CCDA, while PsaF is oxidized by LTO1, resulting in low levels of O_2-reduction. However, the connection of redox regulation of PsaF in vivo with the photoperiod remains to be demonstrated. Besides redox regulation at the PSI complex itself, other redox-regulated proteins are likely to play a role in regulating the partitioning between linear, cyclic flow and the Mehler reaction. Trxm has been shown to regulate negatively cyclic flow (Courteille et al. 2013), and LTO1 may also play a more indirect role by inhibiting cyclic electron flow via the NDH complex (P. Hamel, personal communication).

Under SD conditions, plants show an alteration in the partitioning of assimilated CO_2 in soluble sugars and starch. An upregulation of the Mehler reaction may help the plants to counteract the reduced hours for performing photosynthesis. Thanks to the increased Mehler reaction SD thylakoids build up a larger proton gradient and generate more ATP at a given time and light intensity compared with LD thylakoids (Michelet and Krieger-Liszkay 2012) showing the physiological importance of a redox control of the Mehler reaction. A higher photosynthetic rate and a redistribution of photosynthates between soluble sugars and starch may be advantageous to generate the necessary reserve for the prolonged dark period. Furthermore, higher ROS levels in SD may play an important role as signaling compounds affecting the expression of ROS-responsive genes (Dietz et al. 2016).

Reduction of O_2 in pseudocyclic electron flow is in competition with cyclic electron flow. Both pathways lead to the formation of a proton gradient without generating NADPH. According to Takahashi et al. (2013), the redox state of the chloroplast controls the formation of supercomplexes composed of PSI, Cyt b_6f, LHCs, PGRL1 and FNR. Such supercomplexes are thought to be required for cyclic electron flow (Iwai et al. 2010). The formation of a complex between reduced Trx m and PGRL1 may inhibit cyclic electron flow by preventing the supercomplex formation required for cyclic flow. This suggestion is supported by the recent reports on the interaction between Trx m and PGRL1 (Okegawa and Motohashi 2020; Wolf et al. 2020). As shown recently, Trx x and Trx y play an important role in the acceptor-side regulation of PSI and protection of PSI against photoinhibition under fluctuating light conditions (Okegawa et al. 2023). Future work on the extent of cyclic flow and superoxide production in mutants of the different components of the Trx system will show if both, pseudocyclic and cyclic flow are controlled by the same proteins but in the opposite way. Furthermore, it would be interesting to investigate redoxin mutants under fluctuating light condition to demonstrate the importance of the Mehler reaction under abiotic stress conditions. It has been shown previously that growth of *ntrc* is highly susceptible to fluctuating light conditions (Thormählen et al. 2017).

Materials and methods

Plant material

Arabidopisis (*A. thaliana*) wt (Col-0) and mutants were grown for 6 wk in soil either under SD conditions (8 h continuous white light—160 μmol quanta $m^{-2}s^{-1}$, 21 °C/16 h dark, 18 °C) or LD conditions (16 h continuous white light—160 μmol quanta $m^{-2}s^{-1}$, 21 °C/8 h dark, 18 °C). All mutants and over-expressing plants used were already described in previous studies: the *trxm4* T-DNA mutant (Courteille et al. 2013) and the *trxm1 m2* mutant (Thormählen et al. 2017); the T-DNA insertion mutant of NTRC (*ntrc*) (Lepistö et al. 2009) and transgenic plants overexpressing wt NTRC protein in *ntrc* background (Toivola et al. 2013); the double T-DNA mutant lacking the two 2-Cys Prxs, A and B (*2cpab*) (Ojeda et al. 2018); the T-DNA mutants lacking CCDA isoforms (Page et al. 2004); the T-DNA mutant lacking Cytochrome c_{6A} (Pesaresi et al. 2009).

Extraction of proteins from leaves

Arabidopsis leaves were harvested 1 h after onset of light (light samples) or 1 h before onset of light (dark samples) and ground in liquid nitrogen before homogenization in lysis buffer. The lysis buffer contained 100 mM Tris–HCl pH 6.8, 2% (w/v) SDS, 20 mM EDTA and protease inhibitor cocktail (for plant cell and tissue extracts, 1× final concentration, Sigma-Aldrich, St. Louis, MI, USA).

Extraction of thylakoids from *A. thaliana*

Young fully expanded leaves were ground in 0.33 M sorbitol, 50 mM KCl, 10 mM EDTA, 1 mM $MgCl_2$, 25 mM Mes pH 6.1. After centrifugation, the pellet was washed twice with 0.33 M sorbitol, 60 mM KCl, 2 mM EDTA, 1 mM $MgCl_2$, 25 mM HEPES pH 6.7. After centrifugation, the pellet was resuspended in 0.3 M sorbitol, 50 mM KCl, 1 mM $MgCl_2$, 20 mM HEPES pH 7.6. This procedure was repeated once, and the pellet was resuspended to a final concentration of about 1 mg of chlorophyll (chl) per ml of thylakoids. All centrifugations were performed at 3,000 × *g* for 3 min at 4 °C.

Isolation of PSI

Solubilization buffer (10 mM HEPES pH 7.5) containing 1.2% (w/v) beta-dodecyl maltoside (β-DM) was added to the thylakoid suspension (final chlorophyll [Chl] concentration: 0.5 mg ml^{-1}, β-DM: 0.6% [w/v]). The sample was mixed for 1 min, followed by centrifugation to remove unsolubilized membranes. The supernatant was then loaded onto sucrose gradients (0.1 to 1 M sucrose, 10 mM HEPES pH 7.5, 0.03% [w/v] β-DM) and centrifuged for

145 min at 57,000 rpm using a fixed angle rotor (70.1 Ti). The lower band containing PSI was collected, frozen in liquid nitrogen, and stored at −80 °C.

Room-temperature spin-trapping EPR measurements

Thylakoid membranes generate superoxide in the light, which dismutates either spontaneously or catalyzed by SOD to hydrogen peroxide. To detect $O_2^{\bullet-}$/H_2O_2-derived hydroxyl radicals an assay with the spin trap α-(4-pyridyl-1-oxide)-N-*tert*-butylnitrone (4-POBN, Sigma-Aldrich) was used. Spin-trapping assays were carried out using leaf disks or freshly isolated thylakoid membranes at a concentration of 20 μg Chl ml^{-1}. Leaf disks were vacuum-infiltrated with the buffer containing the spin trap reagents, 50 mM 4-POBN, 4% (v/v) ethanol, 50 μM Fe-EDTA, prior to the illumination and then floating on the same buffer during illumination. Samples were illuminated for a given time with white light (200 μmol quanta m^{-2} s^{-1} in case of leaf disks and 500 μmol quanta m^{-2} s^{-1} in case of thylakoids in the presence of 50 mM 4-POBN), 4% (v/v) ethanol, 50 μM Fe-EDTA, and buffer (25 mM HEPES, pH 7.5, 5 mM $MgCl_2$, 0.3 M sorbitol). When indicated, 200 μM NADPH, 0.3 μM Trxm4 and 0.3 μM NTRC were added to the assay before starting the illumination.

EPR spectra were recorded at room temperature in a quartz flat cell using an ESP-300 X-band (9.73 GHz) spectrometer (Bruker, Rheinstetten, Germany). The following parameters were used: microwave frequency 9.73 GHz, modulation frequency 100 kHz, modulation amplitude: 1G, microwave power: 6.3 mW in 4-POBN assays, receiver gain: 2×10^4, time constant: 40.96 ms; number of scans: 4.

O_2 consumption

Measurements of O_2 consumption were performed in a Liquid-Phase Oxygen Electrode Chamber (Hansatech Instruments, Norfolk, England) using isolated PSI (10 μg Chl ml^{-1}) in Tricine 20 mM pH 8.0, in the presence of 5 mM $MgCl_2$, 30 mM NaCl, and 5 mM ascorbate, 30 μM 2,6-dichlorophenolindophenol (DCPIP) as exogenous electron donors to $P700^+$.

SDS-PAGE and immunoblotting

SDS-PAGE was performed using 8% or 4% to 20% (w/v) polyacrylamide gels. Proteins were blotted onto a nitrocellulose or a PVDF membrane. Labeling of the membranes with polyclonal antibodies, produced in the lab (anti-Trxm; anti-NTRC; anti-2-Cys PRX) or commercially available (PsaF and β-subunit of ATP synthase; Agrisera, Vännäs, Sweden), was carried out at room temperature in 50 mM Tris–HCl pH 7.6, 150 mM NaCl, 0.1% (v/v) Tween-20% and 5% (w/v) nonfat milk powder. After washing, bound antibodies were revealed with a peroxidase-conjugated secondary antirabbit antibody (Agrisera, Vännäs, Sweden) and visualized by enhanced chemiluminescence.

Redox state of PsaF

Total leaf protein samples were prepared as described above with 2 mM AMS (ThermoFisher Scientific, MW 536.44 Da) or mPEG-mal(24) (MM(PEG)24 Methyl-PEG-Maleimide, ThermoFisher Scientific, MW 1239.44 Da) added to the extraction buffer. 50 μg protein samples were precipitated (addition of 7 vol. cold ethanol, overnight incubation at—20 °C), after spinning (11,000 *g* 10 min at room temperature) protein pellets were dried and resuspended in nonreducing electrophoresis loading buffer. After SDS-PAGE (4% to 20% [w/v] polyacrylamide gel), PsaF was immuno-detected (PVDF membrane/Chemiluminescence) using a Chemidoc ISV0025 (BioRad) and signals corresponding to reduced (pegylated) and oxidized forms were quantified using ImageLab software (BioRad).

Statistical analyses

All statistical analyses were conducted as indicated in the figure legends using Tukey or Student's *t*-test. The number of replicates is given in the legends. A difference was considered significant when its adjusted *P*-value was < 0.05.

Accession numbers

CCDA : AT5G54290 Cyt c6A : AT5G45040 2CPA : AT3G11630 2CPB : AT5G06290 LTO1 : AT4G35760 NTRC : AT2G41680 TRXm1 : AT1G03680 Trxm2 : AT4G03520 Trxm4 : AT3G15360

Acknowledgments

We would like to thank Patrice Hamel (Ohio State University, USA) for scientific discussions and for sending us the seeds of the *lto1* mutants.

Author contributions

E.I.-B. and A.K.-L. designed the project; U.H., B.N., G.S., C.E., H.V., E.I.-B., and A.K.-L. performed the experiments and analyzed the data; P.S. and E.R. participated in discussions; A.K.-L. wrote the initial version of the manuscript that was read and revised by all the authors.

Supplementary data

The following materials are available in the online version of this article.

Supplementary Figure S1. Immunoblot analysis of NTRC, Trx-m, and 2-Cys Prx proteins under long- and short-day conditions.

Supplementary Figure S2. Attachment of Trx m2 and m4 to thylakoid membranes.

Supplementary Figure S3. PsaF immunodetection in thylakoid membranes.

Supplementary Figure S4. Immunodetection and redox state of PsaF in leaf extracts.

Supplementary Figure S5. Light-induced hydroxyl radical formation in SD and LD leaf disks of *psan*.

Supplementary Figure S6. 6 Reduction tests of Trxs m by NTRC in vitro.

Funding

This work was supported by the Labex Saclay Plant Sciences-SPS (ANR-17-EUR-0007) and the platform of Biophysics of the I2BC supported by the French Infrastructure for Integrated Structural Biology (FRISBI; grant number ANR-10-INSB-05) and the Infrastructures en Biologie Santé et Agronomie (IBiSA). U.H. was supported by a CNRS PhD fellowship. B.N. acknowledges funding by MCIN/AEI/10.13039/501100011033, grant IJC2019-040972-I and E.R. by the Jane and Aatos Erkko Foundation (Finland).

Conflict of interest statement. None declared.

Data availability

Data will be made available on demand.

References

Benitez-Alfonso Y, Cilia M, San Roman A, Thomas C, Maule A, Hearn S, Jackson D. Control of Arabidopsis meristem development by thioredoxin-dependent regulation of intercellular transport. *Proc Natl Acad Sci U S A*. 2009:106(9):3615–3620. https://doi.org/10.1073/pnas.0808717106

Bohrer A-S, Massot V, Innocenti G, Reichheld J-P, Issakidis-Bourguet E, Vanacker H. New insights into the reduction systems of plastidial thioredoxins point out the unique properties of thioredoxin z from *Arabidopsis*. *J Exp Bot*. 2012:6315–6323. https://doi.org/10.1093/jxb/ers283

Bolte S, Marcon E, Jaunario M, Moyet L, Paternostre M, Kuntz M, Krieger-Liszkay A. Dynamics of the localization of the plastid terminal oxidase inside the chloroplast. *J Exp Bot*. 2020:71(9):2661–2669. https://doi.org/10.1093/jxb/eraa074

Buchanan BB. The path to thioredoxin and redox regulation in chloroplasts. *Annu Rev Plant Biol*. 2016:67(1):1–24. https://doi.org/10.1146/annurev-arplant-043015-111949

Carrillo LR, Froehlich JE, Cruz JA, Savage LJ, Kramer DM. Multi-level regulation of the chloroplast ATP synthase: the chloroplast NADPH thioredoxin reductase C (NTRC) is required for redox modulation specifically under low irradiance. *Plant J*. 2016:87(6):654–663. https://doi.org/10.1111/tpj.13226

Cejudo FJ, Ojeda V, Delgado-Requerey V, González M, Pérez-Ruiz JM. Chloroplast redox regulatory mechanisms in plant adaptation to light and darkness. *Front Plant Sci*. 2019:10:380. https://doi.org/10.3389/fpls.2019.00380

Courteille A, Vesa S, Sanz-Barrio R, Cazale AC, Becuwe-Linka N, Farran I, Havaux M, Rey P, Rumeau D. Thioredoxin m4 controls photosynthetic alternative electron pathways in Arabidopsis. *Plant Physiol*. 2013:161(1):508–520. https://doi.org/10.1104/pp.112.207019

Dietz KJ, Turkan I, Krieger-Liszkay A. Redox- and reactive oxygen species-dependent signaling into and out of the photosynthesizing chloroplast. *Plant Physiol*. 2016:1541–1550. https://doi.org/10.1104/pp.16.00375

Iwai M, Takizawa K, Tokutsu R, Okamuro A, Takahashi Y, Minagawa J. Isolation of the elusive supercomplex that drives cyclic electron flow in photosynthesis. *Nature*. 2010:464(7292):1210–1213. https://doi.org/10.1038/nature08885

Johnson GN. Thiol regulation of the thylakoid electron transport chain–a missing link in the regulation of photosynthesis? *Biochemistry*. 2003:42(10):3040–3044. https://doi.org/10.1021/bi027011k

Kang ZH, Wang GX. Redox regulation in the thylakoid lumen. *J Plant Physiol*. 2016:192:28–37. https://doi.org/10.1016/j.jplph.2015.12.012

Karamoko M, Cline S, Redding K, Ruiz N, Hamel PP. Lumen thiol oxidoreductase1, a disulfide bond-forming catalyst, is required for the assembly of photosystem II in Arabidopsis. *Plant Cell*. 2011:23-(12):4462–4475. https://doi.org/10.1105/tpc.111.089680

Karamoko M, Gabilly ST, Hamel PP. Operation of trans-thylakoid thiol-metabolizing pathways in photosynthesis. *Front Plant Sci*. 2013:4:476. https://doi.org/10.3389/fpls.2013.00476

König J, Baier M, Horling F, Kahmann U, Harris G, Schürmann P, Dietz KJ. The plant-specific function of 2-Cys peroxiredoxin-mediated detoxification of peroxides in the redox-hierarchy of photosynthetic electron flux. *Proc Natl Acad Sci U S A*. 2002:99(8):5738–5743. https://doi.org/10.1073/pnas.072644999

Kozuleva M, Petrova A, Milrad Y, Semenov A, Ivanov B, Redding KE, Yacoby I. Phylloquinone is the principal Mehler reaction site within photosystem I in high light. *Plant Physiol*. 2021:186(4):1848–1858. https://doi.org/10.1093/plphys/kiab221

Krieger-Liszkay A, Shimakawa G, Sétif P. Role of the two PsaE isoforms on O2 reduction at photosystem I in *Arabidopsis thaliana*. *Biochim Biophys Acta Bioenerg*. 2020:1861(1):148089. https://doi.org/10.1016/j.bbabio.2019.148089

Lepistö A, Kangasjärvi S, Luomala EM, Brader G, Sipari N, Keränen M, Keinänen M, Rintamäki E. Chloroplast NADPH-thioredoxin reductase interacts with photoperiodic development in Arabidopsis. *Plant Physiol*. 2009:149(3):1261–1276. https://doi.org/10.1104/pp.108.133777

Lepistö A, Pakula E, Toivola J, Krieger-Liszkay A, Vignols F, Rintamaki E. Deletion of chloroplast NADPH-dependent thioredoxin reductase results in inability to regulate starch synthesis and causes stunted growth under short-day photoperiods. *J Exp Bot*. 2013:64-(12):3843–3854. https://doi.org/10.1093/jxb/ert216

Marcaida MJ, Schlarb-Ridley BG, Worrall JA, Wastl J, Evans TJ, Bendall DS, Luisi BF, Howe CJ. Structure of cytochrome c6A, a novel dithio-cytochrome of *Arabidopsis thaliana*, and its reactivity with plastocyanin: implications for function. *J Mol Biol*. 2006:360(5):968–977. https://doi.org/10.1016/j.jmb.2006.05.065

Mazor Y, Borovikova A, Nelson N. The structure of plant photosystem I super-complex at 2.8 Å resolution. *Elife*. 2015:4:e07433. https://doi.org/10.7554/eLife.07433

Michalska J, Zauber H, Buchanan BB, Cejudo FJ, Geigenberger P. NTRC links built-in thioredoxin to light and sucrose in regulating starch synthesis in chloroplasts and amyloplasts. *Proc Natl Acad Sci U S A*. 2009:106(24):9908–9913. https://doi.org/10.1073/pnas.0903559106

Michelet L, Krieger-Liszkay A. Reactive oxygen intermediates produced by photosynthetic electron transport are enhanced in short-day grown plants. *Biochim Biophys Acta*. 2012:1817(8):1306–1313. https://doi.org/10.1016/j.bbabio.2011.11.014

Motohashi K, Hisabori T. HCF164 receives reducing equivalents from stromal thioredoxin across the thylakoid membrane and mediates reduction of target proteins in the thylakoid lumen. *J Biol Chem*. 2006:281(46):35039–35047. https://doi.org/10.1074/jbc.M605938200

Motohashi K, Hisabori T. Ccda is a thylakoid membrane protein required for the transfer of reducing equivalents from stroma to thylakoid lumen in the higher plant chloroplast. *Antioxid Redox Signal*. 2010:13(8):1169–1176. https://doi.org/10.1089/ars.2010.3138

Muthuramalingam M, Seidel T, Laxa M, Nunes de Miranda SM, Gärtner F, Ströher E, Kandlbinder A, Dietz KJ. Multiple redox and non-redox interactions define 2-cys peroxiredoxin as a regulatory hub in the chloroplast. *Mol Plant*. 2009:2(6):1273–1288. https://doi.org/10.1093/mp/ssp089

Naranjo B, Mignee C, Krieger-Liszkay A, Hornero-Mendez D, Gallardo-Guerrero L, Cejudo FJ, Lindahl M. The chloroplast NADPH thioredoxin reductase C, NTRC, controls non-photochemical quenching of light energy and photosynthetic electron transport in Arabidopsis. *Plant Cell Environ*. 2016:39(4):804–822. https://doi.org/10.1111/pce.12652

Naranjo B, Penzler J-F, Rühle T, Leister D. NTRC effects on non-photochemical quenching depends on PGR5. *Antioxidants*. 2021:10(6):900. https://doi.org/10.3390/antiox10060900

Nikkanen L, Toivola J, Rintamaki E. Crosstalk between chloroplast thioredoxin systems in regulation of photosynthesis. *Plant Cell Environ*. 2016:39(8):1691–1705. https://doi.org/10.1111/pce.12718

Nikkanen L, Toivola J, Trotta A, Diaz MG, Tikkanen M, Aro EM, Rintamäki E. Regulation of cyclic electron flow by chloroplast NADPH-dependent thioredoxin system. *Plant Direct*. 2018:2(11):e00093. https://doi.org/10.1002/pld3.93

Ojeda V, Perez-Ruiz JM, Cejudo FJ. 2-Cys peroxiredoxins participate in the oxidation of chloroplast enzymes in the dark. *Mol Plant*. 2018:11(11):1377–1388. https://doi.org/10.1016/j.molp.2018.09.005

Ojeda V, Perez-Ruiz JM, Gonzalez M, Najera VA, Sahrawy M, Serrato AJ, Geigenberger P, Cejudo FJ. NADPH thioredoxin reductase C and thioredoxins act concertedly in seedling development. *Plant Physiol*. 2017:174(3):1436–1448. https://doi.org/10.1104/pp.17.00481

Okegawa Y, Motohashi K. Chloroplastic thioredoxin m functions as a major regulator of Calvin cycle enzymes during photosynthesis in vivo. *Plant J*. 2015:84(5):900–913. https://doi.org/10.1111/tpj.13049

Okegawa Y, Motohashi K. M-type thioredoxins regulate the PGR5/PGRL1-dependent pathway by forming a disulfide-linked complex with PGRL1. *Plant Cell*. 2020:32(12):3866–3883. https://doi.org/10.1105/tpc.20.00304

Okegawa Y, Sato N, Nakakura R, Murai R, Sakamoto W, Motohashi K. x- and y-type thioredoxins maintain redox homeostasis on photosystem I acceptor side under fluctuating light. *Plant Physiol*. 2023:193(4):2498–2512. https://doi.org/10.1093/plphys/kiad466

Page ML, Hamel PP, Gabilly ST, Zegzouti H, Perea JV, Alonso JM, Ecker JR, Theg SM, Christensen SK, Merchant S. A homolog of prokaryotic thiol disulfide transporter CcdA is required for the assembly of the cytochrome b6f complex in Arabidopsis chloroplasts. *J Biol Chem*. 2004:279(31):32474–32482. https://doi.org/10.1074/jbc.M404285200

Pan X, Ma J, Su X, Cao P, Chang W, Liu Z, Zhang X, Li M. Structure of the maize photosystem I supercomplex with light-harvesting complexes I and II. *Science (1979)*. 2018:360(6393):1109–1113. https://doi.org/10.1126/science.aat1156

Perez-Ruiz JM, Guinea M, Puerto-Galan L, Cejudo FJ. NADPH thioredoxin reductase C is involved in redox regulation of the Mg-chelatase I subunit in *Arabidopsis thaliana* chloroplasts. *Mol Plant*. 2014:7(7):1252–1255. https://doi.org/10.1093/mp/ssu032

Perez-Ruiz JM, Naranjo B, Ojeda V, Guinea M, Cejudo FJ. NTRC-dependent redox balance of 2-Cys peroxiredoxins is needed for optimal function of the photosynthetic apparatus. *Proc Natl Acad Sci U S A*. 2017:114(45):12069–12074. https://doi.org/10.1073/pnas.1706003114

Pesaresi P, Scharfenberg M, Weigel M, Granlund I, Schröder WP, Finazzi G, Rappaport F, Masiero S, Furini A, Jahns P, *et al*. Mutants, overexpressors, and interactors of Arabidopsis plastocyanin isoforms: revised roles of plastocyanin in photosynthetic electron flow and thylakoid redox state. *Mol Plant*. 2009:2(2):236–248. https://doi.org/10.1093/mp/ssn041

Qin X, Suga M, Kuang T, Shen JR. Photosynthesis. Structural basis for energy transfer pathways in the plant PSI-LHCI supercomplex. *Science (1979)*. 2015:348(6238):989–995. https://doi.org/10.1126/science.aab0214

Ramos CL, Pou S, Britigan BE, Cohen MS, Rosen GM. Spin trapping evidence for myeloperoxidase-dependent hydroxyl radical formation by human neutrophils and monocytes. *J Biol Chem*. 1992:267(12):8307–8312. https://doi.org/10.1016/S0021-9258(18)42443-X

Rey P, Sanz-Barrio R, Innocenti G, Ksas B, Courteille A, Rumeau D, Issakidis-Bourguet E, Farran I. Overexpression of plastidial thioredoxins f and m differentially alters photosynthetic activity and response to oxidative stress in tobacco plants. *Front Plant Sci*. 2013:4:390. https://doi.org/10.3389/fpls.2013.00390

Richter AS, Peter E, Rothbart M, Schlicke H, Toivola J, Rintamaki E, Grimm B. Posttranslational influence of NADPH-dependent thioredoxin reductase C on enzymes in tetrapyrrole synthesis. *Plant Physiol*. 2013:162(1):63–73. https://doi.org/10.1104/pp.113.217141

Serrato AJ, Perez-Ruiz JM, Spinola MC, Cejudo FJ. A novel NADPH thioredoxin reductase, localized in the chloroplast, which deficiency causes hypersensitivity to abiotic stress in *Arabidopsis thaliana*. *J Biol Chem*. 2004:279(42):43821–43827. https://doi.org/10.1074/jbc.M404696200

Ströher E, Dietz KJ. The dynamic thiol-disulphide redox proteome of the *Arabidopsis thaliana* chloroplast as revealed by differential electrophoretic mobility. *Physiol Plant*. 2008:133(3):566–583. https://doi.org/10.1111/j.1399-3054.2008.01103.x

Takahashi H, Clowez S, Wollman FA, Vallon O, Rappaport F. Cyclic electron flow is redox-controlled but independent of state transition. *Nat Commun*. 2013:4(1):1954. https://doi.org/10.1038/ncomms2954

Telman W, Liebthal M, Dietz KJ. Redox regulation by peroxiredoxins is linked to their thioredoxin-dependent oxidase function. *Photosynth Res*. 2020:145:31–41. https://doi.org/10.1007/s11120-019-00691-0

Thormählen I, Meitzel T, Groysman J, Ochsner AB, von Roepenack-Lahaye E, Naranjo B, Cejudo FJ, Geigenberger P. Thioredoxin f1 and NADPH-dependent thioredoxin reductase C have overlapping functions in regulating photosynthetic metabolism and plant growth in response to varying light conditions. *Plant Physiol*. 2015:169(3):1766–1786. https://doi.org/10.1104/pp.15.01122

Thormählen I, Zupok A, Rescher J, Leger J, Weissenberger S, Groysman J, Orwat A, Chatel-Innocenti G, Issakidis-Bourguet E, Armbruster U, *et al*. Thioredoxins play a crucial role in dynamic acclimation of photosynthesis in fluctuating light. *Mol Plant*. 2017:10(1):168–182. https://doi.org/10.1016/j.molp.2016.11.012

Toivola J, Nikkanen L, Dahlström KM, Salminen TA, Lepistö A, Vignols HF, Rintamäki E. Overexpression of chloroplast NADPH-dependent thioredoxin reductase in *Arabidopsis* enhances leaf growth and elucidates *in vivo* function of reductase and thioredoxin domains. *Front Plant Sci*. 2013:4:389. https://doi.org/10.3389/fpls.2013.00389

Vaseghi MJ, Chibani K, Telman W, Liebthal MF, Gerken M, Schnitzer H, Mueller SM, Dietz KJ. The chloroplast 2-cysteine peroxiredoxin functions as thioredoxin oxidase in redox regulation of chloroplast metabolism. *Elife*. 2018:7:e38194. https://doi.org/10.7554/eLife.38194

Wang P, Liu J, Liu B, Feng D, Da Q, Wang P, Shu S, Su J, Zhang Y, Wang J, *et al*. Evidence for a role of chloroplastic m-type thioredoxins in the biogenesis of photosystem II in Arabidopsis. *Plant Physiol*. 2013:163(4):1710–1728. https://doi.org/10.1104/pp.113.228353

Wolf BC, Isaacson T, Tiwari V, Dangoor I, Mufkadi S, Danon A. Redox regulation of PGRL1 at the onset of low light intensity. *Plant J*. 2020:103(2):715–725. https://doi.org/10.1111/tpj.14764

Hani *et al.*

Sup. Fig. 1 (A). Immunoblot analysis of NTRC, Trx-m and 2-Cys Prx proteins under long- and short-day conditions.

Immunodetection of NTRC, Trx-m and 2-Cys Prx in total leaf extracts prepared from wild-type plants grown either in short day (SD) or long day (LD) conditions during 3 and 6 weeks, respectively. Samples corresponding to 4, 2 and 1 mg fresh weight (100, 50 and 25%, respectively) were fractionated by SDS-PAGE under reducing conditions, transferred onto nitrocellulose membranes and immunodetected using specific antibodies against NTRC, 2-Cys Prx and Trx-m. Representative blots from four biologically replicates from two independent experiments are presented, as well as the average of the band quantifications (n=4) relative to LD-100 (100%) ± standard deviation (SD).

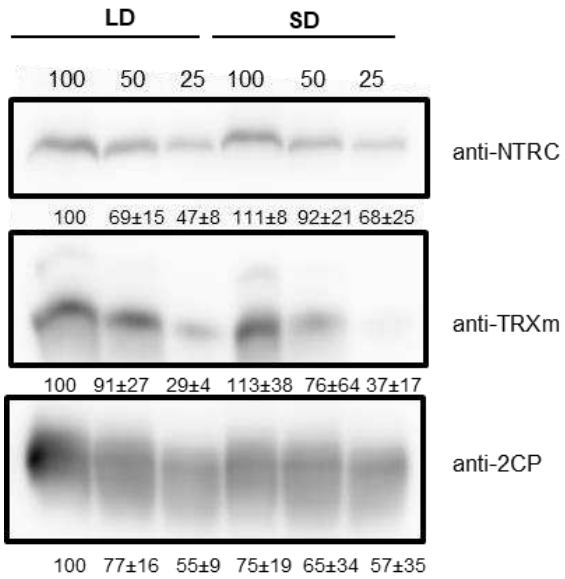

Note: With the anti-Trx-m antibodies used here, the different sized bands correspond to the different Trxs-m: Trx-m1 and -m2 (lower band) and Trx-m4 (higher band). See Delgado-Requerey et al. 2023. Antioxidants 2023, 12(5), 1041; https://doi.org/10.3390/antiox12051041

Method:

For quantification of NTRC, Trx-m and 2-Cys Prx proteins, wild-type plants grown under LD and SD conditions during 3 and 6 weeks, respectively, were used. Rosette leaves were ground with liquid nitrogen and homogenized in 2× Tricine buffer containing 8% [w/v] SDS, 24% [w/v] glycerol, 15 mM DTT, and 100 mM Tris/HCl pH 6.8. The homogenate was incubated for 5 min at 70°C and centrifuged for 10 min at 13,000 × *g*. Solubilized leaf proteins corresponding to 4, 2 and 1 mg fresh weight (100, 50 and 25%, respectively) were loaded onto 15% Tris-Glycine-SDS polyacrylamide gels and subjected to electrophoresis, transferred onto nitrocellulose membranes, and immunodetected using specific antibodies. Anti-NTRC and anti-2-Cys Prx-specific antibodies were kindly provided by Dr. Cejudo (Universidad de Sevilla, Spain), while anti-Trx-m was kindly provided by Dr. Buchanan (Department of Plant and Microbial Biology, University of California, Berkeley, CA, USA). Staining of the membranes with Ponceau served as loading control.

Sup. Fig. 2 Attachment of Trx m2 and m4 to thylakoid membranes.

Experiment performed as described in Fig. 3 caption.

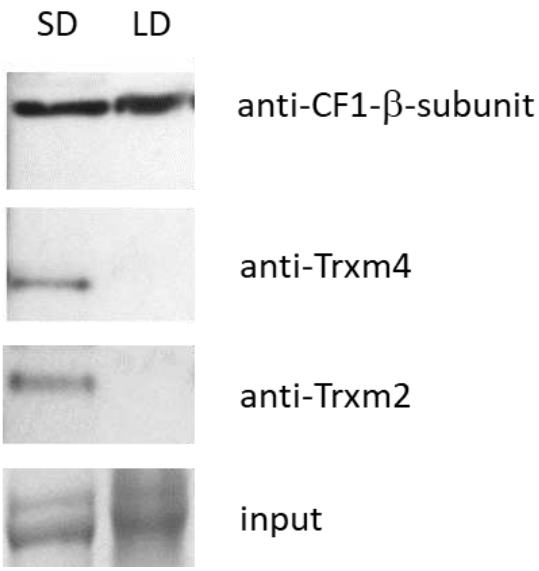

Sup. Fig. 3 PsaF immunodetection in thylakoid membranes

Thylakoid proteins from wt plants grown in SD or LD were treated or not with the reducing chemical TCEP prior to thiol alkylation with AMS. Proteins (equivalent to 2-3 µg chlorophylls) were electrophoresed (SDS-PAGE) and stained with Coomassie blue, or electro-transferred onto a PVDF membrane for immuno-detection of psaF. 1: SD thylakoids untreated; 2: LD thylakoids untreated; 3: SD thylakoids reduced; 4: LD thylakoids reduced. Arrows and asterisk indicate redox variants and unspecific signal, respectively.

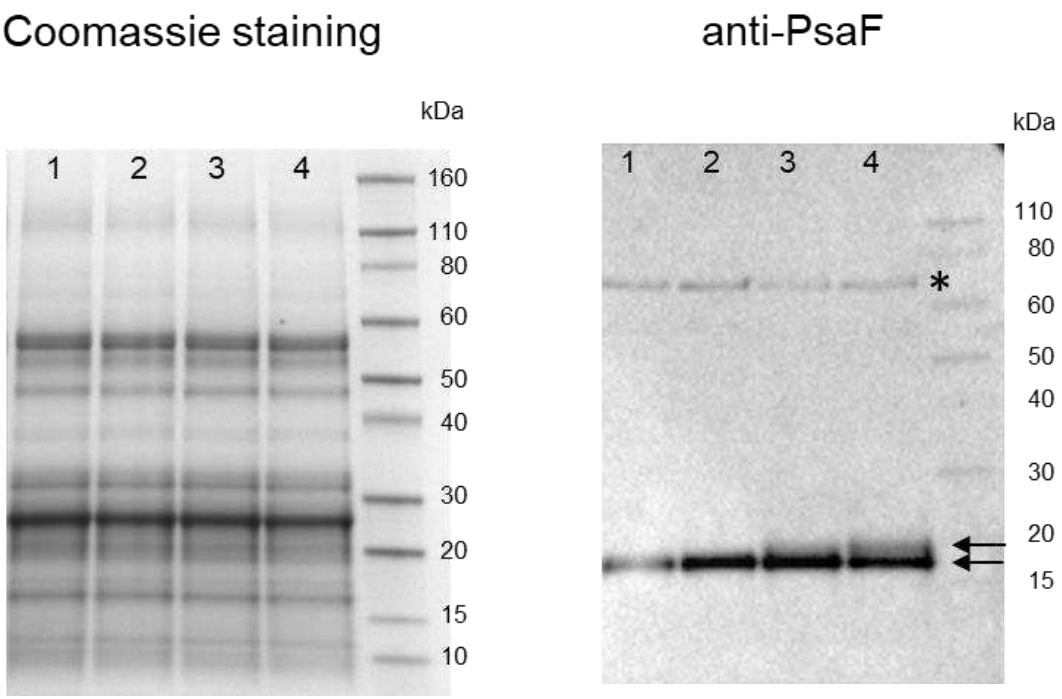

Sup. Fig. 4 Immunodetection and redox state of PsaF in leaf extracts

In order to establish the quantity of leaf extract (Col-0 samples) required to enable a quantitative detection of PsaF the protein samples were prepared in the presence of a reducing chemical (TCEP). Leaf extracts, ranging from 12.5 to 150 µg, were separated by gel electrophoresis (SDS-PAGE under reducing conditions), and transferred onto a PVDF membrane prior to immuno-detection of PsaF. The corresponding signal (chemi-luminescence) was quantified using ImageLab software (BioRad). The PsaF signal was plotted against leaf extract to generate a calibration curve.

(A) Western blot, ECL signal; (B) Densitometry analysis.

For redox western analyses of PsaF, preliminary tests allowed to distinguish oxidized and reduced (pegylated form with mPEG-mal(24)) (C), using 50 µg protein leaf samples electrophoresed in non-reducing conditions. An example of redox western result obtained with dark samples is shown in (D). MWM : molecular weight marker (kDa).

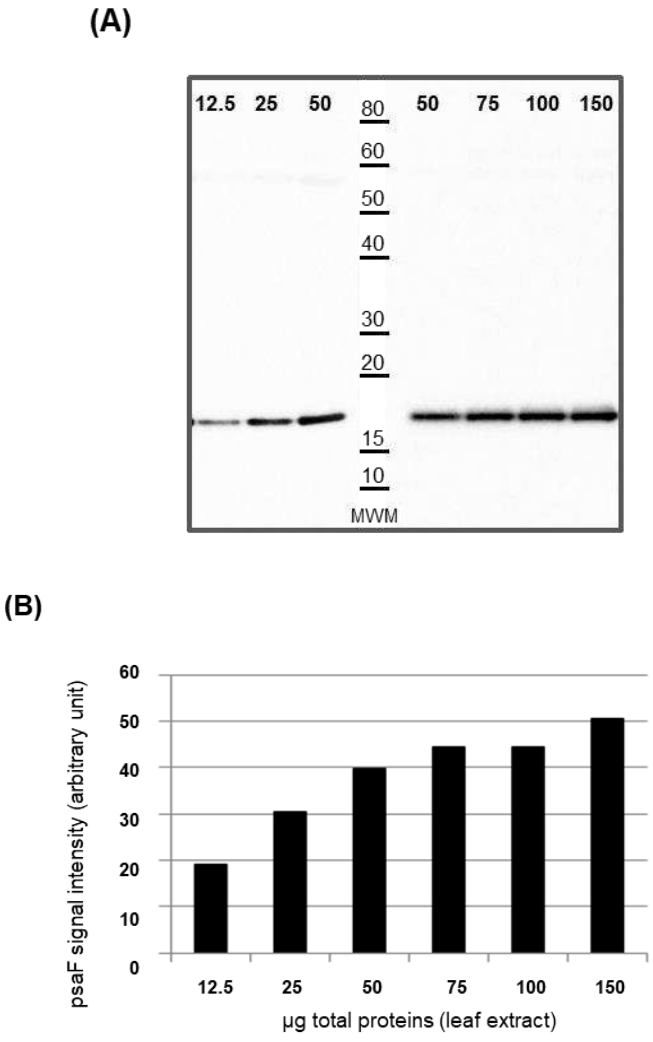

Hani *et al*.

Sup. Fig 4. (C)

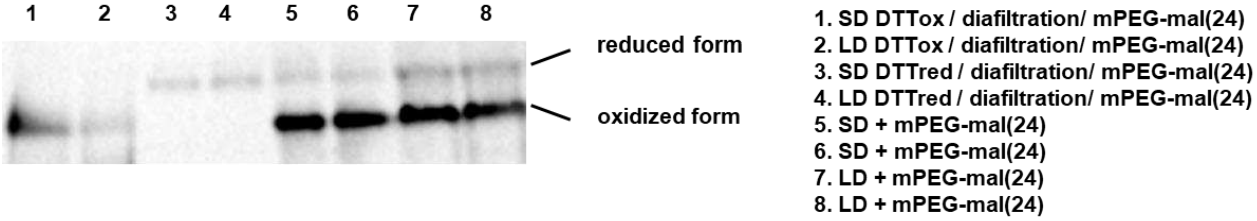

- Extracts without mPEG-mal (lanes 1-4), treated with DTTox (lanes 1 and 2) or DTTred (lanes 3 and 4) (10 mM, 15 min, RT), then diafiltered (amicon ultra, cut-off 10 kDa) then treated with mPEG-mal(24) (2 mM, 30 min, 30°C)

- Extracts with mPEG-mal(24) (lanes 5-8) at 2 mM, incubated 30 min 30°C

- All samples, precipitated (+ 7 vol. cold ethanol, overnight – 20°C), spin (max. speed 10 min RT) and pellet re-suspension in loading blue (non-reducing)

Hani *et al*.

Sup. Fig. 4 (D)

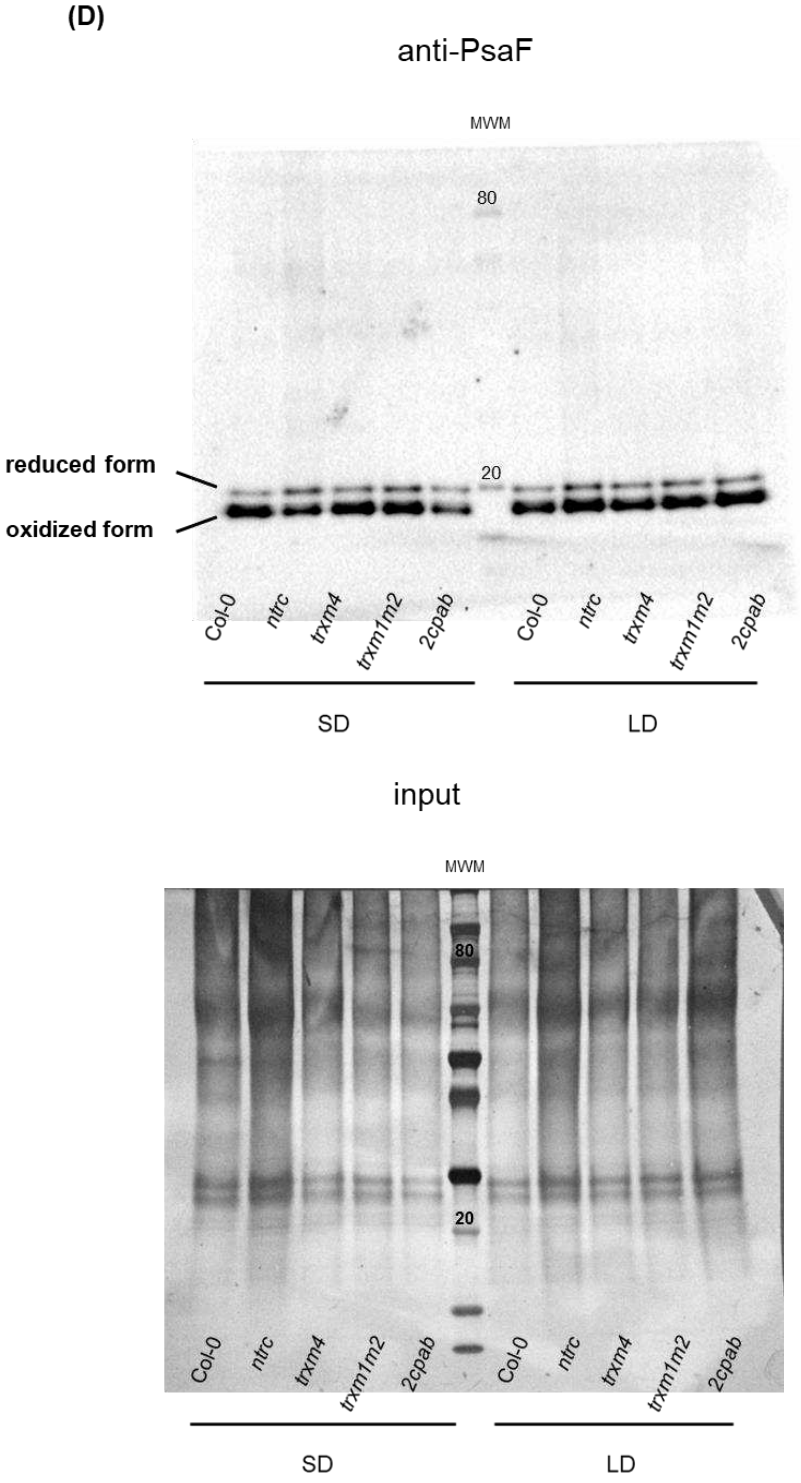

Sup. Fig. 5 Light-induced hydroxyl radical formation in SD and LD leaf disks of *psan*

Generation of hydroxyl radicals originating from $O_2^{\bullet-}/H_2O_2$ was detected by spin trapping with 4-POBN.

Mean values are shown (n=4, biological replicates; *, P <0.05 according to Tukey test.

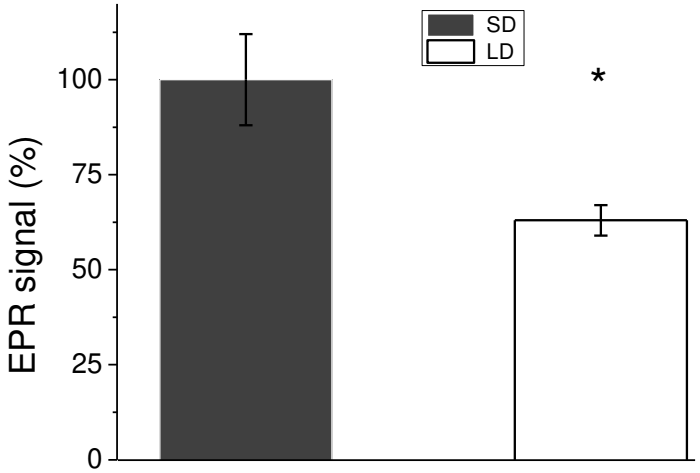

Sup. Fig. 6 Reduction tests of Trxs m by NTRC *in vitro*

Thiols were spectrophotometrically followed by the reduction of the thiol reagent DTNB. NADPH (150 µM) and NTRC (20 nM) were mixed and then TRX (10 µM) was added. Kinetics were started with the addition of DTNB (1 mM).

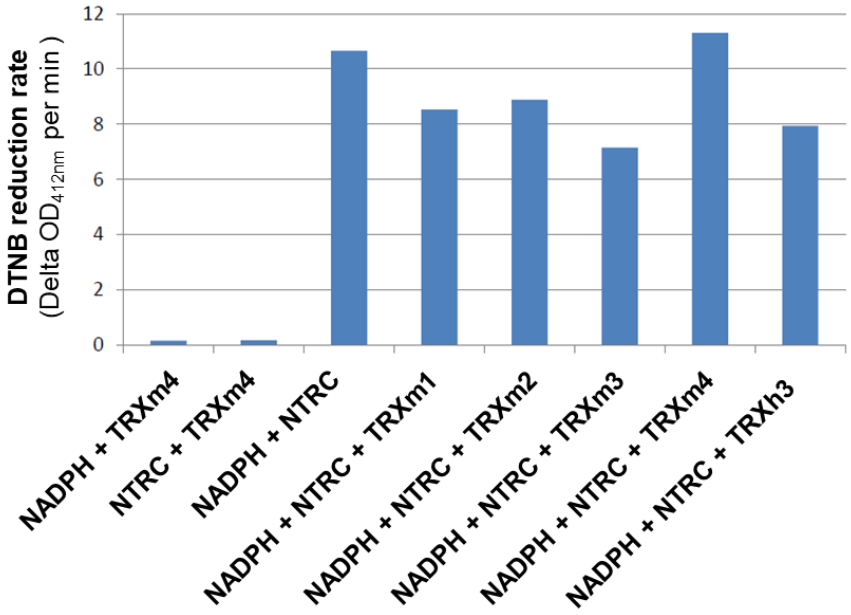

4.3. Characterization of *ccda* and *cytc$_6$a* in *Arabidopsis thaliana*

It has been shown in our publication (Article 3) that CCDA has an important role as an electron carrier in transferring the reducing powers from stroma to the lumen in *A. thaliana* (Hani et al., 2024). However, cyt *c$_6$a* seems not be involved. Plants (*ccda* lines and *cytc$_6$a*) when grown in two different light regimes (Short day(SD)/ Long day(LD)), showed no obvious phenotype (Fig 12). It was already known previously that lack of *cytc$_6$a* has no obvious phenotype in *A. thaliana* (Gupta et al., 2002). To further characterize the plants, 3.5 weeks old plants grown under LD conditions were exposed to different light intensities (upto 600 µmol photons $m^{-2}s^{-1}$) and several photosynthetic parameters were recorded as shown in (Fig. 13-A). However, no obvious differences were seen among the mutants in comparison with wild type (Col-0). Moreover, photoinhibition (Fig 13-B) was studied and Fv/Fm was followed during exposure to high light (700 µmol photons $m^{-2}s^{-1}$) for 120 minutes and the recovery at room light. Fv/Fm remained unchanged in the mutants like in Col-0. No changes in NPQ was seen when plants were illuminated with fluctuating light intensity (Fig 13-C) altered between 55 µmol photons $m^{-2}s^{-1}$ (LL) and 800 µmol photons $m^{-2}s^{-1}$ (HL). The rest of parameters also remained unchanged (not shown here). In order to know if any phenotype exist for these plants under different temperatures, plants were grown at three different temperatures (4, 20 and 27°C), however we did not observe any significant differences in growth (This data is not shown here). Note that the results are only shown for *ccda-3*(as *ccda-4* behaved similar) and *cytc$_6$a* grown under LD conditions SD behaved in a similar way and no differences were observed among two light regimes.

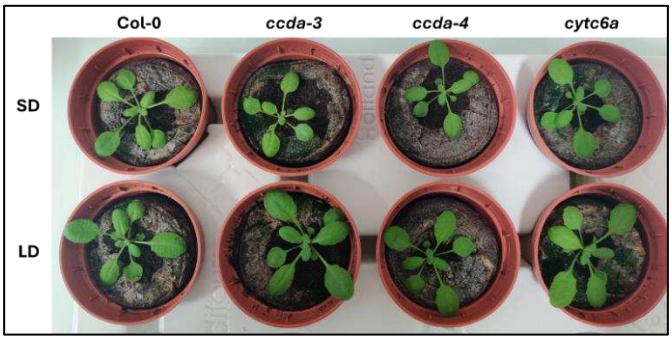

Fig 12- Photo taken for 3 weeks old *Arabidopsis thaliana* plants (Col-0, *ccda-3*, *ccda-4* and *cytc$_6$a*) grown under short day (8h light/16h dark) and long day (16h light/8h dark) conditions.

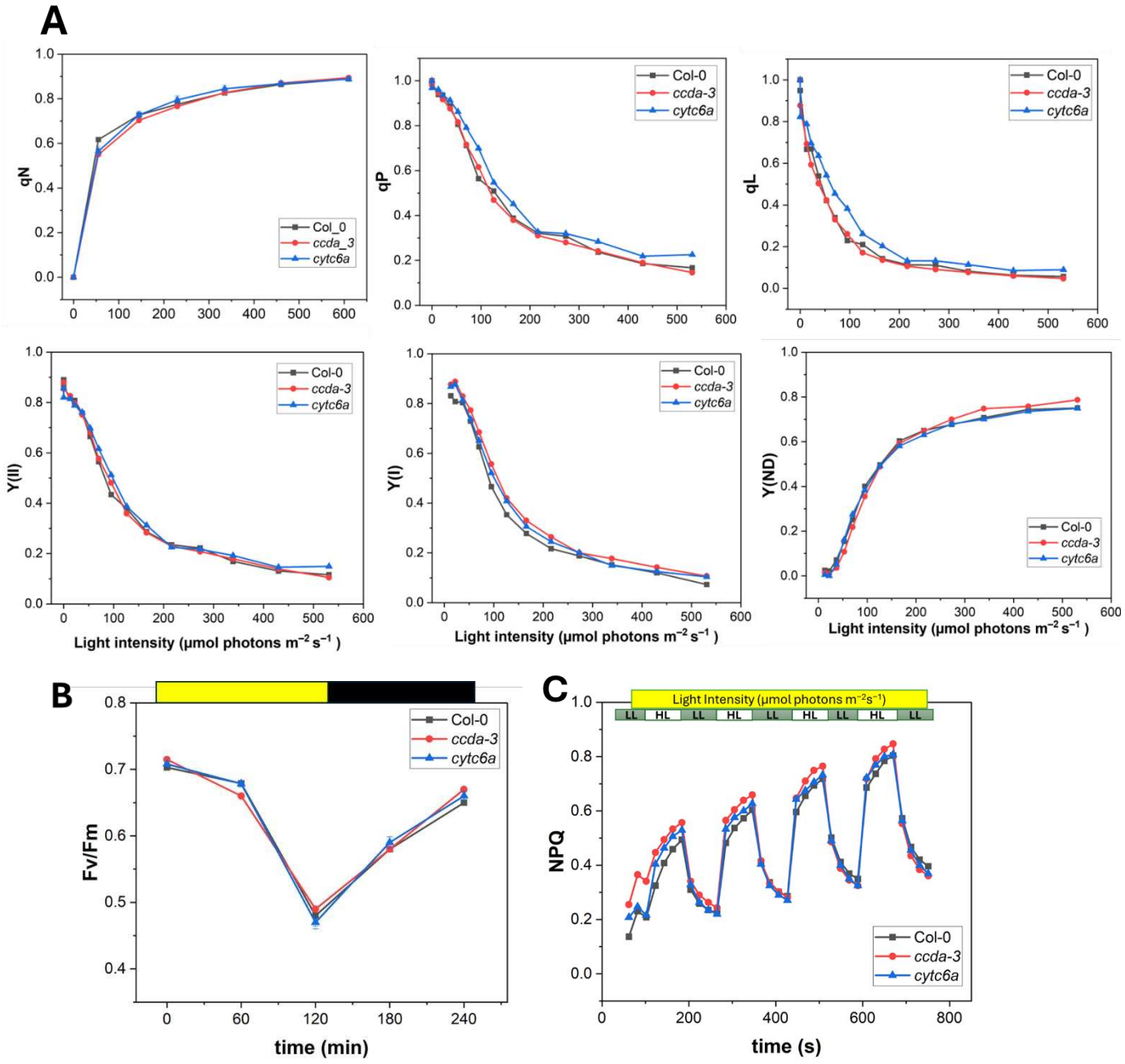

Fig 13. Photosynthetic parameters measured in *Arabidopsis* as a function of different light intensities ranging from 0-600 µmol photons $m^{-2} s^{-1}$ (A).Photoinhibition in *Arabidopis* mutants, where plants were exposed to 700 µmol photons $m^{-2} s^{-1}$ for 120 minutes and recovery was studied at room light (B). Changes in NPQ upon illumination with fluctuating light intensity (50 µmol photons $m^{-2} s^{-1}$ and 800 µmol photons $m^{-2} s^{-1}$ as low and high light intensities respectively) as a function of time (C).

Chapter 5: General Discussions

During the course of my PhD, I was specifically interested in alternative electron transports and how they are regulated. The physiological design of the electron transport chain comes with many feedback mechanisms, that makes it a bit complicated to explore and distinguish these regulatory mechanisms in an in vivo study. Here, I have concentrated only on thioredoxin-mediated redox regulations and ferredoxin-dependent cyclic electron transport under different conditions in two different model plants (*Arabidopsis* and *Marchantia*). I have shown that under Mn deficiency, cyclic electron flow might come into play to protect PSII. Moreover, thanks to KLAS-NIR, that enables us to visualize the real-time redox changes in P700 and PC, I was able to investigate the turnover of P700 and PC. Slower oxidation and faster re-reduction kinetics of P700 and PC support our hypothesis about the possibility of supercomplex formation around PSI and Cyt b_6f complex. On the other hand, we have shown that thioredoxins and certain other lumenal and stromal proteins are involved in the redox regulation of pseudocyclic electron transport under different photoperiod growth.

Taken together, these observations point to the possibilities of interesting interconnection among these two electron flows, but surely, some challenges will be encountered during future studies regarding the regulation of these complex pathways. So now, let's first discuss how we can link cyclic and pseudocyclic keeping in mind what we got during our research.

It is known already that conserved cysteines of PGRL1 protein play a more decisive role in CET activity and that PGRL1 is redox-regulated. Further, Courteille et al., (2013) and Okegawa and Motohashi (2020) have shown that redox factors like Trxm are negatively regulating the PGR5/PGRL1-dependent cyclic electron transport. We have shown that, in contrast, PCET is activated under reducing conditions and we suggest that the reduction of a disulphide bridge of PsaF allows a higher activity of O_2 reduction at PSI (Chapter 4). The questions that we think will need to be addressed in the field in the next years are: If CET and PCET compete in the context of the role of Trxm? If yes, then what about the role of Trxm in the supercomplex formation around CET and what are the other players besides Trxs that could be involved in the redox regulation of CET and PCET? Besides that, another small protein called thylakoid soluble phosphoprotein (TSP9) has been identified in cryo-EM structures of Cyt b_6f. It is known to bind

to the site, where potential n-type electron donor protein is thought to interact with Cyt b_6f and could have a role in CET (Sarewicz et al., 2023). TSP9 possibly also has a role in photosynthetic state transitions. This makes it even more interesting to study it further since state transitions have been proposed to have a role in activating CET and ultimately in the putative supercomplex formation (see for example Kalra et al., 2023). However, the role of state transitions for activation of CET has been ruled out earlier in *Chlamydomonas reinhardtii* (Takahashi et al., 2013). Based on these speculations, we can say that TSP9 might not be directly a part of the supercomplex around CET but could have a more regulatory role in balancing linear and cyclic electron transport or it might be the long-searched docking site for Fd. A detailed sequential study using mutants lacking TSP9 is needed to solve this puzzle.

Talking about the redox regulation of oxygen reduction at the PSI acceptor side, still there are many open questions. With the additional knowledge about the redox systems, more new players were identified, and cross-talks unveiled. However, still, the interactions among several players are not very clear. Let's say, we are still in doubt about the role of NTRC in the redox regulation of oxygen reduction. Is NTRC directly or indirectly regulating the redox status of Trxm-4 or if it somehow functions as a support system to the FTR enzyme? And what about the role of other thioredoxins isoforms in this kind of redox regulation? Moreover, the reversible attachment of Trxm-4 and 2-Cys Prx also needs to be addressed further. In the context of redox regulation of PCET, it will be important to develop a method to trap the redox state of PsaF. Another open question is if indeed LTO1 is involved in mediating the redox state of PsaF or if other, yet unknown lumenal proteins are involved in redox regulation in the thylakoid lumen. Thus, to gain further insights into the redox regulation in chloroplasts, a wide range of potential partners needs to be addressed and investigated in combination.

Moreover, regarding the redox regulations of CET in bryophytes, with the presence of FLV proteins, it seems obvious that the moss redox system in chloroplasts is potentially different from angiosperms. Moreover, we also have not studied the redox changes in Fd under Mn deficiency throughout our study in *Marchantia*, since the Fd signals were too noisy to be confidently analysed. Differences in the redox state of Fd could be attributed in addition to LEF and CET to the function of FLV protein (Sétif et al.,2019), and it would be interesting to study Fd reduction and oxidation in parallel with NADPH generation and reoxidation. It’s always interesting to

study photosynthesis from an evolutionary point of view. Comparing the thioredoxin-mediated redox regulations in mosses and angiosperms will introduce new topics in the field. Furthermore, we can speculate that bryophytes might also possess greater backup capacity in redox regulation, which could be an indication of unknown electron sinks for the reduction mechanism. Taken together, these redox regulatory modifications from simpler to complex systems need to be completely uncovered in the near future.

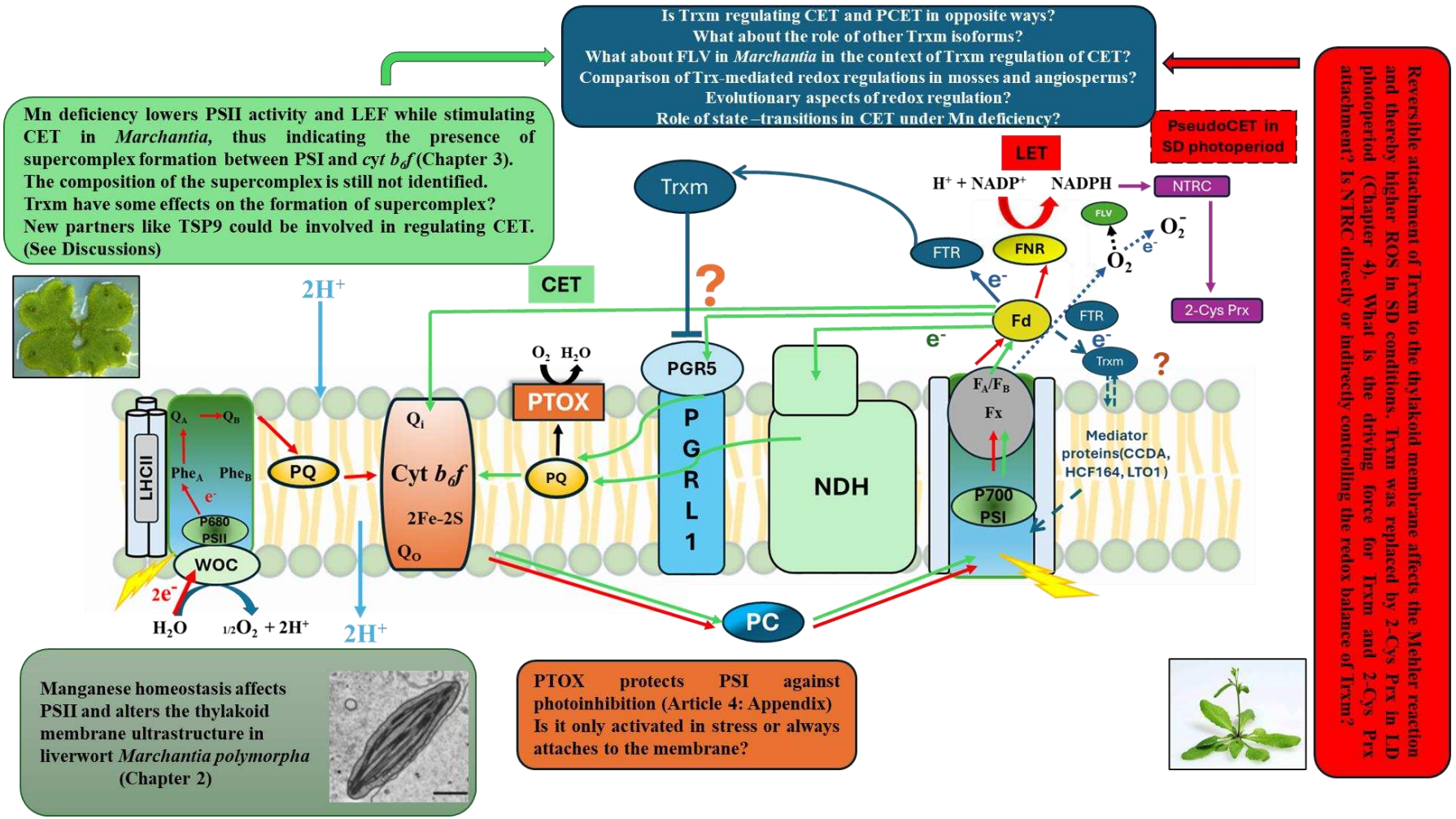

Fig 14: Summary Diagram, Regulation of Cyclic and Pseudocyclic electron transport. A general overview of each chapter is given in the colored boxes

Conclusions and Perspectives

The main objectives of the thesis were :

1. To study the effect of manganese homeostasis on photosynthesis in liverwort *Marchantia polymorpha.*
2. To study the role of thioredoxins, stromal and lumenal proteins in redox regulation of oxygen reduction at the Photosystem I acceptor side under different light regimes in *Arabidopsis thaliana*.

1. Effect of Manganese homeostasis on photosynthesis in liverwort *Marchantia polymorpha*

Manganese (Mn) is an important constituent of water splitting complex at the donor side of PSII, thus playing an important role in photosynthesis. In our study (Messant et al., 2023; Chapter 2) we have used liverwort *Marchantia polymorpha* and have shown the effects of both Mn excess and deficiency on photosynthesis. We have shown that *Marchantia* can accumulate upto 25 mg Mn. g DW^{-1}, which does not classify it a hyperaccumulator, but could point out towards the fact that some sort of protection mechanisms might exist that allow *Marchantia* to efficiently withstand the metal stress. Another explanation could be specific transport mechanisms that might differ from *Arabidopsis thaliana*. Moreover, metabolomic analyses revealed the presence of some metabolites that were absent in *Arabidopsis,* this might indicate the presence of different metabolic pathways in *Marchantia.* It would be interesting to further address these questions by focusing mainly on evolutionary aspects of land plants in relation to other transition metals stress. Moreover, one of the challenging task during this study was to create Mn deficiency in *Marchantia,* which was achieved by using starch as a gelling agent instead of Agar. Mn deficiency overall indicated a change in the thylakoid membrane structure, and this also indicates the role of ion homeostasis in modulating thylakoid membrane dynamics. Interestingly, under Mn deficiency an increase in NPQ pointed towards enhanced cyclic electron transport (CET).

Further, I continued the project by looking deeper into the effects of Mn deficiency on photosynthetic electron transport in *Marchantia* (Hani and Krieger-Liszkay, 2024; Chapter 3). With the help of KLAS-NIR spectrophotometer, we have shown the in vivo redox changes in

P700 and PC under Mn deficiency. We reported a drastic decrease in the PC content relative to P700 signal, which suggests that it has an effect on electron donation to P700. Decrease of PC have also been reported in tobacco and barley during the early stages of senescence (Schöttler et al., 2004; Shimakawa et al., 2020). Moreover, using far-red light , we have shown slower P700 oxidation and faster re-reduction kinetics of $P700^+$ and PC^+ under Mn deficiency, that suggests an increase in the electron transport or availability of electron donors. This speaks for enhanced CET under Mn deficiency rather than chlororespiration, since we observed less donor side limitation under red actinic light. The faster re-reduction kinetics of both $P700^+$, PC^+ and less pool size of PC under Mn deficiency might suggest structural re-organization and some sort of supercomplex formation between Fd-PSI-Cyt b_6f and PC. Here we also propose that changes in the thylakoid membrane organization under Mn deficiency may also favor such kind of supercomplex formation.

Moreover, contrary to the above, we observed slower re-reduction kinetics of $P700^+$ and PC^+ under Mn deficiency in the presence of uncoupler nigericin, which rather indicates photosynthetic control. So here, it can be hypothesized that faster reduction kinetics observed under Mn deficiency without the uncoupler could be because of enhanced CET and less photosynthetic control and vice versa. Another explanation could be the NADPH-driven reverse electron flow, thus providing electrons for $P700^+$ and PC^+ in the presence of uncoupler.

However, experiments are needed to confirm whether CET is dependent on certain pool size of proton gradient or pH dependent changes. In addition to that, it's important to identify the putative supercomplex formation under Mn deficiency. Further, it would be really interesting to further characterize TSP9 protein (see Discussions). I have already started designing the CRISPR mutants for TSP9 and it would be interesting to characterize them and further check them under different conditions (like Mn deficiency). The identification of supercomplex will help in understanding the role of CET under different stress conditions and it would further pave the way to study the changes in photosynthetic electron flow under deprivation of micronutrients other than Mn.

Furthermore, to study the effects of Mn deficiency on *Arabidopsis thaliana,* I was successful in achieving Mn deficiency by growing plants hydroponically. Now the plan is to

perform mass spectrometry and to see if there is any post translational modifications (Acetylation), as there is also involvement of state transitions in CET and may be important for supercomplex formation. Comparison between *Arabidopsis* and *Marchantia* will broaden our understanding of CET under stressful conditions.

2. The role of thioredoxins, stromal and lumenal proteins in redox regulation of oxygen reduction at the Photosystem I acceptor side under different light regimes in *Arabidopsis thaliana*

In the second project, we studied the redox regulation of Mehler reaction under growth photoperiod in *A. thaliana*. It is known that Trx-m negatively regulates CET and that's why both pathways (cyclic and pseudocyclic) compete with each other. We have shown a higher ROS production in wild type plants grown under short day (SD) than in long day (LD). However, this difference was lost in Trxm mutants, showing the reversible attachment of Trxm to the thylakoid membrane under SD and vice versa. Moreover, an interesting finding was the involvement of CCDA as a mediator protein in the transfer of reducing equivalents from stroma to the lumen. Further, we proposed that under SD, PsaF is the subunit of PSI, that may be redox regulated as it has two cysteines in the lumen. However, the redox western for PsaF was not convincing as it was not easy to catch the redox state during the isolation procedure. This needs to be done again either by labelling reduced cysteine thiols with *N*-ethylmaleimide (NEM) or cysteine trapping to see which cysteines are shifted. NEM infiltrated leaves can then be used to perform westerns. Another possibility is to have *psaF* mutant, but its lethal since its involved in docking plastocyanin to the PSI complex. Further, it would be interesting to assess the biochemical behavior of ferredoxin with reduced PsaF to show if Fd docking is different because of reduced PsaF. Besides all that, flash induced absorption changes in isolated PSI should be studied.

The role of CCDA needs to be addressed, whether it is PSI dependent or not. It could be done by tracking the redox changes in P700. Moreover, performing westerns or checking the transcript levels of CCDA should be done to see if there is less CCDA under different photoperiods. Moreover, TCEP activity could be checked in this mutant. Another important

question that should be addressed is what drives the membrane attachment of Trxm-4. Here we propose that high salt concentrations or the changes in pH might disrupt the membrane association. Trxm-4 could also have a structural role but one should also look into the real activity of Trxm-4 on PSI, by checking P700 activity to show if there is less cyclic electron transport. We cannot deny the fact that besides redox regulation at PSI complex itself, other redox regulated proteins are likely to play a role in regulating the portioning between linear, cyclic and pseudocyclic electron flow. So based on our findings it could be hypothesized that LTOI may also play a more indirect role by inhibiting cyclic electron flow via the NDH complex. This way we can say that maybe Trxm-4 and LTOI are players in the opposite ways.

To conclude, in order to establish connection between two projects, a lot of future work is needed to see if interaction between Trx-m and PGRLI inhibit the putative supercomplex formation required for cyclic flow. Moreover, further studies on the extent of cyclic flow and superoxide production in mutants of the different components of the Trx system will show if both pseudocyclic and cyclic flow are controlled by the same proteins but in the opposite way.

Resume

Photosynthesis is a complex but highly efficient light powered process which is critical for the existence of all life forms on this planet earth. The overall process involves capturing of sunlight energy and its conversion into the chemical energy via specialized complexes embedded in the "thylakoid membrane"; which itself is housed in the chloroplast. Many of us know the famous equation for the overall chemical reaction of photosynthesis that produces sugar and oxygen which is ultimately used for aerobic respiration.

$$\mathbf{6CO_2 + 6H_2O + light\ energy \rightarrow C_6H_{12}O_6 + 6O_2}$$

Driven by the sunlight, the most important biochemical event that allows the water splitting and release of molecular oxygen is the water oxidizing complex (WOC) of photosystem II. It is also called Manganese (Mn) cluster (Mn_4CaO_5), since Mn is one of the essential element in catalyzing this reaction. Although the overall process might appear simpler to many of us, but the answer to many questions still remains unknown. For example, one of the common questions that I asked myself during my PhD thesis was: "What about regulation", how the electron transport is regulated under different physiological conditions? Plants need to maintain the redox balance especially under conditions when the amount of energy produced exceeds the demands for metabolism. This situation can lead to overreduction of electron transport chain (ETC) and ultimately the production of reactive oxygen species (ROS). To maintain the more oxidized state, plants have alternative electron sinks in the chloroplast like cyclic electron transport (CET) around PSI, Mehler reaction or pseudocyclic electron transport (PCET) and plastoquinol terminal oxidase (PTOX). They have been proposed as mechanisms that can be upregulated or induced to relieve the reductive pressure on the ETC.

In the first part of my PhD thesis, I have studied the effects of manganese homeostasis on photosynthetic electron transport chain in the liverwort *Marchantia polymorpha.* For this project, *Marchantia* was grown in both Mn excess and deficiency to deeply study the effects on both metabolism and photosynthesis. This plant was able to hyperaccumulate Mn upto 25 mg Mn g DW^{-1} but were not declared as hyperaccumulator since it showed signs of stress. Results from gas chromatography (GC-MS) showed an important influence of Mn excess at metabolism level. Metabolites that are known to have role in protecting plants from heavy metal stress were

increased under Mn excess and interestingly some new metabolites that were absent in *Arabidopsis* were also found in *Marchantia.* Moreover, chlorophyll fluorescence data showed a change in stoichiometry between PSI and PSII, which points towards some sort of photoprotection mechanism, that could be CET. Further, results from microscopy reveals changes in the chloroplast structure and thylakoid membrane (Article 1). To continue, I focused mainly on Mn deficiency and studied its effects on cyclic electron transport (CET). With the use of KLAS-NIR spectrophotometer, I was successful in confirming that its indeed the CET, that is enhanced under Mn deficiency. By using the Far-red light, in vivo oxidation reduction kinetics of P700 and plastocyanin were studied that points towards a supercomplex formation around PSI (Article 2).

The second part of my PhD project involves studying the redox regulation of oxygen reduction at the photosystem I acceptor side. I used *Arabidopsis thaliana* and growing it under different photoperiod generated different amounts of ROS. I tried to link it with thioredoxins (Trxs), that are best known for redox regulation of target proteins. With electron paramagnetic resonance spectroscopy , I have shown that increased amount of ROS under short day photoperiod is linked with the reversible of attachment of Trxm isoform to the thylakoid membrane and certain lumenal and stromal players are involved in the transfer of reducing equivalents from stroma to the lumen (Article 3).

Résumé

La photosynthèse est un processus complexe mais efficace qui consiste à convertir l'énergie solaire en énergie chimique via des complexes spécialisés intégrés dans la "membrane thylakoïdienne" du chloroplaste. Beaucoup d'entre nous connaissent la célèbre équation de la réaction chimique globale de la photosynthèse, qui produit du sucre et de l'oxygène, lesquels sont finalement utilisés pour la respiration aérobie.

$$\mathbf{6CO_2 + 6H_2O + énergie\ lumineuse \rightarrow C_6H_{12}O_6 + 6O_2}$$

Sous l'effet de la lumière, la réaction biochimique la plus importante permettant la photolyse de l'eau et la libération d'oxygène moléculaire est réalisée par cluster de manganèse (Mn_4CaO_5) du photosystème II, le Mn étant l'éléments le plus important pour catalyser cette réaction. Bien que le processus global puisse sembler simple, la réponse à de nombreuses questions reste encore inconnue. Par exemple, l'une des questions que je me suis posée durant ma thèse était : "Qu'en est-il de la régulation ?", comment le transport d'électrons est-il régulé dans les conditions physiologiques différentes ? Les plantes doivent maintenir l'équilibre redox, surtout lorsque la quantité d'énergie produite dépasse les besoins du métabolisme. Cette situation peut entraîner une réduction excessive de la chaîne de transport d'électrons (CTE), générant ainsi la production d'espèces réactives de l'oxygène (ROS). Pour maintenir un état plus oxydé, les plantes disposent de puits d'électrons alternatifs dans le chloroplaste, tels que le transport cyclique d'électrons (TCE) autour du PSI, le transport pseudo-cyclique d'électrons, et l'oxydase terminale à plastoquinol (PTOX). Ces mécanismes ont été proposés comme pouvant être régulés à la hausse ou induits pour soulager la pression réductrice sur la CTE.

Dans la première partie de ma thèse de doctorat, j'ai étudié les effets de l'homéostasie du manganèse sur la CTE photosynthétique dans l'hépatique *Marchantia polymorpha*. Pour ce projet, *Marchantia* a été cultivée dans des conditions d'excès et de carence en Mn afin d'étudier en profondeur ces effets sur le métabolisme et la photosynthèse. Les résultats de la chromatographie en phase gazeuse (GC-MS) ont révélé que l'excès de Mn influence fortement le métabolisme, augmentant les métabolites connus pour leur rôle dans la protection des plantes contre le stress dû aux métaux lourds et, fait intéressant, certains nouveaux métabolites absents chez *Arabidopsis* ont également été trouvés chez *Marchantia*. De plus, les données de

fluorescence chlorophyllienne ont montré un changement de stœchiométrie entre PSI et PSII, suggérant une sorte de mécanisme de photoprotection, qui pourrait être le TCE. En outre, les résultats de la microscopie révèlent des changements dans la structure du chloroplaste et la membrane des thylakoïdes (article 1). Ensuite, je me suis concentré sur la carence en Mn en étudiant ses effets sur le TCE. L'utilisation du spectrophotomètre KLAS-NIR, m'a permis de confirmer que c'est bien le TCE qui est amélioré en cas de carence en Mn. L'étude de la cinétique d'oxydo-réduction in vivo du P700 et de la plastocyanine en utilisant la lumière rouge lointaine, indique la formation d'un supercomplexe autour de la PSI (article 2)

La deuxième partie de mon doctorat consiste à étudier la régulation redox de la réduction de l'oxygène du côté de l'accepteur du photosystème I. J'ai utilisé *Arabidopsis thaliana* en la cultivant sous différentes photopériodes, ce qui a généré différentes quantités de ROS. J'ai essayé d'établir un lien avec les thiorédoxines (Trxs), connues pour la régulation redox des protéines cibles. Grâce à la spectroscopie de résonance paramagnétique électronique, j'ai montré que l'augmentation de la quantité de ROS sous une photopériode de courte durée est liée à l'attachement réversible de l'isoforme Trxm à la membrane thylakoïdienne, et que certains acteurs du lumen et du stroma sont impliqués dans le transfert d'équivalents réducteurs du stroma vers le lumen (article 3).

References:

Ahmad, N., Khan, M. O., Islam, E., Wei, Z. Y., McAusland, L., Lawson, T., Johnson, G. N., & Nixon, P. J. (2020). Contrasting Responses to Stress Displayed by Tobacco Overexpressing an Algal Plastid Terminal Oxidase in the Chloroplast. Frontiers in Plant Science, 11, 501. https://doi.org/10.3389/fpls.2020.00501

Alboresi, A., Caffarri, S., Nogue, F., Bassi, R., & Morosinotto, T. (2008). In silico and biochemical analysis of Physcomitrella patens photosynthetic antenna: identification of subunits which evolved upon land adaptation. PloS one, 3(4), e2033. https://doi.org/10.1371/journal.pone.0002033

Allahverdiyeva, Y., Ermakova, M., Eisenhut, M., Zhang, P., Richaud, P., Hagemann, M., Cournac, L., & Aro, E. M. (2011). Interplay between flavodiiron proteins and photorespiration in Synechocystis sp. PCC 6803. The Journal of Biological Chemistry, 286(27), 24007–24014. https://doi.org/10.1074/jbc.M111.223289

Amunts, A., & Nelson, N. (2009). Plant photosystem I design in the light of evolution. Structure (London, England : 1993), 17(5), 637–650. https://doi.org/10.1016/j.str.2009.03.006

Anderson J. M. (1982). The role of chlorophyll-protein complexes in the function and structure of chloroplast thylakoids. *Molecular and cellular biochemistry*, *46*(3), 161–172. https://doi.org/10.1007/BF00239665

Ares, Á., Itouga, M., Kato, Y., & Sakakibara, H. (2018). Differential Metal Tolerance and Accumulation Patterns of Cd, Cu, Pb and Zn in the Liverwort Marchantia polymorpha L. Bulletin of environmental contamination and toxicology, 100(3), 444–450. https://doi.org/10.1007/s00128-017-2241-0

Arnon D. I. (1959). Conversion of light into chemical energy in photosynthesis. Nature, 184, 10–21. https://doi.org/10.1038/184010a0

Asada K. (1999). The water-water cycle in chloroplasts: Scavenging of Active Oxygens and Dissipation of Excess Photons. Annual review of plant physiology and plant molecular biology, 50, 601–639. https://doi.org/10.1146/annurev.arplant.50.1.601

Asada K. (2000). The water-water cycle as alternative photon and electron sinks. Philosophical transactions of the Royal Society of London. Series B, Biological sciences, 355(1402), 1419–1431. https://doi.org/10.1098/rstb.2000.0703

Asada, K., Kiso, K., & Yoshikawa, K. (1974). Univalent reduction of molecular oxygen by spinach chloroplasts on illumination. The Journal of biological chemistry, 249(7), 2175–2181.

Badger, M. R., von Caemmerer, S., Ruuska, S., & Nakano, H. (2000). Electron flow to oxygen in higher plants and algae: rates and control of direct photoreduction (Mehler reaction) and rubisco oxygenase. Philosophical transactions of the Royal Society of London. Series B, Biological sciences, 355(1402), 1433–1446. https://doi.org/10.1098/rstb.2000.0704

Bell, A. J., Frankel, L. K., & Bricker, T. M. (2015). High Yield Non-detergent Isolation of Photosystem I-Light-harvesting Chlorophyll II Membranes from Spinach Thylakoids: IMPLICATIONS FOR THE ORGANIZATION OF THE PS I ANTENNAE IN HIGHER PLANTS. The Journal of biological chemistry, 290(30), 18429–18437. https://doi.org/10.1074/jbc.M115.663872

BENSON, A. A., BASSHAM, J. A., CALVIN, M., HALL, A. G., HIRSCH, H. E., KAWAGUCHI, S., LYNCH, V., & TOLBERT, N. E. (1952). The path of carbon in photosynthesis. XV. Ribulose and sedoheptulose. The Journal of biological chemistry, 196(2), 703–716. https://doi.org/10.2172/915054

Bernal-Bayard, P., Hervás, M., Cejudo, F. J., & Navarro, J. A. (2012). Electron transfer pathways and dynamics of chloroplast NADPH-dependent thioredoxin reductase C (NTRC). The Journal of biological chemistry, 287(40), 33865–33872. https://doi.org/10.1074/jbc.M112.388991

Bloom A. J. (2019). Metal regulation of metabolism. Current opinion in chemical biology, 49, 33–38. https://doi.org/10.1016/j.cbpa.2018.09.017

Bloom, A. J., & Lancaster, K. M. (2018). Manganese binding to Rubisco could drive a photorespiratory pathway that increases the energy efficiency of photosynthesis. Nature plants, 4(7), 414–422. https://doi.org/10.1038/s41477-018-0191-0

Boekema, E. J., Jensen, P. E., Schlodder, E., van Breemen, J. F., van Roon, H., Scheller, H. V., & Dekker, J. P. (2001). Green plant photosystem I binds light-harvesting complex I on one side of the complex. Biochemistry, 40(4), 1029–1036. https://doi.org/10.1021/bi0015358

Boekema, E. J., van Roon, H., Calkoen, F., Bassi, R., & Dekker, J. P. (1999). Multiple types of association of photosystem II and its light-harvesting antenna in partially solubilized photosystem II membranes. Biochemistry, 38(8), 2233–2239. https://doi.org/10.1021/bi9827161

Borisova-Mubarakshina, M. M., Vetoshkina, D. V., & Ivanov, B. N. (2019). Antioxidant and signaling functions of the plastoquinone pool in higher plants. Physiologia plantarum, 166(1), 181–198. https://doi.org/10.1111/ppl.12936

Bowman J. L. (2022). The liverwort Marchantia polymorpha, a model for all ages. Current topics in developmental biology, 147, 1–32. https://doi.org/10.1016/bs.ctdb.2021.12.009

Bowman, J. L., Kohchi, T., Yamato, K. T., Jenkins, J., Shu, S., Ishizaki, K., Yamaoka, S., Nishihama, R., Nakamura, Y., Berger, F., Adam, C., Aki, S. S., Althoff, F., Araki, T., Arteaga-

Vazquez, M. A., Balasubrmanian, S., Barry, K., Bauer, D., Boehm, C. R., Briginshaw, L., … Schmutz, J. (2017). Insights into Land Plant Evolution Garnered from the Marchantia polymorpha Genome. Cell, 171(2), 287–304.e15. https://doi.org/10.1016/j.cell.2017.09.030

Bowman, J. L., Sakakibara, K., Furumizu, C., & Dierschke, T. (2016). Evolution in the Cycles of Life. Annual review of genetics, 50, 133–154. https://doi.org/10.1146/annurev-genet-120215-035227

Bricker, T. M., Roose, J. L., Fagerlund, R. D., Frankel, L. K., & Eaton-Rye, J. J. (2012). The extrinsic proteins of Photosystem II. Biochimica et biophysica acta, 1817(1), 121–142. https://doi.org/10.1016/j.bbabio.2011.07.006

Brooks, M. D., Sylak-Glassman, E. J., Fleming, G. R., & Niyogi, K. K. (2013). A thioredoxin-like/β-propeller protein maintains the efficiency of light harvesting in Arabidopsis. Proceedings of the National Academy of Sciences of the United States of America, 110(29), E2733–E2740. https://doi.org/10.1073/pnas.1305443110

Buchanan B. B. (2016). The Path to Thioredoxin and Redox Regulation in Chloroplasts. Annual review of plant biology, 67, 1–24. https://doi.org/10.1146/annurev-arplant-043015-111949

Büchel C. (2015). Evolution and function of light harvesting proteins. Journal of plant physiology, 172, 62–75. https://doi.org/10.1016/j.jplph.2014.04.018

Buchert, F. E. (2020). Chloroplast ATP synthase from green microalgae. In Advances in Botanical Research (Vol. 96, pp. 75-118). Academic Press. https://doi.org/10.1016/bs.abr.2020.07.001

Buchert, F., Mosebach, L., Gäbelein, P., & Hippler, M. (2020). PGR5 is required for efficient Q cycle in the cytochrome b6f complex during cyclic electron flow. The Biochemical journal, 477(9), 1631–1650. https://doi.org/10.1042/BCJ20190914

Busch, A., & Hippler, M. (2011). The structure and function of eukaryotic photosystem I. Biochimica et biophysica acta, 1807(8), 864–877. https://doi.org/10.1016/j.bbabio.2010.09.009

Caffarri, S., Croce, R., Cattivelli, L., & Bassi, R. (2004). A look within LHCII: differential analysis of the Lhcb1-3 complexes building the major trimeric antenna complex of higher-plant photosynthesis. Biochemistry, 43(29), 9467–9476. https://doi.org/10.1021/bi036265i

Caffarri, S., Kouril, R., Kereïche, S., Boekema, E. J., & Croce, R. (2009). Functional architecture of higher plant photosystem II supercomplexes. The EMBO journal, 28(19), 3052–3063. https://doi.org/10.1038/emboj.2009.232

Caffarri, S., Tibiletti, T., Jennings, R. C., & Santabarbara, S. (2014). A comparison between plant photosystem I and photosystem II architecture and functioning. Current protein & peptide science, 15(4), 296–331. https://doi.org/10.2174/1389203715666140327102218

Candiano, G., Bruschi, M., Musante, L., Santucci, L., Ghiggeri, G. M., Carnemolla, B., Orecchia, P., Zardi, L., & Righetti, P. G. (2004). Blue silver: a very sensitive colloidal Coomassie G-250 staining for proteome analysis. Electrophoresis, 25(9), 1327–1333. https://doi.org/10.1002/elps.200305844

Cao, P., Su, X., Pan, X., Liu, Z., Chang, W., & Li, M. (2018). Structure, assembly and energy transfer of plant photosystem II supercomplex. Biochimica et biophysica acta. Bioenergetics, 1859(9), 633–644. https://doi.org/10.1016/j.bbabio.2018.03.007

Carol, P., & Kuntz, M. (2001). A plastid terminal oxidase comes to light: implications for carotenoid biosynthesis and chlororespiration. Trends in plant science, 6(1), 31–36. https://doi.org/10.1016/s1360-1385(00)01811-2

Carol, P., Stevenson, D., Bisanz, C., Breitenbach, J., Sandmann, G., Mache, R., Coupland, G., & Kuntz, M. (1999). Mutations in the Arabidopsis gene IMMUTANS cause a variegated phenotype by inactivating a chloroplast terminal oxidase associated with phytoene desaturation. The Plant cell, 11(1), 57–68. https://doi.org/10.1105/tpc.11.1.57

Cazzonelli, C. I., & Pogson, B. J. (2010). Source to sink: regulation of carotenoid biosynthesis in plants. Trends in plant science, 15(5), 266–274. https://doi.org/10.1016/j.tplants.2010.02.003

Cejudo, F. J., Ferrández, J., Cano, B., Puerto-Galán, L., & Guinea, M. (2012). The function of the NADPH thioredoxin reductase C-2-Cys peroxiredoxin system in plastid redox regulation and signalling. FEBS letters, 586(18), 2974–2980. https://doi.org/10.1016/j.febslet.2012.07.003

Cejudo, F. J., González, M. C., & Pérez-Ruiz, J. M. (2021). Redox regulation of chloroplast metabolism. Plant physiology, 186(1), 9–21. https://doi.org/10.1093/plphys/kiaa062

Cejudo, F. J., Ojeda, V., Delgado-Requerey, V., González, M., & Pérez-Ruiz, J. M. (2019). Chloroplast Redox Regulatory Mechanisms in Plant Adaptation to Light and Darkness. Frontiers in plant science, 10, 380. https://doi.org/10.3389/fpls.2019.00380

Chen, Y., Xu, B., Yao, R., Chen, C., & Zhang, C. (2022). Mimicking the Oxygen-Evolving Center in Photosynthesis. Frontiers in plant science, 13, 929532. https://doi.org/10.3389/fpls.2022.929532

Chiu, Y. F., & Chu, H. A. (2022). New Structural and Mechanistic Insights Into Functional Roles of Cytochrome b559 in Photosystem II. Frontiers in plant science, 13, 914922. https://doi.org/10.3389/fpls.2022.914922

Corpas, F. J., Barroso, J. B., Palma, J. M., & Rodriguez-Ruiz, M. (2017). Plant peroxisomes: A nitro-oxidative cocktail. Redox biology, 11, 535–542. https://doi.org/10.1016/j.redox.2016.12.033

Courteille, A., Vesa, S., Sanz-Barrio, R., Cazalé, A. C., Becuwe-Linka, N., Farran, I., Havaux, M., Rey, P., & Rumeau, D. (2013). Thioredoxin m4 controls photosynthetic alternative electron pathways in Arabidopsis. Plant physiology, 161(1), 508–520. https://doi.org/10.1104/pp.112.207019

Couturier, J., Chibani, K., Jacquot, J. P., & Rouhier, N. (2013). Cysteine-based redox regulation and signaling in plants. Frontiers in plant science, 4, 105. https://doi.org/10.3389/fpls.2013.00105

Cramer, W. A., Zhang, H., Yan, J., Kurisu, G., & Smith, J. L. (2004). Evolution of photosynthesis: time-independent structure of the cytochrome b6f complex. Biochemistry, 43(20), 5921–5929. https://doi.org/10.1021/bi049444o

Crepin, A., & Caffarri, S. (2018). Functions and Evolution of Lhcb Isoforms Composing LHCII, the Major Light Harvesting Complex of Photosystem II of Green Eukaryotic Organisms. Current protein & peptide science, 19(7), 699–713. https://doi.org/10.2174/1389203719666180222101534

Crepin, A., Kučerová, Z., Kosta, A., Durand, E., & Caffarri, S. (2020). Isolation and characterization of a large photosystem I-light-harvesting complex II supercomplex with an additional Lhca1-a4 dimer in Arabidopsis. The Plant journal : for cell and molecular biology, 102(2), 398–409. https://doi.org/10.1111/tpj.14634

Crofts A. R. (2004). The Q-cycle - A Personal Perspective. Photosynthesis research, 80(1-3), 223–243. https://doi.org/10.1023/B:PRES.0000030444.52579.10

DalCorso, G., Pesaresi, P., Masiero, S., Aseeva, E., Schünemann, D., Finazzi, G., Joliot, P., Barbato, R., & Leister, D. (2008). A complex containing PGRL1 and PGR5 is involved in the switch between linear and cyclic electron flow in Arabidopsis. Cell, 132(2), 273–285. https://doi.org/10.1016/j.cell.2007.12.028

Dangoor, I., Peled-Zehavi, H., Wittenberg, G., & Danon, A. (2012). A chloroplast light-regulated oxidative sensor for moderate light intensity in Arabidopsis. The Plant cell, 24(5), 1894–1906. https://doi.org/10.1105/tpc.112.097139

Dekker, J. P., & Boekema, E. J. (2005). Supramolecular organization of thylakoid membrane proteins in green plants. Biochimica et biophysica acta, 1706(1-2), 12–39. https://doi.org/10.1016/j.bbabio.2004.09.009

Dietz, K. J., Turkan, I., & Krieger-Liszkay, A. (2016). Redox- and Reactive Oxygen Species-Dependent Signaling into and out of the Photosynthesizing Chloroplast. Plant physiology, 171(3), 1541–1550. https://doi.org/10.1104/pp.16.00375

Eisenhut, M., Hoecker, N., Schmidt, S. B., Basgaran, R. M., Flachbart, S., Jahns, P., Eser, T., Geimer, S., Husted, S., Weber, A. P. M., Leister, D., & Schneider, A. (2018). The Plastid Envelope CHLOROPLAST MANGANESE TRANSPORTER1 Is Essential for Manganese Homeostasis in Arabidopsis. Molecular plant, 11(7), 955–969. https://doi.org/10.1016/j.molp.2018.04.008

Eliyahu, E., Rog, I., Inbal, D., & Danon, A. (2015). ACHT4-driven oxidation of APS1 attenuates starch synthesis under low light intensity in Arabidopsis plants. Proceedings of the National Academy of Sciences of the United States of America, 112(41), 12876–12881. https://doi.org/10.1073/pnas.1515513112

Ferreira, K. N., Iverson, T. M., Maghlaoui, K., Barber, J., & Iwata, S. (2004). Architecture of the photosynthetic oxygen-evolving center. Science (New York, N.Y.), 303(5665), 1831–1838. https://doi.org/10.1126/science.1093087

Foyer C. H. (2018). Reactive oxygen species, oxidative signaling and the regulation of photosynthesis. Environmental and experimental botany, 154, 134–142. https://doi.org/10.1016/j.envexpbot.2018.05.003

Fromme, P., Jordan, P., & Krauss, N. (2001). Structure of photosystem I. Biochimica et biophysica acta, 1507(1-3), 5–31. https://doi.org/10.1016/s0005-2728(01)00195-5

Fuad, N., Day, D. A., Ryrie, I. J., & Thorne, S. W. (1983). A photosystem II light-harvesting chlorophyll-protein complex with a high fluorescence emission at 736 nm. Photobiochemistry and photobiophysics, 5, 255-262.

Furt, F., Oostende, C.v, Widhalm, J. R., Dale, M. A., Wertz, J., & Basset, G. J. (2010). A bimodular oxidoreductase mediates the specific reduction of phylloquinone (vitamin K_1) in chloroplasts. The Plant journal : for cell and molecular biology, 64(1), 38–46. https://doi.org/10.1111/j.1365-313X.2010.04305.x

Galka, P., Santabarbara, S., Khuong, T. T., Degand, H., Morsomme, P., Jennings, R. C., Boekema, E. J., & Caffarri, S. (2012). Functional analyses of the plant photosystem I-light-harvesting complex II supercomplex reveal that light-harvesting complex II loosely bound to photosystem II is a very efficient antenna for photosystem I in state II. The Plant cell, 24(7), 2963–2978. https://doi.org/10.1105/tpc.112.100339

Gamborg, O. L., Miller, R. A., & Ojima, K. (1968). Nutrient requirements of suspension cultures of soybean root cells. Experimental cell research, 50(1), 151–158. https://doi.org/10.1016/0014-4827(68)90403-5

Geigenberger, P., Thormählen, I., Daloso, D. M., & Fernie, A. R. (2017). The Unprecedented Versatility of the Plant Thioredoxin System. Trends in plant science, 22(3), 249–262. https://doi.org/10.1016/j.tplants.2016.12.008

Gerotto, C., Trotta, A., Bajwa, A. A., Morosinotto, T., & Aro, E. M. (2022). Role of serine/threonine protein kinase STN7 in the formation of two distinct photosystem I supercomplexes in Physcomitrium patens. Plant physiology, 190(1), 698–713. https://doi.org/10.1093/plphys/kiac294

Gisriel, C. J., & Brudvig, G. W. (2022). Comparison of PsbQ and Psb27 in photosystem II provides insight into their roles. Photosynthesis research, 152(2), 177–191. https://doi.org/10.1007/s11120-021-00888-2

Gisriel, C. J., Shen, G., Flesher, D. A., Kurashov, V., Golbeck, J. H., Brudvig, G. W., Amin, M., & Bryant, D. A. (2023). Structure of a dimeric photosystem II complex from a cyanobacterium acclimated to far-red light. *The Journal of biological chemistry*, *299*(1), 102815. https://doi.org/10.1016/j.jbc.2022.102815

Goldschmidt-Clermont, M., & Bassi, R. (2015). Sharing light between two photosystems: mechanism of state transitions. Current opinion in plant biology, 25, 71–78. https://doi.org/10.1016/j.pbi.2015.04.009

Grieco, M., Suorsa, M., Jajoo, A., Tikkanen, M., & Aro, E. M. (2015). Light-harvesting II antenna trimers connect energetically the entire photosynthetic machinery - including both photosystems II and I. Biochimica et biophysica acta, 1847(6-7), 607–619. https://doi.org/10.1016/j.bbabio.2015.03.004

Gupta, R., He, Z., & Luan, S. (2002). Functional relationship of cytochrome c(6) and plastocyanin in Arabidopsis. Nature, 417(6888), 567–571. https://doi.org/10.1038/417567a

Guskov, A., Kern, J., Gabdulkhakov, A., Broser, M., Zouni, A., & Saenger, W. (2009). Cyanobacterial photosystem II at 2.9-A resolution and the role of quinones, lipids, channels and chloride. Nature structural & molecular biology, 16(3), 334–342. https://doi.org/10.1038/nsmb.1559

Hall, M., Mata-Cabana, A., Akerlund, H. E., Florencio, F. J., Schröder, W. P., Lindahl, M., & Kieselbach, T. (2010). Thioredoxin targets of the plant chloroplast lumen and their implications for plastid function. Proteomics, 10(5), 987–1001. https://doi.org/10.1002/pmic.200900654

Hani, U ., Naranjo, B., Shimakawa, G., Vanacker, H., Espinasse, C., ... , Issakidis-Bourguet, E & Krieger-Liszkay, A. (2023). A complex and dynamic redox network regulating oxygen reduction at photosystem I. bioRxiv, 2023-09

Hanke, G., & Mulo, P. (2013). Plant type ferredoxins and ferredoxin-dependent metabolism. Plant, cell & environment, 36(6), 1071–1084. https://doi.org/10.1111/pce.12046

Harbinson J, Woodward FI (1987) The use of light-induced absorbance changes at 820 nm to monitor the oxidation state of P-700 in leaves. Plant Cell Environ 10:131-140

Harbinson, J., & Hedley, C. L. (1993). Changes in P-700 Oxidation during the Early Stages of the Induction of Photosynthesis. Plant physiology, 103(2), 649–660. https://doi.org/10.1104/pp.103.2.649

Harrer R. (2003). Associations between light-harvesting complexes and Photosystem II from Marchantia polymorpha L. determined by two- and three-dimensional electron microscopy. Photosynthesis research, 75(3), 249–258. https://doi.org/10.1023/A:1023952832255

Hasan, S. S., Yamashita, E., Baniulis, D., & Cramer, W. A. (2013). Quinone-dependent proton transfer pathways in the photosynthetic cytochrome b6f complex. Proceedings of the National Academy of Sciences of the United States of America, 110(11), 4297–4302. https://doi.org/10.1073/pnas.1222248110

Hertle, A. P., Blunder, T., Wunder, T., Pesaresi, P., Pribil, M., Armbruster, U., & Leister, D. (2013). PGRL1 is the elusive ferredoxin-plastoquinone reductase in photosynthetic cyclic electron flow. Molecular cell, 49(3), 511–523. https://doi.org/10.1016/j.molcel.2012.11.030

Heyno, E., Gross, C. M., Laureau, C., Culcasi, M., Pietri, S., & Krieger-Liszkay, A. (2009). Plastid alternative oxidase (PTOX) promotes oxidative stress when overexpressed in tobacco. The Journal of biological chemistry, 284(45), 31174–31180. https://doi.org/10.1074/jbc.M109.021667

Hoh, D., Froehlich, J. E., & Kramer, D. M. (2023). Redox regulation in chloroplast thylakoid lumen: The pmf changes everything, again. Plant, cell & environment, 10.1111/pce.14789. Advance online publication. https://doi.org/10.1111/pce.14789

Hohmann-Marriott, M. F., & Blankenship, R. E. (2011). Evolution of photosynthesis. Annual review of plant biology, 62, 515–548. https://doi.org/10.1146/annurev-arplant-042110-103811

Horton, P., & Ruban, A. (2005). Molecular design of the photosystem II light-harvesting antenna: photosynthesis and photoprotection. Journal of experimental botany, 56(411), 365–373. https://doi.org/10.1093/jxb/eri023

Houille-Vernes, L., Rappaport, F., Wollman, F. A., Alric, J., & Johnson, X. (2011). Plastid terminal oxidase 2 (PTOX2) is the major oxidase involved in chlororespiration in Chlamydomonas. Proceedings of the National Academy of Sciences of the United States of America, 108(51), 20820–20825. https://doi.org/10.1073/pnas.1110518109

Husted, S., Laursen, K. H., Hebbern, C. A., Schmidt, S. B., Pedas, P., Haldrup, A., & Jensen, P. E. (2009). Manganese deficiency leads to genotype-specific changes in fluorescence induction kinetics and state transitions. Plant physiology, 150(2), 825–833. https://doi.org/10.1104/pp.108.134601

Ibrahim, M., Fransson, T., Chatterjee, R., Cheah, M. H., Hussein, R., Lassalle, L., Sutherlin, K. D., Young, I. D., Fuller, F. D., Gul, S., Kim, I. S., Simon, P. S., de Lichtenberg, C., Chernev, P., Bogacz, I., Pham, C. C., Orville, A. M., Saichek, N., Northen, T., Batyuk, A., … Yano, J. (2020). Untangling the sequence of events during the S2 → S3 transition in photosystem II and implications for the water oxidation mechanism. Proceedings of the National Academy of Sciences of the United States of America, 117(23), 12624–12635. https://doi.org/10.1073/pnas.2000529117

Ifuku, K., & Noguchi, T. (2016). Structural Coupling of Extrinsic Proteins with the Oxygen-Evolving Center in Photosystem II. Frontiers in plant science, 7, 84. https://doi.org/10.3389/fpls.2016.00084

Ivanov, B. N., Khorobrykh, S. A., Kozuleva, M. A., & Borisova-Mubarakshina, M. M. (2014). The role of oxygen and its reactive forms in photosynthesis. Contemporary Problems of Photosynthesis, 407-460.

Jackowski, G., Kacprzak, K., & Jansson, S. (2001). Identification of Lhcb1/Lhcb2/Lhcb3 heterotrimers of the main light-harvesting chlorophyll a/b-protein complex of Photosystem II (LHC II). Biochimica et biophysica acta, 1504(2-3), 340–345. https://doi.org/10.1016/s0005-2728(00)00262-0

Jansson S. (1999). A guide to the Lhc genes and their relatives in Arabidopsis/IT>. Trends in plant science, 4(6), 236–240. https://doi.org/10.1016/s1360-1385(99)01419-3

Jensen, P. E., Bassi, R., Boekema, E. J., Dekker, J. P., Jansson, S., Leister, D., Robinson, C., & Scheller, H. V. (2007). Structure, function and regulation of plant photosystem I. Biochimica et biophysica acta, 1767(5), 335–352. https://doi.org/10.1016/j.bbabio.2007.03.004

Johnson G. N. (2011). Physiology of PSI cyclic electron transport in higher plants. Biochimica et biophysica acta, 1807(3), 384–389. https://doi.org/10.1016/j.bbabio.2010.11.009

Johnson, X., Steinbeck, J., Dent, R. M., Takahashi, H., Richaud, P., Ozawa, S., Houille-Vernes, L., Petroutsos, D., Rappaport, F., Grossman, A. R., Niyogi, K. K., Hippler, M., & Alric, J. (2014). Proton gradient regulation 5-mediated cyclic electron flow under ATP- or redox-limited conditions: a study of ΔATpase pgr5 and ΔrbcL pgr5 mutants in the green alga Chlamydomonas reinhardtii. Plant physiology, 165(1), 438–452. https://doi.org/10.1104/pp.113.233593

Joliot, P., & Johnson, G. N. (2011). Regulation of cyclic and linear electron flow in higher plants. Proceedings of the National Academy of Sciences of the United States of America, 108(32), 13317–13322. https://doi.org/10.1073/pnas.1110189108

Joliot, P., Béal, D., & Joliot, A. (2004). Cyclic electron flow under saturating excitation of dark-adapted Arabidopsis leaves. Biochimica et biophysica acta, 1656(2-3), 166–176. https://doi.org/10.1016/j.bbabio.2004.03.010

Jordan, P., Fromme, P., Witt, H. T., Klukas, O., Saenger, W., & Krauss, N. (2001). Three-dimensional structure of cyanobacterial photosystem I at 2.5 A resolution. Nature, 411(6840), 909–917. https://doi.org/10.1038/35082000

Kalra, I., Wang, X., Zhang, R., & Morgan-Kiss, R. (2023). High salt-induced PSI-supercomplex is associated with high CEF and attenuation of state transitions. Photosynthesis research, 157(2-3), 65–84. https://doi.org/10.1007/s11120-023-01032-y

Kambakam, S., Bhattacharjee, U., Petrich, J., & Rodermel, S. (2016). PTOX Mediates Novel Pathways of Electron Transport in Etioplasts of Arabidopsis. Molecular plant, 9(9), 1240–1259. https://doi.org/10.1016/j.molp.2016.06.008

Kang, Z. H., & Wang, G. X. (2016). Redox regulation in the thylakoid lumen. Journal of plant physiology, 192, 28–37. https://doi.org/10.1016/j.jplph.2015.12.012

Kang, Z., Qin, T., & Zhao, Z. (2019). Thioredoxins and thioredoxin reductase in chloroplasts: A review. Gene, 706, 32–42. https://doi.org/10.1016/j.gene.2019.04.041

Karamoko, M., Gabilly, S. T., & Hamel, P. P. (2013). Operation of trans-thylakoid thiol-metabolizing pathways in photosynthesis. Frontiers in plant science, 4, 476. https://doi.org/10.3389/fpls.2013.00476

Kargul, J., Nield, J., & Barber, J. (2003). Three-dimensional reconstruction of a light-harvesting complex I-photosystem I (LHCI-PSI) supercomplex from the green alga Chlamydomonas reinhardtii. Insights into light harvesting for PSI. The Journal of biological chemistry, 278(18), 16135–16141. https://doi.org/10.1074/jbc.M300262200

Kato, H., Yasui, Y., & Ishizaki, K. (2020). Gemma cup and gemma development in Marchantia polymorpha. The New phytologist, 228(2), 459–465. https://doi.org/10.1111/nph.16655

Kato, Y., Odahara, M., Fukao, Y., & Shikanai, T. (2018). Stepwise evolution of supercomplex formation with photosystem I is required for stabilization of chloroplast NADH dehydrogenase-like complex: Lhca5-dependent supercomplex formation in Physcomitrella patens. The Plant journal : for cell and molecular biology, 96(5), 937–948. https://doi.org/10.1111/tpj.14080

Keryer, E., Collin, V., Lavergne, D., Lemaire, S., & Issakidis-Bourguet, E. (2004). Characterization of Arabidopsis Mutants for the Variable Subunit of Ferredoxin:thioredoxin Reductase. Photosynthesis research, 79(3), 265–274. https://doi.org/10.1023/B:PRES.0000017173.46185.3e

Kirchhoff H. (2019). Chloroplast ultrastructure in plants. The New phytologist, 223(2), 565–574. https://doi.org/10.1111/nph.15730

Klimmek, F., Ganeteg, U., Ihalainen, J. A., van Roon, H., Jensen, P. E., Scheller, H. V., Dekker, J. P., & Jansson, S. (2005). Structure of the higher plant light harvesting complex I: in vivo characterization and structural interdependence of the Lhca proteins. Biochemistry, 44(8), 3065–3073. https://doi.org/10.1021/bi047873g

Klughammer C, Schreiber U (1998) Measuring P700 absorbance changes in the near infrared spectral region with a dual wavelength pulse modulation system. In: Garab G (ed) Photosynthesis: mechanisms and effects, vol V. Kluwer Academic Publishers, Dordrecht, pp 4357–4360

Klughammer, C., & Schreiber, U. (2016). Deconvolution of ferredoxin, plastocyanin, and P700 transmittance changes in intact leaves with a new type of kinetic LED array spectrophotometer. Photosynthesis research, 128(2), 195–214. https://doi.org/10.1007/s11120-016-0219-0

Kohzuma, K., Dal Bosco, C., Kanazawa, A., Dhingra, A., Nitschke, W., Meurer, J., & Kramer, D. M. (2012). Thioredoxin-insensitive plastid ATP synthase that performs moonlighting functions. Proceedings of the National Academy of Sciences of the United States of America, 109(9), 3293–3298. https://doi.org/10.1073/pnas.1115728109

Koskela, M. M., Brünje, A., Ivanauskaite, A., Lopez, L. S., Schneider, D., DeTar, R. A., Kunz, H. H., Finkemeier, I., & Mulo, P. (2020). Comparative analysis of thylakoid protein complexes in state transition mutants nsi and stn7: focus on PSI and LHCII. Photosynthesis research, 145(1), 15–30. https://doi.org/10.1007/s11120-020-00711-4

Kozuleva, M., Petrova, A., Milrad, Y., Semenov, A., Ivanov, B., Redding, K. E., & Yacoby, I. (2021). Phylloquinone is the principal Mehler reaction site within photosystem I in high light. Plant physiology, 186(4), 1848–1858. https://doi.org/10.1093/plphys/kiab221

Krieger-Liszkay A. (2005). Singlet oxygen production in photosynthesis. Journal of experimental botany, 56(411), 337–346. https://doi.org/10.1093/jxb/erh237

Krieger-Liszkay, A., & Shimakawa, G. (2022). Regulation of the generation of reactive oxygen species during photosynthetic electron transport. Biochemical Society transactions, 50(2), 1025–1034. https://doi.org/10.1042/BST20211246

Laemmli U. K. (1970). Cleavage of structural proteins during the assembly of the head of bacteriophage T4. Nature, 227(5259), 680–685. https://doi.org/10.1038/227680a0

Lane B. G. (2002). Oxalate, germins, and higher-plant pathogens. IUBMB life, 53(2), 67–75. https://doi.org/10.1080/15216540211474

Laugier, E., Tarrago, L., Courteille, A., Innocenti, G., Eymery, F., Rumeau, D., Issakidis-Bourguet, E., & Rey, P. (2013). Involvement of thioredoxin y2 in the preservation of leaf methionine sulfoxide reductase capacity and growth under high light. Plant, cell & environment, 36(3), 670–682. https://doi.org/10.1111/pce.12005

Laureau, C., De Paepe, R., Latouche, G., Moreno-Chacón, M., Finazzi, G., Kuntz, M., Cornic, G., & Streb, P. (2013). Plastid terminal oxidase (PTOX) has the potential to act as a safety valve for excess excitation energy in the alpine plant species Ranunculus glacialis L. Plant, cell & environment, 36(7), 1296–1310. https://doi.org/10.1111/pce.12059

Lee, E. S., Kang, C. H., Park, J. H., & Lee, S. Y. (2018). Physiological Significance of Plant Peroxiredoxins and the Structure-Related and Multifunctional Biochemistry of Peroxiredoxin 1. Antioxidants & redox signaling, 28(7), 625–639. https://doi.org/10.1089/ars.2017.7400

Leister D. (2020). Alternative electron pathways in photosynthesis: strength in numbers. The New phytologist, 228(4), 1166–1168. https://doi.org/10.1111/nph.16911

Lepistö, A., Kangasjärvi, S., Luomala, E. M., Brader, G., Sipari, N., Keränen, M., Keinänen, M., & Rintamäki, E. (2009). Chloroplast NADPH-thioredoxin reductase interacts with photoperiodic development in Arabidopsis. Plant physiology, 149(3), 1261–1276. https://doi.org/10.1104/pp.108.133777

Liu, Z., Yan, H., Wang, K., Kuang, T., Zhang, J., Gui, L., An, X., & Chang, W. (2004). Crystal structure of spinach major light-harvesting complex at 2.72 A resolution. Nature, 428(6980), 287–292. https://doi.org/10.1038/nature02373

Loll, B., Kern, J., Saenger, W., Zouni, A., & Biesiadka, J. (2005). Towards complete cofactor arrangement in the 3.0 A resolution structure of photosystem II. Nature, 438(7070), 1040–1044. https://doi.org/10.1038/nature04224

Lu, Y., Du, J. J., Yu, Z. B., Peng, J. J., Xu, J. N., & Wang, X. Y. (2014). Identification of potential targets for thylakoid oxidoreductase AtVKOR/LTO1 in chloroplasts. Protein and peptide letters, 22(3), 219–225. https://doi.org/10.2174/09298665216661411211531 38

Lunde, C., Jensen, P. E., Haldrup, A., Knoetzel, J., & Scheller, H. V. (2000). The PSI-H subunit of photosystem I is essential for state transitions in plant photosynthesis. Nature, 408(6812), 613–615. https://doi.org/10.1038/35046121

Malnoë, A. (2011). A genetic suppressor approach to the biogenesis, quality control and function of photosynthetic complexes in Chlamydomonas reinhardtii (Doctoral dissertation, Université Paris Sud-Paris XI).

Malone, L. A., Proctor, M. S., Hitchcock, A., Hunter, C. N., & Johnson, M. P. (2021). Cytochrome b6f - Orchestrator of photosynthetic electron transfer. Biochimica et biophysica acta. Bioenergetics, 1862(5), 148380. https://doi.org/10.1016/j.bbabio.2021.148380

Marcaida, M. J., Schlarb-Ridley, B. G., Worrall, J. A., Wastl, J., Evans, T. J., Bendall, D. S., Luisi, B. F., & Howe, C. J. (2006). Structure of cytochrome c6A, a novel dithio-cytochrome of Arabidopsis thaliana, and its reactivity with plastocyanin: implications for function. Journal of molecular biology, 360(5), 968–977. https://doi.org/10.1016/j.jmb.2006.05.065

Maréchal E. (2018). Primary Endosymbiosis: Emergence of the Primary Chloroplast and the Chromatophore, Two Independent Events. Methods in molecular biology (Clifton, N.J.), 1829, 3–16. https://doi.org/10.1007/978-1-4939-8654-5_1

Margulis, K., Zer, H., Lis, H., Schoffman, H., Murik, O., Shimakawa, G., Krieger-Liszkay, A., & Keren, N. (2020). Over Expression of the Cyanobacterial Pgr5-Homologue Leads to Pseudoreversion in a Gene Coding for a Putative Esterase in Synechocystis 6803. Life (Basel, Switzerland), 10(9), 174. https://doi.org/10.3390/life10090174

Margulis, L. (1971). The Origin of Plant and Animal Cells: The serial symbiosis view of the origin of higher cells suggests that the customary division of living things into two kingdoms should be reconsidered. *American scientist*, *59*(2), 230-235.

Mazor, Y., Borovikova, A., Caspy, I., & Nelson, N. (2017). Structure of the plant photosystem I supercomplex at 2.6 Å resolution. Nature plants, 3, 17014. https://doi.org/10.1038/nplants.2017.14

MEHLER A. H. (1951). Studies on reactions of illuminated chloroplasts. I. Mechanism of the reduction of oxygen and other Hill reagents. Archives of biochemistry and biophysics, 33(1), 65–77. https://doi.org/10.1016/0003-9861(51)90082-3

Messant, M., Hani, U., Lai, T. L., Wilson, A., Shimakawa, G., & Krieger-Liszkay, A. (2024). Plastid terminal oxidase (PTOX) protects photosystem I and not photosystem II against photoinhibition in Arabidopsis thaliana and Marchantia polymorpha. The Plant journal : for cell and molecular biology, 117(3), 669–678. https://doi.org/10.1111/tpj.16520

Messant, M., Krieger-Liszkay, A., & Shimakawa, G. (2021). Dynamic Changes in Protein-Membrane Association for Regulating Photosynthetic Electron Transport. Cells, 10(5), 1216. https://doi.org/10.3390/cells10051216

Meurer, J., Meierhoff, K., & Westhoff, P. (1996). Isolation of high-chlorophyll-fluorescence mutants of Arabidopsis thaliana and their characterisation by spectroscopy, immunoblotting and northern hybridisation. Planta, 198(3), 385–396. https://doi.org/10.1007/BF00620055

Meyer, Y., Belin, C., Delorme-Hinoux, V., Reichheld, J. P., & Riondet, C. (2012). Thioredoxin and glutaredoxin systems in plants: molecular mechanisms, crosstalks, and functional significance. Antioxidants & redox signaling, 17(8), 1124–1160. https://doi.org/10.1089/ars.2011.4327

Michelet, L., & Krieger-Liszkay, A. (2012). Reactive oxygen intermediates produced by photosynthetic electron transport are enhanced in short-day grown plants. Biochimica et biophysica acta, 1817(8), 1306–1313. https://doi.org/10.1016/j.bbabio.2011.11.014

Minagawa, J., & Takahashi, Y. (2004). Structure, function and assembly of Photosystem II and its light-harvesting proteins. Photosynthesis research, 82(3), 241–263. https://doi.org/10.1007/s11120-004-2079-2

Mishler BD, Churchill SP. 1984. A cladistic approach to the phylogeny of the 'Bryophytes'. Brittonia 36: 406.

Mitchell P. (1975). The protonmotive Q cycle: a general formulation. FEBS letters, 59(2), 137–139. https://doi.org/10.1016/0014-5793(75)80359-0

Mittler, R., Zandalinas, S. I., Fichman, Y., & Van Breusegem, F. (2022). Reactive oxygen species signalling in plant stress responses. Nature reviews. Molecular cell biology, 23(10), 663–679. https://doi.org/10.1038/s41580-022-00499-2

Motohashi, K., & Hisabori, T. (2006). HCF164 receives reducing equivalents from stromal thioredoxin across the thylakoid membrane and mediates reduction of target proteins in the thylakoid lumen. The Journal of biological chemistry, 281(46), 35039–35047. https://doi.org/10.1074/jbc.M605938200

Motohashi, K., & Hisabori, T. (2010). CcdA is a thylakoid membrane protein required for the transfer of reducing equivalents from stroma to thylakoid lumen in the higher plant chloroplast. Antioxidants & redox signaling, 13(8), 1169–1176. https://doi.org/10.1089/ars.2010.3138

Müller, P., Li, X. P., & Niyogi, K. K. (2001). Non-photochemical quenching. A response to excess light energy. Plant physiology, 125(4), 1558–1566. https://doi.org/10.1104/pp.125.4.1558

Munekage, Y., Hashimoto, M., Miyake, C., Tomizawa, K., Endo, T., Tasaka, M., & Shikanai, T. (2004). Cyclic electron flow around photosystem I is essential for photosynthesis. Nature, 429(6991), 579–582. https://doi.org/10.1038/nature02598

Munekage, Y., Hojo, M., Meurer, J., Endo, T., Tasaka, M., & Shikanai, T. (2002). PGR5 is involved in cyclic electron flow around photosystem I and is essential for photoprotection in Arabidopsis. Cell, 110(3), 361–371. https://doi.org/10.1016/s0092-8674(02)00867-x

Murata N. (1969). Control of excitation transfer in photosynthesis. I. Light-induced change of chlorophyll a fluorescence in Porphyridium cruentum. Biochimica et biophysica acta, 172(2), 242–251. https://doi.org/10.1016/0005-2728(69)90067-x

Naranjo, B., Mignée, C., Krieger-Liszkay, A., Hornero-Méndez, D., Gallardo-Guerrero, L., Cejudo, F. J., & Lindahl, M. (2016). The chloroplast NADPH thioredoxin reductase C, NTRC, controls non-photochemical quenching of light energy and photosynthetic electron transport in Arabidopsis. Plant, cell & environment, 39(4), 804–822. https://doi.org/10.1111/pce.12652

Nawrocki, W. J., Bailleul, B., Picot, D., Cardol, P., Rappaport, F., Wollman, F. A., & Joliot, P. (2019). The mechanism of cyclic electron flow. Biochimica et biophysica acta. Bioenergetics, 1860(5), 433–438. https://doi.org/10.1016/j.bbabio.2018.12.005

Nawrocki, W. J., Buchert, F., Joliot, P., Rappaport, F., Bailleul, B., & Wollman, F. A. (2019b). Chlororespiration Controls Growth Under Intermittent Light. Plant physiology, 179(2), 630–639. https://doi.org/10.1104/pp.18.01213

Nawrocki, W. J., Liu, X., Raber, B., Hu, C., de Vitry, C., Bennett, D. I. G., & Croce, R. (2021). Molecular origins of induction and loss of photoinhibition-related energy dissipation qI. Science advances, 7(52), eabj0055. https://doi.org/10.1126/sciadv.abj0055

Nawrocki, W. J., Tourasse, N. J., Taly, A., Rappaport, F., & Wollman, F. A. (2015). The plastid terminal oxidase: its elusive function points to multiple contributions to plastid physiology. Annual review of plant biology, 66, 49–74. https://doi.org/10.1146/annurev-arplant-043014-114744

Nelson, N., & Yocum, C. F. (2006). Structure and function of photosystems I and II. Annual review of plant biology, 57, 521–565. https://doi.org/10.1146/annurev.arplant.57.032905.105350

Nikkanen, L., & Rintamäki, E. (2019). Chloroplast thioredoxin systems dynamically regulate photosynthesis in plants. The Biochemical journal, 476(7), 1159–1172. https://doi.org/10.1042/BCJ20180707

Nikkanen, L., Guinea Diaz, M., Toivola, J., Tiwari, A., & Rintamäki, E. (2019). Multilevel regulation of non-photochemical quenching and state transitions by chloroplast NADPH-dependent thioredoxin reductase. Physiologia plantarum, 166(1), 211–225. https://doi.org/10.1111/ppl.12914

Nikkanen, L., Toivola, J., & Rintamäki, E. (2016). Crosstalk between chloroplast thioredoxin systems in regulation of photosynthesis. Plant, cell & environment, 39(8), 1691–1705. https://doi.org/10.1111/pce.12718

Nikkanen, L., Toivola, J., Diaz, M. G., & Rintamäki, E. (2017). Chloroplast thioredoxin systems: prospects for improving photosynthesis. Philosophical transactions of the Royal Society of London. Series B, Biological sciences, 372(1730), 20160474. https://doi.org/10.1098/rstb.2016.0474

Noctor, G., & Foyer, C. H. (1998). ASCORBATE AND GLUTATHIONE: Keeping Active Oxygen Under Control. Annual review of plant physiology and plant molecular biology, 49, 249–279. https://doi.org/10.1146/annurev.arplant.49.1.249

Nowicka, B., Trela-Makowej, A., Latowski, D., Strzalka, K., & Szymańska, R. (2021). Antioxidant and Signaling Role of Plastid-Derived Isoprenoid Quinones and Chromanols. International journal of molecular sciences, 22(6), 2950. https://doi.org/10.3390/ijms22062950

Oja, V., Eichelmann, H., Peterson, R. B., Rasulov, B., & Laisk, A. (2003). Deciphering the 820 nm signal: redox state of donor side and quantum yield of Photosystem I in leaves. Photosynthesis research, 78(1), 1–15. https://doi.org/10.1023/A:1026070612022

Ojeda, V., Pérez-Ruiz, J. M., González, M., Nájera, V. A., Sahrawy, M., Serrato, A. J., Geigenberger, P., & Cejudo, F. J. (2017). NADPH Thioredoxin Reductase C and Thioredoxins Act Concertedly in Seedling Development. Plant physiology, 174(3), 1436–1448. https://doi.org/10.1104/pp.17.00481

Okegawa, Y., & Motohashi, K. (2015). Chloroplastic thioredoxin m functions as a major regulator of Calvin cycle enzymes during photosynthesis in vivo. The Plant journal : for cell and molecular biology, 84(5), 900–913. https://doi.org/10.1111/tpj.13049

Okegawa, Y., Basso, L., Shikanai, T., & Motohashi, K. (2020). Cyclic Electron Transport around PSI Contributes to Photosynthetic Induction with Thioredoxin f. Plant physiology, 184(3), 1291–1302. https://doi.org/10.1104/pp.20.00741

Okegawa, Y., Long, T. A., Iwano, M., Takayama, S., Kobayashi, Y., Covert, S. F., & Shikanai, T. (2007). A balanced PGR5 level is required for chloroplast development and optimum operation of cyclic electron transport around photosystem I. Plant & cell physiology, 48(10), 1462–1471. https://doi.org/10.1093/pcp/pcm116

Ono, T. A., Noguchi, T., Inoue, Y., Kusunoki, M., Matsushita, T., & Oyanagi, H. (1992). X-ray Detection of the Period-Four Cycling of the Manganese Cluster in Photosynthetic Water Oxidizing Enzyme. Science (New York, N.Y.), 258(5086), 1335–1337. https://doi.org/10.1126/science.258.5086.1335

Ort, D. R., & Baker, N. R. (2002). A photoprotective role for O(2) as an alternative electron sink in photosynthesis?. Current opinion in plant biology, 5(3), 193–198. https://doi.org/10.1016/s1369-5266(02)00259-5

Page, C. C., Moser, C. C., Chen, X., & Dutton, P. L. (1999). Natural engineering principles of electron tunnelling in biological oxidation-reduction. Nature, 402(6757), 47–52. https://doi.org/10.1038/46972

Page, M. L., Hamel, P. P., Gabilly, S. T., Zegzouti, H., Perea, J. V., Alonso, J. M., Ecker, J. R., Theg, S. M., Christensen, S. K., & Merchant, S. (2004). A homolog of prokaryotic thiol disulfide transporter CcdA is required for the assembly of the cytochrome b6f complex in Arabidopsis chloroplasts. The Journal of biological chemistry, 279(31), 32474–32482. https://doi.org/10.1074/jbc.M404285200

Pan, X., Cao, P., Su, X., Liu, Z., & Li, M. (2020). Structural analysis and comparison of light-harvesting complexes I and II. Biochimica et biophysica acta. Bioenergetics, 1861(4), 148038. https://doi.org/10.1016/j.bbabio.2019.06.010

Pan, X., Li, M., Wan, T., Wang, L., Jia, C., Hou, Z., Zhao, X., Zhang, J., & Chang, W. (2011). Structural insights into energy regulation of light-harvesting complex CP29 from spinach. Nature structural & molecular biology, 18(3), 309–315. https://doi.org/10.1038/nsmb.2008

Passarini, F., Wientjes, E., Hienerwadel, R., & Croce, R. (2009). Molecular basis of light harvesting and photoprotection in CP24: unique features of the most recent antenna complex. The Journal of biological chemistry, 284(43), 29536–29546. https://doi.org/10.1074/jbc.M109.036376

Peltier, G., Aro, E. M., & Shikanai, T. (2016). NDH-1 and NDH-2 Plastoquinone Reductases in Oxygenic Photosynthesis. Annual review of plant biology, 67, 55–80. https://doi.org/10.1146/annurev-arplant-043014-114752

Pérez-Ruiz, J. M., Naranjo, B., Ojeda, V., Guinea, M., & Cejudo, F. J. (2017). NTRC-dependent redox balance of 2-Cys peroxiredoxins is needed for optimal function of the photosynthetic apparatus. Proceedings of the National Academy of Sciences of the United States of America, 114(45), 12069–12074. https://doi.org/10.1073/pnas.1706003114

Peter, G. F., & Thornber, J. P. (1991). Biochemical composition and organization of higher plant photosystem II light-harvesting pigment-proteins. The Journal of biological chemistry, 266(25), 16745–16754.

Petrova, A. A., Boskhomdzhieva, B. K., Milanovsky, G. E., Koksharova, O. A., Mamedov, M. D., Cherepanov, D. A., & Semenov, A. Y. (2017). Interaction of various types of photosystem I complexes with exogenous electron acceptors. Photosynthesis research, 133(1-3), 175–184. https://doi.org/10.1007/s11120-017-0371-1

Porra, R. J., Thompson, W. A., & Kriedemann, P. E. (1989). Determination of accurate extinction coefficients and simultaneous equations for assaying chlorophylls a and b extracted with four different solvents: verification of the concentration of chlorophyll standards by atomic absorption spectroscopy. Biochimica et Biophysica Acta (BBA)-Bioenergetics, 975(3), 384-394.

Prakash, J. S., Baig, M. A., & Mohanty, P. (2001). Senescence induced structural reorganization of thylakoid membranes in Cucumis sativus cotyledons; LHC II involvement in reorganization of thylakoid membranes. Photosynthesis research, 68(2), 153–161. https://doi.org/10.1023/A:1011876412537

Pulido, P., Spínola, M. C., Kirchsteiger, K., Guinea, M., Pascual, M. B., Sahrawy, M., Sandalio, L. M., Dietz, K. J., González, M., & Cejudo, F. J. (2010). Functional analysis of the pathways for 2-Cys peroxiredoxin reduction in Arabidopsis thaliana chloroplasts. Journal of experimental botany, 61(14), 4043–4054. https://doi.org/10.1093/jxb/erq218

Qin, K., Fernie, A. R., & Zhang, Y. (2021). The Assembly of Super-Complexes in the Plant Chloroplast. Biomolecules, 11(12), 1839. https://doi.org/10.3390/biom11121839

Qin, X., Suga, M., Kuang, T., & Shen, J. R. (2015). Photosynthesis. Structural basis for energy transfer pathways in the plant PSI-LHCI supercomplex. Science (New York, N.Y.), 348(6238), 989–995. https://doi.org/10.1126/science.aab0214

Radmer, R. J., & Kok, B. (1976). Photoreduction of O(2) Primes and Replaces CO(2) Assimilation. Plant physiology, 58(3), 336–340. https://doi.org/10.1104/pp.58.3.336

Raines C. A. (2003). The Calvin cycle revisited. *Photosynthesis research*, *75*(1), 1–10. https://doi.org/10.1023/A:1022421515027

Rantala, M., Rantala, S., & Aro, E. M. (2020). Composition, phosphorylation and dynamic organization of photosynthetic protein complexes in plant thylakoid membrane. Photochemical & photobiological sciences : Official journal of the European Photochemistry Association and the European Society for Photobiology, 19(5), 604–619. https://doi.org/10.1039/d0pp00025f

Richter, A. S., Pérez-Ruiz, J. M., Cejudo, F. J., & Grimm, B. (2018). Redox-control of chlorophyll biosynthesis mainly depends on thioredoxins. FEBS letters, 592(18), 3111–3115. https://doi.org/10.1002/1873-3468.13216

Rochaix J. D. (2014). Regulation and dynamics of the light-harvesting system. Annual review of plant biology, 65, 287–309. https://doi.org/10.1146/annurev-arplant-050213-040226

Rochaix, J. D., Lemeille, S., Shapiguzov, A., Samol, I., Fucile, G., Willig, A., & Goldschmidt-Clermont, M. (2012). Protein kinases and phosphatases involved in the acclimation of the photosynthetic apparatus to a changing light environment. Philosophical transactions of the

Royal Society of London. Series B, Biological sciences, 367(1608), 3466–3474. https://doi.org/10.1098/rstb.2012.0064

Rosso, D., Ivanov, A. G., Fu, A., Geisler-Lee, J., Hendrickson, L., Geisler, M., Stewart, G., Krol, M., Hurry, V., Rodermel, S. R., Maxwell, D. P., & Hüner, N. P. (2006). IMMUTANS does not act as a stress-induced safety valve in the protection of the photosynthetic apparatus of Arabidopsis during steady-state photosynthesis. Plant physiology, 142(2), 574–585. https://doi.org/10.1104/pp.106.085886

Ruban, A., Foyer, C., & Murchie, E. (Eds.). (2022). Photosynthesis in Action: Harvesting Light, Generating Electrons, Fixing Carbon. Academic Press.

Rühle, T., Dann, M., Reiter, B., Schünemann, D., Naranjo, B., Penzler, J. F., Kleine, T., & Leister, D. (2021). PGRL2 triggers degradation of PGR5 in the absence of PGRL1. Nature communications, 12(1), 3941. https://doi.org/10.1038/s41467-021-24107-7

Samecka-Cymerman, A., Marczonek, A., & Kempers, A. J. (1997). Bioindication of heavy metals in soil by liverworts. Archives of environmental contamination and toxicology, 33(2), 162–171. https://doi.org/10.1007/s002449900238

Sarewicz, M., Szwalec, M., Pintscher, S., Indyka, P., Rawski, M., Pietras, R., Mielecki, B., Koziej, Ł., Jaciuk, M., Glatt, S., & Osyczka, A. (2023). High-resolution cryo-EM structures of plant cytochrome b6f at work. Science advances, 9(2), eadd9688. https://doi.org/10.1126/sciadv.add9688

Sárvári, E., & Nyitrai, P. (1994). Separation of chlorophyll-protein complexes by Deriphat polyacrylamide gradient gel electrophoresis. Electrophoresis, 15(8-9), 1068–1071. https://doi.org/10.1002/elps.11501501159

Sárvári, É., Gellén, G., Sági-Kazár, M., Schlosser, G., Solymosi, K., & Solti, Á. (2022). Qualitative and quantitative evaluation of thylakoid complexes separated by Blue Native PAGE. Plant methods, 18(1), 23. https://doi.org/10.1186/s13007-022-00858-2

Schägger, H., & von Jagow, G. (1991). Blue native electrophoresis for isolation of membrane protein complexes in enzymatically active form. Analytical biochemistry, 199(2), 223–231. https://doi.org/10.1016/0003-2697(91)90094-a

Schlarb-Ridley, B. G., Nimmo, R. H., Purton, S., Howe, C. J., & Bendall, D. S. (2006). Cytochrome c(6A) is a funnel for thiol oxidation in the thylakoid lumen. FEBS letters, 580(9), 2166–2169. https://doi.org/10.1016/j.febslet.2006.03.052

Schmidt, S. B., Jensen, P. E., & Husted, S. (2016). Manganese Deficiency in Plants: The Impact on Photosystem II. Trends in plant science, 21(7), 622–632. https://doi.org/10.1016/j.tplants.2016.03.001

Schneider, A., Steinberger, I., Herdean, A., Gandini, C., Eisenhut, M., Kurz, S., Morper, A., Hoecker, N., Rühle, T., Labs, M., Flügge, U. I., Geimer, S., Schmidt, S. B., Husted, S., Weber, A. P., Spetea, C., & Leister, D. (2016). The Evolutionarily Conserved Protein PHOTOSYNTHESIS AFFECTED MUTANT71 Is Required for Efficient Manganese Uptake at the Thylakoid Membrane in Arabidopsis. The Plant cell, 28(4), 892–910. https://doi.org/10.1105/tpc.15.00812

Schöttler, M. A., & Tóth, S. Z. (2014). Photosynthetic complex stoichiometry dynamics in higher plants: environmental acclimation and photosynthetic flux control. Frontiers in plant science, 5, 188. https://doi.org/10.3389/fpls.2014.00188

Schöttler, M. A., Kirchhoff, H., & Weis, E. (2004). The role of plastocyanin in the adjustment of the photosynthetic electron transport to the carbon metabolism in tobacco. Plant physiology, 136(4), 4265–4274. https://doi.org/10.1104/pp.104.052324

Schreiber U, Klughammer C, Neubauer C (1988) Measuring P700 absorbance changes around 830 nm with a new type of pulse modulation system. Zeitschrift für Naturforschung C, vol 43.

Schreiber U. (2017). Redox changes of ferredoxin, P700, and plastocyanin measured simultaneously in intact leaves. Photosynthesis research, 134(3), 343–360. https://doi.org/10.1007/s11120-017-0394-7

Schreiber, U., & Klughammer, C. (2016). Analysis of Photosystem I Donor and Acceptor Sides with a New Type of Online-Deconvoluting Kinetic LED-Array Spectrophotometer. Plant & cell physiology, 57(7), 1454–1467. https://doi.org/10.1093/pcp/pcw044

Schuller, J. M., Birrell, J. A., Tanaka, H., Konuma, T., Wulfhorst, H., Cox, N., Schuller, S. K., Thiemann, J., Lubitz, W., Sétif, P., Ikegami, T., Engel, B. D., Kurisu, G., & Nowaczyk, M. M. (2019). Structural adaptations of photosynthetic complex I enable ferredoxin-dependent electron transfer. Science (New York, N.Y.), 363(6424), 257–260. https://doi.org/10.1126/science.aau3613

Schürmann, P., & Buchanan, B. B. (2008). The ferredoxin/thioredoxin system of oxygenic photosynthesis. Antioxidants & redox signaling, 10(7), 1235–1274. https://doi.org/10.1089/ars.2007.1931

Schwenkert, S., Legen, J., Takami, T., Shikanai, T., Herrmann, R. G., & Meurer, J. (2007). Role of the low-molecular-weight subunits PetL, PetG, and PetN in assembly, stability, and dimerization of the cytochrome b6f complex in tobacco. Plant physiology, 144(4), 1924–1935. https://doi.org/10.1104/pp.107.100131

Sekiguchi, T., Yoshida, K., Okegawa, Y., Motohashi, K., Wakabayashi, K. I., & Hisabori, T. (2020). Chloroplast ATP synthase is reduced by both f-type and m-type thioredoxins.

Biochimica et biophysica acta. Bioenergetics, 1861(11), 148261. https://doi.org/10.1016/j.bbabio.2020.148261

Serrato, A. J., Pérez-Ruiz, J. M., Spínola, M. C., & Cejudo, F. J. (2004). A novel NADPH thioredoxin reductase, localized in the chloroplast, which deficiency causes hypersensitivity to abiotic stress in Arabidopsis thaliana. The Journal of biological chemistry, 279(42), 43821–43827. https://doi.org/10.1074/jbc.M404696200

Sétif, P., Boussac, A., & Krieger-Liszkay, A. (2019). Near-infrared in vitro measurements of photosystem I cofactors and electron-transfer partners with a recently developed spectrophotometer. Photosynthesis research, 142(3), 307–319. https://doi.org/10.1007/s11120-019-00665-2

Sétif, P., Mutoh, R., & Kurisu, G. (2017). Dynamics and energetics of cyanobacterial photosystem I:ferredoxin complexes in different redox states. Biochimica et biophysica acta. Bioenergetics, 1858(7), 483–496. https://doi.org/10.1016/j.bbabio.2017.04.001

Sétif, P., Shimakawa, G., Krieger-Liszkay, A., & Miyake, C. (2020). Identification of the electron donor to flavodiiron proteins in Synechocystis sp. PCC 6803 by in vivo spectroscopy. Biochimica et biophysica acta. Bioenergetics, 1861(10), 148256. https://doi.org/10.1016/j.bbabio.2020.148256

Sharma, S. (2007). Marchantia polymorpha L.: A bioaccumulator. Aerobiologia, 23(3), 181-187.

Shen J. R. (2015). The Structure of Photosystem II and the Mechanism of Water Oxidation in Photosynthesis. Annual review of plant biology, 66, 23–48. https://doi.org/10.1146/annurev-arplant-050312-120129

Shevela, D., Kern, J. F., Govindjee, G., & Messinger, J. (2023). Solar energy conversion by photosystem II: principles and structures. Photosynthesis research, 156(3), 279–307. https://doi.org/10.1007/s11120-022-00991-y

Shikanai T. (2007). Cyclic electron transport around photosystem I: genetic approaches. Annual review of plant biology, 58, 199–217. https://doi.org/10.1146/annurev.arplant.58.091406.110525

Shikanai T. (2014). Central role of cyclic electron transport around photosystem I in the regulation of photosynthesis. Current opinion in biotechnology, 26, 25–30. https://doi.org/10.1016/j.copbio.2013.08.012

Shimakawa G. (2023). Electron transport in cyanobacterial thylakoid membranes: are cyanobacteria simple models for photosynthetic organisms?. Journal of experimental botany, 74(12), 3476–3487. https://doi.org/10.1093/jxb/erad118

Shimakawa, G., Hanawa, H., Wada, S., Hanke, G. T., Matsuda, Y., & Miyake, C. (2021). Physiological Roles of Flavodiiron Proteins and Photorespiration in the Liverwort Marchantia polymorpha. Frontiers in plant science, 12, 668805. https://doi.org/10.3389/fpls.2021.668805

Shimakawa, G., Ishizaki, K., Tsukamoto, S., Tanaka, M., Sejima, T., & Miyake, C. (2017). The Liverwort, Marchantia, Drives Alternative Electron Flow Using a Flavodiiron Protein to Protect PSI. Plant physiology, 173(3), 1636–1647. https://doi.org/10.1104/pp.16.01038

Shimakawa, G., Shaku, K., Nishi, A., Hayashi, R., Yamamoto, H., Sakamoto, K., Makino, A., & Miyake, C. (2015). FLAVODIIRON2 and FLAVODIIRON4 proteins mediate an oxygen-dependent alternative electron flow in Synechocystis sp. PCC 6803 under CO2-limited conditions. Plant physiology, 167(2), 472–480. https://doi.org/10.1104/pp.114.249987

Standfuss, J., & Kühlbrandt, W. (2004). The three isoforms of the light-harvesting complex II: spectroscopic features, trimer formation, and functional roles. The Journal of biological chemistry, 279(35), 36884–36891. https://doi.org/10.1074/jbc.M402348200

Standfuss, J., Terwisscha van Scheltinga, A. C., Lamborghini, M., & Kühlbrandt, W. (2005). Mechanisms of photoprotection and nonphotochemical quenching in pea light-harvesting complex at 2.5 A resolution. The EMBO journal, 24(5), 919–928. https://doi.org/10.1038/sj.emboj.7600585

Steinbeck, J., Ross, I. L., Rothnagel, R., Gäbelein, P., Schulze, S., Giles, N., Ali, R., Drysdale, R., Sierecki, E., Gambin, Y., Stahlberg, H., Takahashi, Y., Hippler, M., & Hankamer, B. (2018). Structure of a PSI-LHCI-cyt b6f supercomplex in Chlamydomonas reinhardtii promoting cyclic electron flow under anaerobic conditions. Proceedings of the National Academy of Sciences of the United States of America, 115(41), 10517–10522. https://doi.org/10.1073/pnas.1809973115

Strand, D. D., Fisher, N., & Kramer, D. M. (2017). The higher plant plastid NAD(P)H dehydrogenase-like complex (NDH) is a high efficiency proton pump that increases ATP production by cyclic electron flow. The Journal of biological chemistry, 292(28), 11850–11860. https://doi.org/10.1074/jbc.M116.770792

Stroebel, D., Choquet, Y., Popot, J. L., & Picot, D. (2003). An atypical haem in the cytochrome b(6)f complex. Nature, 426(6965), 413–418. https://doi.org/10.1038/nature02155

Su, X., Ma, J., Wei, X., Cao, P., Zhu, D., Chang, W., Liu, Z., Zhang, X., & Li, M. (2017). Structure and assembly mechanism of plant C2S2M2-type PSII-LHCII supercomplex. Science (New York, N.Y.), 357(6353), 815–820. https://doi.org/10.1126/science.aan0327

Takahashi H. (2022). Cyclic electron flow A to Z. Journal of plant research, 135(4), 539–541. https://doi.org/10.1007/s10265-022-01402-y

Takahashi, H., Clowez, S., Wollman, F. A., Vallon, O., & Rappaport, F. (2013). Cyclic electron flow is redox-controlled but independent of state transition. Nature communications, 4, 1954. https://doi.org/10.1038/ncomms2954

Telfer, A., Bishop, S. M., Phillips, D., & Barber, J. (1994). Isolated photosynthetic reaction center of photosystem II as a sensitizer for the formation of singlet oxygen. Detection and quantum yield determination using a chemical trapping technique. The Journal of biological chemistry, 269(18), 13244–13253.

Terentyev V. V. (2022). Macromolecular conformational changes in photosystem II: interaction between structure and function. Biophysical reviews, 14(4), 871–886. https://doi.org/10.1007/s12551-022-00979-x

Thormählen, I., Meitzel, T., Groysman, J., Öchsner, A. B., von Roepenack-Lahaye, E., Naranjo, B., Cejudo, F. J., & Geigenberger, P. (2015). Thioredoxin f1 and NADPH-Dependent Thioredoxin Reductase C Have Overlapping Functions in Regulating Photosynthetic Metabolism and Plant Growth in Response to Varying Light Conditions. Plant physiology, 169(3), 1766–1786. https://doi.org/10.1104/pp.15.01122

Thormählen, I., Ruber, J., von Roepenack-Lahaye, E., Ehrlich, S. M., Massot, V., Hümmer, C., Tezycka, J., Issakidis-Bourguet, E., & Geigenberger, P. (2013). Inactivation of thioredoxin f1 leads to decreased light activation of ADP-glucose pyrophosphorylase and altered diurnal starch turnover in leaves of Arabidopsis plants. Plant, cell & environment, 36(1), 16–29. https://doi.org/10.1111/j.1365-3040.2012.02549.

Thormählen, I., Zupok, A., Rescher, J., Leger, J., Weissenberger, S., Groysman, J., Orwat, A., Chatel-Innocenti, G., Issakidis-Bourguet, E., Armbruster, U., & Geigenberger, P. (2017). Thioredoxins Play a Crucial Role in Dynamic Acclimation of Photosynthesis in Fluctuating Light. Molecular plant, 10(1), 168–182. https://doi.org/10.1016/j.molp.2016.11.012

Thornton, L. E., Ohkawa, H., Roose, J. L., Kashino, Y., Keren, N., & Pakrasi, H. B. (2004). Homologs of plant PsbP and PsbQ proteins are necessary for regulation of photosystem ii activity in the cyanobacterium Synechocystis 6803. The Plant cell, 16(8), 2164–2175. https://doi.org/10.1105/tpc.104.023515

Tikhonov A. N. (2013). pH-dependent regulation of electron transport and ATP synthesis in chloroplasts. Photosynthesis research, 116(2-3), 511–534. https://doi.org/10.1007/s11120-013-9845-y

Tikhonov A. N. (2014). The cytochrome b6f complex at the crossroad of photosynthetic electron transport pathways. Plant physiology and biochemistry : PPB, 81, 163–183. https://doi.org/10.1016/j.plaphy.2013.12.011

Tikhonov A. N. (2023). Electron Transport in Chloroplasts: Regulation and Alternative Pathways of Electron Transfer. Biochemistry. Biokhimiia, 88(10), 1438–1454. https://doi.org/10.1134/S0006297923100036

Toivola, J., Nikkanen, L., Dahlström, K. M., Salminen, T. A., Lepistö, A., Vignols, H. F., & Rintamäki, E. (2013). Overexpression of chloroplast NADPH-dependent thioredoxin reductase in Arabidopsis enhances leaf growth and elucidates in vivo function of reductase and thioredoxin domains. Frontiers in plant science, 4, 389. https://doi.org/10.3389/fpls.2013.00389

Turkan, I., Uzilday, B., Dietz, K. J., Bräutigam, A., & Ozgur, R. (2018). Reactive oxygen species and redox regulation in mesophyll and bundle sheath cells of C4 plants. Journal of experimental botany, 69(14), 3321–3331. https://doi.org/10.1093/jxb/ery064

Ueda, M., Kuniyoshi, T., Yamamoto, H., Sugimoto, K., Ishizaki, K., Kohchi, T., Nishimura, Y., & Shikanai, T. (2012). Composition and physiological function of the chloroplast NADH dehydrogenase-like complex in Marchantia polymorpha. The Plant journal : for cell and molecular biology, 72(4), 683–693. https://doi.org/10.1111/j.1365-313X.2012.05115.x

Ueda, M., Kuniyoshi, T., Yamamoto, H., Sugimoto, K., Ishizaki, K., Kohchi, T., Nishimura, Y., & Shikanai, T. (2012). Composition and physiological function of the chloroplast NADH dehydrogenase-like complex in Marchantia polymorpha. The Plant journal : for cell and molecular biology, 72(4), 683–693. https://doi.org/10.1111/j.1365-313X.2012.05115.x

Ueda, M., Tanaka, A., Sugimoto, K., Shikanai, T., & Nishimura, Y. (2014). chlB requirement for chlorophyll biosynthesis under short photoperiod in Marchantia polymorpha L. Genome biology and evolution, 6(3), 620–628. https://doi.org/10.1093/gbe/evu045

Umena, Y., Kawakami, K., Shen, J. R., & Kamiya, N. (2011). Crystal structure of oxygen-evolving photosystem II at a resolution of 1.9 Å. Nature, 473(7345), 55–60. https://doi.org/10.1038/nature09913

van Bezouwen, L. S., Caffarri, S., Kale, R. S., Kouřil, R., Thunnissen, A. W. H., Oostergetel, G. T., & Boekema, E. J. (2017). Subunit and chlorophyll organization of the plant photosystem II supercomplex. Nature plants, 3, 17080. https://doi.org/10.1038/nplants.2017.80

Vinyard, D., Yocum, C. F., & Bricker, T. M. (2022). Preface: special issues on photosystem II. Photosynthesis research, 152(2), 87–90. https://doi.org/10.1007/s11120-022-00930-x

Wang, D., & Fu, A. (2016). The Plastid Terminal Oxidase is a Key Factor Balancing the Redox State of Thylakoid Membrane. The Enzymes, 40, 143–171. https://doi.org/10.1016/bs.enz.2016.09.002

Wang, P., Liu, J., Liu, B., Feng, D., Da, Q., Wang, P., Shu, S., Su, J., Zhang, Y., Wang, J., & Wang, H. B. (2013). Evidence for a role of chloroplastic m-type thioredoxins in the biogenesis of photosystem II in Arabidopsis. Plant physiology, 163(4), 1710–1728. https://doi.org/10.1104/pp.113.228353

Wei, X., Su, X., Cao, P., Liu, X., Chang, W., Li, M., Zhang, X., & Liu, Z. (2016). Structure of spinach photosystem II-LHCII supercomplex at 3.2 Å resolution. Nature, 534(7605), 69–74. https://doi.org/10.1038/nature18020

Wientjes, E., & Croce, R. (2011). The light-harvesting complexes of higher-plant Photosystem I: Lhca1/4 and Lhca2/3 form two red-emitting heterodimers. The Biochemical journal, 433(3), 477–485. https://doi.org/10.1042/BJ20101538

Wolf, B. C., Isaacson, T., Tiwari, V., Dangoor, I., Mufkadi, S., & Danon, A. (2020). Redox regulation of PGRL1 at the onset of low light intensity. The Plant journal : for cell and molecular biology, 103(2), 715–725. https://doi.org/10.1111/tpj.14764

Wu, J., Rong, L., Lin, W., Kong, L., Wei, D., Zhang, L., Rochaix, J. D., & Xu, X. (2021). Functional redox links between lumen thiol oxidoreductase1 and serine/threonine-protein kinase STN7. Plant physiology, 186(2), 964–976. https://doi.org/10.1093/plphys/kiab091

Wulff, R. P., Lundqvist, J., Rutsdottir, G., Hansson, A., Stenbaek, A., Elmlund, D., Elmlund, H., Jensen, P. E., & Hansson, M. (2011). The activity of barley NADPH-dependent thioredoxin reductase C is independent of the oligomeric state of the protein: tetrameric structure determined by cryo-electron microscopy. Biochemistry, 50(18), 3713–3723. https://doi.org/10.1021/bi200058a

Xu, Q., Yu, L., Chitnis, V. P., & Chitnis, P. R. (1994). Function and organization of photosystem I in a cyanobacterial mutant strain that lacks PsaF and PsaJ subunits. The Journal of biological chemistry, 269(5), 3205–3211

Yadav, K. N., Semchonok, D. A., Nosek, L., Kouřil, R., Fucile, G., Boekema, E. J., & Eichacker, L. A. (2017). Supercomplexes of plant photosystem I with cytochrome b6f, light-harvesting complex II and NDH. Biochimica et biophysica acta. Bioenergetics, 1858(1), 12–20. https://doi.org/10.1016/j.bbabio.2016.10.006

Yamamoto, H., Peng, L., Fukao, Y., & Shikanai, T. (2011). An Src homology 3 domain-like fold protein forms a ferredoxin binding site for the chloroplast NADH dehydrogenase-like complex in Arabidopsis. The Plant cell, 23(4), 1480–1493. https://doi.org/10.1105/tpc.110.080291

Yamashita, E., Zhang, H., & Cramer, W. A. (2007). Structure of the cytochrome b6f complex: quinone analogue inhibitors as ligands of heme cn. Journal of molecular biology, 370(1), 39–52. https://doi.org/10.1016/j.jmb.2007.04.011

Yamori, W., & Shikanai, T. (2016). Physiological Functions of Cyclic Electron Transport Around Photosystem I in Sustaining Photosynthesis and Plant Growth. Annual review of plant biology, 67, 81–106. https://doi.org/10.1146/annurev-arplant-043015-112002

Yamori, W., Sakata, N., Suzuki, Y., Shikanai, T., & Makino, A. (2011). Cyclic electron flow around photosystem I via chloroplast NAD(P)H dehydrogenase (NDH) complex performs a significant physiological role during photosynthesis and plant growth at low temperature in rice. The Plant journal : for cell and molecular biology, 68(6), 966–976. https://doi.org/10.1111/j.1365-313X.2011.04747.x

Yamori, W., Shikanai, T., & Makino, A. (2015). Photosystem I cyclic electron flow via chloroplast NADH dehydrogenase-like complex performs a physiological role for photosynthesis at low light. Scientific reports, 5, 13908. https://doi.org/10.1038/srep13908

Yano, J., & Yachandra, V. (2014). Mn4Ca cluster in photosynthesis: where and how water is oxidized to dioxygen. Chemical reviews, 114(8), 4175–4205. https://doi.org/10.1021/cr4004874

Yeremenko, N., Jeanjean, R., Prommeenate, P., Krasikov, V., Nixon, P. J., Vermaas, W. F., Havaux, M., & Matthijs, H. C. (2005). Open reading frame ssr2016 is required for antimycin A-sensitive photosystem I-driven cyclic electron flow in the cyanobacterium Synechocystis sp. PCC 6803. *Plant & cell physiology*, *46*(8), 1433–1436. https://doi.org/10.1093/pcp/pci147

Yoshida, K., & Hisabori, T. (2016). Two distinct redox cascades cooperatively regulate chloroplast functions and sustain plant viability. Proceedings of the National Academy of Sciences of the United States of America, 113(27), E3967–E3976. https://doi.org/10.1073/pnas.1604101113

Yoshida, K., & Hisabori, T. (2017). Distinct electron transfer from ferredoxin-thioredoxin reductase to multiple thioredoxin isoforms in chloroplasts. The Biochemical journal, 474(8), 1347–1360. https://doi.org/10.1042/BCJ20161089

Yoshida, K., Hara, S., & Hisabori, T. (2015). Thioredoxin Selectivity for Thiol-based Redox Regulation of Target Proteins in Chloroplasts. The Journal of biological chemistry, 290(23), 14278–14288. https://doi.org/10.1074/jbc.M115.647545

Yu, L., Vassiliev, I. R., Jung, Y. S., Bryant, D. A., & Golbeck, J. H. (1995). Modified ligands to FA and FB in photosystem I. II. Characterization of a mixed ligand [4Fe-4S] cluster in the C51D mutant of PsaC upon rebinding to P700-Fx cores. The Journal of biological chemistry, 270(47), 28118–28125. https://doi.org/10.1074/jbc.270.47.28118

Zaitsev, S. Y., Volchenkova, T. A., Kalabina, N. A., Schaefer, C., & Zubov, V. P. (1998, December). Purification and monolayer study of the thylacoid lipids of moss marchantia

polymorpha. In Macromolecular symposia (Vol. 136, No. 1, pp. 119-129). Weinheim, Germany: WILEY-VCH Verlag GmbH & Co. KGaA.

Zelitch, I. (1979). Photorespiration: studies with whole tissues. In *Photosynthesis II: Photosynthetic Carbon Metabolism and Related Processes* (pp. 353-367). Berlin, Heidelberg: Springer Berlin Heidelberg.

Zhang, B., Zhang, C., Liu, C., Jing, Y., Wang, Y., Jin, L., Yang, L., Fu, A., Shi, J., Zhao, F., Lan, W., & Luan, S. (2018). Inner Envelope CHLOROPLAST MANGANESE TRANSPORTER 1 Supports Manganese Homeostasis and Phototrophic Growth in Arabidopsis. Molecular plant, 11(7), 943–954. https://doi.org/10.1016/j.molp.2018.04.007

Zhang, C., Römheld, V., & Marschner, H. (1995). Retranslocation of iron from primary leaves of bean plants grown under iron deficiency. Journal of Plant Physiology, 146(3), 268-272.

Zhang, S., Tang, K., Yan, Q., Li, X., Shen, L., Wang, W., He, Y. K., Kuang, T., Han, G., Shen, J. R., & Zhang, X. (2023). Structural insights into a unique PSI-LHCI-LHCII-Lhcb9 supercomplex from moss Physcomitrium patens. Nature plants, 9(5), 832–846. https://doi.org/10.1038/s41477-023-01401-4

Zhou, Q., Wang, C., Yamamoto, H., & Shikanai, T. (2022). PTOX-dependent safety valve does not oxidize P700 during photosynthetic induction in the Arabidopsis pgr5 mutant. Plant physiology, 188(2), 1264–1276. https://doi.org/10.1093/plphys/kiab541

Appendix

Article 4: Plastid terminal oxidase (PTOX) protects photosystem I and not photosystem II against photoinhibition in *Arabidopsis thaliana* and *Marchantia* polymorpha (published)

Introduction

Besides non-photochemical quenching mechanism and alternative electron flows, several regulatory proteins are also involved in protective mechanism. Plastid terminal oxidase (PTOX) is one of them which acts as a "safety valve" for protecting photosystem II (PSII) *Marchantia polymorpha* was chosen for this study because of its emerging importance as an evolutionary land plant. An earlier study (Messant et al., 2021) has shown the presence of two PTOX isoforms (PTOXa and PTOXb), with PTOXa showing some similarity with algae and PTOXb with angiosperms. However, not much information is available regarding the exact role of plant and agal-type PTOX isoforms. In this study, PTOX mutant from *Arabidopsis* (*immutans)* was complemented with bacterial desaturase CrtI (to avoid the possible effect of mutation on carotenoid biosynthesis). In addition, a PTOX double mutant was constructed in *Marchantia polymorpha.* Photosynthetic electron transport and susceptibility of PSI and PSII to photoinhibition was investigated. In the absence of PTOX, PSI was more susceptible to photoinhibition while PSII was relatively more stable.

My contributions to this paper only involves performing RT-qPCR (Fig S7) and analyzing data. Moreover, I participated in reading the manuscript.

the plant journal

SEB SOCIETY FOR EXPERIMENTAL BIOLOGY

The Plant Journal (2024) **117,** 669–678 doi: 10.1111/tpj.16520

Plastid terminal oxidase (PTOX) protects photosystem I and not photosystem II against photoinhibition in *Arabidopsis thaliana* and *Marchantia polymorpha*

Marine Messant[1], Umama Hani[1], Thanh-Lan Lai[1], Adjélé Wilson[1], Ginga Shimakawa[1,2] and Anja Krieger-Liszkay[1,*]

[1]*Institute for Integrative Biology of the Cell (I2BC), Université Paris-Saclay, CEA, CNRS, 91198 Gif-sur-Yvette cedex, France, and*

[2]*Department of Bioscience, School of Biological and Environmental Sciences, Kwansei-Gakuin University, 1 Gakuen-Uegahara, Sanda, Hyogo 669-1330, Japan*

Received 20 April 2023; revised 1 October 2023; accepted 21 October 2023; published online 3 November 2023.
*For correspondence (e-mail anja.liszkay@i2bc.paris-saclay.fr).

SUMMARY

The plastid terminal oxidase PTOX controls the oxidation level of the plastoquinone pool in the thylakoid membrane and acts as a safety valve upon abiotic stress, but detailed characterization of its role in protecting the photosynthetic apparatus is limited. Here we used PTOX mutants in two model plants *Arabidopsis thaliana* and *Marchantia polymorpha*. In Arabidopsis, lack of PTOX leads to a severe defect in pigmentation, a so-called variegated phenotype, when plants are grown at standard light intensities. We created a green Arabidopsis PTOX mutant expressing the bacterial carotenoid desaturase CRTI and a double mutant in Marchantia lacking both PTOX isoforms, the plant-type and the alga-type PTOX. In both species, lack of PTOX affected the redox state of the plastoquinone pool. Exposure of plants to high light intensity showed in the absence of PTOX higher susceptibility of photosystem I to light-induced damage while photosystem II was more stable compared with the wild type demonstrating that PTOX plays both, a pro-oxidant and an anti-oxidant role *in vivo*. Our results shed new light on the function of PTOX in the protection of photosystem I and II.

Keywords: *Arabidopsis thaliana, Marchantia polymorpha*, photosynthesis, photoinhibition, regulation.

INTRODUCTION

In nature, plants have to cope with sudden changes in light intensity. Light intensities higher than needed for CO_2 assimilation saturate the photosynthetic electron transport chain and can cause oxidative stress leading to damage to the photosystems. Photosynthetic organisms have a multitude of regulation mechanisms to protect the photosynthetic apparatus in excess light. Among these protection mechanisms, there are processes that lead to the dissipation of excess energy as heat, downregulation of the photosynthetic electron transport and even the degradation and repair of photosystem II (PSII) that is sacrificed protecting photosystem I (PSI) against photodamage (Oguchi et al., 2021; Sonoike, 2011). PSII, different from PSI, has an efficient damage repair cycle so that damage of PSII is not very costly (Li et al., 2018). Alternative electron transport routes like cyclic electron flow and Mehler/Mehler-like reactions are important to protect PSI against photoinhibition (Alboresi et al., 2019). Furthermore, the plastid terminal oxidase PTOX has been shown to be an important sink for electrons upon stress (Stepien & Johnson, 2009, 2018; Streb et al., 2005). PTOX is a non-heme diiron carboxylate enzyme that catalyzes the oxidation of plastoquinol, reducing oxygen to water. Depending on the quinol availability, it can have an anti-oxidant or a pro-oxidant function as has been shown *in vitro* using recombinant PTOX protein (Yu et al., 2014). Upregulation of PTOX expression has been reported for several stress-tolerant plant species acclimated to harsh environments such as drought, high light, and high temperature (Ibáñez et al., 2010; Quiles, 2006), high salinity (Stepien & Johnson, 2009), low temperature (Ivanov et al., 2012; Streb et al., 2005), and high levels of UV light (Laureau et al., 2013). PTOX is believed to act as a stress-induced safety valve that keeps the acceptor side of PSII oxidized, thereby helping to protect PSII from photodamage (Ivanov et al., 2012; Quiles, 2006; Stepien & Johnson, 2009; Streb et al., 2005). However, overexpression of PTOX1 from *Chlamydomonas reinhardtii* promotes photoinhibition via the production of reactive oxygen species (Ahmad et al., 2020; Heyno et al., 2009) while overexpression

of PTOX from *A. thaliana* does not alter the light susceptibility of PSII (Rosso et al., 2006). This may be caused either by a difference in the protein content in the two overexpression systems or by a difference in the regulation between alga- and plant-type PTOX isoforms.

The genome of angiosperms encodes one PTOX while most other photosynthetic organisms possess two isoforms that can either be closely related or belong to a plant-type or an alga-type family (Messant et al., 2021). PTOX mutants called *immutans* (*im*) in *Arabidopsis thaliana* and *ghost* in tomato show, depending on the light intensity, a very strong variegated phenotype (Wetzel et al., 1994). In angiosperms, PTOX is crucial for carotenoid biosynthesis (Carol et al., 1999). Plant carotenoid desaturases use plastoquinone (PQ) as electron acceptor and depend on PTOX for reoxidation of plastoquinol (PQH_2) to PQ. Single mutants of PTOX in *Chlamydomonas reinhardtii* or in *Marchantia polymorpha* show normal pigmentation (Houille-Vernes et al., 2011; Messant et al., 2021).

The importance of PTOX for protection of the photosynthetic apparatus against photoinhibition remains unclear. Here we use PTOX mutants of Arabidopsis and Marchantia to study the susceptibility of the photosynthetic apparatus to high light stress. To overcome the strong impact on carotenoid biosynthesis in *im*, we crossed *im* with Arabidopsis expressing the bacterial carotene desaturase (CRTI) (Schaub et al., 2005). CRTI introduces conjugation in phytoene by adding four double bonds using oxygen as electron acceptor and, therefore, being independent of PQ. In addition, we generated double mutants of PTOXa and PTOXb in Marchantia to show the importance of PTOX in an organism that contains, different to angiosperms, flavodiiron enzymes allowing Mehler-like reaction as additional route of alternative electron flow and keeping the electron transport chain oxidized. Furthermore, we determined the enzymatic activity of both, PTOXa and PTOXb using an *in vitro* approach.

RESULTS

PTOX affects the redox state of the electron transport chain in *A. thaliana* and *M. polymorpha*.

We crossed *im* with Arabidopsis expressing the bacterial carotene desaturase (CRTI) and used chlorophyll fluorescence induction curves and post-illumination fluorescence for screening the F2 generation (Figure 1). Mutants lacking PTOX in the F2 generation of the *im*CRTI lines show homogeneously green leaves under normal growth light (Figure 1) and also under fluctuating light (Supplemental Figure S1). There were no significant differences in chlorophyll a/b and chlorophyll/carotenoid ratio between wild type and *im*CRTI lines (Table S1). Two *im*CRTI lines were selected for this study hereafter called *im*CRTI_1 and *im*CRTI_2. Upon illumination with low-intensity actinic light, in the wild type, the fluorescence level reached within the first 10 sec a steady state level very close to the minimum fluorescence level Fo, while both *im*CRTI lines showed a higher fluorescence level in the light (Figure 1b). This shows that the plastoquinone pool is more reduced in the mutants as expected when PTOX activity is lacking. Moreover, the so-called post-illumination fluorescence rise is higher in *im*CRTI than in Col-0, reflecting a more reduced PQ pool due to the absence of PTOX activity and the loss of chlororespiratory activity (Figure 1c).

To investigate whether in Marchantia lack of PTOX has the same effect on pigment composition and on the reduction state of the PQ pool as in Arabidopsis, we created mutants lacking the two PTOX isoforms PTOXa and PTOXb. Marchantia Δ*ptoxaptoxb_1* and Δ*ptoxaptoxb_2* construction is shown in Figure 2a. Different from *Arabidopsis*, PTOX mutants in Marchantia do not show a phenotype independent of the light regime (Figure 2b). When the growth light intensity was doubled, all genotypes contained less chlorophyll and carotenoids (Figure S2). No variegated phenotype was observed in the double mutants, showing that carotenoid biosynthesis was not affected in the absence of PTOX (SI Table 1) in contrast to the variegated phenotype reported in the *im* mutant. To challenge the photosynthetic apparatus even more, plants were grown in fluctuating light. The double mutants were not more stressed than the other genotypes, only the wild type, Tak-1, was a bit paler than the mutants (Figure S2).

Both PTOX enzymes, PTOXa and PTOXb, contribute to keeping the redox state of the PQ pool oxidized as shown by chlorophyll fluorescence induction upon illumination with actinic light (Figure 2c). Fluorescence induction was measured by applying a moderate light intensity of red light (I = 53 μmol quanta m^{-2} sec^{-1}). At this light intensity, the maximum level of fluorescence was reached faster in the mutants compared with the wild type (Figure 2c, inset). The single mutants Δ*ptoxa* and Δ*ptoxb* showed a fast rise followed by a fluorescence decrease. This transient phase is lacking in the double mutants, and it can be attributed to the remaining PTOX activity in the single mutants. When instead a saturating flash was used like usually done for measuring OJIP fluorescence induction curves, there was no difference, indicating that the size of the PQ pool was the same in all genotypes. The absence of an effect in the mutants in a short saturating flash could be explained by a low activity of PTOX. When the light was switched off, the fluorescence level remained higher in Δ*ptoxaptoxb*_1 showing that the reoxidation of PQH_2 in the dark was retarded in the absence of PTOX. The faster fluorescence rise in the first second after the onset of actinic light was observed in all mutants, also when only one PTOX isoform was lacking (Figure 2d).

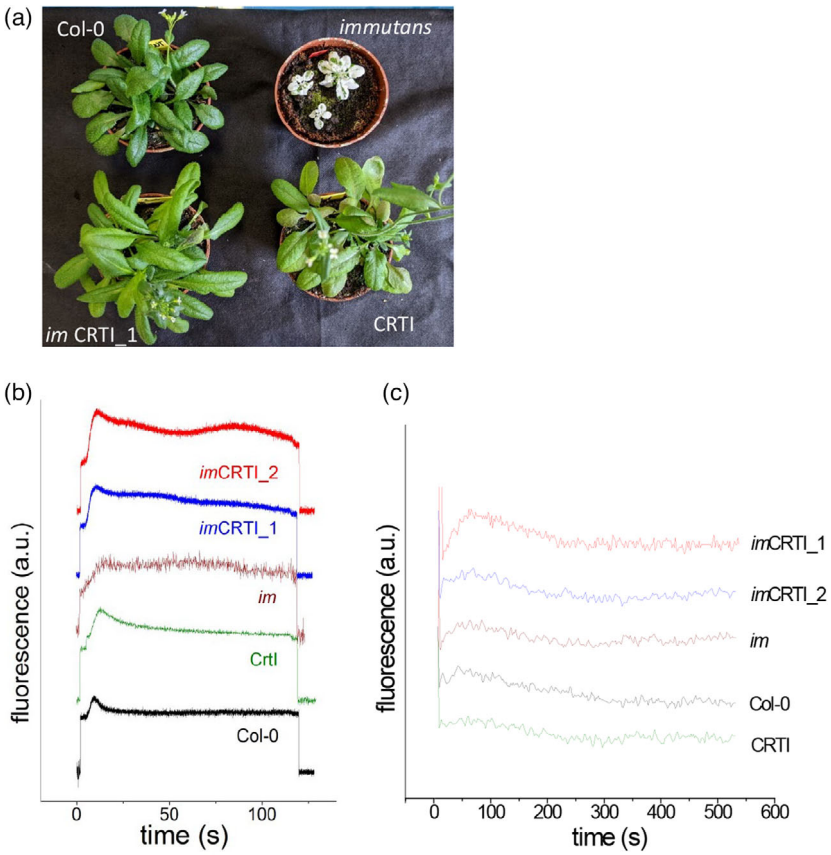

Figure 1. Characterization of Arabidopsis *im* x CRTI lines.
(a) The photo shows 5-week-old plants, wild-type Col-0, PTOX mutant *im*, plant-expressing bacterial desaturase CRTI, and *im*CRTI_1 mutant; grown in long-day conditions at 100 μmol quanta m^{-2} sec^{-1}.
(b) Chlorophyll fluorescence induction curves of Col-0 and the *im*CRTI_1 and *im*CRTI_2 lines. Fv/Fm values for Col-0: 0.853 ± 0.001; *im*CRTI_1: 0.850 ± 0.012; *im*CRTI_2: 0.851 ± 0.023. c. Post-illumination fluorescence rise of Col-0 and both *im*CRTI lines after 10 min actinic light (530 μmol quanta m^{-2} sec^{-1}). The flash indicates the turning of the actinic light. Representative curves are shown (n = 4 for each genotype).

Comparison of PTOXa and PTOXb recombinant proteins

We further studied the enzymatic properties of the two PTOX isoforms using recombinant protein and an *in vitro* activity assay. As shown in Figure S3, there are differences in the amino acid sequence of the two proteins, especially with respect to the length at the N-terminal site[16]. In the catalytic site, starting from α-helix 1, fully conserved residues represent 64% of the total sequences whereas conservative and semi-conservative exchanges are 26% and 6%, respectively. We used purified recombinant PTOXa and PTOXb proteins to determine the maximum catalytic activity of the two isoforms using saturating concentrations of decylplastoquinol as substrate (Table 1). For PTOXb, the N-terminal extension had been removed since the full-length gene was not expressed in *E. coli*. The enzyme activity of PTOXa was 3 times higher than that of PTOXb.

PTOX activity affects the quantum efficiency of PSI

PTOX competes to a certain extent with linear electron flow from PSII via the PQ pool, the cytochrome b_6f complex, and plastocyanin to PSI. Since PTOX oxidizes PQH_2, it reduces at the same time the number of electrons available for reduction of $P700^+$. The number of available electrons determines the level of the so-called donor-side limitation of PSI, Y(ND). When Marchantia thalli were exposed to fluctuating light intensities, Y(ND) was high at high light intensities and low at low light intensities independent of the genotype (Figure 3a). However, the switch from high Y(ND) to low Y(ND) was immediate in the double mutant while this transition was slower in Tak-1, indicating that PTOX oxidizes partly the PQ pool and limits electron donation upon the change from high light to low light. Similar results were obtained for all mutants (Figure S4). Accordingly, less donor-side limitation (Y(ND)) was observed in the mutants when plants were illuminated with increasing light intensity (Figure 3b). Each intensity was applied for 3 min before the measurement was taken to ensure that the photosynthetic apparatus was acclimated to the given light intensity. At all light intensities, there was less donor-side limitation in the double mutant than in the single mutant while Tak-1 showed the highest Y(ND). The lower donor-side limitation in the mutants resulted in a higher PSI yield (Figure 3c), while the effective quantum yield of PSII (Y(II)) was the same in all genotypes (Figure 3d). Acceptor-side limitation (Y(NA)) was very low in all genotypes (Figure S5) thanks to the presence of flavodiiron proteins (Shimakawa et al., 2017). No differences in non-photochemical quenching (NPQ) were found in the different genotypes (Figure S5).

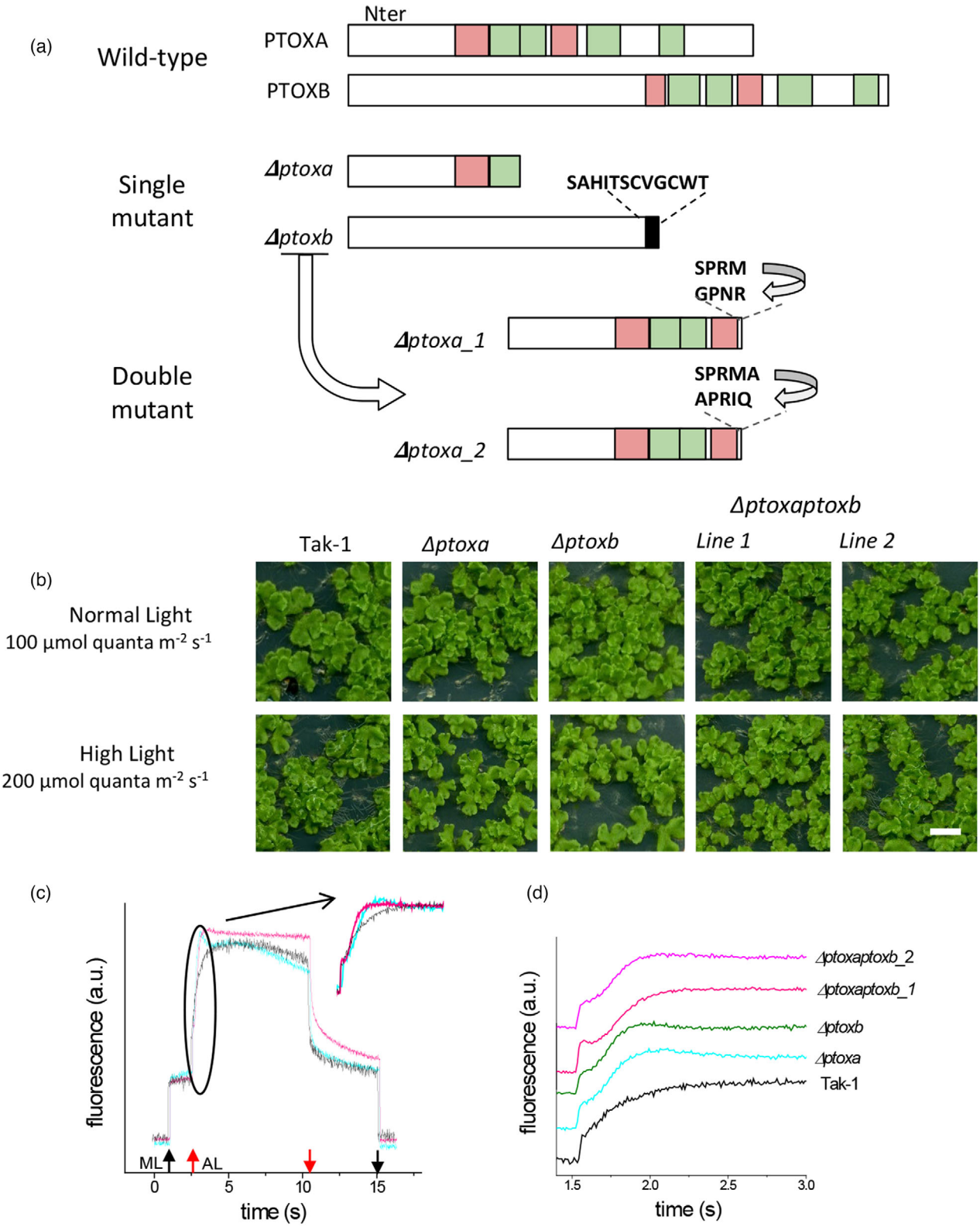

Figure 2. Characterization of *Marchantia polymorpha* PTOX mutant lines.
(a) Design of the PTOX mutants using CRISP/Cas9 technology. Marchantia has a 'plant-type' and an 'alga-type' PTOX (PTOXa and PTOXb, respectively). Two membrane-associated (red) and four α-helices which contain the six iron binding site motifs necessary for the catalytic activity (green) are shown in colored bars. PTOXB possesses a long Nter part. The double mutants were generated by the transformation of Δptoxb. All mutants have frameshift mutation in PTOX genes, resulting in shorter polypeptides of PTOX (see details in Materials and Methods and Figure S3).
(b) Images of the different genotypes grown for 3 weeks at 100 μmol quanta m^{-2} sec^{-1} and at 200 μmol quanta m^{-2} sec^{-1}.
(c)Chlorophyll fluorescence induction curves measured at low actinic light (I = 53 μmol quanta m^{-2} sec^{-1}). Arrows indicate the set on/off of the measuring light and of the actinic light. The inset shows a zoom of the fluorescence change upon the onset of the actinic light. Black: Tak-1, blue: Δ*ptoxa*, pink: Δ*ptoxaptoxb_1*.
(d) Fluorescence induction curves upon onset of actinic light for all genotypes starting from the F_0 level corresponding to the zoom in e. Fv/Fm values for Tak-1: 0.766 ± 0.001; Δ*ptoxa*: 0.774 ± 0.003; Δ*ptoxb*: 0.775 ± 0.001; Δ*ptoxaptoxb_1*: 0.764 ± 0.016; Δ*ptoxaptoxb_2*: 0.744 ± 0.012. Representative curves are shown (*n* = 4 for each genotype).

Table 1 Activity of purified recombinant MBP-MpPTOXa and MBP-MpPtoxb-Δ*Nter*

Sample	Activity (μmol O_2 mg protein^{-1} min^{-1})
MBP-MpPTOXa	149 +/− 16
MBP-MpPtoxb-Δ*Nter*	46 +/− 6

The assay contained 10 μg protein per 700 μl final volume, 100 μM decyl-plastoquinone, 200 μM NADH, 10 μg DT-diaphorase, 50 mM Tris–HCl pH 8.0, 2.5 mM $MgCl_2$. Activities were determined by measuring O_2 consumption at 25°C with a Clark-type electrode.

PTOX protects PSI from photoinhibition and promotes photoinhibition of PSII

Next, we investigated the protective effect of PTOX against light-induced damage of the two photosystems. Both, *Arabidopsis* leaves and *Marchantia* thalli, were exposed for 3 h to high light (1250 μmol quanta m^{-2} sec^{-1}), and photoinhibition of PSI was followed as a loss in the absorption signal at 830 nm, the so-called Pm value, while photoinhibition of PSII was monitored by the loss of the maximum quantum yield of PSII (Fv/Fm). At this light intensity, the donor-side limitation of PSI was higher in the wild types than in the mutants (Figure S6). PSI was more susceptible to photoinhibition in *im*CRTI lines and in Δ*ptoxaptoxb* mutants (Figure 4a, c) than in the respective wild types. The opposite was observed for PSII (Figure 4b, d). PSII was more damaged in respective wild types than in the PTOX-lacking mutants. This may be due to the pro-oxidant role of PTOX that has been previously observed in tobacco overexpressing PTOX (Ahmad et al., 2012, 2020; Heyno et al., 2009). In *Marchantia*, PTOX single mutants showed no increase in PSII photoinhibition compared with the double mutants, showing that one PTOX isoform is enough to allow sufficient accumulation of $P700^+$ that protects against the destruction of the FeS clusters in PSI (Sonoike et al., 1995). On the other hand, one PTOX isoform was also sufficient to protect PSII.

DISCUSSION

The *Arabidopsis im*CRTI lines are homogeneously green and grow well in high light. This makes this mutant an ideal tool to study the effect of PTOX activity on photosynthetic electron transport in angiosperms. Previously the study of PTOX activity in angiosperms was limited to plants grown at low light intensity, a growth condition that permits to avoid the variegated phenotype (Trouillard et al., 2012). Despite in angiosperms, no knockout mutants of PTOX have been reported in another organism of the green lineage. In Chlamydomonas, a mutant of PTOX2 had been obtained while no mutant of PTOX1 could be isolated (Houille-Vernes et al., 2011). The double mutant in Marchantia is the first mutant that lacks all PTOX activity in a plant besides angiosperms.

In vivo experiments showed a higher PTOX activity *in C. reinhardtii* (Houille-Vernes et al., 2011) than in the vascular plant tomato (Trouillard et al., 2012) or in *Eutrema salsugine* (Stepien & Johnson, 2009). In *M. polymorpha*, *in vivo*, the deletion of PTOXb has a larger effect on the redox state of the PSII acceptor side than that of PTOXa (Messant et al., 2021). This difference cannot be explained by a difference in the activity of the enzymes but rather by differences in the regulation of the enzyme activities. Both purified recombinant PTOXa and PTOXb proteins from *M. polymorpha* showed higher activity (Table 1) than has been previously reported for rice PTOX (Yu et al., 2014). Here and in the previous study on OsPTOX, the enzymes were expressed as MBP fusion proteins to ensure their solubility. A V_{max} for MBP-OsPTOX of 16.6 ± 0.8 μmol O_2 mg^{-1} min^{-1} has been determined using soluble decyl-PQ at saturating concentration as substrate, while here, using the same enzymatic assay, a 3-fold higher V_{max} was determined for the truncated MBP-MpPTOXb and a 10-fold higher V_{max} for MBP-MpPTOXa (Table 1). The difference in activity between the MpPTOX isoforms may be caused by the changes in the amino acid sequence that may affect the substrate accessibility to the catalytic center (Figure S3). It seems rather unlikely that the N-terminal extension of MpPTOXb affects the catalytic activity in the *in vitro* assay since the helices harboring the catalytic center are unaltered. The N-terminal extension of MpPTOXb may be important for anchoring PTOX permanently to the membrane as has been suggested by Nawrocki et al. (2015). MpPTOXa, the enzyme that is more closely related

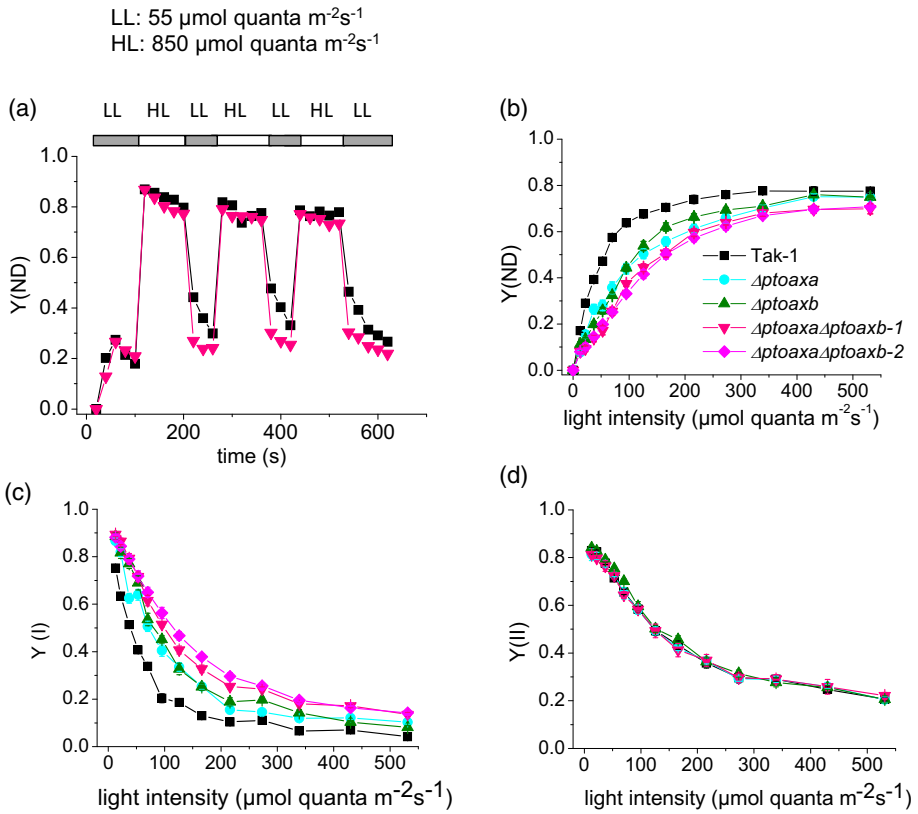

Figure 3. Chlorophyll fluorescence and P700 absorption parameters measured in Marchantia.
(a) Changes in PSI donor-side limitation Y(ND) upon illumination with fluctuating light. Light intensity was altered between 55 µmol quanta m^{-2} sec^{-1} (LL) and 850 µmol quanta m^{-2} sec^{-1} (HL). For clarity, only values of a single representative measurement for Tak-1 (black squares) and the double mutant line Δ*ptoaxb_1* (pink triangle) are shown.
(b) PSI donor-side limitation Y(ND) as a function of the light intensity.
(c) Quantum yield of PSI, Y(I), as a function of the light intensity.
(d) Effective quantum yield of PSII, Y(II) as a function of the light intensity. B–D: Three replicates from four different independently grown sets of plants, n = 12, mean and SD are given.

to angiosperm PTOX isoforms (Messant et al., 2021) may be more loosely attached to the membrane. PTOX in angiosperms has been shown either to migrate within the thylakoid membrane from stroma lamellae to grana stacks (Stepien & Johnson, 2018) or to associate with the thylakoid membrane only in the presence of a high proton motive force (Bolte et al., 2020). Anchoring of the enzyme to the membrane is required for the access to its membrane-localized substrate PQH_2 and PTOXa is supposed to be regulated via relocalization to the membrane under conditions when photosynthetic electron transport is saturated.

In the literature, PTOX is discussed as a safety valve that protects the photosynthetic apparatus and especially PSII upon exposure of plants to oxidative stress conditions such as high light, high salinity, and extreme temperatures (Quiles, 2006; Stepien & Johnson, 2009; Stepien & Johnson, 2018). However, as shown in Figure 4 for both, Arabidopsis and Marchantia, PSII is more susceptible to photoinhibition in the wild types than in the PTOX mutants while the opposite was observed for PSI. Increase in donor-side limitation to PSI and a high level of $P700^+$ accumulation is known to protect PSI against photoinhibition (Cerqueira et al., 2019; Sejima et al., 2014). We note that the PTOX mutants still can sustain a high level of P700 oxidation, which should be due to other electron sinks such as Calvin-Benson cycle and flavodiiron proteins (Shimakawa et al., 2017). More surprising than the protective effect of PTOX activity on PSI is the higher PSII damage observed in the wild types compared with the mutants. The higher damage of PSII suggests that a larger amount of reactive oxygen species is generated in wild-type plants than in the mutants. It has been shown that overexpression of PTOX1 from *Chlamydomonas reinhardtii* in tobacco promotes oxidative stress, especially the production of superoxide anion radicals ($O_2^{\bullet-}$) (Heyno et al., 2009). In this overexpressor PSII is highly susceptible to photoinhibition (Ahmad et al., 2012, 2020; Heyno et al., 2009). *In vitro*, as a function of the decyl-plastoquinol concentration and pH value, PTOX has an anti-oxidant or a pro-oxidant role (Yu et al., 2014). At

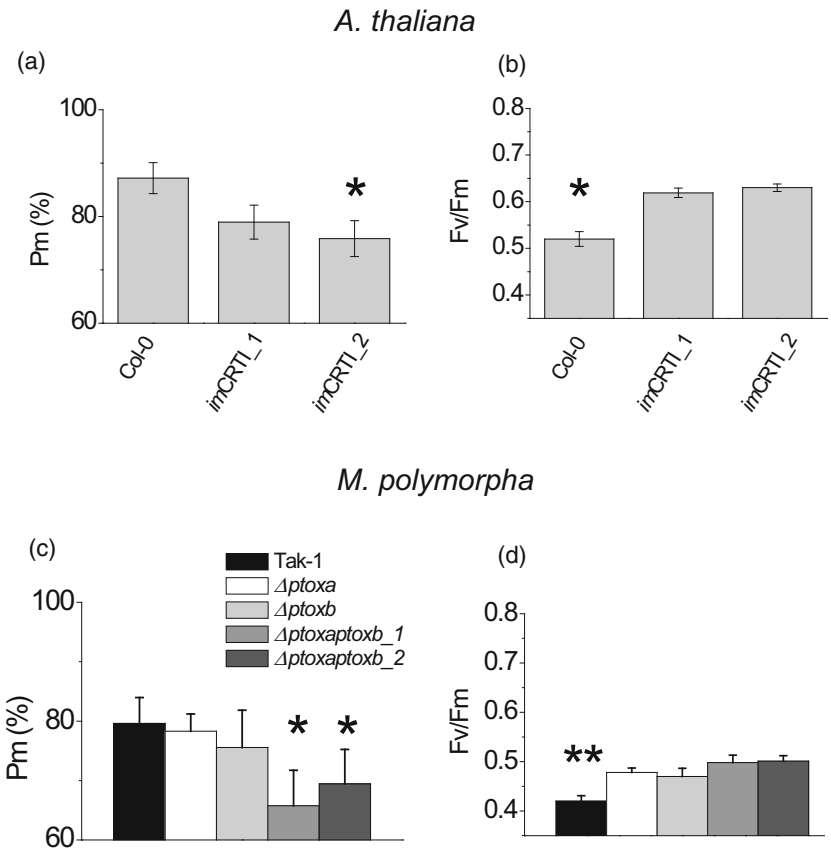

Figure 4. Photoinhibition of PSI and PSII in Arabidopsis (a, b) and Marchantia (c, d). Leaves and thalli were exposed to high light (1250 μmol quanta m^{-2} sec^{-1}) for 3 h. Left, percentage of the loss of maximum absorption change of P700 (Pm) compared to the Pm value prior to the photoinhibition treatment. Fv/Fm values prior to the photoinhibitory treatment for Col-0 were: 0.813 ± 0.006, *im*CRTI_1: 0.814 ± 0.011, *im*CRTI_2: 0.809 ± 0.012 and for Marchantia Tak-1: 0.766 ± 0.005, Δ*ptoxa*: 0.767 ± 0.011, Δ*ptoxb*: 0.766 ± 0.008, Δ*ptoxaptoxb_1*: 0.769 ± 0.06, Δ*ptoxaptoxb_2*: 0.758 ± 0.016. Three replicates from four different independently grown sets of plants, $n = 12$, mean and SD are given. Stars indicate significant differences, compared to the control condition, based on a Mann and Whitney test (* $P < 0.05$, ** $P < 0.01$).

slightly alkaline pH (pH 8.0), PTOX activity favors the production of $O_2^{\bullet-}$ when the substrate concentration is high. $O_2^{\bullet-}$ production at pH 8.0 is likely caused by the pH-dependent stabilization of the semiquinone $PQ^{\bullet-}$ that reduced O_2 to $O_2^{\bullet}$ or by the peroxo intermediate of the Fe-Fe cluster. When the substrate concentration is low, PTOX has an anti-oxidant effect lowering the yield of $O_2^{\bullet-}$ production. This said, PTOX only promotes $O_2^{\bullet-}$ production when the PQ pool is highly reduced. This is the case at high light intensities largely exceeding the light required for photosynthetic electron transport.

CONCLUSION

According to the data presented here, PTOX plays an important role under high light stress, protecting PSI against photoinhibition. Thanks to its PQH_2 oxidizing activity removing thereby electrons from the electron transport chain. In high light, less electrons are available to reduce $P700^+$. At the same time, lack of PTOX activity protects PSII against photoinhibition. The negative impact of PTOX on PSII stability in high light is most likely caused by its pro-oxidant role leading to $O_2^{\bullet-}$ production. Overall, it is beneficial for the plant to sacrifice PSII upon high light stress. Photoinhibition of PSII protects PSI against photoinhibition since it limits electron donation and favors the accumulation of $P700^+$. Sonoike has proposed that PSII photoinhibition can be regarded as a protection mechanism for PSI (Sonoike, 2011). PSI photoinhibition is irreversible in the short term compared with the efficient damage repair cycle of PSII (Li et al., 2018).

MATERIALS AND METHODS

Plant material

Arabidopsis thaliana

Arabidopsis thaliana (Col-0), the PTOX mutant *im*, a transgenic *Arabidopsis* line expressing *CRTI* under 35S promoter control as described in Schaub et al., 2005 here called CRTI, and two lines of crosses *im* x CRTI were grown for 3–4 weeks in soil under a light–dark cycle (16 h-light, 22°C, 100 μmol quanta m^{-2} sec^{-1}, white

fluorescent lamp/8 h-dark, 20°C). The lines of the F2 generation that showed no PTOX activity were named *im*CRTI_1 and *im*CRTI_2. RT-PCR showed that the expression level is low in these lines (Figure S7).

Marchantia polymorpha

A male accession of *M. polymorpha*, Takaragaike (Tak)-1, and all mutants were asexually cultured on one-half-strength Gamborg's B5 agar medium (Gamborg et al., 1968) in the same light conditions as used for *Arabidopsis*. For physiological measurements, 2–3 weeks old thalli were used.

RT-PCR

For quantitative RT-PCR analysis, plants were subjected to 16 h-light (22°C, 100 μmol quanta m^{-2} sec^{-1}, white, fluorescent lamp/8 h-dark, 20°C) for 2 weeks. Total RNAs were extracted using the Plant Mini RNeasy kit (Qiagen, Venlo, Netherlands) according to the manufacturer's instructions and quantified using a NanoDrop Spectroscope (Nanodrop 2000, Ozyme, Saint-Cyr-l'École, France). To perform RT reactions, the SuperScript IV Reverse Transcriptase kit (Invitrogen, Carlsbad, USA) was used. qPCR was done using a LightCycler 96 Instrument (Roche, Penzberg, Germany). cDNA was diluted three times with LightCycler 480 SYBR Green I Master (Roche, Penzberg, Germany) reaction medium (1X final concentration) containing 250 nM of each primer (Table S2). mRNA levels were normalized to two reference housekeeping genes (UBIQUITIN CARRIER PROTEIN 21 and YELLOW-LEAF-SPECIFIC GENE). Three technical replicates were performed for each qPCR.

Genome editing by CRISPR/Cas9 system

The construction of plasmids allowing the transformation of *M. polymorpha* by the CRISPR/Cas9 method was carried out according to the method of Sugano et al., 2014. Six target sequences of interest, three for *PTOXa* and three for *PTOXb*, were inserted into pMpGE_En03 vectors which were transferred into pMpGE010 or pMpGE011 vectors by gateway reaction. Each of the *Δptoxa* and *Δptoxb* single mutants previously characterized (Messant et al., 2021) were transformed with the vectors to mutate the remaining intact PTOX gene. The final transformation of the plants was carried out using the Agar-Trap method (Tsuboyama et al., 2018; Tsuboyama & Kodama, 2014) on thalli and gemmae. After sequencing, two double mutants were obtained from the single *Δptoxb* mutant transformed with a *PTOXa* gene targeting sequence: CCTTATGGAGGCTCTAGG. These different mutants do not differ in the location but in the type of mutation caused by Cas9 (see Figure S8 for more details). Throughout the manuscript, these two double mutants are called *Δptoxaptoxb_1* and *Δptoxaptoxb_2*.

Vector constructions and MBP-MpPTOXa and MBP-MpPTOXbΔNter expression, purification from *E.coli* and enzymatic assay

PETM-40_PTOXa construct. The synthetic optimized gene (Eurofins) of *PTOXa* (Mp3g12150.1) from *Marchantia* was amplified by PCR with the primers [F-PTOXa-Nco1 and R-PTOXa-Xho1]. The amplified fragment was digested with Nco1 and Xho1 and ligated with Nco1/Xho1-digested PETM-40 to produce the vector PETM-40_PTOXa.

PETM-40_Δ33-257-PTOXb (*PETM-40_*Δ**Nter**-*PTOXb) construct*. First, the PTOXb gene (Mp7g11430.1) from *Marchantia* was amplified by PCR using the cDNA of Tak-1 as a template and the primers [F-PTOXb and R-PTOXb]. The amplified fragments were cloned in PETM-40 vector linearized with Nco1 and Xho1 using the In-Fusion HD Cloning Kit (TaKaRa) to generate the vector PETM-40_PTOXb. Then, a deletion of a large part of a sequence encoding the N terminal domain (33–257) of the PTOXb gene (Mp7g11430.1) was introduced by site-directed mutagenesis using the plasmid PETM-40_PTOXb as template and synthetic primers F-PET-PTOXb Del and R-PET-PTOXb Del. All plasmids were checked by sequencing. List of primers in SI Table S3. The obtained plasmids were used to transform BL21 (DE3) *E. coli* cells. 20 ml of overnight cultures were inoculated into 1 L of LB, grown at 37°C to an OD 600 nm between 0.6 and 0.8, and induced with IPTG. After induction overnight at 16°C, the cells were harvested, washed in buffer A (25 mM sodium phosphate buffer pH 7.6, $MgCl_2$ 2.5 mM, NaCl 300 mM, glycerol 15% V/V), and frozen at −80°C. Purification was carried out on ice. Cells were resuspended in buffer A with DNase, PMSF, and lysozyme and sonicated. After centrifugation at 28000 g for 45 min the supernatant was solubilized for 30 min on ice by slowly adding 6 X CMC n-octyl β-D-glucopyranoside (nOG; 1 X CMC = 25 mM) and then applied to Amylose resin. After washing thoroughly with buffer A containing 2 X CMC nOG; the elution was accomplished with buffer B (50 mM Tris–HCl pH 8.0, $MgCl_2$ 2.5 mM, glycerol, 10% V/V, 2 X CMC nOG, and 10 mM maltose). Proteins resolved by SDS-PAGE were detected using Coomassie Brilliant Blue. Protein quantification was done by using the Bradford reagent. The activity of recombinant PTOX was measured as described in Yu et al.2014.

Activity was measured using a coupled enzymatic assay. PQ was reduced to PQH_2 by human DT-diaphorase and PQH_2 was oxidized by PTOX. Standard assay conditions containing 10 μg protein per 700 μl assay volume, 100 μM decyl-plastoquinone, 200 μM NADH, 10 μg human DT-diaphorase (Sigma-Aldrich), 50 mM Tris–HCl pH 8.0, 2.5 mM $MgCl_2$ were used. Activities were determined by measuring O_2 consumption with a Clark-type electrode.

Chlorophyll fluorescence and P700 measurements

Chlorophyll *a* fluorescence and P700 absorption were measured using a Dual-PAM-100 fluorometer (Walz, Effeltrich, Germany). Chlorophyll fluorescence curves were measured using a low actinic light (38 μmol quanta m^{-2} sec^{-1}). Post-illumination fluorescence rise was measured after illumination of *Arabidopsis* leaves for 10 min at 530 μmol quanta m^{-2} sec^{-1}. PSII and PSI parameters were determined as described by Messant et al. (2021). Pm is the maximal P700 signal upon transformation of P700 from the fully reduced to the fully oxidized state. The following definitions were used according to Klughammer and Schreiber (1994): Effective quantum yield of PSII: Y(II) = (Fm′-F)/Fm′; Yield of donor side limitation: Y(ND) = 1-P700red; PSI quantum yield: Y(I) = 1-Y(ND)-Y(NA).

Photoinhibition

Arabidopsis leaves and *Marchantia* thalli were exposed to high light (1250 μmol quanta m^{-2} sec^{-1}) for 3 h. Samples were kept for 15 min at room light (8 μmol quanta m^{-2} sec^{-1}) before determining the maximum value for P700 absorption, Pm, and the maximum quantum yield of PSII, Fv/Fm.

ACKNOWLEDGEMENTS

We would like to thank Anne-Sophie Fiorucci (I2BC) for scientific discussions and her help with RT-PCR experiments. This work was supported by the Labex Saclay Plant Sciences-SPS (ANR-17-EUR-0007) and by the platform of Biophysics of the I2BC supported by the French Infrastructure for Integrated Structural Biology (FRISBI; grant number ANR-10-INSB-05). M.M. is supported by a CEA PhD fellowship.

AUTHOR CONTRIBUTIONS

MM, GS, and AK-L designed the project. MM, UH, T-LL, AW, GS, and AK-L performed the experiments and analyzed the data. AK-L wrote the initial version of the manuscript that was read and revised by all authors.

DATA AVAILABILITY STATEMENT

Data will be made available on demand.

SUPPORTING INFORMATION

Additional Supporting Information may be found in the online version of this article.

Figure S1. Plants grown in different light regimes. a: *Arabidopsis thaliana* (2 weeks old) in long day or for 1 week in fluctuating light condition (LL = 55 μmol quanta m^{-2} sec^{-1}, HL = 850 μmol quanta m^{-2} sec^{-1}). b: *Marchantia polymorpha* (2 weeks old), grown for 1 week in fluctuating light (5 min 55 μmol quanta m^{-2} sec^{-1}, 1 min 850 μmol quanta m^{-2} sec^{-1}).

Figure S2. Pigment composition in *Marchantia polymorpha* genotypes grown at 100 μmol quanta m^{-2} sec^{-1} (normal light, NL) and at 200 μmol quanta m^{-2} sec^{-1} (high light, HL). Pigments were extracted by incubation in 100% acetone. Mean values with standard error are given (n = 3). Stars indicate significant differences, compared to the control condition, based on Student's t-test (* $P < 0.05$). Pigment determination was done in accordance to Lichtenthaler (1987). Ref.: Lichtenthaler H. (1987) Methods in Enzymology 148, pp 350-382.

Figure S3. Sequence alignment of MpPTOXa and Nter truncated MpPTOXb catalytic sites by MUSCLE. Sequence alignment of MpPTOXa and Nter truncated MpPTOXb catalytic sites by MUSCLE. The six helices α-1 (red), α-2 (green), α-4 (yellow), α-5 (magenta) and α-6 (cyan) are framed and the fourth iron binding sites motifs with the six iron binding sites determined by McDonald *et al.*, 2003, are indicated in bold above sequences. The site of truncation of the recombinant protein is indicated by a flash. Ref.: McDonald AE, Amirsadeghi S, Vanlerberghe GC. Prokaryotic orthologues of mitochondrial alternative oxidase and plastid terminal oxidase. *Plant Mol Biol.* 53(6):865-76. (2003). Edgar RC. MUSCLE: multiple sequence alignment with high accuracy and high throughput. *Nucleic Acids Res.* 32(5):1792–7. (2004).

Figure S4. Donor side limitation Y(ND) in fluctuating light condition (LL = 55 μmol quanta m^{-2} sec^{-1}, HL = 850 μmol quanta m^{-2} sec^{-1}) for all Marchantia genotypes. Additional data sets to Figure 3a.

Figure S5. Acceptor side limitation Y(NA) and non-photochemical quenching (NPQ) as a function of the light intensity for all Marchantia genotypes. Additional data to Figure 3a.

Figure S6. Donor-side limitation (Y(ND)) at 1290 μmol quanta m^{-2} sec^{-1}.

Figure S7. mRNA expression levels of ptox in 2-week-old plants determined by RT-PCR. Arabidopsis ecotype *Landsberg erecta, immutans.* and the two lines of crosses between CRTI and *im.* Data are from two different RNA extraction. A third RNA extraction showed the same result but all expression levels were higher likely because of harvesting at a different time of the day. Mean values with standard error are shown (n = 2).

Figure S8. Sequencing of MpPTOXa gene, after CRISPR/Cas9 transformation of *Δptoxb* mutant, in both *Δptoxaptoxb* double mutant lines. The first sequence is MpPTOXa CDS. The two others are the result of CRISPR/cas9 mutations in both double mutant lines. The red frame show the NGG targeted site. The orange frame represents mutations results.

Table S1. Chlorophyll a/b and carotenoid to chlorophyll ratio in *A. thaliana* genotypes.

Table S2. Primer sequences for RT-qPCR.

Table S3. Primer sequences for *PTOX* constructs.

REFERENCES

Ahmad, N., Khan, M.O., Islam, E., Wei, Z.Y., McAusland, L., Lawson, T. *et al.* (2020) Contrasting responses to stress displayed by tobacco overexpressing an algal plastid terminal oxidase in the chloroplast. *Frontiers in Plant Science*, **11**, 501.

Ahmad, N., Michoux, F. & Nixon, P.J. (2012) Investigating the production of foreign membrane proteins in tobacco chloroplasts: expression of an algal plastid terminal oxidase. *PLoS One*, **7**, e41722.

Alboresi, A., Storti, M. & Morosinotto, T. (2019) Balancing protection and efficiency in the regulation of photosynthetic electron transport across plant evolution. *The New Phytologist*, **221**, 105–109.

Bolte, S., Marcon, E., Jaunario, M., Moyet, L., Paternostre, M., Kuntz, M. *et al.* (2020) Dynamics of the localization of the plastid terminal oxidase inside the chloroplast. *Journal of Experimental Botany*, **71**, 2661–2669.

Carol, P., Stevenson, D., Bisanz, C., Breitenbach, J., Sandmann, G., Mache, R. *et al.* (1999) Mutations in the Arabidopsis gene IMMUTANS cause a variegated phenotype by inactivating a chloroplast terminal oxidase associated with phytoene desaturation. *The Plant Cell*, **11**, 57–68.

Cerqueira, J.V.A., Silveira, J.A.G., Carvalho, F.E.L., Cunha, J.R. & Lima Neto, M.C. (2019) The regulation of P700 is an important photoprotective mechanism to NaCl-salinity in Jatropha curcas. *Physiologia Plantarum*, **167**, 404–417.

Gamborg, O.L., Miller, R.A. & Ojima, K. (1968) Nutrient requirements of suspension cultures of soybean root cells. *Experimental Cell Research*, **50**, 151–158.

Heyno, E., Gross, C.M., Laureau, C., Culcasi, M., Pietri, S. & Krieger-Liszkay, A. (2009) Plastid alternative oxidase (PTOX) promotes oxidative stress when overexpressed in tobacco. *The Journal of Biological Chemistry*, **284**, 31174–31180.

Houille-Vernes, L., Rappaport, F., Wollman, F.A., Alric, J. & Johnson, X. (2011) Plastid terminal oxidase 2 (PTOX2) is the major oxidase involved in chlororespiration in Chlamydomonas. *Proceedings of the National Academy of Sciences of the United States of America*, **108**, 20820–20825.

Ibáñez, H., Ballester, A., Muñoz, R. & Quiles, M.J. (2010) Chlororespiration and tolerance to drought, heat and high illumination. *Journal of Plant Physiology*, **15**(167), 732–738.

Ivanov, A.G., Rosso, D., Savitch, L.V., Stachula, P., Rosembert, M., Oquist, G. *et al.* (2012) Implications of alternative electron sinks in increased resistance of PSII and PSI photochemistry to high light stress in cold-acclimated Arabidopsis thaliana. *Photosynthesis Research*, **113**, 191–206.

Klughammer, C. & Schreiber, U. (1994) An improved method, using saturating light pulses, for the determination of photosystem I quantum yield via P700+-absorbance changes at 830 nm. *Planta*, **192**, 261–268.

Laureau, C., De Paepe, R., Latouche, G., Moreno-Chacón, M., Finazzi, G., Kuntz, M. *et al.* (2013) Plastid terminal oxidase (PTOX) has the potential to act as a safety valve for excess excitation energy in the alpine plant species Ranunculus glacialis L. *Plant, Cell & Environment*, **36**, 1296–1310.

Li, L., Aro, E.M. & Millar, A.H. (2018) Mechanisms of Photodamage and protein turnover in Photoinhibition. *Trends in Plant Science*, **23**, 667–676.

Messant, M., Shimakawa, G., Perreau, F., Miyake, C. & Krieger-Liszkay, A. (2021) Evolutive differentiation between alga- and plant-type plastid terminal oxidase: study of plastid terminal oxidase PTOX isoforms in Marchantia polymorpha. *Biochimica et Biophysica Acta—Bioenergetics*, **1862**, 148309.

Nawrocki, W.J., Tourasse, N.J., Taly, A., Rappaport, F. & Wollman, F.A. (2015) The plastid terminal oxidase: its elusive function points to multiple contributions to plastid physiology. *Annual Review of Plant Biology*, **66**, 49–74.

Oguchi, R., Terashima, I. & Chow, W.S. (2021) The effect of different spectral light quality on the photoinhibition of photosystem I in intact leaves. *Photosynthesis Research*, **149**, 83–92.

Quiles, M.J. (2006) Stimulation of chlororespiration by heat and high light intensity in oat plants. *Plant, Cell & Environment*, **29**, 1463–1470.

Rosso, D., **Ivanov, A.G.**, **Fu, A.**, **Geisler-Lee, J.**, **Hendrickson, L.**, **Geisler, M.** ***et al.*** (2006) IMMUTANS does not act as a stress-induced safety valve in the protection of the photosynthetic apparatus of Arabidopsis during steady-state photosynthesis. *Plant Physiology*, **142**, 574–585.

Schaub, P., **Al-Babili, S.**, **Drake, R.** & **Beyer, P.** (2005) Why is golden rice golden (yellow) instead of red? *Plant Physiology*, **138**, 441–450.

Sejima, T., **Takagi, D.**, **Fukayama, H.**, **Makino, A.** & **Miyake, C.** (2014) Repetitive short-pulse light mainly inactivates photosystem I in sunflower leaves. *Plant & Cell Physiology*, **55**, 1184–1193.

Shimakawa, G., **Ishizaki, K.**, **Tsukamoto, S.**, **Tanaka, M.**, **Sejima, T.** & **Miyake, C.** (2017) The liverwort, *Marchantia*, drives alternative electron flow using a Flavodiiron protein to protect PSI. *Plant Physiology*, **173**, 1636–1647.

Sonoike, K. (2011) Photoinhibition of photosystem I. *Physiologia Plantarum*, **142**, 56–64.

Sonoike, K., **Terashima, I.**, **Iwaki, M.** & **Itoh, S.** (1995) Destruction of photosystem I iron-sulfur centers in leaves of Cucumis sativus L. by weak illumination at chilling temperatures. *FEBS Letters*, **362**, 235–238.

Stepien, P. & **Johnson, G.N.** (2009) Contrasting responses of photosynthesis to salt stress in the glycophyte Arabidopsis thaliana and the halophyte Thellungiella halophila. Role of the plastid terminal oxidase as an alternative electron sink. *Plant Physiology*, **149**, 1154–1165.

Stepien, P. & **Johnson, G.N.** (2018) Plastid terminal oxidase requires translocation to the grana stacks to act as a sink for electron transport. *Proceedings of the National Academy of Sciences of the United States of America*, **115**, 9634–9639.

Streb, P., **Josse, E.-M.**, **Galouët, E.**, **Baptist, F.**, **Kuntz, M.** & **Cornic, G.** (2005) Evidence for alternative electron sinks to photosynthetic carbon assimilation in the high mountain plant species Ranunculus glacialis. *Plant Cell Environ*, **28**, 1123–1135.

Sugano, S.S., **Shirakawa, M.**, **Takagi, J.**, **Matsuda, Y.**, **Shimada, T.**, **Hara-Nishimura, I.** ***et al.*** (2014) CRISPR/Cas9-mediated targeted mutagenesis in the liverwort Marchantia polymorpha L. *Plant & Cell Physiology*, **55**, 475–481.

Trouillard, M., **Shahbazi, M.**, **Moyet, L.**, **Rappaport, F.**, **Joliot, P.**, **Kuntz, M.** ***et al.*** (2012) Kinetic properties and physiological role of the plastoquinone terminal oxidase (PTOX) in a vascular plant. *Biochimica et Biophysica Acta*, **1817**, 2140–2148.

Tsuboyama, S. & **Kodama, Y.** (2014) AgarTrap: a simplified agrobacterium-mediated transformation method for sporelings of the liverwort Marchantia polymorpha L. *Plant & Cell Physiology*, **55**, 229–236.

Tsuboyama, S., **Nonaka, S.**, **Ezura, H.** & **Kodama, Y.** (2018) Improved G-AgarTrap: A highly efficient transformation method for intact gemmalings of the liverwort Marchantia polymorpha. *Scientific Reports*, **17**(8), 10800.

Wetzel, C.M., **Jiang, C.Z.**, **Meehan, L.J.**, **Voytas, D.F.** & **Rodermel, S.R.** (1994) Nuclear–organelle interactions: the immutans variegation mutant of Arabidopsis is plastid autonomous and impaired in carotenoid biosynthesis. *The Plant Journal*, **6**, 161–175.

Yu, Q., **Feilke, K.**, **Krieger-Liszkay, A.** & **Beyer, P.** (2014) Functional and molecular characterization of plastid terminal oxidase from rice (Oryza sativa). *Biochimica et Biophysica Acta*, **1837**, 1284–1292.

Fig. S2

Pigment composition in *Marchantia polymorpha* genotypes grown at 100 µmol quanta $m^{-2}s^{-1}$ (normal light, NL) and at 200 µmol quanta $m^{-2}s^{-1}$ (high light, HL)

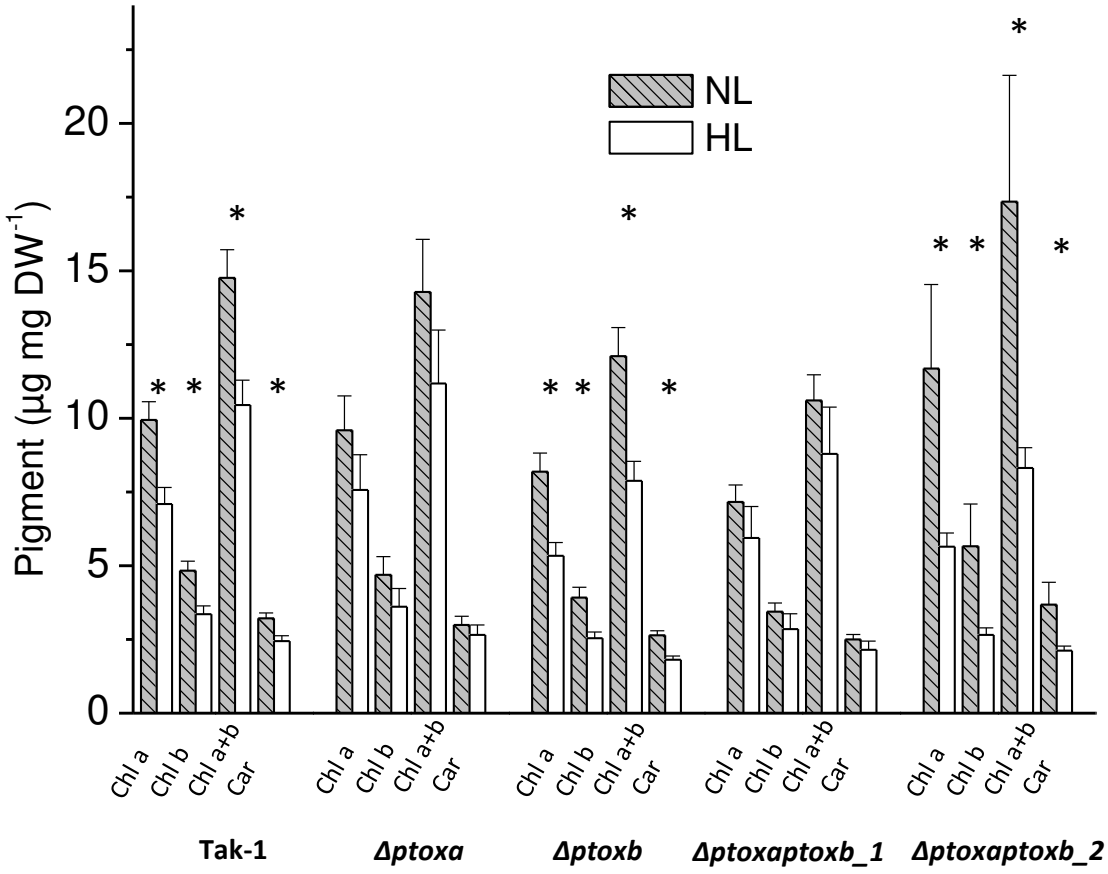

Pigments were extracted by incubation in 100% acetone. Mean values with standard error are given (n=3). Stars indicate significant differences, compared to the control condition, based on Student's t-test (* $p<0.05$).

Pigment determination was done in accordance to Lichtenthaler (1987).
Ref.: Lichtenthaler H. (1987) Methods in Enzymology 148, pp 350-382

Fig. S1

Plants grown in different light regimes.

a*: Arabidopsis thaliana* (2 weeks old) in long day or for 1 week in fluctuating light condition (LL = 55 µmol quanta $m^{-2}s^{-1}$, HL = 850 µmol quanta $m^{-2}s^{-1}$)

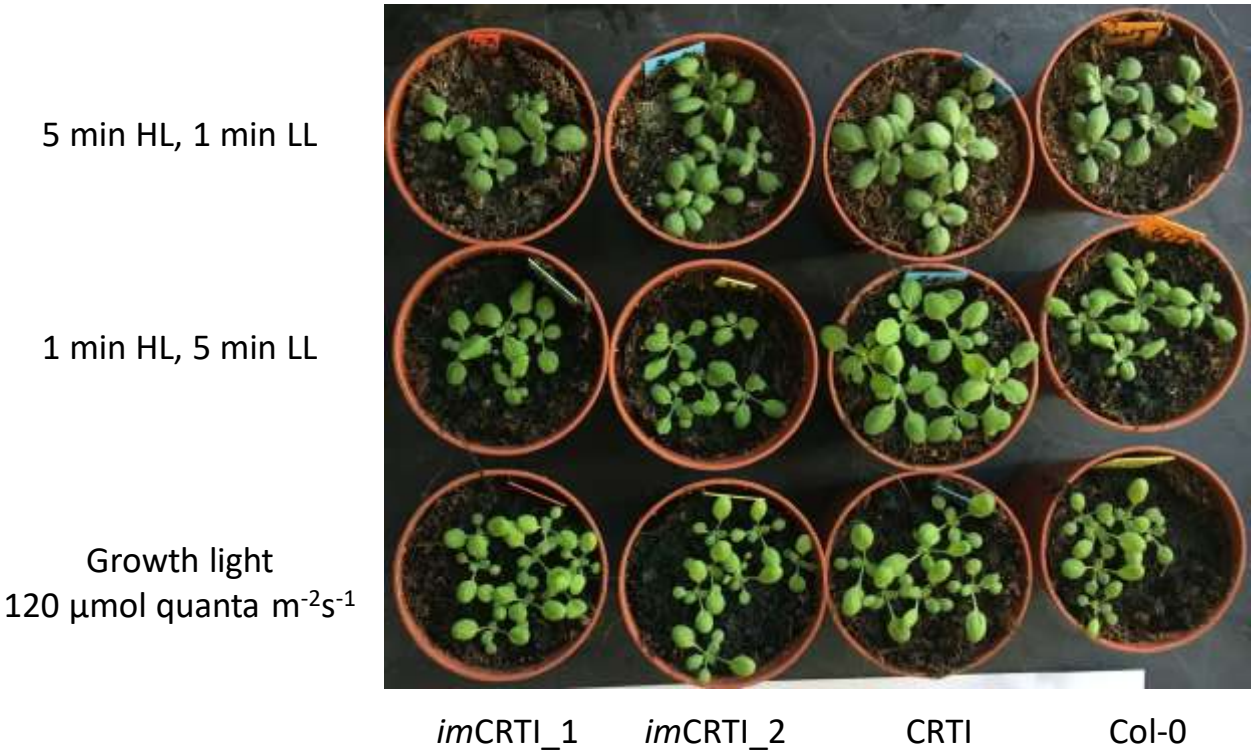

b*: Marchantia polymorpha* (2 weeks old), grown for 1 week in fluctuating light (5 min 55 µmol quanta $m^{-2}s^{-1}$, 1 min 850 µmol quanta $m^{-2}s^{-1}$)

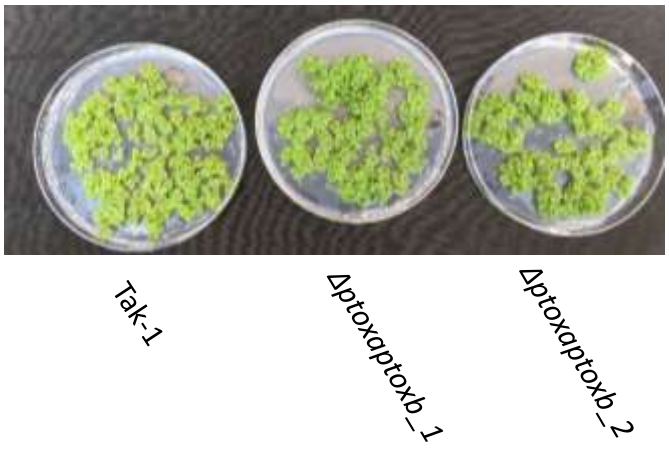

Fig. S3

Sequence alignment of MpPTOXa and Nter truncated MpPTOXb catalytic sites by MUSCLE.

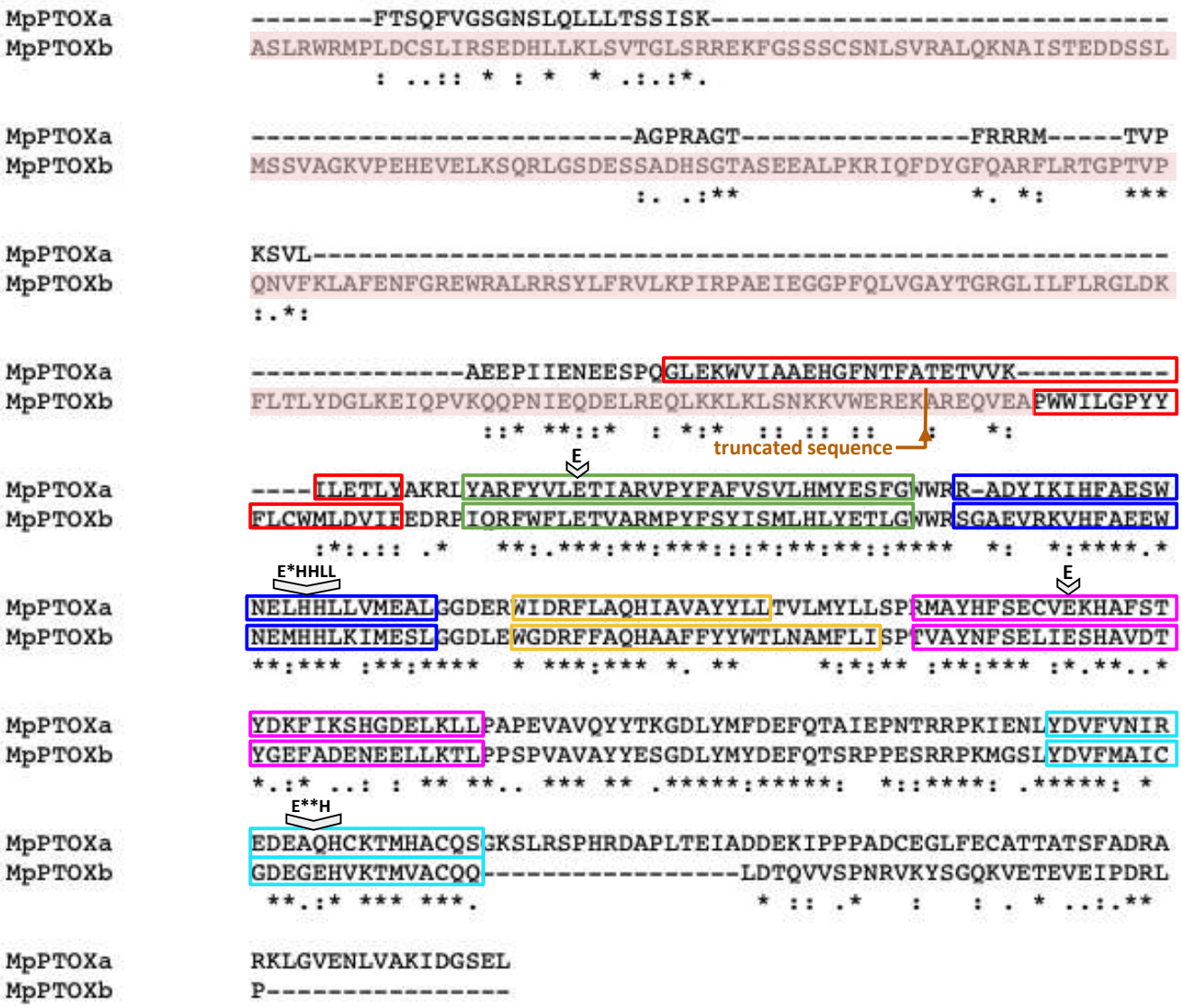

Sequence alignment of MpPTOXa and Nter truncated MpPTOXb catalytic sites by MUSCLE. The six helices **α**-1 (red), **α**-2 (green), **α**-4 (yellow), **α**-5 (magenta) and **α**-6 (cyan) are framed and the fourth iron binding sites motifs with the six iron binding sites determined by McDonald *et al*., 2003, are indicated in bold above sequences. The site of truncation of the recombinant protein is indicated by a flash

Ref.: McDonald AE, Amirsadeghi S, Vanlerberghe GC. Prokaryotic orthologues of mitochondrial alternative oxidase and plastid terminal oxidase. *Plant Mol Biol.* **53**(6):865-76. (2003)

Edgar RC. MUSCLE: multiple sequence alignment with high accuracy and high throughput. *Nucleic Acids Res*. **32**(5):1792-7. (2004)

Fig. S4

Donor side limitation Y(ND) in fluctuating light condition (LL = 55 µmol quanta $m^{-2}s^{-1}$, HL = 850 µmol quanta $m^{-2}s^{-1}$) for all Marchantia genotypes. Additional data sets to Fig. 3a

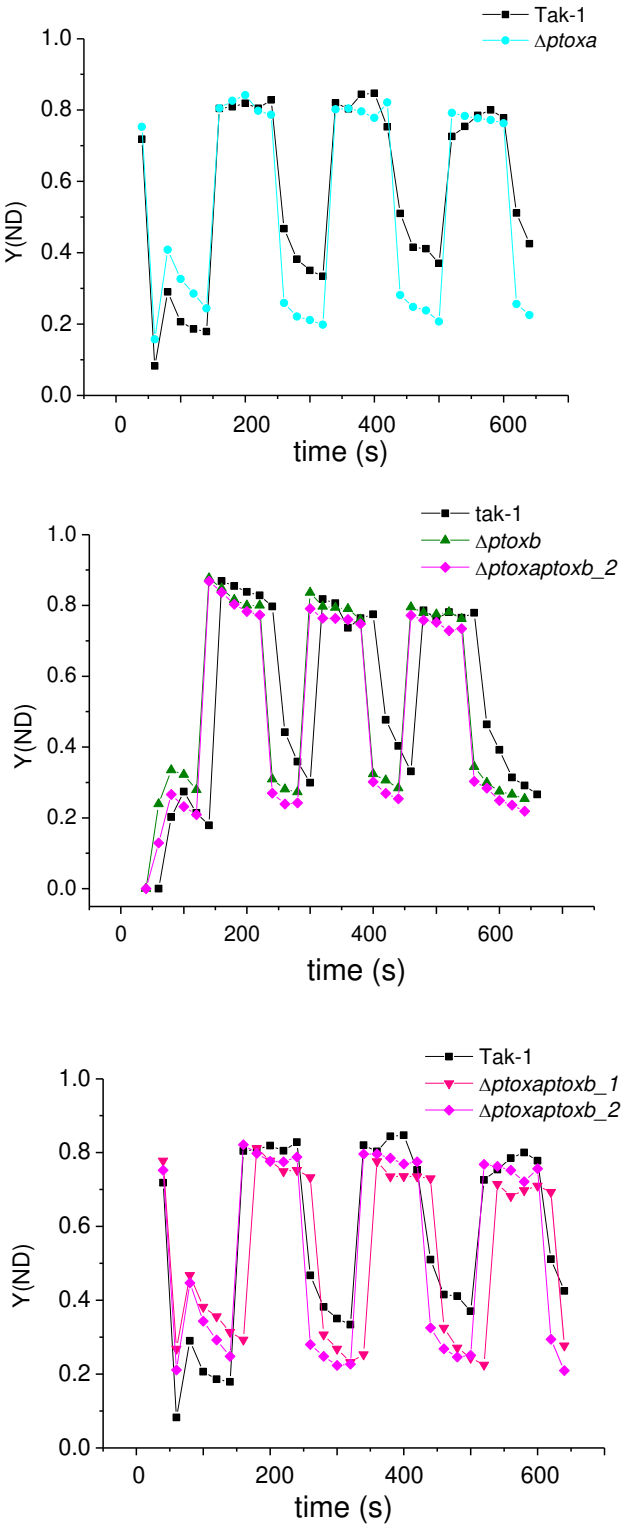

Fig. S5

Acceptor side limitation Y(NA) and non-photochemical quenching (NPQ) as a function of the light intensity for all Marchantia genotypes. Additional data to Fig. 3a

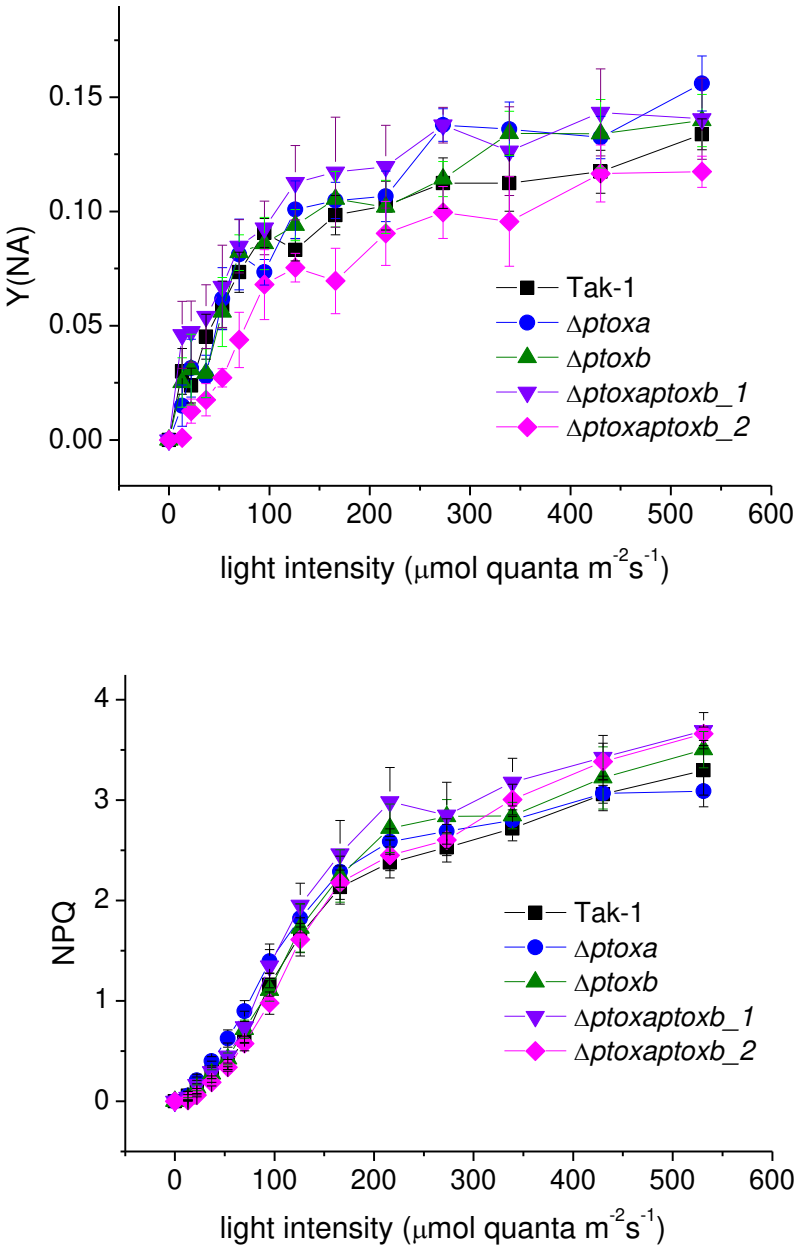

Fig. S6

Donor-side limitation (Y(ND)) at 1290 µmol quanta $m^{-2}s^{-1}$

Arabidopsis thaliana

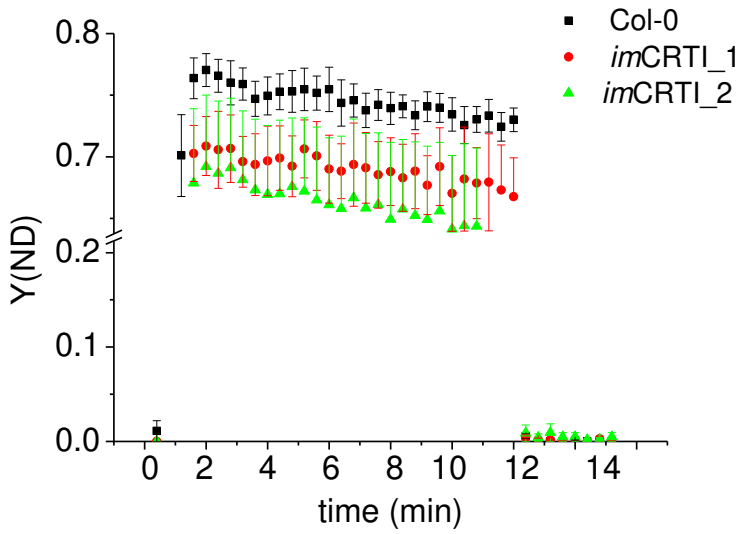

Marchantia polymorpha

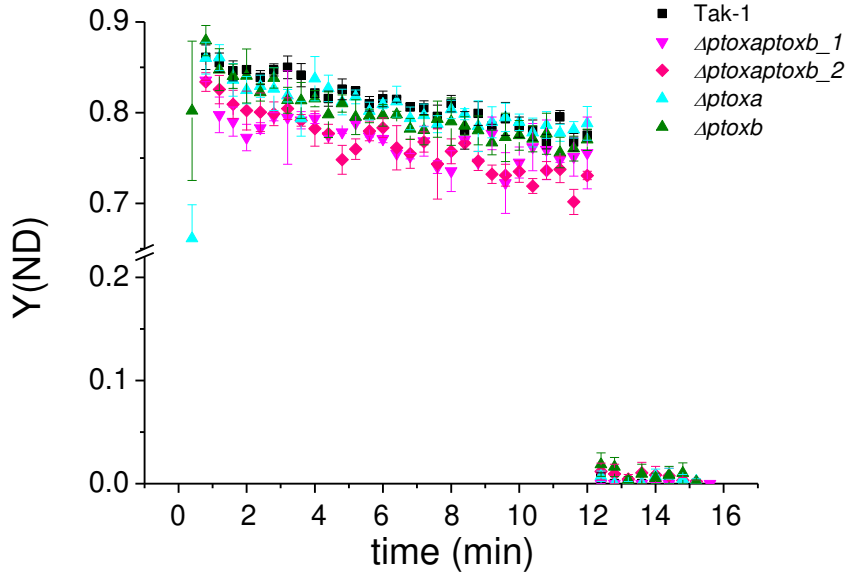

Fig. S7

mRNA expression levels of ptox in 2-week-old plants determined by RT-PCR. : Arabidopsis ecotype *Landsberg erecta , immutans.* and the two lines of crosses between CRTI and *im*.

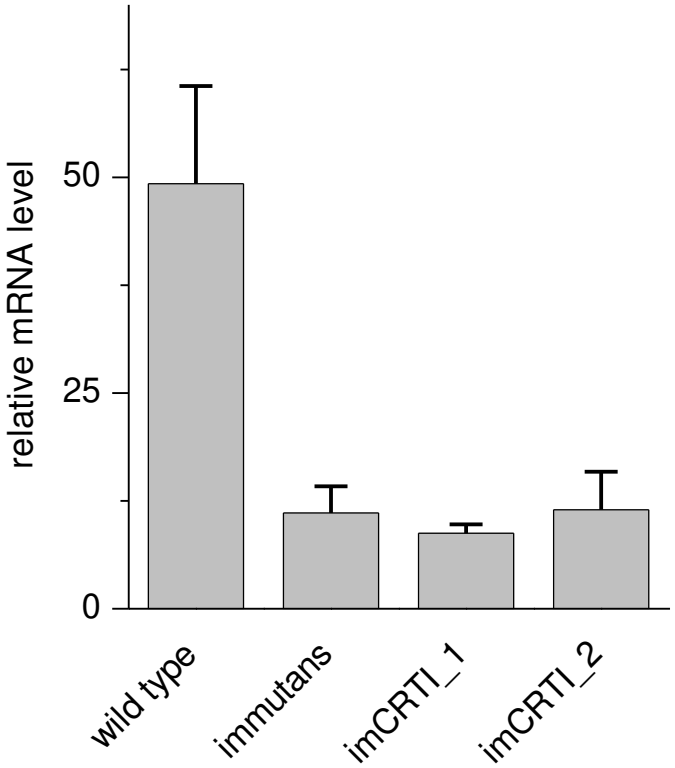

Data are from two different RNA extraction. A third RNA extraction showed the same result but all expression levels were higher likely because of harvesting at a different time of the day. Mean values with standard error are shown (n=2).

Fig. S8

Sequencing of MpPTOXa gene, after CRISPR/Cas9 transformation of *Δptoxb* mutant, in both *Δptoxaptoxb* double mutant lines

>MpPTOXa in *Δptoxb* mutant

ATGGCGTCTGGTCTGAGGATTGCTCCTCTGAATTGTGTATATAATCGCTGTGTGCCATCGGAGTCCCAAGGTTTTGGCTG
TTGCACCCGAACGGGTCGGAATGGGCCGATTTTGGCTGTGGGCGGGAAGCCCGTTCGATTCACTTCGCAGTTTGTGGGGT
CAGGAAATTCTTTGCAGCTTCTCTTGACGAGCTCGATTTCGAAAGCGGGTCCTCGTGCTGGCACATTCAGAAGGCGGATG
ACCGTCCCTAAGTCAGTGCTTGCAGAAGAGCCCATTATTGAAAATGAGGAATCGCCTCAAGGTTTGGAGAAGTGGGTGAT
TGCTGCGGAACATGGATTCAACACCTTTGCCACTGAGACTGTTGTGAAGATACTAGAGACTCTGTACGCGAAGCGCTTGT
ACGCAAGGTTTTACGTTTTAGAAACCATCGCGAGAGTTCCGTACTTTGCTTTTGTATCGGTTTTACACATGTACGAGAGC
TTTGGTTGGTGGAGACGGGCGGACTACATCAAAATTCACTTTGCAGAAAGCTGGAATGAACTACATCATCTTCTGGTTAT
GGAGGCTCTAGGTGGAGACGAGAGGTGGATCGATAGATTTTTGGCTCAGCACATTGCCGTTGCATACTATCTTCTTACTG
TATTAATGTATCTCCTTA-GCCCTAGAATGGCATACCATTTCTCAGAATGTGTCGAGAAGCATGCTTTTTCTACTTACGA
TAAGTTCATAAAGTCACATGGAGATGAGTTGAAGCTGCTTCCTGCTCCGGAGGTCGCAGTCCAATATTATACTAAGGGAG
ATCTATACATGTTTGATGAATTTCAAACTGCCATTGAACCGAACACAAGAAGACCAAAGATAGAAAATCTTTATGACGTT
TTCGTGAACATTCGTGAAGACGAAGCGCAGCATTGCAAGACAATGCATGCCTGTCAATCGGGGAAAAGTTTGAGGTCTCC
ACATAGAGACGCTCCTCTTACAGAGATAGCTGATGACGAGAAGATTCCTCCTCCAGCGGATTGTGAAGGCCTATTTGAAT
GTGCCACCACAGCCACTTCGTTCGCAGACAGGGCACGGAAACTAGGAGTAGAAAATCTTGTCGCAAAAATCGACGGATCA
GAGTTATGA

>MpPTOXa in *Δptoxaptoxb*_1

ATGGCGTCTGGTCTGAGGATTGCTCCTCTGAATTGTGTATATAATCGCTGTGTGCCATCGGAGTCCCAAGGTTTTGGCTG
TTGCACCCGAACGGGTCGGAATGGGCCGATTTTGGCTGTGGGCGGGAAGCCCGTTCGATTCACTTCGCAGTTTGTGGGGT
CAGGAAATTCTTTGCAGCTTCTCTTGACGAGCTCGATTTCGAAAGCGGGTCCTCGTGCTGGCACATTCAGAAGGCGGATG
ACCGTCCCTAAGTCAGTGCTTGCAGAAGAGCCCATTATTGAAAATGAGGAATCGCCTCAAGGTTTGGAGAAGTGGGTGAT
TGCTGCGGAACATGGATTCAACACCTTTGCCACTGAGACTGTTGTGAAGATACTAGAGACTCTGTACGCGAAGCGCTTGT
ACGCAAGGTTTTACGTTTTAGAAACCATCGCGAGAGTTCCGTACTTTGCTTTTGTATCGGTTTTACACATGTACGAGAGC
TTTGGTTGGTGGAGACGGGCGGACTACATCAAAATTCACTTTGCAGAAAGCTGGAATGAACTACATCATCTTCTGGTTAT
GGAGGCTCTAGGTGGAGACGAGAGGTGGATCGATAGATTTTTGGCTCAGCACATTGCCGTTGCATACTATCTTCTTACTG
TATTAATGTATCTCCTAGGCCCCTAGAATAGAA----------

>MpPTOXa in *Δptoxaptoxb*_2

ATGGCGTCTGGTCTGAGGATTGCTCCTCTGAATTGTGTATATAATCGCTGTGTGCCATCGGAGTCCCAAGGTTTTGGCTG
TTGCACCCGAACGGGTCGGAATGGGCCGATTTTGGCTGTGGGCGGGAAGCCCGTTCGATTCACTTCGCAGTTTGTGGGGT
CAGGAAATTCTTTGCAGCTTCTCTTGACGAGCTCGATTTCGAAAGCGGGTCCTCGTGCTGGCACATTCAGAAGGCGGATG
ACCGTCCCTAAGTCAGTGCTTGCAGAAGAGCCCATTATTGAAAATGAGGAATCGCCTCAAGGTTTGGAGAAGTGGGTGAT
TGCTGCGGAACATGGATTCAACACCTTTGCCACTGAGACTGTTGTGAAGATACTAGAGACTCTGTACGCGAAGCGCTTGT
ACGCAAGGTTTTACGTTTTAGAAACCATCGCGAGAGTTCCGTACTTTGCTTTTGTATCGGTTTTACACATGTACGAGAGC
TTTGGTTGGTGGAGACGGGCGGACTACATCAAAATTCACTTTGCAGAAAGCTGGAATGAACTACATCATCTTCTGGTTAT
GGAGGCTCTAGGTGGAGACGAGAGGTGGATCGATAGATTTTTGGCTCAGCACATTGCCGTTGCATACTATCTTCTTACTG
TATTAATGTATCTCCTAG-CCCCTAGAATACAAAA----------

The first sequence is MpPTOXa CDS. The two others are the result of CRISPR/cas9 mutations in both double mutant lines. The red frame show the NGG targeted site. The orange frame represents mutations results.

Table S1:

Chlorophyll a/b and carotenoid to chlorophyll ratio in *A. thaliana* genotypes

Sample	Chla/b	Car/(chla+chlb)
Col-0	3.78±0,11	0.41±0,02
*im*CRTI_1	3,95±0,05	0,41±0,01
*im*CRTI_2	3,94±0,09	0,41±0,01

Pigments were extracted by incubation in 100% acetone. Mean values with standard deviation are given (n=4).

Pigment determination was done in according to Lichtenthaler (1987).

Ref.: Lichtenthaler H. (1987) Methods in Enzymology 148, pp 350-382

Table S2

Primer sequences for RT-qPCR

Primer names		Primer sequences
F-PTOX	F	5'-TGCAGTGTTCTGCTTCATCA-3'
R-PTOX	R	5'-GCACCGGATATCGCAGTAAA-3'
F-UBC21	F	5′-CAGTCTGTGTGTAGAGCTATCATAGCAT-3′
R-UBC21	R	5′-AGAAGATTCCCTGAGTCGCAGTT-3′
F-YLS8	F	5′-TCATTCGTTTCGGCCATGA-3′
R-YLS8	R	5′-CTCAGCAACAGACGCAAGCA-3′

Primers used for qPCR for checking PTOX mRNA expression levels in Arabidopsis ecotype *Landsberg erecta , immutans* and the two lines of crosses between CRTI and *im*. YLS8 and UBC21 corresponds to housekeeping genes.

Table S3

Primer sequences for *PTOX* constructs.

Primer names	Primer sequences	
F-PTOX1-Nco1	F	5'- GAT ATA CCA TGG CTT CTG GCC TGC GCA TTG -3'
R-PTOX1-Xho1	R	5'- GCC GGC CTC GAG TTA TAA TTC GCT GCC ATC -3'
F-PTOX2	F	5'- TTC AGG GCG CCA TGG GCA GTC CTG CCG CAT GCA TGC TTC -3'
R-PTOX2	R	5'- GTG GTG GTG CTC GAG TCA CGG CAG ACG GTC GGG-3'
F-PET-PTOX2 Del	F	5'-GCTACCGACTGCACGGCTGCAGCTCGAGAACAAGTGGAA GCACCTTGG-3'
R-PET-PTOX2 Del	R	5'- TGCAGCCGTGCGTCGGTAGCAGCGGAACTGGGGAGGTG -3'

Primers used for vector constructions for PTOX expression in *E.coli* as described in the Methods section.